Stereoselective Synthesis of Cyanohydrins:
Process Development

Vom Promotionsausschuss der
Technischen Universität Hamburg-Harburg
zur Erlangung des akademischen Grades
Doktor–Ingenieur
genehmigte Dissertation

von
Sebastian Dirk Briechle

aus
Frechen

2013

Vorsitzender des Prüfungsausschusses:	Prof. Dr.-Ing. Michael Schlüter
1. Gutachter:	Prof. Dr. rer. nat. Andreas Liese
2. Gutachter:	Prof. Dr.-Ing. Irina Smirnova
Tag der mündlichen Prüfung:	31. August 2012

urn:nbn:de:gbv:830-tubdok-12054

Danke allen, die diese Arbeit ermöglicht und zu ihrem Gelingen beigetragen haben!

Für Helene, Ida und Eva

Contents

List of Figures

List of Tables

Überblick

Enantiomerenreine Cyanhydrine sind hervorragende Zwischenprodukte für eine Vielzahl von unterschiedlichen, optisch aktiven Molekülen wie Pharmazeutika, Fein- und Agrochemikalien.
In dieser Arbeit wurde eine zweistufige, chemoenzymatische Route zur Synthese enantiomerenreiner Cyanhydrine untersucht, welche einfache und kommerziell erhältliche Aldehyde und Diene als Ausgangsmaterial nutzt. In der ersten Stufe wurde eine funktionalisierte, chirale Cyclohexenyl-Struktur in einer Diels-Alder Reaktion gebildet. Diese Reaktion wurde katalysiert durch einen Salen-Übergangsmetall-Katalysator, welcher kovalent an ein Dendrimer gebunden war, ein sogenanntes *Chemzyme*. Die Reaktion wurde sowohl in Batchreaktionen als auch in einem kontinuierlich betriebenen Membranreaktor untersucht. Zur experimentellen Untersuchung der Reaktionskinetik wurde eine *Medium-Throughput-Assay* mittels eines Laborroboters realisiert. Ein kinetisches Modell konnte entwickelt werden, welches die experimentellen Daten mit einem einzigen kinetischen Parameter gut beschreibt. Der Katalysator konnte in dem untersuchten Reaktionssystem homogen gelöst werden, allerdings zeigte die Untersuchung der Reaktionskinetik auch Charakteristika einer heterogen katalysierten Reaktion. Mit Hilfe des kinetischen Modells wurde ein kontinuierlich betriebener Membranreaktor ausgelegt. Der Membranreaktor konnte über 40 Tage betrieben werden. Aufgrund der geringen Aktivität des Katalysators wurde nur eine Raum-Zeit-Ausbeute von 0.5 $g\,L^{-1}\,d^{-1}$ bei einem maximalen Umsatz von 80 % erreicht.
In der zweiten Stufe wurde das Cyanhydrin durch eine stereoselektive, enzym-katalysierte Addition von Cyanwasserstoff (HCN) an die Aldehydfunktion der Cyclohexenyl-Struktur gebildet. Als Modellsystem wurde die stereoselektive HCN-Addition an Benzaldehyd untersucht, welche katalysiert wurde durch eine Hydroxynitril Lyase aus *Hevea brasiliensis*. Um eine direkte Kopplung der ersten mit der zweiten Reaktion zu ermöglichen, wurde evaluiert, ob die enzymatische Reaktion in einem organischen Lösungsmittel-Reaktionssystem durchgeführt werden kann. Als mögliche Lösungsmittel wurden Toluol und Diisopropylether gefunden. Die Evaluierung unterschiedlicher Immobilisationsmatrizen zeigte, dass das Enzym sowohl auf Celite, porösen Glaskugeln und Nanodiamanten erfolgreich immobilisiert werden konnte. In dem organischen Lösungsmittel-Reaktionssystem konnte mit Celite als Immobilisationsmatrix ein Umsatz von über 95 % und ein Enantiomerenüberschuss von über 99 % erreicht werden. Die Raum-Zeit-Ausbeute lag hier bei 1 $mmol\,L^{-1}\,s^{-1}$. Die Reaktion wurde auch in einem kontinuierlich betriebenen Membranreaktor durchgeführt. Aufgrund des Gefahrenpotenzials von HCN konnte der Reaktor allerdings nur für sechs Stunden betrieben werden, ohne dass ein stationärer Betriebspunkt erreicht werden konnte. Leider konnten beide Reaktionen nicht direkt miteinander gekoppelt werden, da das nicht vollständig umgesetzte Aldehyd der ersten Reaktion (Acrolein) das Enzym sehr schnell inaktiviert hat.
Neben der Analyse der zwei Reaktionsschritte wurde ein modell-basiertes Kalibrationsverfahren entwickelt, welches die Kalibration eines Multiwellenlängen-Photospektrometers mit der Bestimmung der Parameter eines kinetischen Modells direkt verknüpft. Der Vergleich unterschiedlicher experimenteller Designs (Anfangsreaktionsgeschwindigkeitsmessungen und Verlaufskurvenanalyse) zeigte, dass mit dem entwickelten Verfahren die Anzahl der Experimente deutlich reduziert werden konnte, ohne die Signifikanz der Modellparameter zu verschlechtern.

1 Introduction

Biotechnology has been defined by the Organisation for Economic Co-operation and Development [1] as "The application of science and technology to living organisms, as well as parts, products and models thereof, to alter living or non-living materials for the production of knowledge, goods and services.". The definition describes the broadness of the field of biotechnology which has a deep impact on the daily life of people in the world. While the definition focuses on the "application" to "biological systems" the "modern biotechnology" takes an additional step and focuses also on the techniques and tools which "biological systems" apply to achieve their individual goal. "Imitation of nature" is a process which is used knowingly or unknowingly in all applications of science and technology, and biotechnology is predestined for it. From the viewpoint of a bioprocess engineer the following aspects of nature are of main interest:

- catalysis: make reactions possible and save energy
- reaction sequences: build complex chemical compounds out of simple building blocks
- chirality: the optimal architectural design
- membranes: separation and conjunction
- iterative optimisation: trial and error under the pressure of survival

The mentioned aspects play an important role in this thesis, which main objective is to show the feasibility of a continuous production of a cyanohydrin, synthesised in a two step reaction sequence. Starting from simple building blocks a functionalised cyclohexenyl structure is synthesised, catalysed by a polymer supported organometallic catalyst. The cyclohexenyl structure is processed into the cyanohydrin by the enzymatically and enantioselectively catalysed addition of hydrogen cyanide.

1.1 Catalysis: make reactions possible and save energy

According to the Nobel prize winner Wilhelm Ostwald a catalyst enhances the reaction rate of a chemical reaction without consumption of the catalyst [2]. A catalyst changes the path of the reaction, which normally reduces the activation energy (E_a) for the relevant reaction, figure 1.1, for the forward as well as reverse reaction. The

position of the thermodynamic equilibrium ($\Delta_r H$) is not affected but the rate to equilibrate. The catalyst and reactants react to a transition state, the so called catalyst-substrate complexes. It is defined as the state corresponding to the highest energy ($E_a(k_1)$ and $E_a(k_2)$) along this reaction coordinate r, but the energy level is lower compared to the uncatalysed path [3]. The product is formed and then released from the catalyst. It can be distinguished between two types of catalyses. The heterogeneous catalysis is characterised by two non-mixible phases while in the homogeneous catalysis the reactants and the catalyst are located in one phase [4]. Most common industrial metal/(metal)-organic catalysed reaction systems are heterogeneous, but also homogeneously catalysed are found. Biologically catalysed reactions can be homogeneous as well as heterogeneous. Here the reactions are catalysed by proteins, the so called enzymes.

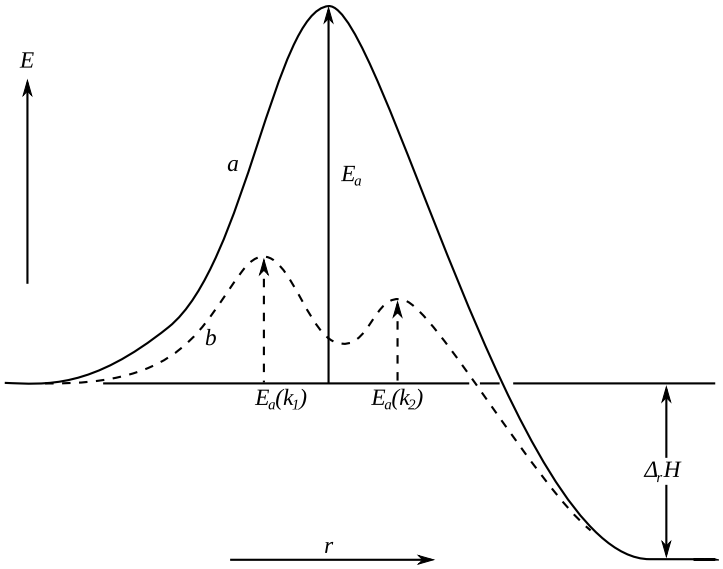

Figure 1.1: Generic energy diagram of a non-catalysed (a) and a catalysed (b) chemical reaction along the reaction path r [3]

1.2 Chirality: the optimal architectural design

Isomers are compounds which share the same molecular formula but differ in the structure. Depending on the type of the structural difference a distinction between *constitutional* and *stereoisomerism* can be made. The constitutional isomers, like propanol or dimethyl ether, differ in their *constitution*. The differences between constitutional isomeres are in the type and sequence of bounds, how the atoms are linked to each other. Stereoisomers have the same constitution but differ in their *configuration*. The three-dimensional arrangement of the atoms and atom groups is unequal.

Depending on the type of structural differences they can be *enantiomers* or *diastereomers (diastereoisomers)*. The structure of an enantiomer (b and c figure 1.2) are picture and mirror picture while for diastereomers this is not true (a and b, a and c, respectively) [5]. To describe the relative orientation of functional groups within a diastere-

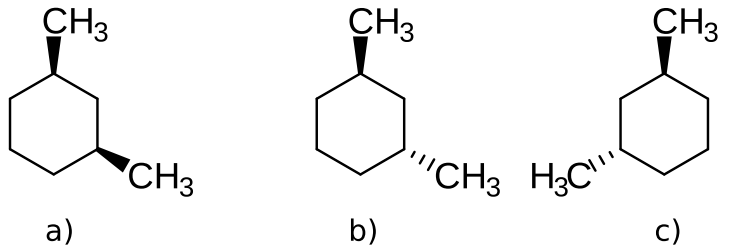

Figure 1.2: Stereoisomers of 1,3-Dimethylcyclohexan [5]

omeric molecule the prefixes *cis* and *trans* are used. The prefix *cis* terms any configuration where two functional groups are attached to different atoms point to the same site of the plane of ring structure, while *trans* describes a configuration where the two functional groups point into opposite directions. The isomers of a molecule with one chiral centre are called enantiomers and a mixture of 1:1 of such isomers is called a racemate. The Cahn-Ingold-Prelog priority rules [6] can be used to name the stereoisomers of a molecule[1]. According to the distribution of the substituents at a chiral centre the configuration is named either (*R*)- or (*S*)-configuration.

The term chiral is used to describe an object that is non-superimposable on its mirror image. This is a basic architectural design of many biostructures and it can be discovered in all scales. For example, the human hands are chiral, because they can not be superimposed on each other, the ears are another example. In small scale many biologically active compounds like the naturally occurring amino acids, sugars or the proteins are chiral. The role of chirality can be seen as an additional information, beyond the constitution of the molecule's atoms. Enantiomers have similar physical and chemical properties in a non-chiral environment. The additional information of chirality comes in to play when they are interacting with a chiral environment. Now physical and chemical properties differ in the interaction with the non-chiral environment. Therefore in biological systems molecular chirality plays an essential role in the interaction of chiral biological compounds like DNA, enzymes, antibodies and hormones. Normally the type and activity of interaction differ for the different enantiomers. One of the most popular examples is limonene. The monoterpene (*R*)-

[1] *R* or *S* according to a system by which its substituents are each assigned a priority, according to the Cahn-Ingold-Prelog priority rules, based on atomic number. If the centre is oriented so that the lowest-priority of the four is pointed away from a viewer, the viewer will then see two possibilities: If the priority of the remaining three substitutes decreases in clockwise direction, it is labeled *R* (for *rectus*), if it decreases in counterclockwise direction, it is *S* (for *sinister*)

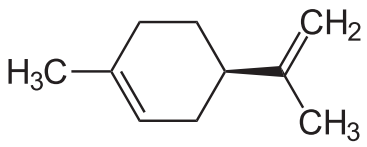

Figure 1.3: Chemical structure of (*R*)-limonene [7]

limonene (Figure 1.3) smells like orange. The corresponding (*S*)-limonene interacts in a different way with the receptors of the scent and smells unpleasing like mint to turpentine. In high concentrations, among the intensive turpentine smell, also a slight citrus aroma can be sensed [7].

The composition of a mixture of enantiomers is called *enantiomeric excess (ee)* and is expressed as follows:

$$ee = \frac{e_1 - e_2}{e_1 + e_2} \tag{1.1}$$

The term e_1 describes the fraction of the enantiomer in excess and e_2 the corresponding fraction of the other enantiomer. The *ee*-value ranges from 0 (racemate) to 1 (100%), respectively. A value of zero corresponds to a racemic mixture while a value of 1 (100%) is an enantiopure solution. An enantiomeric excess equal to 90% corresponds to a fraction of the racemate in the mixture of 10%. The rest of 90% is the excess of one isomer. The fraction of this enantiomer accounts for 95%, and the other enantiomer for 5% [5].

The *diastereomeric excess* (*de*) is defined analogous to the enantiomeric excess (equation 1.2) and describes the fraction of the pure diastereomers in a mixture [7].

$$de = \frac{D_1 - D_2}{D_1 + D_2} \tag{1.2}$$

As synonym for a chiral molecule *optical active substance* is often used, because in solutions of chiral molecules the plane of linearly polarised light is rotated. The angle of optical rotation of plane-polarised light passing through a sample of materia can be measured with a *polarimeter*.

1.2.1 Stereoselective synthesis

A reaction in which one of two or more possible stereoisomers is favoured or exclusively synthesised is called *stereo selective*. A stereoselective reaction in which different quantities of two enantiomers are produced is named *enantioselective*, which is true for all *asymmetric synthesis*. If two or more chiral centres exist then the reaction can be *diastereoselective*. The asymmetric synthesis is a subgroup of the stereoselective synthesis. It uses chiral, non racemic compounds often only as auxiliary material,

which is not an element of the end product. Their function is the transfer of the chiral information from the auxiliary material to a non chiral starting substances. Auxiliary material belongs to chiral modified reagents like borane with chiral substituents, chiral solvents, chiral catalysts like enzymes or chiral reagent which are temporarily covalently bound to the starting material or intermediate, to perform a diastereoselective synthesis [7].

The production of enantiopure compounds is of increasing importance in the chemical and biochemical industry. Particularly the pharma industry focuses more and more on the production of enantiopure compounds, but also the agricultural and food chemistry, for example the production of flavouring agents (e.g. limomeme), are an area of application for enantiopure compounds. For a pharmaceutical the control of the chirality of the active ingredient is an important factor of safety, because often only one enantiomer has the desired biological activity, while the other has no or even a strong toxic effect [8]. As example can be mentioned the Parkinson drug L-Dopa (3,4-dihydroxy-L-phenylalanine). Only the (*S*)-enantiomer has the desired activity, while the (*R*)-enantiomer particulate heavy adverse effect [9]. The US Food and Drug Administration (FDA) as well as the European Committee for Proprietary Medicinal Products claim for the conferral of admission of a stereoisomeric drug that the physiological effect of each enantiomer is characterised.

Also in agricultural industry the control of the chirality of the active ingredient can be on importance. For example the acitve ingriedent Indoxacarb (Methyl- 7-Chloro-2,5-dihydro-2-[[(methoxycarbonyl)[4-(trifluoromethoxy)phenyl] amino]carbonyl]indeno[1,2-e][1,3,4]oxadiazine-4a(3H)-carboxylate) exist as (*S*)- and (*R*)-enantiomer. The (*R*)-enantiomer showed no biocidal effect, but can have an effect on mammals [10].

Consequently it is desirable to produce a drug, flavouring agent and acrop protection product in an enantiopure formulation. In general the following methods are applied:

- enzymatic or chemical catalysed asymmetric synthesis
- synthesis via chiral 'building blocks' out of a 'chiral pool'
- production of racemates with subsequent separation of a racemate into its components, the pure enantiomers (chiral resolution) [11]

The asymmetric synthesis is the method of choice, because there is no cost intensive separation of a racemate into its enantiomers required. The economic advantage of the asymmetric synthesis relies on the conversion of a low amount of asymmetric information – conserved in the catalysed – into a large quantity of chiral compounds [8]. A low amount of an optical active catalyst has the ability to produce a large quantity of natural or synthetic compounds. This so called amplification rate of chiral multiplication can theoretically reach any value. In this aspect the asymmetric synthesis differs from the intra- and intermolecular chiral group transfer reaction, where

the increase of chiral centres is limited. Hence there is the ambition to develop new asymmetric reactions and to optimise the established reactions in enantioselectivity and productivity.

For example, metal-mediated asymmetric catalysis has been intensively studies over the last four decades since the first report of homogeneous Cu-catalysed asymmetric cyclopropanation [8]. Although, at first, entantioselectivity was only modest, notable advances have been achieved during the last three decades [8]. And in the last century several asymmetric catalysed reactions have been established in industrial scale (table 1.1) [12]. A milestone for the research on the area of asymmetric synthesis was the Nobel prize award for the research work of Noyori, Sharpless and Knowles in the year 2001 [13].

year	inventor	catalyst	reaction
1966	Nozaki	Schiff-Base copper complex	production of Cyclopropancarboxylate
1968	Knowles	Wilkinson's catalyst	hydrogenation of Olefines
1980	Sharpless	*tert*-Butyl hydro peroxide	epoxidation of allyl alcohols
1991	Jacobsen	manganese (III)-Salen complex	epoxidation of olefines

Table 1.1: Development of transition metal catalysed asymmetric synthesis [14, 15, 16, 17]

Today an enantiomeric excess of more the 98% can be obtained using asymmetric synthesis and the application areas are by now even the dehydroxilation of carbon-carbon double bounds, the organo metallic catalysed addition of aldehydes, alkylation, the Diels-Alder-Reaction, thw Mannich-Reaction and the Michael-Reaction amongst others [18]. With more then 10.000 tons per anno still one of the largest industrial application of a chemical asymmetric synthesis is the production of an intermidiate in the synthesis of the herbicide Metolachlor from Syngenta [19, 20, 21].

Despite the great successes in the research field of asymmetric synthesis the majority of the production processes of stereoisomeric drugs still deals with chiral resolution, because the often extremely short developing times do not favour the development of an asymmetric synthesis. Furthermores, the proprietary rights of an innovative process are to some extent a barrier for a fast industrial realisation [22].

1.3 Membranes: separation and conjunction

Membranes are the main structural element in an organism. A cell is composed of nucleic acids, proteins and other biochemicals surrounded by a *membrane* built from lipids [23]. While the cell membrane separates the outer from the inner cell, the inner cellular membranes compard the cell in functional sections. All cell membranes

have in common that they are selective in the way which type of molecule or information (signal transduction) can pass the membrane or not. Membranes in living cells separate reactions and at the same time permit the exchange of substrates and products through the membranes [24]. This idea of separation and conjunction has been transferred to reaction engineering and process development in the application of the *membrane reactor* .

1.3.1 The application of the membrane reactor

In the asymmetric catalysis reaction engineering and process development have a pivotal role. This is true for chemical and biochemical catalysts as well. An important parameter for the classification of a catalyst in reaction engineering is the *turnover number (ton)*. It describes the ratio of the number of moles of substrate that a mole of catalyst can convert before becoming inactive (equation 1.3).

$$\text{turnover number} = \frac{\text{amount substrate [mol]}}{\text{amount catalyst [mol]}} \tag{1.3}$$

The activity of a catalyst is described by the *turnover frequency (tof)* (equation 1.4) [25]. Depending on the scale of the industrial application the activity should be from 1.000 h^{-1} up to 10.000 h^{-1} [26].

$$\text{turnover frequency} = \frac{\text{converted substrate [mol]}}{\text{time [h]} \cdot \text{ amount catalyst [mol]}} \tag{1.4}$$

Many promising developments have not reached industrial scale, because only a low turnover number could be realised, for example with a Lewis-acid as chiral catalyst a turnover number of only 10 to 50 could be achieved [27].

One possibility to optimise the efficiency of a catalyst is the decoupling of the residence time of the reactants and the catalyst. This can be achieved by the retention of a costintensive catalysator in the reactor or by recycling the catalyst in the process. In figure 1.4 methods for the decoupling are shown. Methods for the retention are the immobilisation of the catalyst in a packed bed or in a second phase, or the application of *membrane reactors*, where the catalyst is homogeneously solubilised in the bulk phase and retained by a membrane [12]. The main problems related to a packed bed are the nonuniform and partly unknown structures of the heterogeneous catalysts, mass transport limitation due to hindered diffusion, and a low catalytic activity. [28]. These problems can partly be solved by the application of membrane reactors. Membrane reactors are a standard tool in biotechnical processes [29]. They are used for catalyst retention, substrate dosage and product removal [30]. The *enzyme membrane reactor (EMR)* was developed by Evonik Industries AG, formerly Degussa AG, and their partners: Wandrey and Kula, in early 1980s [31]. In this concept, enzymes are

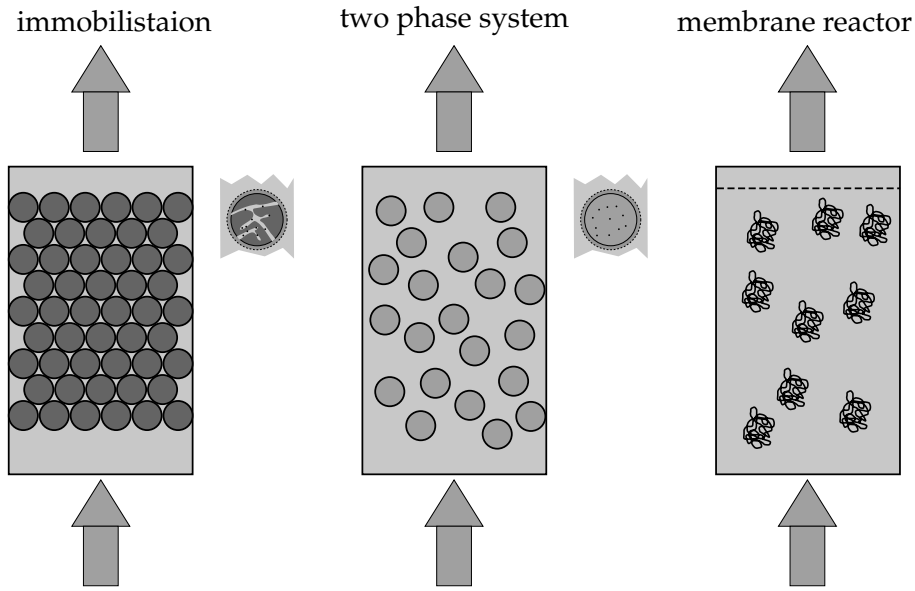

Figure 1.4: Methods for decoupling the residence time of reactant and catalyst according to [12]

retained by ultrafiltration membrane. This technology was introduced by Degussa AG for acylase process in 1981 and is in production since then [32, 33].

$$R = 1 - \frac{c_{Permeate}}{c_{Retentate}} \tag{1.5}$$

The membrane reactor is a subcategory of the filtration: the principle of the operation of the membrane filtration is the separation of the particles according to their size. The driving force is the pressure difference across the membrane. The different types of filtration are classified according the mean particle size they retain, cf. figure 1.5, whereas in most cases ultra- or nanofiltration is used for catalyst separation and recycling [34]. An important parameter of a membrane is the molecular weight cut-off (MWCO), which can be defined as the molecular weight at which 90% of the solute are retained by the membrane. This is amongst others depending on the mean pore size of the membrane and in the case of organic membranes also on the solvents and the temperature [35]. An important factor for the application of homogeneous catalysis in a membrane reactor is the retention R, equation 1.5. The retention factor has to be close to 1 (100 %), to avoid a wash out of the catalyst. The leaching (retention factor < 100 %) gives rise to two problems: the loss of expensive catalyst and the contamination of the product with the catalyst [34]. For definitions of *retentate* and *permeate* see figure 1.7. It can be differentiated between a *dead end* and a *cross-flow filtration*. In the case of a dead end filtration the flux is directed in a rectangular way

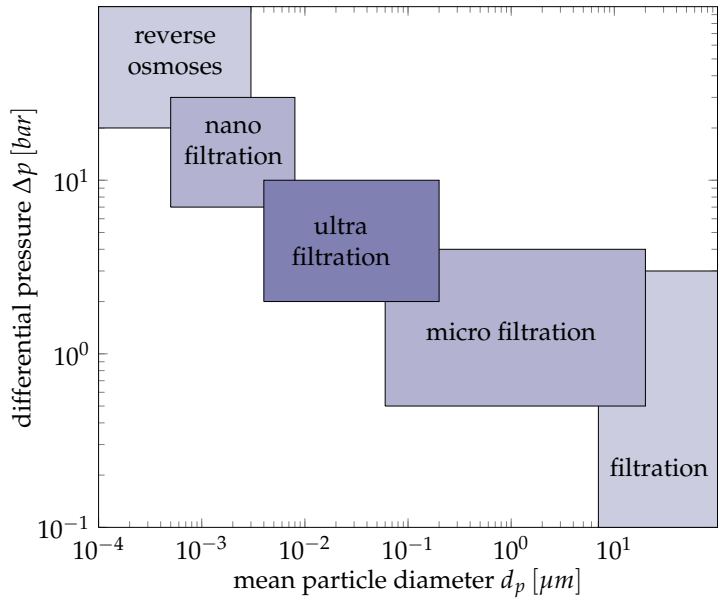

Figure 1.5: Classification of membrane processes [29]

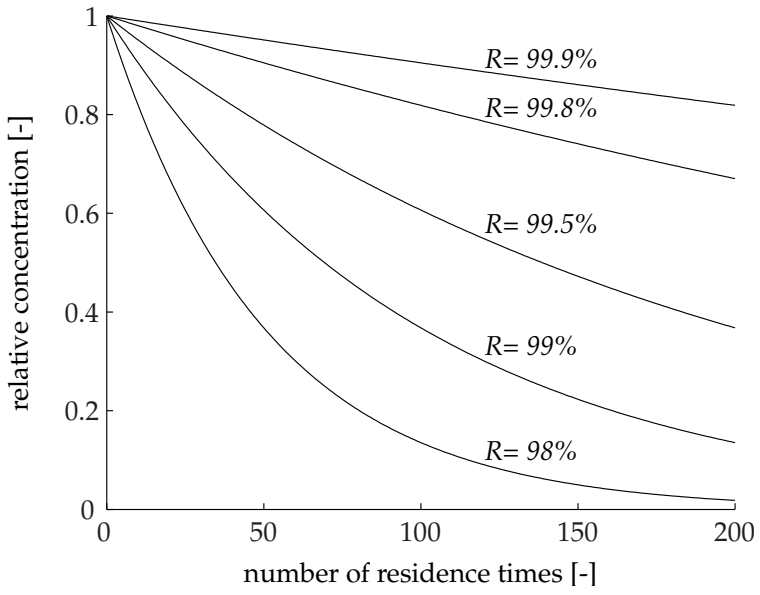

Figure 1.6: Relative catalyst concentration as function of retention and number of residence time

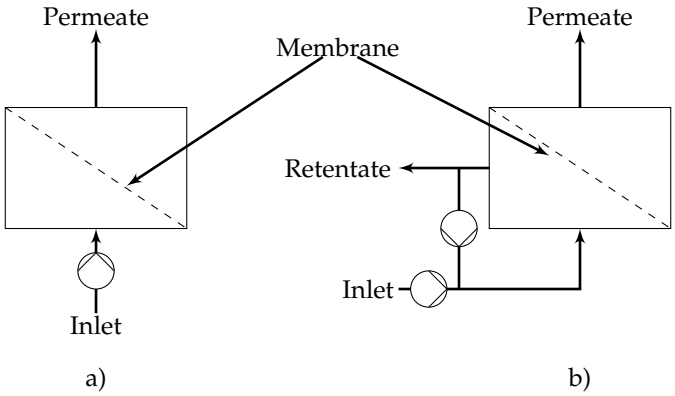

Figure 1.7: Schematic drawing of a dead end (a) and crossflow filtration (b)

to the surface of the membrane. In contrast, the direction of the flux is parallel to the surface of the membrane in the crossflow filtration. The dead end filtration operating method provides the advantage of a simple set up. Just one pump feeding the inflow is necessary. The main drawback for the application of a dead end filtration in a membrane reactor is the concentration polarisation at the surface of the membrane and the accumulation of retained material on the membrane. As shown in figure 1.7, for the realisation of a cross flow filtration commonly a second pump is integrated for the circulation flow to assure the essential tangential flow to minimise the fouling of the membrane. Fouling is the formation of a solid layer which leads to a change of the characteristic of the membrane: reduced cut off, decreased transmembrane flow at a constant pressure drop over the membrane [35, 34, 36]. The application of a dead end filtration in a membrane reactor allows a separation and reaction in one operation unit, while for cross flow filtration in most cases a separate separation unit has to be installed beside the reactor [29]. Besides the maximising of the total turnover number membrane techniques as integrated process unit have even more advantages. The downstream processing is simplified, because the retention of the catalyst can be seen as first purification step. The product stream is free from the catalyst and a further, cost intensive separation of the product and the catalyst is not necessary [12].

Membrane techniques can only be realised if the molecules to retain have a sufficient diameter. For enzymes this is given by their three dimensional macro molecular structure. The diameter of the iron-storage protein ferritin was measured with 7.5 nm [37]. Common chemical catalysts do not satisfy this criterion without a modification. To apply chemical catalysts in a membrane process, the molecular weight of the catalyst must be increased [12]. This can be achieved by coupling the chemical catalysed to different types of carrier materials, so that the separation of the reactants and the product from the catalyst can be done according to their size. Different types of supports can be used, such as dendrimers, hyperbranched polymers, nano-

structured materials or stabilised nano-particles [34]. When using a soluble support, the chemical catalyst will be still homogeneously soluble in the reaction medium. Due to the similarity of such a system with a biological catalyst the names *Chemzyme* or *Synzyme* have been coined [30]. Compared to an enzyme the chemzyme is not so specific with respect to their substrate, because the catalytic centre is often less complex. Therefore such chemzyme reaction systems are mainly of interest for reactions where no or no applicable enzyme is known [12] and where the compatibility to organic solvents is required. According to the *enzyme-membrane-reactor (EMR)* a *chemzyme-membrane-reactor (CMR)* is applied to retain a polymeric bound, homogeneously soluble, chemical catalyst (figure 1.8) [12]. The enzyme membrane reactor is nowadays

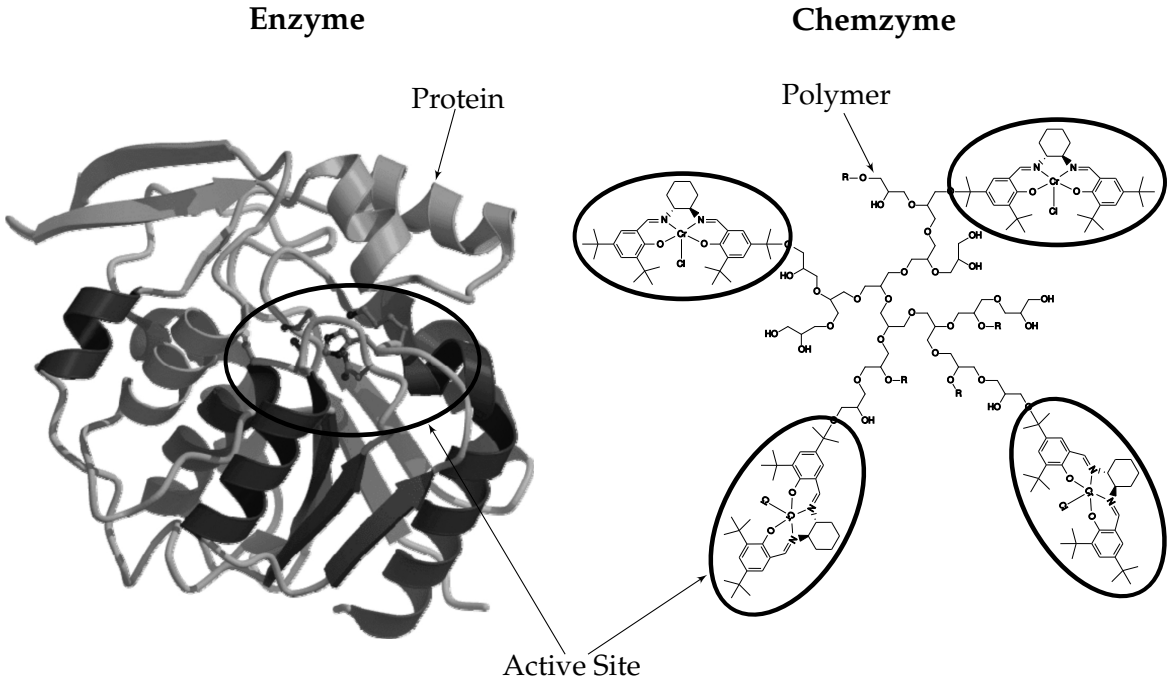

Figure 1.8: Comparison of an enzyme and chemzyme, (enzyme image: [38])

an established technology [29]. New knowledge in polymer chemistry, ceramic materials and new analytic methods facilitates the production of membranes with well defined characteristics like mean pore diameter, hydrophobicity/hydrophilicity, stability against extreme pH and organic solvents, pressure resistance, ionspecifity and sterilisability [30], so that new areas of application open up for the membrane technology. One of the first examples for a reaction catalysed by a chemical catalyst bound to a polymer was the reduction of ketones with a polymeric bound oxazaboroline

catalyst in 1998 [27]. In a first trial the oxazaboroline catalyst had been bound to the polystyrene gel. Due to the macroscopic structure of the gel a mass transport limitation occurred, giving rise to a loss of enantioselectivity. By binding the catalyst to a homogeneously soluble polymer the mass transport limitations could be overcome. With this approach 560 *mol* product per *mol* catalyst could be synthesised in a membrane reactor [27]. This would correspond to a catalyst content of 0.18 *mol*% in a batch reaction, which would be not sufficient for the desired enantioselectivity. The optical active alcoholes had been synthesised in the continuous process with an enantiomeric excess of more then 99% and a space time yield of 1.4 $kg^{-1}\, L^{-1}_{Reactor\ volume}\, d^{-1}$. In recent years an enormous improvement regarding the catalyst retention of different chemzymes could be achieved in the field of enantioselective carbon-carbon bond formation as well as redox reactions, which is essential for the maximal achievable total turnover number [12].

The mode of operation of a membrane reactor as a continuously-operated, stirred-tank reactor (CSTR) enables an operation in the steady state a high conversion and low substrate concentrations, respectively. The reaction proceeds at the reaction rate associated with the final (output) concentration, which is characterised by low concentrations of the starting material and high concentration of the product. Due to the low substrate concentrations the formation of byproducts formed with the substrate is represseed. The repression of the formation of byproducts in a membrane reactor using chemzymes could be shown in the example of the reaction of oxazaborolidines [27]. This is of advantage especially, when the asymmetric catalysed reaction competes with a racemic side reaction. In comparison to a stoichiometric reaction of reaction order one, which results in the racemate, at low starting material concentrations the asymmetric synthesis is more selective [39, 27].

In a continuous operation mode a system with membrane separation works stable in general, because the conditions of the reaction can be controlled easily, although a gradual deactivation of the catalyst can be observed [27], which leads to a reduction of the turn over frequence proceeding with time. Several possible reasons for this behaviour have to be considered:

- Deactivation of the catalyst due to thermal exposure
- Deactivation of the catalyst due to chemical interactions with the starting material, products, solvent and impurities
- Loss of the catalyst due to leaching of the catalyst or parts of it like the coordinated metal ions

Intermediates of the reaction or transition states can form a complex with the ligands or the starting materials, which can cause a chemical deactivation of the catalyst. Such a complex can be quite stable, but inefficient for the catalysis [35]. Especially in the case of enzymes the three dimensional structure is essential for activity, all actions which alter the tertiary and quaternary structure can lead to deactivation. The

actions can be conformational changes due to a changed polarity of the surrounding environment, the break of inner molecular hydrogen bounds, reaction of functional groups on the surface with substances of the surrounding environment (for example oxidation and polymerisation) or the removal of water bound to the enzyme in a water free environment. But the advantage of the application of a homogeneous catalyst is that fresh catalyst can be supplemented easily, when the loss of activity, because of leaching or deactivation, exceeds a target value. This is difficult in a fixed bed reactor [28].

Combinig a proper catalyst and its support – like polymers – with membrane techniques important improvements could be achieved in the area of homogeneous catalysis, which in a continuous process combines the advantage of the homogeneous and heterogeneous catalysis [34]. In future applications the main focus will be on new reaction systems, the application of new polymers and solvent resistant membranes [12]. This will be completed with the development of reaction sequences, where chemically and biologically catalysed reactions will be coupled in serial [40].

1.4 Reaction sequences: build complex chemical compounds out of simple building blocks

Reaction sequences (*metabolic pathways*) are the main characteristics of the chemistry in a cell and a huge scientific community is analysing the metabolic networks to understand the function of a cell. As an example for a well known passway the glycolysis can be mentioned, utilising glucose to gain pyruvate and energy in a ten step cascade. In these pathways compartments within the cell and therefore membranes often play an important role, because not all reactions take place in the cytoplasm, but are distributed to different parts of the cell like the nucleus or mitochondrion. This compartments are separated by selective membranes and the product of one reaction is transported via the membrane to another compartment where it is used as the starting material for a second reaction. For example Acetyl-CoA synthesised in the mitochondrion is transported to the cytosol, were it is used for fatty acid synthesis [23]. This system is the model for the reaction sequence investigated in this work – the idea of a combination of membrane reactor, where two reactions are separated by membranes. The connection of the reaction is the mass flow over the membrane of the first to the second reaction. Finally the catalyst is retained in the second reactor also by a membrane resulting in a liquid flow containing mainly the product of interest and a solvent.

1.5 Iterative optimisation: trail and error under the pressure of survival

The last topic on the list is the *iterative optimisation*. In this study *this principle of evolution* played an important role in the context of optimising a mathematic model describing the kinetics of the investigated systems using modern computing. The principle of evolution was for the fist time transferred to the world of modern computing by Alex S. Fraser:

> *Fraser was one of the first to conceive and execute computer simulations of genetic systems, and his efforts in the 1950s and 1960s had a profound impact on computational models of evolutionary systems. The simulation algorithms he used were important not only in the simulation of genetical problems, but provided a menu of techniques that enriched the entire simulation effort in any problem that involved probability sampling among a population of alternatives, the heart of Monte Carlo methods [41].*

Nowadays the basic idea has been implemented in modern optimisation algorithms and the power of the evolution algorithms make them an important tool as mathematical optimiser for different tasks in engineering science.

1.6 Cyanohydrin, high potential chiral building blocks

Cyanohydrins are valuable starting materials for various optically active compounds such as pharmaceuticals, fine chemicals and agrochemicals [42]. Cyanohydrins, bearing two functional groups, possess a massive synthetic potential. Thus, these α-substituted carboxylic acid derivatives give access to a great variety of important classes of compounds [43]. Starting from enantiomerically enriched cyanohydrins renders them even more interesting building blocks offering a wide variety of synthetic possibilities for the production of optically pure intermediates and products with potential biological activity [44].

The follow-up chemistry of the cyanohydrins is closely discussed elsewhere, c.f. [45, 43, 46]. Possible follow up transformations of cyanohydrins are presented in figure 1.9; the transformations concerning the hydroxy group and the reactions affecting the nitrile functionality were investigated. An important observation for the investigated reaction was, that all these functional group transformations proceed (with almost no exception) without any substantial decrease of the enantiomeric purity of the starting material [46]. Table 1.2 gives an overview of the products of the transformations of a cyanohydrins.

Product	Citation
α-hydroxy carboxylic acids	[48, 49]
primary β-hydroxyamines	[50, 51]
secondary β-hydroxyamines	[52]
aziridines	[53]
α-aminonitriles	[54, 55]
α-azidonitriles	[56]
α-fluoronitriles	[57]
α-hydroxyketones (acyloins)	[58]
α-amino-β-hydroxy carboxylic acids	[51]
2-cyanotetrahydrofuran and -pyran	[59]
2,3-disubstituted piperidines	[60]
azacycloalkan-3-ols	[50]
carboxylic acid cyanohydrin esters	[61, 62]
vinyl ethers	[63, 64]
silyl ethers	[65, 66]
α-amino-β-hydroxy carboxylic acids	[51]
D- and L-sphingosines	[67]
prostacyclin mimic	[68]
tetronic acids	[69, 70, 71, 72]
adrenaline and ephedrine analogues	[73, 74, 75]
L-2-deoxypentoses	[76]
a tumor agent fragment	[77]
2-amino-1,3-diols	[78]
α-hydroxy-β-amino carboxylic acids	[79, 80]
chiral heterocycles	[50, 81, 60, 82]
chiral nitrones for cycloaddition reactions	[83]

Table 1.2: Products of the transformations of a cyanohydrin

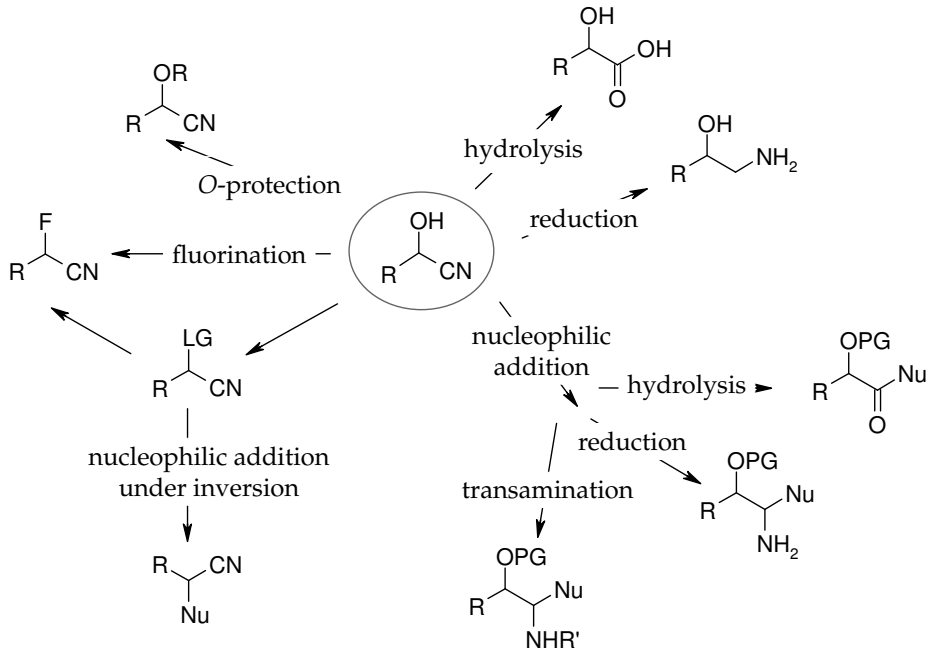

Figure 1.9: Possible follow up transformations of cyanohydrins [43, 47]

1.7 The objectives

This investigation was part of the CERC3 transnational projekt *Sustainability By Advanced Chemoenzymatic Technologies*. A competitive production route for the synthesis of the cyanohydrins starting with simple, commercially available building blocks as valuable intermediates is of major interest. The reaction sequence, Diels-Alder reaction followed by cyanohydrin formation, would represent a powerful tool to synthesise complex molecules from simple building blocks, due to the applicability of α,β-unsaturated aldehydes as dienophiles for the Diels-Alder reaction [43]. In figure 1.10 the reaction sequence is presented. In the first step simple building blocks – a diene and an aldehyde – react to form a functionalised cyclohexenyl structure with chiral side chains in the Diels-Alder reaction. The formed aldehyde finds then application as chiral auxiliary in an asymmetric reaction to synthesis the cyanohydrin – marked in figure 1.10 – with an additional chiral centre.

The main objective of this study is to show the feasibility of a continuous production of the cyanohydrin according to the reaction sequence presented in figure 1.10 whereas the first reaction is catalysed by a chemzyme and the second by an enzyme. The follow-up reactions are not considered.

The task is to lay the basis for the establishment of the continouos process to pro-

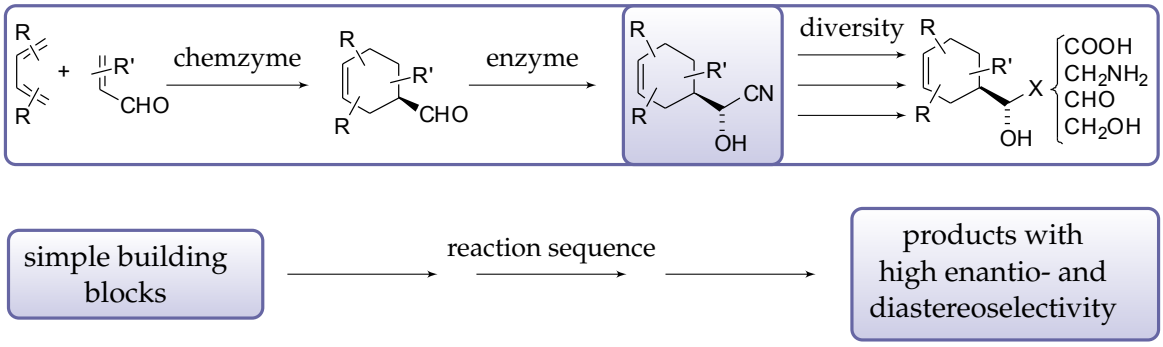

Figure 1.10: The two step synthesis of chiral cyanohydrins starting with simple building blocks; the cyanohydrin is marked.

duce the enantiopure cyanohydrins. The aim is to couple both reactions without an intermediate purification of the liquid stream. For a substantiated process development tools are evaluated to investigate the kinetics of both reactions applied, which allows a reasonable design of the process of the continuous synthesis of optical active cyanohydrin.

A goal of the investigation is the application of membrane reactors for both reactions. For this purpose the immobilisation and retention of the catalysts by a membrane has to be evaluated as well as the selection of one suitable solvent.

The work is structured as follows: in chapter 2 the first step of the reaction sequence, the Diels-Alder reaction, is described. The reaction is catalysed by salen transition metal catalyst with macromolecular properties, a so called *chemzyme*. The application in a batch as well as in a continuous operated membrane reactor is studied. A focus is on the investigation of the kinetics of the reaction. For a straightforward experimental evaluation of the kinetic a liquid handling robot procedure has to be developed, to obtain sufficient experimental results for the formulation and validation of a suitable kinetic model, which facilitates the simulation of the reaction for a reasonable design of the process.

In the second part (chapter 3) the hydroxynitrile lyase (HNL) catalysed, enantioselective hydrogen cyanide (HCN) addition to an aldehyde is investigated. First the HCN production has to be established along with the necessary precautions for handling the toxic and explosive substance. The cyanohydrin synthesis in an aqueous phase batch reaction is investigated. Here the focus is on the development of a strategy, evaluating the information recorded by a multi-wavelength photospectrometer for the investigation of the kinetic of the reaction. The evaluation is usually based on chemometric modelling using for their calibration procedure off-line measurements of the desired process variables [84]. Due to the data driven approach lots of off-line measurements are required. A methodology is evaluated – a model driven approach –, which enables to perform a calibration procedure of uni- as well as mul-

tivariate chemometric models simultaneously with the parameter determination of a kinetic model, without a prior calibration step.

The aldehydes of interest are poorly soluble in the natural aqueous medium, which leads to low reaction rates and large reaction volumes. In addition, undesired site reactions and degradation of organic compounds often occur in water [43], the thermodynamic equilibrium is unfavourable and product recovery can be difficult. Working in an organic solvent avoids these problems. Enzymes often show a beneficial behaviour in such systems [43, 85, 86, 87, 46]. On industrial scale, the enzymatic cyanohydrin synthesis is preferably carried out with isolated nonimmobilized HNLs in a biphasic aqueous-organic emulsion system with methanol-free *tert*-butyl methyl ether as the organic solvent [46]. *tert*-Butyl methyl ether is not a suitable solvent for the Diels-Alder reaction catalysed by salen transition metal catalyst[2], therefore a different organic solvent has to be found which is usable for both reaction steps. The biphasic aqueous-organic emulsion system already published [88, 43, 44, 89] is developed for (semi)-batch operations. For the transfer of the process into a continuous operating plant the mixing and the separation of the organic and water phase has to be especially evaluated, because vigorous stirring is essential to effect a highly productive reaction by providing an optimal contact between the phases in the aqueous-organic emulsion system [89]. The enzymes have to withstand the shear stress caused by this measures. At the same time huge interphases favour the deactivation of the enzyme [29]. Also special equipment is necessary to separate the organic and water phase in a continuous fashion. A system with only one liquid phase and a solid phase would be favourable. The focus of this study is therefore the application of a liquid/solid phase reaction system, which can be applied in a continuous operated membrane reactor.

The third part (chapter 4) addresses the coupling of both reaction steps to enable the continuous synthesis of the optical active cyanohydrins out of simple building blocks.

[2] I would like to thank Prof. Dr. Rainer Haag from the Institute of Chemistry and Biochemistry - Organic Chemistry, Freie Universität Berlin, Dendritic Polymer Research Group, for this information

2 Synthesis of functionalised cyclohexenyl structures

In the following chapter the investigation of the Diels-Alder reaction is presented. The application was studied in a batch as well as in a continuously operated membrane reactor. A focus was put on the investigation of the kinetics of the reaction. For a straightforward experimental evaluation of the kinetic a liquid handling robot procedure had to be developed to obtain sufficient experimental results for the formulation and validation of a suitable kinetic model, which facilitates the simulation of the reaction for a reasonable design of the process.

After short descriptions of the Diels-Alder reaction, the Salen transition metal catalyst with macromolecular properties and the investigated reaction system is discussed. The developed liquid handling robot procedure is described as well as fundamental kinetics of homogeneously and heterogeneously catalysed reactions. On the bases of the experimental results a simple kinetic is deduced. The *Materials and Methods* are described in appendix A and only the results (2.6) and the deduction of a kinetic model (2.6.3) are discussed here. Finally the application of the chemzyme in a membrane reactor is discussed in chapter 2.8.

2.1 The Diels-Alder reaction

The **Diels-Alder reaction** had been discovered by Otto Diels and Kurt Alder in 1928 [90] and their work was honoured with the Nobel Prize in Chemistry in the year 1950 [91]. It is a [4+2]-cycloaddition between a conjugated diene and a substituted alkene, commonly termed the dienophile, to form a substituted cyclohexene system [90]. Several bounds are formed or cleaved simultaneously via a cyclic tran-

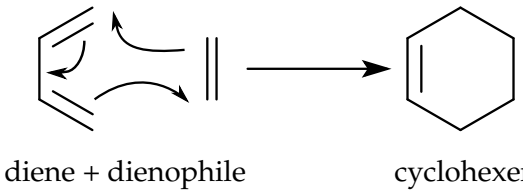

Figure 2.1: The Diels-Alder reaction [90].

sition state. The alkene (dienophile) has to be activated by neighbouring polar substituents. The commonly used dienophiles are unsaturated carbonyl compounds like maleic anhydride or acrolein [92]. The cycloaddition is basically reversible and is then called **retro Diels-Alder Reaction** [93]. The Diels-Alder reaction forms a heterocylic

carbon ring with four possible connected stereocentres in a single reaction step. The control of these stereocentres is the goal of the application of the asymmetric synthesis of the Diels-Alder reaction [94]. It has been shown that in the presence of a chiral Lewis acid or a chiral salen catalyst the stereocentre can be controlled [95, 96].

2.2 Salen transition metal catalyst with macromolecular properties

In asymmetric synthesis organometallic catalysts are often applied, whose selectivity and reactivity are determined by the specific combination of a catalyst, the starting materials and the reaction conditions. The catalytic activity thereby commonly depends on the metallic central atom, whereas the selectivity is influenced more by the organic chiral ligand. The interaction of charges and steric effects characterise the efficiency of an organometallic catalyst. The chiral ligand is significant for the intermolecular transfer of the chirality (information transfer) from the catalyst to the substrates. One disadvantage encountered when anchoring catalytic metal sites to polymers is the difficulty of any accurate control of the number and location of these sites [97]. This could be shown for ligands with a central as well as axial and planar chirality [8]. A wide variety of organometallic catalysts with chiral ligands is known, but the large number of possible combinations of an organic ligand with a transition metal opens up room for further developments. For a successful optimisation new chiral ligands as well as a deeper understanding of the relevant mechanisms of the reaction is necessary. Unfortunately, it is difficult to know the precise transition state of an asymmetric reaction at present. Both screening and rational optimisation through mechanistic studies are required to achieve highly enantioselective metal-catalysed asymmetric methods [8].

In the sixties of the last century the coupling of a chiral ligand with a macromolecule has been reported for the first time [98]. To enlarge the molecular size of an organometallic catalyst the bondage to a dendrimer is particular suitable. Dendrimers are polymers, which consist of repetitive units and form a hyperbranched structure. One disadvantage encountered when anchoring catalytic metal sites to linear polymers is the difficulty of accurate control of the number and location of these sites [97]. But dendrimers represent nanoscopic catalysts with physical characteristics such as size, solubility and dispersity of the catalytic sites that – unlike those in related systems with conventional polymers – are defined very precisely, so that these molecules offer advantageous properties for physical separation and catalyst recycling [97]. Such a dendrimeric catalyst has been successfully employed as homogeneous catalyst for the first time in the Kharasch addition [97]. The catalytic activity is similar to a monomeric organometallic complex, because the active centres are sterically separated at the end of the extremity of the dendrimers.

As an alternative to the exodendral location of the active centre an endodendral attachment can also be realised, where the catalyst is bound within the den-

drimeric structure, c.f. figure 2.2. It is important, that by binding the catalyst to a

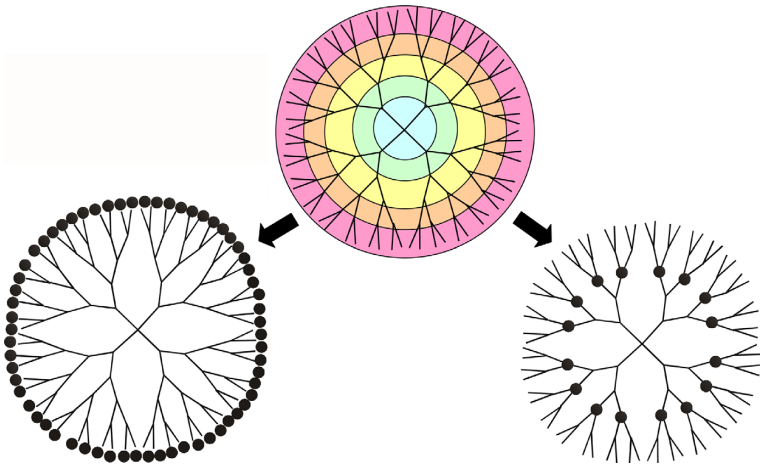

Figure 2.2: The fixation of catalytic metal centres (represented by the black spheres) in exodendral (left) and endodendral (right) positions of dendrimers [99].

macro-molecule, the desired properties like activity, stability and selectivity, are not changed. The linker and spacer units employed in the fixation of the catalysts may be crucial in this respect as well as the functional groups present in the dendrimer. Regarding the dendrimer core structure itself, the length and conformational rigidity of the branches and spacers are important factors when evaluating a dendritic catalyst. For immobilised asymmetric catalysts even subtle conformational changes may significantly influence their stereoselectivity. The interplay of all these factors will generally determine negative or beneficial dendrimer effects in catalyst performance [99]. Most commonly, carbosilane, polyphenylene, poly(benzyl ether), DAB, PANAM and PPI dendrimers have been applied for the immobilisation of transition-metal complexes. [34].

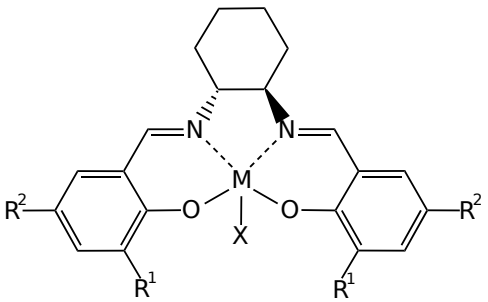

Figure 2.3: Schematic drawing of a salen ligand with transition metal (M) and counter ion (X) [17].

Jacobsen et al. applied an *optical active salen-Mn(III)-complex* in the year 1991 the first time in the epoxidation of alkens [17]. Since then a diversity of highly selective asymmetric reactions has been discovered, which all has been catalysed by such an *optical active salen-metal-complex* [17, 100, 101, 102], figure 2.3. Salen was first synthesised by A. Combes in 1889 [103]. Commonly it is synthesised by the uncatalysed condensation of salicylaldehyd with a 1,2-diamine. The word 'salen' (*N,N'*-bis(salicylaldehyde)ethylenediamaine)[1] is a short form for the family of the bisimine, whose structure is derived from the ethylene diamines [104]. The functional imine group enclosed in salen, which is also called 'Schiff-Base', is stabilised by the complexation with a metal ion [104] and already in 1933 Pfeiffer and coworkers described a salen-metal-complex [105]. For most transition metals the complexation with salen is known. Different metal complexes of salen bearing aluminium, chromium, cobalt, copper, manganese, palladium, ruthenium, silver, titanium, vanadium or zinc as the metal centre have been successfully applied in a multitude of asymmetric reactions [106]. The sterical configuration of the complex can be a described as distorted square in a plane or as a pyramid with a square base depending on the coordination with regard to the metallic centre. Salen ligands can be synthesised easily and their sterical configuration can be controlled well [107]. Due to it's multifarious configuration the chiral salen-metal-complex is a versatile catalyst and the reactions catalysed by such a salen ligand include epoxidation, asymmetric epoxide-ring opening, sulfoxidation, C-H oxidation, aziridination, sulfimidation, C-H amination, S-ylide formation, hydrocyanation, silylcyanation, aerobic oxidative coupling and cycloaddition processes such as the Diels-Alder reaction, hetero-Diels-Alder reaction and cyclopropanation [104].

2.3 The Diels-Alder reaction model system

As model system the Diels-Alder reaction of acrolein with 1-methoxy-1,3-butadiene to form a 2-methoxy-cyclohexen-carbaldehyde catalysed by a polyglycerol-supported asymmetrical salen ligand was chosen, c.f figure 2.4. The polyglycerol-supported asymmetrical chromium salen ligand was synthesised by Hajji et al. [102][2] and was successfully used as supported catalyst for hetero-Diels-Alder reactions between Danishefsky's diene and benzaldehyde and the asymmetric epoxidation of olefins [108] as well as the hydrolytic kinetic resolution of terminal epoxides [108]. This polymeric catalyst showed outstanding catalytic activities and selectivities (up to 78 % *ee*), that are comparable to the original catalysts reported by Jacobsen, thus proving the effectiveness of our design criteria [102]. The polymeric catalyst showed

[1] Furthermore, this name is abbreviated as salen ligand.

[2] I would like to thank Prof. Dr. Rainer Haag and Dipl.-Chem. Juliane Keilitz from the Institute of Chemistry and Biochemistry - Organic Chemistry, Freie Universität Berlin, Dendritic Polymer Research Group, for the supply of the catalyst.

a high retention in the membrane reactor ($\geq$ 99 %) [106].

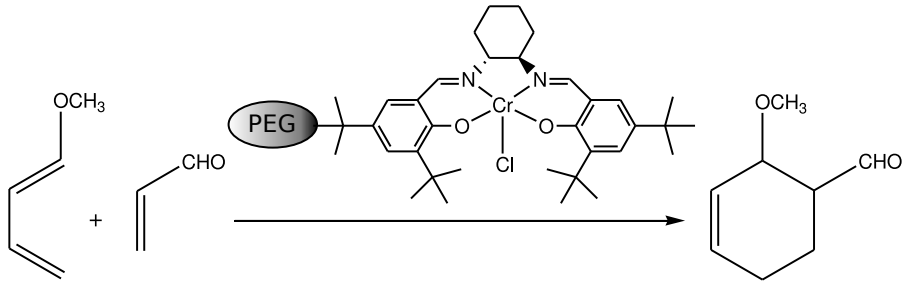

Figure 2.4: Investigated reaction system for the Diels-Alder reaction

Hajji et al. [109] reported the successful conversion of acrolein with 1-methoxy-1,3-butadiene to 2-methoxycyclohex-3-enecarbaldehyde using the polyglycerol-supported asymmetric chromium salen ligand. The four possible stereoisomers are presented in figure 2.5. If the reaction is carried out under thermal conditions a *trans/cis* ratio of 6/1 could be achieved. By applying the Jacobsen catalyst, either as free catalyst or immobilised on polyglycerol, the *trans/cis* ratio is increased to 9/1, but the product is racemic [43, 109]. The coupling of the Diels-Alder reaction with the enantioselective enzymatic catalysed addition of HCN was first performed by Avi in 2007 [43]. Using HNL from *Hevea brasiliensis* (*Hb*HNL) and from *Prunus amygdalus* (*Pa*HNL) as a catalyst, complementary selectivities with respect to the new stereocentre were obtained [43].

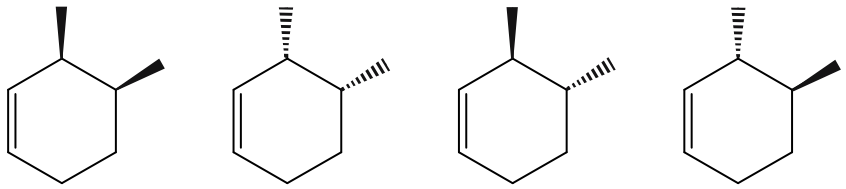

Figure 2.5: Enantiomers of the *cis* (a and b) and *trans* (c and d) configuration of the product.

2.4 The kinetic of homogeneously catalysed reactions

The mechanism of homogeneously catalytic reactions is complex even, when only a single reaction is involved, since the catalytic cycle consists of several stoichiometric reactions. Due to the various complexities involved, the kinetics of a homogeneous reaction are often represented by non-linear rate equations, some purely empirical

and some based on a mechanism [110]. In table 2.1 some examples of homogeneous

Reaction	Catalyst	Rate equation
Hydroformylation of propylene	$HCo(CO)_4$	$r = \frac{k\, c_{substrate}\, c_{catalyst}\, c_{H_2}}{c_{CO}}$
Hydroformylation of propylene	$Co_2(CO)_8$	$r = \frac{k\, c_{substrate}^{0,87}\, c_{catalyst}^{0,75}\, c_{H_2}^{0,55}\, c_{CO}}{(1 + K_2\, c_{CO})^2}$
Oxidation of cyclohexane	$Mn(OAc)_2$	$r = \frac{k\, c_{substrate}\, c_{catalyst}}{K_1 + K_2\, c_{catalyst}}$
Carbonylation of methanol	$NiCl_2$	$r = \frac{k\, c_{substrate}\, c_{CO}}{(1 + K_1\, c_{CO})(1 + K_2\, c_{substrate})(1 + K_3\, c_{H_2O})^2}$

Table 2.1: Examples of homogeneous catalysed reactions [111, 112, 113, 114, 110].

catalysed reactions are shown. It can be noted that the mathematical forms of the rate equations used range from simple power law types to hyperbolic forms to those based on mechanisms already established. In some cases, a close analogy to the rate equations used in heterogeneous catalysis is obvious, except that in homogeneous catalysis the mechanism considered involves molecular level description of the catalytic intermediate species [110]. In some cases, like hydroformylation, the rate equation used is empirical due to complexities such as the substrate inhibition with CO and also olefines, even though the catalytic cycle is reasonably well established. All in all it would be more appropriate to develop rate equations based on a molecular level and correlate the trends observed with the mechanism [110]. Because of the analogy with a heterogeneous catalytic reaction the two best established mechanistic kinetic models are presented in the next chapter.

2.4.1 The kinetics of a heterogeneous catalysed reaction

Catalytic reactions occur when the reacting species are associated with the catalyst. In heterogeneous catalysis this happens at a surface, in homogeneous catalysis in a complex formed with the catalyst molecule. In terms of kinetics, the catalyst must be included as a participating species that leaves the reaction unaltered. In the following, the general catalytic reaction presented in equation 2.1 is considered.

$$A + B \overset{catalyst}{\rightleftharpoons} P \tag{2.1}$$

The catalytic process consists of a sequence of elementary steps that form a cycle from which the catalyst emerges unaltered [115]. Two fundamental kinetic models can be formulated. The Langmuir-Hinshelwood kinetics assume that all species are adsorbed and accommodated (in thermal equilibrium) with the surface before they

take part in any reactions [115]. Hence, species react in the chemisorbed state[3] on the surface. This is the predominant mechanism in heterogeneous catalysis. Another possibility is the so called Eley-Rideal mechanism, in which one of the reactants reacts directly out of the gas phase, without being accommodated at the surface [115].

The Langmuir-Hinshelwood kinetics

Langmuir and Hinshelwood proposed a mechanism where both molecules adsorb and the adsorbed molecules undergo a bimolecular reaction. The elementary reaction steps of the catalysed reaction between A and B in steps elementary according to the Langmuir-Hinshelwood mechanism can be presented as follows (equations 2.2), S represents the surface:

$$\begin{aligned}
&(1) \quad A + S \underset{k_{-1}}{\overset{k_{+1}}{\rightleftharpoons}} AS \\
&(2) \quad B + S \underset{k_{-2}}{\overset{k_{+2}}{\rightleftharpoons}} BS \\
&(3) \quad AS + BS \underset{k_{-3}}{\overset{k_{+3}}{\rightleftharpoons}} PS + S \\
&(4) \quad PS \underset{k_{-4}}{\overset{k_{+4}}{\rightleftharpoons}} P + S
\end{aligned} \tag{2.2}$$

Note that in the final desorption step the equilibrium constant for adsorption of P equals $\frac{1}{K_4}$, whereas for the other adsorption steps it is defined as

$$K_x = \frac{k_{+x}}{k_{-x}} \tag{2.3}$$

where k_+ describes the adsorption. In step (4), k_{+4} represents the desorption. In drafting a catalytic cycle as in equations 2.2 we naturally have to ensure that the reaction steps are thermodynamically and stoichiometrically consistent [115]. For instance, the number of sites consumed in the adsorption and dissociation steps must equal the number of sites liberated in the formation and desorption steps to fulfil the criterion that the catalyst is unaltered by the catalytic cycle. The symbol θ_R is used to indicate the fraction of occupied sites occupied by species R. Because Langmuir and Hinshelwood formulated the mechanism for a reaction of gases, the concentrations are expressed as partial pressures: p_x/p^0 where p^0 is the reference pressure ($p^0 = 1$

[3] Chemisorption = adsorption by means of chemical instead of physical forces [115].

bar)[4]

$$\begin{aligned}
(1) \quad & r_1 = k_{+1} p_A \theta_S - k_{-1} \theta_A \\
(2) \quad & r_2 = k_{+2} p_B \theta_S - k_{-2} \theta_B \\
(3) \quad & r_3 = k_{+3} \theta_A \theta_B - k_{-3} \theta_{PS} \theta_S \\
(4) \quad & r_4 = k_{+4} \theta_P - k_{-4} p_P \theta_S
\end{aligned} \tag{2.4}$$

The number of sites on a catalyst is constant and hence all species of active site – empty and occupied – should always add up to unity, as expressed by the following balance of sites:

$$\theta_S + \theta_A + \theta_B + \theta_P = 1 \tag{2.5}$$

To solve the kinetics for the most general case we need the full set of differential equations describing the coverage of all species participating in the reaction[5]. But in the following we will assume the following simplifications:

1. The surface reaction to PS (step 3, equation 2.2) is the rate-determining step (RDS), while all other steps are sufficiently fast so that they can be considered as being in **quasi-equilibrium**.
2. The reaction is not reversible.

Then the rate equations 2.4 can be simplified to:

$$\begin{aligned}
(1) \quad & 0 \simeq k_{+1} p_A \theta_S - k_{-1} \theta_A \Rightarrow \theta_A = K_1 p_A \theta_S \\
(2) \quad & 0 \simeq k_{+2} p_B \theta_S - k_{-2} \theta_B \Rightarrow \theta_B = K_2 p_B \theta_S \\
(3) \quad & r_3 = k_{+3} \theta_A \theta_B \\
(4) \quad & 0 \simeq k_{+4} \theta_P - k_{-4} p_P \theta_S \Rightarrow \theta_P = K_4^{-1} p_P \theta_S
\end{aligned} \tag{2.6}$$

By substituting θ_A and θ_B in the rate expression for the rate determining step we finally obtain:

$$r = r_{+3} = k_3 \frac{K_1 K_2 p_A p_B}{(1 + K_1 p_A + K_2 p_B + K_4^{-1} p_P)^2} \tag{2.7}$$

With the assumption that the active centres are equally distributed in the reaction volume, like it is in a homogeneous catalytic reactions, and that the density is constant, which is true in most of the cases for reaction in a liquid phase [29], we can modify equation 2.7 and express all participating substances as molar concentrations. The

[4] For simplification the reference pressure p^0 will not be included, but it is implicitly assumed that p_x represents a relative quantity.

[5] For more details confer to [115].

sum of the molar concentrations of all active sites occupied or empty is constant, $c_{S,0}$. Equation 2.5 is changed to:

$$c_S + c_{SA} + c_{SB} + c_{SP} = c_{S,0} \tag{2.8}$$

The substitution of the partial pressures and applying equation 2.8 to equation 2.7 leads to the following expression:

$$r = r_3 = k_3^+ c_{S,0}^2 \frac{K_1 K_2 c_A c_B}{(1 + K_1 c_A + K_2 c_B + K_4^{-1} c_P)^2} \tag{2.9}$$

The Eley-Rideal mechanism

The Eley-Rideal mechanism is based on the assumption that one substance (A), adsorbed on the surface of the catalyst, reacts with an unbound substrate molecule (B) to form the product (P). The initial step is the adsorption of the compound A to the catalyst (equation 2.10 (1)), followed by the product formation with the compound B (equation 2.10 (2)). The cycle is closed with the desorption of the product (equation 2.10 (2)).

$$\begin{aligned} &(1) \quad A + S \underset{k_{-1}}{\overset{k_{+1}}{\rightleftharpoons}} AS \\ &(2) \quad AS + B \underset{k_{-2}}{\overset{k_{+2}}{\rightleftharpoons}} PS \\ &(3) \quad PS \underset{k_{-3}}{\overset{k_{+3}}{\rightleftharpoons}} P + S \end{aligned} \tag{2.10}$$

With the assumption that step 2 is the rate determining step and that the reaction is not reversible and considering a quasi-equilibrium the equation for the rate is obtained to:

$$r = r_2 = k_2^+ c_{S,0} \frac{K_1 c_A c_B}{1 + K_1 c_A + K_3^{-1} c_P} \tag{2.11}$$

2.5 A medium throughput experimental kinetic investigation

The kinetic investigation of the studied Diels-Alder reaction was realised in a medium-throughput experimental design using a three-axis-robotic liquid handling system (figure 2.6). The liquid handling robot consisted of a syringe pump (Dilutor 40199) and the three axis robot (Gilson Abimed 231) itself. The reaction vessels, 2 ml glass vials, were located in a double walled rack, which was connected to an external water bath for temperature control. The syringe pump was connected via a valve and a flexible tube with the needle located at the robot's arm. With this setup it was possible to handle 16 X 5 glass vials with the maximum of 2 ml. The dilutor and the

position of the needle were controlled by the micro controller of the liquid handling robot, which enabled a free programming of the position of the needle in the XY-plan (vial position) as well as in the Z-plan (height of the needle tip) and of the aspirated and dispensed volumes. The robotic liquid handling system can be programed using a BASIC-like programming languages and with loops, jump instruction and timer functions as well as prompts for user interactions, highly flexible programs could be implemented designed for individual purposes. The working volume of a single liq-

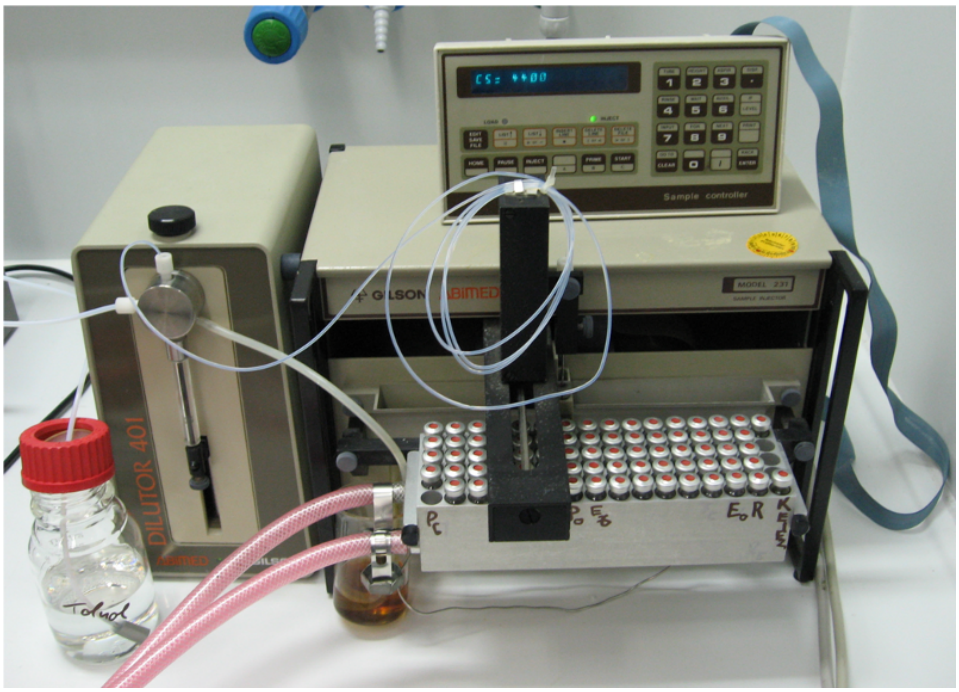

Figure 2.6: The liquid handling robot; Gilson Abimed 231 and Dilutor 401.

uid transfer ranged from 1 to 500 μl with an experimentally determined error of only 3 %, c.f. appendix A.1.2.

The procedure of the addition of compounds and the probing is illustrated in figure 2.7. The rack was divided in four zones, holding:

1. Substrates and catalyst
2. The reactors
3. Dilution vials
4. Sample vials.

The substrates and catalyst were automatically added into the reactors, samples were taken from the reactor, diluted and then stored in the sample vials. The whole

procedure was controlled by the micro controller enabling the automated, simultaneous investigation of five independent reactions. Placing micro inserts into the vials to reduce the inner volume to 300 μl the amount of catalyst, substrates and the sampling volume could be reduced. Mixing was performed within the inserts, sequentially aspirating and dispensing approximately 50 % of the liquid in the insersts up to five times by the diluter. A more detailed description of the experimental liquid handling process is given in appendix A.1.1.

An estimation of the propagation of the uncertainty of the liquid transfer in the sampling and dilution steps and the comparison with the uncertainty of GC-analysis showed, that the uncertainty of the liquid transfer was with only 4 % in the same range of the uncertainty of the GC-analysis, c.f. chapter A.1.4.

2.6 Results and discussion: batch reaction and kinetics

In the following chapter the results of the batch reactions carried out with the liquid handling robot are discussed. The focus was to derive a suitable kinetic model describing the reaction. The used materials and methods, like GC-analysis, calibration, catalyst purification and characterisation and experimental design are presented in appendix A.

2.6.1 Analysis of the catalyst

The elementary analysis of the chromium content of the catalyst gave a mass ratio of 61.4 mg chromium per 1 g catalyst, expressed as a concentration of active centres 1.18 $mmol$ chromium per 1 g catalyst. In the range of the measurement accuracy no difference could be observed between the purified and raw material. In the following and for all calculations the concentration of the active centres is used, because this is the important factor for the kinetic description. The approximate molar mass of the hyperbranched polyglycerol was known with 8000 $g\,mol^{-1}$ [106, 102] and the average loading of active centres of one polymer molecule could be calculated to 9.4. The hyperbranched polyglycerol bears a high density of hydroxy functionalisations (up to 14 $mmol\,g^{-1}$) [106]. So the obtained loading was less than one tenths of the theoretically maximal loading, but the loading is comparable to reported loadings. For example with a salen ligand supported by polysiloxan a loading of active centres per polymer molecule was approximately 5 [26]. For other reaction systems higher loadings are reported, for example for the asymmetric rhodium catalysed hydrogenation of prochiral alkenes catalysed by chiral ferrocenyl diphospines ('Josiphos') immobilised at the endgroups of dendrimers, thus obtaining systems of up to 24 chiral metal centres in the periphery [99]. Another example is the metallation of the multisite phosphines with $[Rh(COD)_2]BF_4$ with cleanly yielded cationic rhododendrimers containing up to 32 metal centres [99].

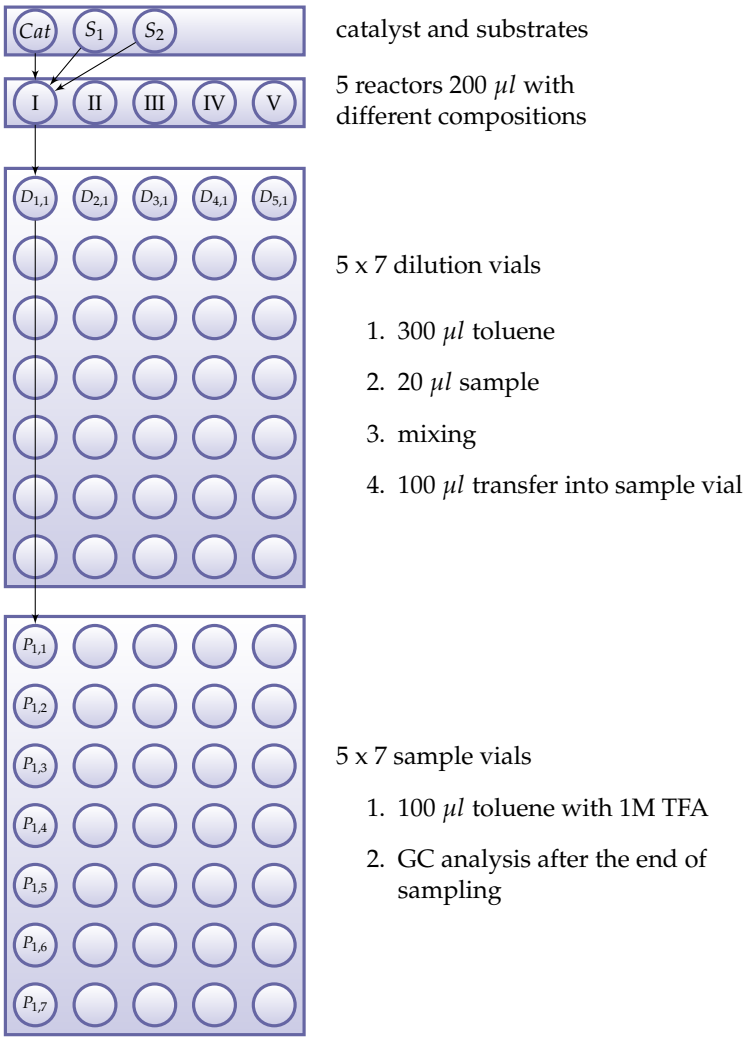

Figure 2.7: Function diagram of the liquid handling process

2.6.2 Kinetic investigations

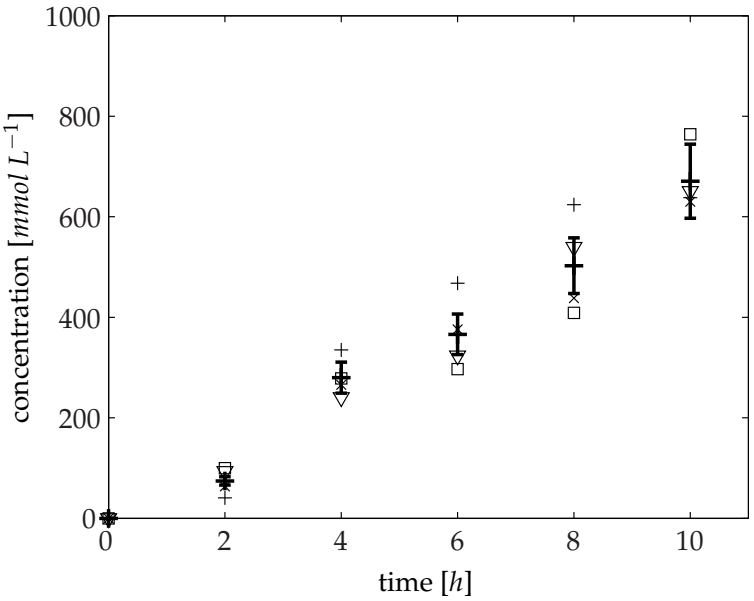

Figure 2.8: Reproducibility of the kinetic investigations. Four times repeated experiment (+, ×, ▽, □) with fixed starting conditions. The error bars indicate the uncertainty calculated of the mean values at each point.
$c_{0,acrolein} = c_{0,butadiene} = 1\,mol\,L^{-1}$, $c_{catalyst} = 35\,mmol\,L^{-1}$, $T = 25\,°C, solvent: toluene$

An important factor for the kinetic investigations is the reproducibility of the procedure. A reproducibility was given, but the uncertainty of the obtained values was bigger than predicted with the uncertainty of measured concentrations of 5 %, c.f. chapter A.1.4. The reason might be the solubility of the catalyst. Differing from the communicated solubility ([116], the catalyst was not as soluble as expected. Even at concentrations of 0.05 $g\,ml^{-1}$ small particles were suspended in the solution, which tended to sediment. The particles could partly be broken by ultrasonication. But the catalyst tended also to adhere to the glass walls of the reaction vials (figure 2.9). The concentration in the stock vial for the catalyst could not be reduced further, because then large volumes of catalyst solution had to be added to the reaction vials to reach the target starting conditions. Due to the particles and the adhesion of the catalyst the reproducibility was reduced to an uncertainty of approximately 16 %. The adhesion effect increased with decreasing fluid volumes and especially the last samples were error-prone, therefore they were not be included in the evaluation. It is to mention that the volumes examined were small (reaction volume 200 μl and smallest transferred volume 1 μl). Handling such small volumes is error-prone and thus the error was in an acceptable range, yet open to improvements.

The solubility problem is conditional upon the reaction system and can be solved

Figure 2.9: Adhered catalyst at the glass walls of the reaction vial after sampling

by a solvent change. A more polar solvent might increase the solubility and reduce the adhesion. This could not be done in this study, because of the coupling with the enzymatic step, c.f. chapter 3.10.1.

An uncatalysed reaction could be neglected. No significant reaction could be measured without the addition of a catalyst within a reaction time of ten hours, c.f. figure 2.10. Also the assumption of an irreversable reaction could be confirmed. Over the reaction time of ten hours no significant reduction of the product concentration could be observed in the presence of the catalyst.

Investigated were the influence of the starting concentration, the influence of the ratio of the concentrations of starting materials as well as the concentration of the catalyst. In figure 2.11 different ratios of starting concentrations are compared, equimolar [6] and one reactant in excess. Interestingly, the excess had no significant influence on the time course of the product concentration, no matter which starting material was in excess. No significant increase of the reaction rate could be observed with one compound in excess and the reaction rates were only dependent on the lower concentrated substrate, this could be acrolein as well as butadiene, as long as the sum of the concentration of both substrates were larger 400 $mmol\ L^1$. This could not only be observed at a starting concentration of 400 $mmol\ L^1$ but also for concentrations of the lower dosed substrate of 600 and 800 $mmol\ L^{-1}$.

For low starting concentrations of both substrates in combination with high catalyst concentrations a different behaviour was visible. In the case of an equimolar addition of 200 $mmol\ L^{-1}$ and a catalyst concentration of 35 $mmol\ L^{-1}$ only a marginal conversion could be observed, c.f. figure 2.12. But increasing the concentration of one reactant to 1000 $mmol\ L^{-1}$, a conversion of over 80 % could be reached. The time courses differed here for the two different substrates in excess, because the butadiene

[6] Due to the precision of 1 μl of the dilutor an exact equimolar ratio could not be applied.

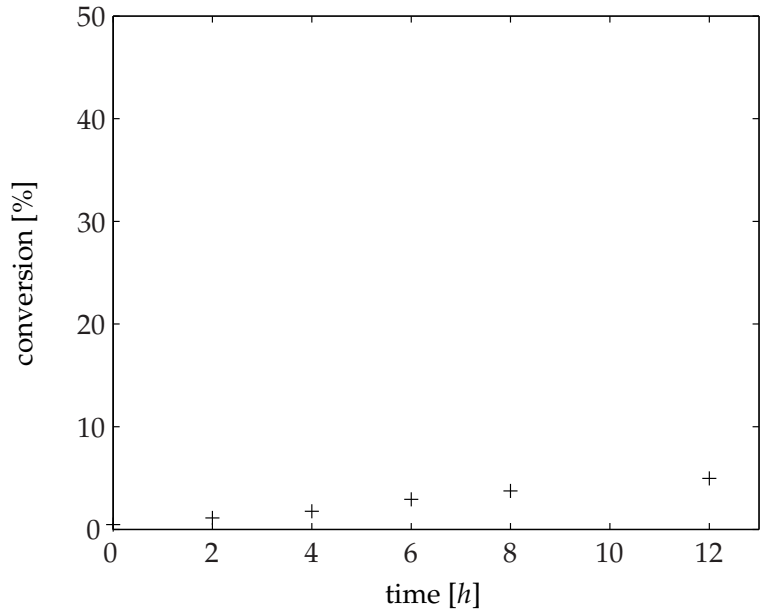

Figure 2.10: Non-catalysed formation of the carbaldehyde;
$(+)$: $c_{0,butadiene} = c_{0,acrolein} = 1\,mol\,L^{-1}$, $c_{catalyst} = 0\,mmol\,L^{-1}$, $T = 25\,°C$, $solvent$: $toluene$

concentration was at a nominal concentration of 200 $mmol\,L^{-1}$ with 190 $mmol\,L^{-1}$ about 18 % lower compared to the acrolein concentration (230 $mmol\,L^{-1}$) due to the precision of the liquid handling robot.

As important parameters for the reaction rate the concentration of the starting materials as well as the catalyst concentrations have been identified. Because of the observation, that at concentrations higher than 200 $mmol L^{-1}$ the reaction rate is independent on the ratio of the starting material, in the following only equimolar starting concentrations were considered. In figure 2.13 the increase of the reaction rate with an increased starting concentration is clearly visible. The initial reaction rates were approximated, the linear slopes from time zero to six hours are illustrated and the values of slopes are specified with m ($mmol\,L^{-1}\,h^{-1}$). In the minor graph (figure 2.13) the initial reaction rates are presented as the function of the initial concentrations. The initial rate was linearly dependent on the initial concentration, but the interception with the x-axis ($m = f(0\,mmol\,L^{-1})$) was at a concentration of 200 $mmol\,L^{-1}$. This observation confirmed the results presented above, that a minimal concentration exist at which the reaction starts. Possibly an unspecific adsorption of the reactants could explain the observation, c.f. chapter 2.6.4. An explanation could not be found why the threshold for the sum of the concentrations of both substrate to start the reaction was 400 $mmol L^{-1}$. The phenomenon was not closer investigated, because the focus of the investigation was the establishment of the continuously operated process.

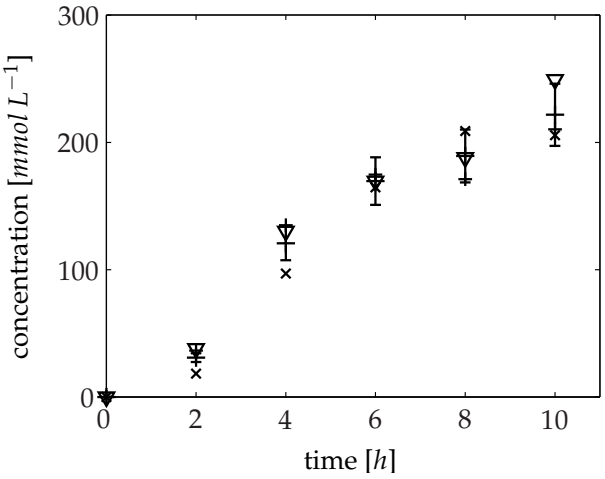

Figure 2.11: Excess of starting material without influence.
$(+), (\times), (\triangledown)$: $c_{catalyst} = 35\,mmol\,L^{-1}$, $T = 25\,°C$, $solvent:\ toluene$
$(+)$: $c_{0,butadiene} = 400\,mmol\,L^{-1}$, $c_{0,acrolein} = 1000\,mmol\,L^{-1}$; $c_{0,acrolein}/c_{0,butadiene} = 2.5$
$(\times)$: $c_{0,butadiene} = 400\,mmol\,L^{-1}$, $c_{0,acrolein} = 350\,mmol\,L^{-1}$; $c_{0,butadiene}/c_{0,Acrolein} = 1.14$
$(\triangledown)$: $c_{0,butadiene} = 1000\,mmol\,L^{-1}$, $c_{0,acrolein} = 350\,mmol\,L^{-1}$; $c_{0,butadiene}/c_{0,acrolein} = 2.8$
The error bars indicate the uncertainty calculated of the mean values at each point.

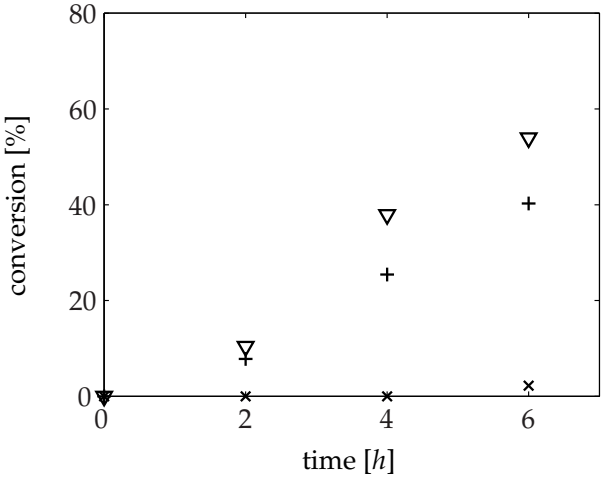

Figure 2.12: Excess of starting material with influence at low catalyst to starting material concentration ratios;
$(+), (\times), (\triangledown)$: $c_{catalyst} = 35\,mmol\,L^{-1}$, $T = 25\,°C$, $solvent:\ toluene$
$(\times)$: $c_{0,butadiene} = 190\,mmol\,L^{-1}$, $c_{0,acrolein} = 230\,mmol\,L^{-1}$; $c_{0,acrolein}/c_{0,butadiene} = 0.83$
$(+)$: $c_{0,butadiene} = 190\,mmol\,L^{-1}$, $c_{0,acrolein} = 980\,mmol\,L^{-1}$; $c_{0,acrolein}/c_{0,butadiene} = 5.1$
$(\triangledown)$: $c_{0,butadiene} = 990\,mmol\,L^{-1}$, $c_{0,acrolein} = 230\,mmol\,L^{-1}$; $c_{0,butadiene}/c_{0,acrolein} = 4.3$

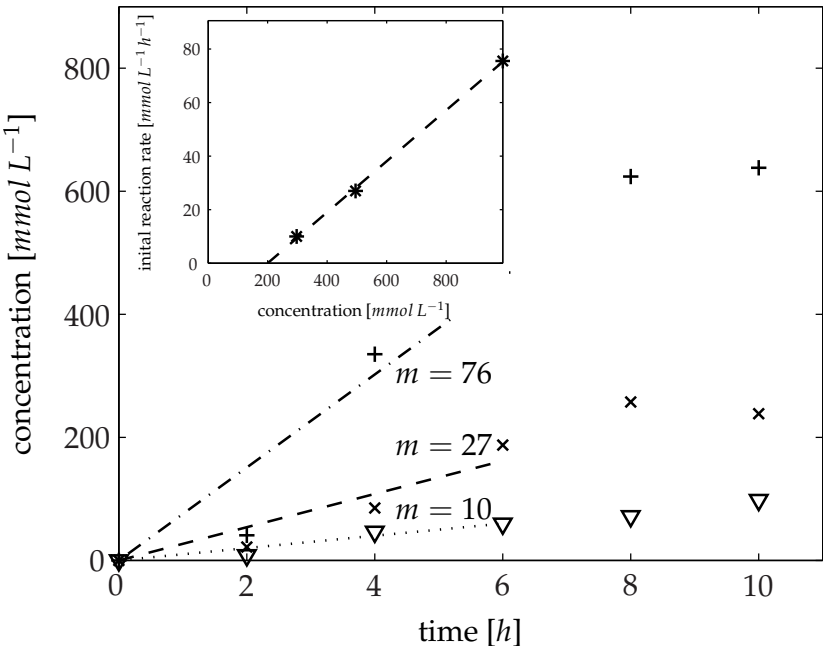

Figure 2.13: Influence of starting material concentration on the reaction rate;
$(+), (\times), (\triangledown)$: $c_{catalyst} = 35\,mmol\,L^{-1}$, $T = 25\,°C$, $solvent$: $toluene$
$(+)$: $c_{0,butadiene} = c_{0,acrolein} = 1000\,mmol\,L^{-1}$, $c_0/c_{catalyst} = 28.6$
$(\times)$: $c_{0,butadiene} = c_{0,acrolein} = 500\,mmol\,L^{-1}$, $c_0/c_{catalyst} = 14.3$
$(\triangledown)$: $c_{0,butadiene} = c_{0,acrolein} = 300\,mmol\,L^{-1}$, $c_0/c_{catalyst} = 8.6$
linear slope approximated form time zero to six hours $m = [mmol\,L^{-1}\,h^{-1}]$

Changing of the catalyst concentration gave the expected results, c.f. table 2.2. The conversion after ten hours increased with increasing catalyst concentration. The apparent reaction rate coefficients k were about the same size. The apparent reaction rate coefficient at the lowest catalyst concentration of 9 $mmol\ L^{-1}$ was slightly increased, which could be an effect of the experimental error, possibly also an unspecific adsorption could be the reason, c.f. chapter 2.6.4.

catalyst $[mmol\ L^{-1}]$	catalyst/substrate $[-]$	conversion after ten hours $[-]$	apparent reaction rate coefficients[1] $[h^{-1}]$
35	0.035	0.64	1.8
18	0.018	0.29	1.6
9	0.009	0.20	2.2

[1] The reaction rate coefficients are calculated by $k = \frac{\Delta c}{\Delta t}\frac{1}{c_{cat}}$.

Table 2.2: Conversion as function of the catalyst concentration; $c_{0,butadiene} = c_{0,acrolein} = 1\ mol\ L^{-1}$

In general, the kinetic of the investigated Diels-Alder reaction catalysed by a polymer supported salen ligand with a chromium insert can be characterised as rather complex. The reaction rate was mainly a function of the starting material concentration as well as the catalyst concentration. The ratio of the two starting materials has no significant influence on the reaction rate, as long as the concentration is higher than 200 $mmol L^{-1}$. An enantioselectivity of the catalyst for the investigated reaction system could not be observed, which was already reported by our cooperation partners [43, 109]. But the enhanced diastereoselectivity was clearly visible, c.f. figure A.2. The diastereomeric excess in all samples could be calculated to $de = 74\,\%$ with a standard deviation of 4 %. The measured *de* was independent of the starting conditions. The diastereomeric excess was consequently 20 % lower compared the reference sample for the calibration which was kindly provided by the Institute of Chemistry and Biochemistry - Organic Chemistry, Freie Universität Berlin, Dendritic Polymer Research Group, Prof. Dr. Rainer Haag. The diastereomeric excess of the reference sample was confirmed by NMR [7]. The measured *cis*/*trans* ratio confirmed the results reported by Avi [43] and Hajji [109]. The selectivity of an unsymmetrical salen catalyst can be influenced by the water content in the reaction. Hence, one reason for the lower *de* could be that the reference sample was synthesised under low moist conditions, while for the kinetic measurements no special arrangements for low

[7] The NMR measurements of the reference sample were carried out at the Institute of Chemistry and Biochemistry - Organic Chemistry, Freie Universität Berlin, Dendritic Polymer Research Group, Prof. Dr. Rainer Haag.

moist conditions were taken, because this would have increased the experimental effort drastically.

2.6.3 A random Eley-Rideal mechanism

The observations presented in chapter 2.6.2 can be partly described with a random bireaction mechanism inspired by the Eley-Rideal mechanism. In this chapter first the developed mechanism is outlined and then applied to the measurements. Eley and Rideal developed the mechanism for a gas phase reaction, were one substrate is adsorbed to a solid surface. The mechanism described here is developed for a homogeneous reaction and the substrate is bound to a catalytic centre. The forces involved in the binding in the investigated case are not known and the binding might be better described by a chemisorption. But to keep the similarity to the Eley-Rideal mechanism, in the following the binding of a substrate is called "adsorption".

The mechanism proposed by Eley and Rideal is outlined in chapter 2.4.1. The basic idea is that one reactant of a bireaction system is adsorbed – bound and coordinated – to the catalyst C and the second reactant reacts directly with the adsorbed molecule. In the classic Eley-Rideal mechanism the sequence is ordered. For example compound A is always adsorbed and substance B interacts with the bound substance to form the product P. As figure 2.14 indicates this mechanism can not describe the

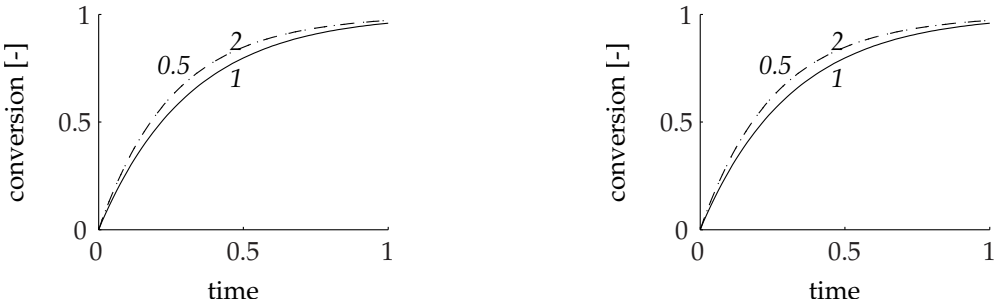

Figure 2.14: Illustration of the conversion as function of the ratio of the starting concentrations; left: classical Eley-Rideal mechanism; right: simplified, symmetric, random Eley-Rideal mechanism. The numbers represent the ratio of the starting material A to B. To generalise the illustation the plots are normelised.

behaviour shown in figure 2.11, because the conversion predicted by the Eley-Rideal mechanism is a function of the ratio of the starting material. The Eley-Rideal mechanism is ordered and therefore for the reaction progress it is also important which starting material is in excess.

A possible elementary mechanism of a bireaction system, inspired by the Eley-Rideal, which can describe the experimental observation is outlined in the following. The basic idea is, that both substrates (A and B) can bound and compete for the active

centres (C). Then the transition complex of the catalyst and one of the compounds reacts with free molecules in the bulk solution forming the product, which is then released into the solution. The elementary reaction steps of the catalytic reaction between A and B in elementary steps are presented in equations 2.12.

$$\begin{aligned}
(I) \quad & A + C \underset{k_{-1}}{\overset{k_{+1}}{\rightleftharpoons}} AC \\
(II) \quad & B + C \underset{k_{-2}}{\overset{k_{+2}}{\rightleftharpoons}} BC \\
(III) \quad & AC + B \underset{k_{-3}}{\overset{k_{+3}}{\rightleftharpoons}} PC \\
(IV) \quad & BC + A \underset{k_{-4}}{\overset{k_{+4}}{\rightleftharpoons}} PC \\
(V) \quad & PC \underset{k_{-5}}{\overset{k_{+5}}{\rightleftharpoons}} P + C
\end{aligned} \tag{2.12}$$

The full set of differential equations describing all species participating in the reaction on the basis of concentrations is given in the equations 2.13.

$$\begin{aligned}
(1) \quad & \frac{d\,c_A}{d\,t} = k_{-1}c_{AC} - k_{+1}c_A\,c_C - k_{+4}c_{BC}\,c_A + k_{-4}c_{PC} \\
(2) \quad & \frac{d\,c_B}{d\,t} = k_{-2}c_{BC} - k_{+2}c_B\,c_C - k_{+3}c_{AC}\,c_B + k_{-3}c_{PC} \\
(3) \quad & \frac{d\,c_P}{d\,t} = k_{+5}c_{PC} - k_{-5}c_P\,c_C \\
(4) \quad & \frac{d\,c_{AC}}{d\,t} = k_{+1}c_A\,c_C - k_{-1}c_{AC} - k_{+3}c_{AC}\,c_B + k_{-3}c_{PC} \\
(5) \quad & \frac{d\,c_{BC}}{d\,t} = k_{+2}c_B\,c_C - k_{-2}c_{BC} - k_{+4}c_{BC}\,c_A + k_{-4}c_{PC} \\
(6) \quad & \frac{d\,c_{PC}}{d\,t} = k_{+3}c_{AC}\,c_B + k_{+4}c_{BC}\,c_A - k_{-3}c_{PC} - k_{-4}c_{PC} \\
(7) \quad & \frac{d\,c_C}{d\,t} = k_{-1}c_{AC} - k_{+1}c_A\,c_C + k_{-2}c_{BC} - k_{+2}c_B\,c_C + k_{+5}c_{PC} - k_{-5}c_P\,c_C
\end{aligned} \tag{2.13}$$

The number of sites on a catalyst is constant and hence the concentration of the sum of all transition complexes and free active sites is constant:

$$c_C + c_{AC} + c_{BC} + c_{PC} = c_{C,0} \tag{2.14}$$

For the investigated case the equation system can be simplified. It can be assumed, that the rate determining steps are the product formation steps III and IV in equa-

tion 2.12. All other steps are sufficiently fast that they can be considered as being in a quasi-equilibrium. Furthermore it can be assumed that the product binds weakly to the active centres and hence $k_{+5} >> k_{-5}$. The product is directly released from the active site and the concentration of the transition complex with the product is almost zero ($c_{PC} = 0$). This can be the reason for the observed irreversibility of the reaction. Mathematically the irreversibility can also be expressed by setting k_{-3} and k_{-4} to zero. In combination with a weak bond of the product to the catalyst, the reaction equation V in the reaction sequence 2.12 has no influence on the globally observed production rate of the product. The system can by simplified furthermore and in equation III and IV no transition complex with the product is formed, but the product is directly released into the bulk phase, c.f. equation 2.15.

$$\begin{aligned} (IIIa) \quad & AC + B \underset{k_{-3}}{\overset{k_{+3}}{\rightleftharpoons}} P + C \\ (IVa) \quad & BC + A \underset{k_{-4}}{\overset{k_{+4}}{\rightleftharpoons}} P + C \end{aligned} \tag{2.15}$$

With this assumption the differential equation system (2.13) is simplified to:

$$\begin{aligned} (1a), (2a) \quad & \frac{d\,c_A}{d\,t} = \frac{d\,c_B}{d\,t} = -\frac{d\,c_P}{d\,t} \\ (3a) \quad & \frac{d\,c_P}{d\,t} = r = k_{+3} c_{AC}\, c_B + k_{+4} c_{BC}\, c_A \\ (4a) \quad & 0 \simeq k_{+1} c_A\, c_C - k_{-1} c_{AC} - k_{+3} c_{AC}\, c_B \\ (5a) \quad & 0 \simeq k_{+2} c_B\, c_C - k_{-2} c_{BC} - k_{+4} c_{BC}\, c_A \end{aligned} \tag{2.16}$$

The influence of the reactants on the reaction rate was for both substrats the same. Therefore the reaction rate equation must be symmetric with respect to the substrates. Therefore the reaction rates k_{+3} and k_{+4} can be set equal. Due to symmetry also the adsorption rates of the substrates are set equal ($k_{+1} = k_{+2}$ and $k_{-1} = k_{-2}$).

By substitution of the transition complex concentrations, the rate equation can be obtained for the rate determining step of the simplified, symmetric random Eley-Rideal mechanism:

$$r = c_{C,0}\, k_{+3}\, \frac{c_A^2\, c_B + 2\, K_b\, c_A\, c_B + c_B^2\, c_A}{c_A^2 + K_a\,(c_A + c_B) + K_b\, K_a + K_b\,(c_A + c_B) + c_B^2 + \frac{K_a}{K_b}\, c_B\, c_A} \tag{2.17}$$

with:

$\frac{k_{-1}}{k_{+1}} = K_1^{-1} = K_a$: ratio of desorption to adsorption rate; reciprocal equilibrium constant for the adsorption.

$\frac{k_{-1}}{k_{+3}} = K_b$: ratio of desorption to reaction rate

For the developed model the influence of the catalyst concentration on the reaction rate is linear at constant starting concentrations. As it is visible in figure 2.15 on the left site, the influence of the concentration of the starting material is also linear as long as the initial ratio of the substrate concentrations is constant. The reaction rate displays only low dependency on the ratio of the substrate concentration with a maximal increase of 40 %, c.f. figure 2.15, right. Consequently the time-conversion plot is also not much influenced by the ratio, as presented in figure 2.14 on the right site.

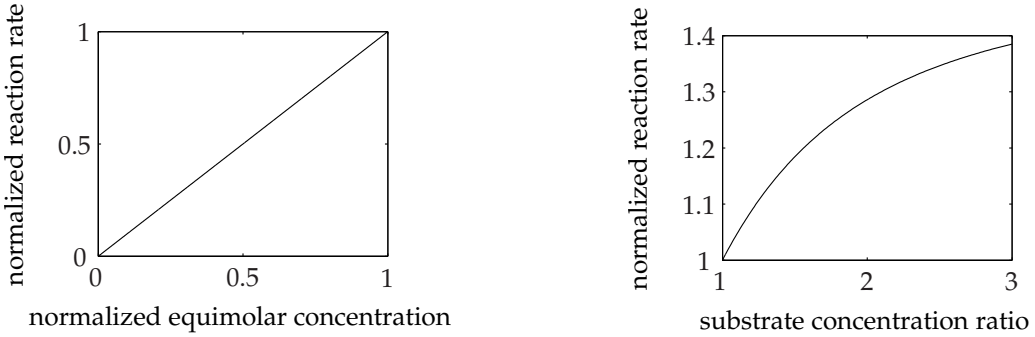

Figure 2.15: Illustration of the reaction rate as function of equimolar substrate concentrations (left) and as function of the ratio of the substrate concentrations (right). The plots are calculated with the solution of the quasi-equilibrium approach, equation 2.17; $k_{+3} = 0.02\,L\,mmol^{-1}\,h^{-1}$, $k_a = k_b = 0.1\,mmol\,L^{-1}$. To generalise the illustation the plots are normelised.

A closer look has to be taken on the substrate concentrations which are in the range of the catalyst concentrations ($c_A = c_B \simeq c_{S,0}$). In this range the assumption of a quasi-equilibrium is not valid, as seen in figure 2.16. In the upper plot the conversions calculated on the base of product formation are shown ($U = \frac{c_P}{c_{A,0}}$), the mid plot represents the conversions calculated on the base of substrate consumption ($U = \frac{c_{A,0}-c_A}{c_{A,0}}$) and in the lower plot the reaction rates of the substrate–catalyst–complexes is shown ($\frac{c_{AC}}{dt}$ $\frac{c_{BC}}{dt}$). In the case of high substrate to catalyst ratios the reaction rates of the substrate-catalyst-complexes drop at the beginning almost immediately to zero (quasi-equilibrium). But the reaction rates declines slowly when the substrate concentrations are equal to the catalyst concentration. Then a quasi-equilibrium

does not exist. The consequence becomes visible comparing the conversion plots. The conversion based on the substrate consumption do not differ for both cases (mid plot), but for the conversion based on the product formation (upper plot) clearly a difference is visible. Here also the reaction rate shows an acceleration – counterclockwise curvature – in the first phase of the reaction, c.f. also figure 2.17, right. This can be explained by the adsorption of the substrate to the catalyst. First the substrate is adsorbed and the concentration in the bulk phase is reduced, but no product is released. When the quasi-equilibrium is reached the product is formed and released in the same rate as the substrate is adsorbed, thus the reaction rate accelerates until the quasi-equilibrium is reached. As it can be seen in figure 2.17 the time-conversion plot for substrate concentrations is also more sensitive in that range of concentrations. The influence of the ratio of the substrates is increased when the substrate concentration is in the range of the catalyst concentration.

The measurements show a similar characteristics. The reaction rate is depending on the catalyst as well as on the equimolar starting concentrations, c.f. figures 2.13 and 2.2, and the influence of the ratio of the substrates on the reaction rate is quite low at high substrate concentrations, c.f. figures 2.11. But the influence is increased at high catalyst to substrate ratios (figure 2.12). In all plots an acceleration of the reaction rate is visible comparing the time range 0 to 1 hour and 1 to 2 hours.

2.6.4 Determination of the model parameters and interpretation of the observations

The model parameters were obtained by minimising the fitness function 2.18. The fitness function was expressed as the root mean square error (RMSE):

$$\mathrm{RMSE} = \sqrt{\frac{\sum_{i=1}^{n} (\overline{x}_i - x_i)^2}{n}} \tag{2.18}$$

with the residual of the measured concentration, $\overline{x}_i$, and the simulated concentration of the product, x_i at each measurement time point i. n was the number of measurements. The parameters of the simulation are altered in that way, that the RMSE is minimised, obtaining an optimised set of model parameters.

The optimisation was done with Matlab 7.4 (R2007a), The MathWorks, including the Optimisation, the Genetic Algorithm and Direct Search and the Statistics Toolboxes. A combination of two optimisation strategies has been applied. For a rough global optimisation the genetic algorithm `ga` was applied and the solution was furthermore improved using the solver `lsqnonlin` (trust-region-reflective algorithm), c.f. sample code in appendix B.2

28 measurements have been used simultaneously for optimisation. To estimate the contribution of the measurements uncertainty on the RMSE, the RMSE for the measurement's uncertainty of 16 % was calculated to 52.6 $mmol L^{-1}$. For the analysis

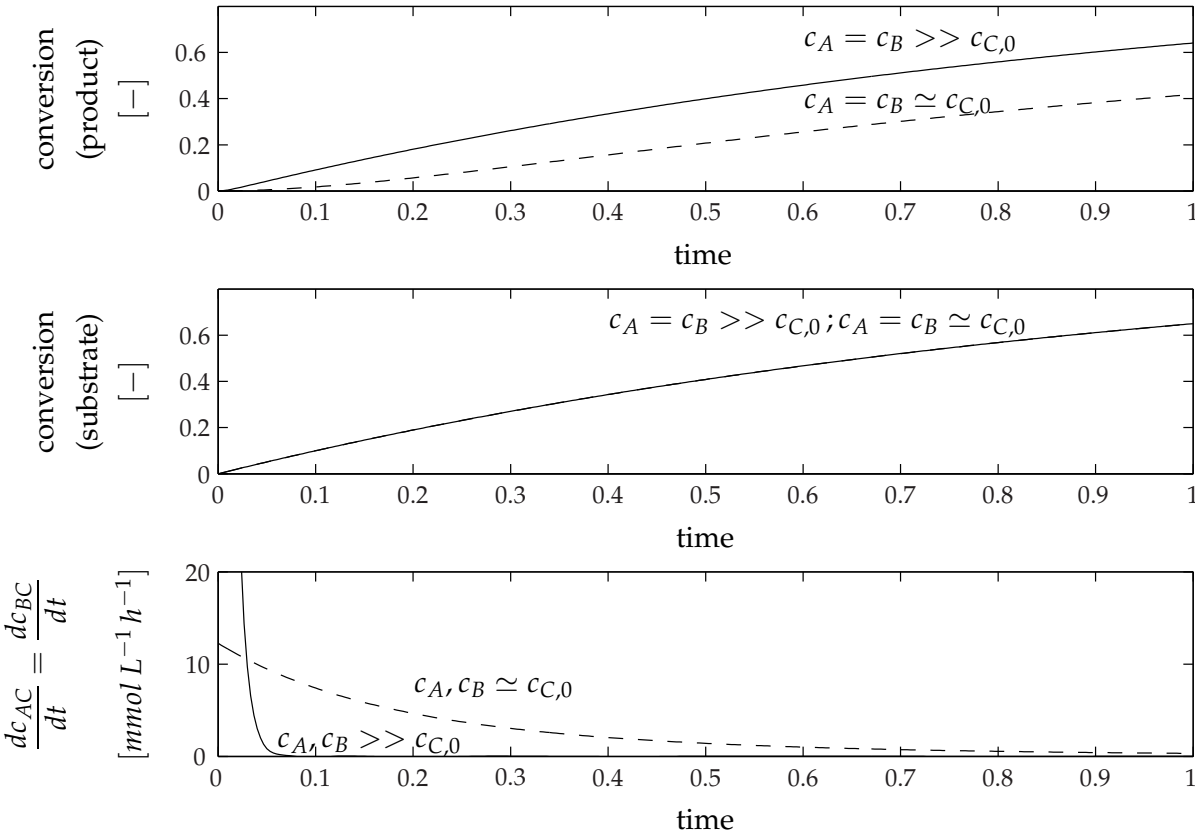

Figure 2.16: Illustration of the conversion based on product formation $U = \frac{c_P}{c_{A,0}}$ (upper plot), conversion based on substrate consumption $U = \frac{c_{A,0} - c_A}{c_{A,0}}$ (mid plot) and reaction rates of the substrate–catalyst complexes ($\frac{c_{AC}}{dt}$ $\frac{c_{BC}}{dt}$) (lower plot) calculated by the simplified, symmetric random Eley-Rideal mechanism at high $\frac{c_A}{c_{C_0}} = \frac{c_B}{c_{C_0}} > 25$ and low substrate to catalyst concentration ratios; $c_A = c_B \simeq c_{C_0}$. The plots are calculated with the set of differential equations 2.13 and the simplifications, but not assuming a quasi-equilibrium; $k_{+3} = 0.02\,L\,mmol^{-1}\,h^{-1}\,; k_{+1} = 0.01\,L\,mol^{-1}h^{-1}\,; \frac{k_{+1}}{k_{-1}} = 10\,L\,mol^{-1}$. To generalise the illustation the plots are normelised.

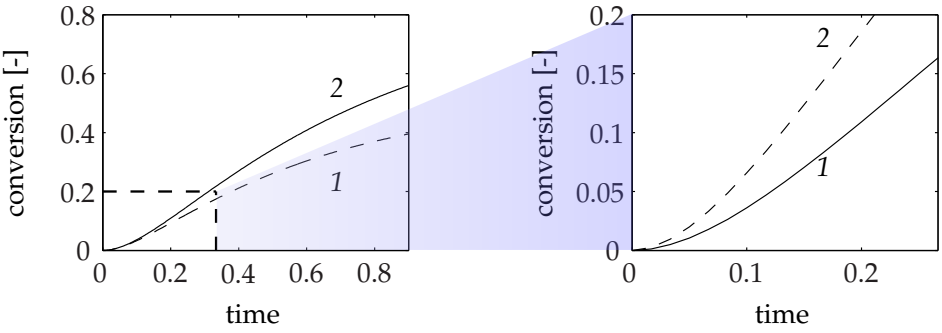

Figure 2.17: Illustration of the conversion based on product formation as function of the ratio of the starting concentration of the simplified, symmetric random Eley-Rideal mechanism at low starting concentrations; $c_A, c_B \simeq c_{C_0}$, right: magnification of the first stage. The numbers represent the ratio of the starting material A to B. The plots are calculated with the set of differential equations 2.13 and the simplifications, but not assuming a quasi-equilibrium; $k_{+3} = 0.02\,L\,mmol^{-1}\,h^{-1}$; $k_{+1} = 0.01\,L\,mol^{-1}h^{-1}$; $\frac{k_{+1}}{k_{-1}} = 10\,L\,mol^{-1}$. To generalise the illustation the plots are normelised.

of the sensitive the 95 % confidence intervals for all parameters have been calculated.

The results for the parameter estimation using equation 2.17 are presented in table 2.3. Noticeable was the parameter K_a, which tended to zero, and a high uncer-

Parameter	Unit	Value	Confidential interval
k_{+3}	$[L\,mmol^{-1}\,h^{-1}]$	$2.4 * 10^{-3}$	$\pm 1.6 * 10^{-4}$
K_a	$[mmol L^{-1}]$	$\rightarrow 0$	> 1
K_b	$[mmol L^{-1}]$	0.05	> 1000
$RMSE$	$[mmol L^{-1}]$	96.21	-

Table 2.3: Estimated parameters for the symmetric random Eley-Rideal mechanism

tainty. Also the parameter k_b had a huge uncertainty and hence these parameters were not sensitive. Therefore the equation 2.17 could be simplified further and K_a could set to zero. The quotient K_a/K_b tended also to zero, because the ratio of the desorption rate to the reaction rate (K_b) was always larger than K_a, due to the fact that the reaction rate k_{+3} was much slower than the adsorption rate k_{+1}. The parameter estimation, setting K_a equal to zero, revealed that also the K_b value tended to zero, so that also K_b could be set to zero. Than we obtain for the simplest rate equation:

$$r = c_{C,0}\,k_{+3}\,\frac{c_A^2\,c_B + c_B^2\,c_A}{c_B^2 + c_A^2} \tag{2.19}$$

With this rate equation the same RMSE and k_{+3} values as presented in table 2.3 had been obtained. The comparison of the model and the measured data showed a good correlation, likewise for high concentrations and for low concentrations, for concentration ratios unequal to one as well as different catalyst concentrations, c.f. figure 2.18. The low value and sensitivity of the parameters K_a and K_b strengthened the assumption of the rate limiting step. The adsorption of the substrate to the catalyst k_{+1} was several magnitudes faster than the desorption rate k_{-1} and the reaction rate k_{+3} was faster than the desorption rate k_{-1}, so that $K_a = k_{-1}/k_{+1} \rightarrow 0$ as well as $K_b = k_{-1}/k_{+3} \rightarrow 0$.

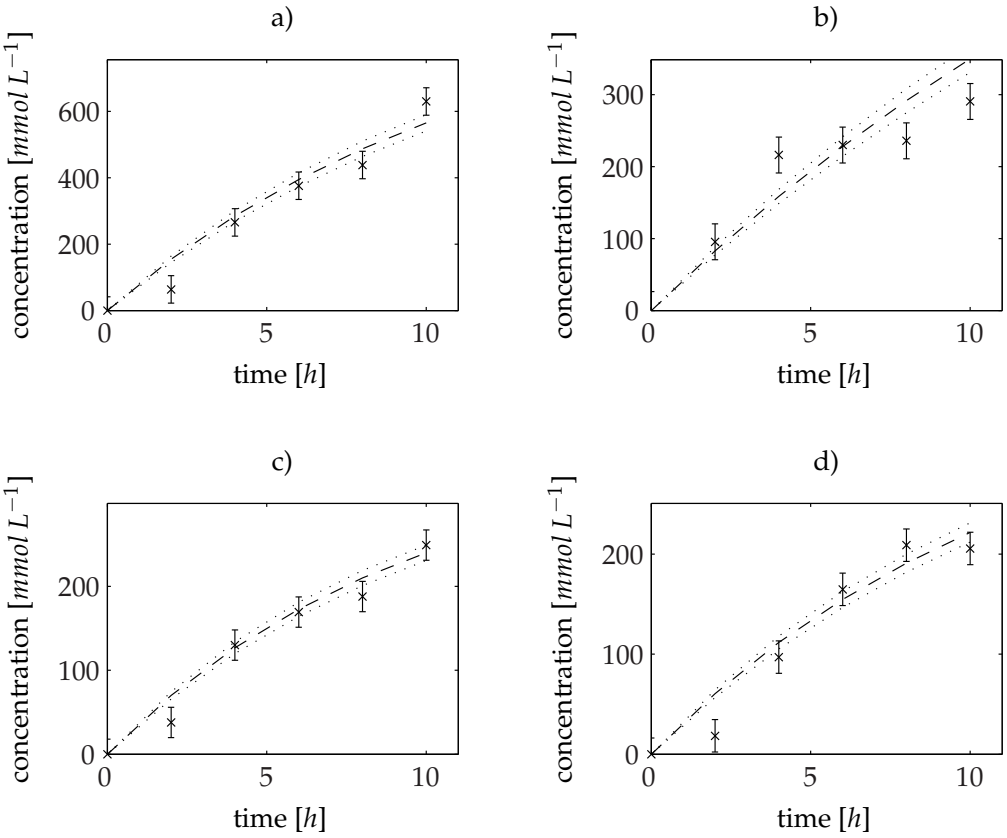

Figure 2.18: Comparison simulation and measurements.
a) $c_{0,butadiene} = 990\,mmol\,L^{-1}$, $c_{0,acrolein} = 980\,mmol\,L^{-1}$, $c_{catalyst} = 35\,mmol\,L^{-1}$; $c_{0,butadiene}/c_{0,acrolein} = 1$
b) $c_{0,butadiene} = 990\,mmol\,L^{-1}$, $c_{0,acrolein} = 980\,mmol\,L^{-1}$, $c_{catalyst} = 18\,mmol\,L^{-1}$; $c_{0,butadiene}/c_{0,acrolein} = 1$
c) $c_{0,butadiene} = 990\,mmol\,L^{-1}$, $c_{0,acrolein} = 380\,mmol\,L^{-1}$, $c_{catalyst} = 35\,mmol\,L^{-1}$; $c_{0,butadiene}/c_{0,acrolein} = 2.6$
d) $c_{0,butadiene} = 400\,mmol\,L^{-1}$, $c_{0,acrolein} = 380\,mmol\,L^{-1}$, $c_{catalyst} = 35\,mmol\,L^{-1}$; $c_{0,butadiene}/c_{0,acrolein} = 1.05$

High catalyst to substrate ratios (larger than 0.10) could not be mapped by the model. As shown in figures 2.19 the observed product concentration was much lower

than the concentration predicted by the model. The acceleration of the reaction rates, which was visible in all measurements during the first reaction hours, could not be displayed by the model, because in all reaction the substrate concentrations were more than ten times higher than the catalyst concentrations whereas the model predicted a reduced reaction rate only at catalyst concentrations in the range of the substrate concentration.

This observation can possibly be explained by an unspecific adsorption of the substrates and the product to the polymer, which was not integrated into the kinetic model, but has a large similarity to the kinetic model at substrate concentrations equal to catalyst concentration (c.f. figures 2.16 and 2.17. The principle idea of the reaction mechanism was that a reaction occurs, when a molecule bound by the catalyst interacts with a free molecule in the bulk phase. When the concentrations of the substrate was reduced significantly by unspecific adsorption during the start phase, the likelihood of interaction would also be reduced so that the reaction between a bound and a free molecule would be unlikely, hence the reaction rate would be reduced as well as the final conversion. After the saturation of the polymer the observed production rate would increase and with increasing product concentrations the adsorption sites would be covered more and more with product instead of substrates. Such an adsorption would also explain the reduced reaction rate at low substrate to catalyst ratios. The substrate concentrations in the bulk phase would be reduced by adsorption to such a degree, that the reaction would not proceed.

If the concentration of one compound was increased, the concentration in the solution would not be reduced so drastically by adsorption and the likelihood of an interaction would increase so that the reaction could occur. For higher concentrations the effects of the adsorption would be less pronounced, because a sufficient number of free molecules would be always in solution. For the observed behaviour the substrate concentration would have to be reduced to a value of the concentration of the active sites, so that the unspecific adsorption can be roughly estimated to seven molecules per polymer molecule. The hyperbranched polyglycerol bore a high density of hydroxy functionalisations (up to 14 $mmol\,g^{-1}$) [106]. And less than one tenth of the hydroxy functions had been blocked by a catalytic site. The polar hydroxy functions could be adsorption sites for the substrates and product which also had polar regions. Especially in an unpolar solvent like toluene the adsorption equilibrium could moved to the adsorption.

The adsorption of a starting material and product on the polymer could not be proved experimentally, because no sufficiently sensitive analytic method was available for the substrates in particular, but similar observations were reported by the cooperation partners in Berlin [8]. The phenomena could not be proved by a model either, because the uncertainty in the measured data was too large to determine sen-

[8] Institute of Chemistry and Biochemistry - Organic Chemistry, Freie Universität Berlin, Dendritic Polymer Research Group, Prof. Dr. Rainer Haag.

sitive parameters describing the unspecific adsorption.

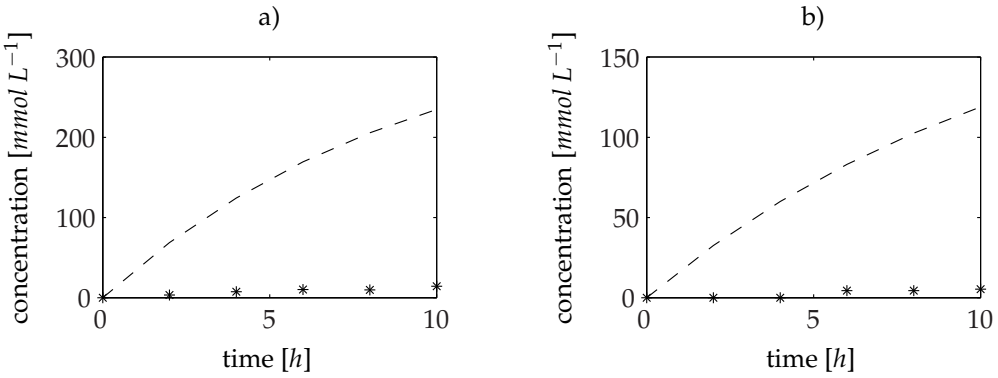

Figure 2.19: Comparison simulation and measurements high catalyst to substrate ratio.
a) $c_{0,butadiene} = 350\,mmol\,L^{-1}$, $c_{0,acrolein} = 380\,mmol\,L^{-1}$, $c_{catalyst} = 44\,mmol\,L^{-1}$; $c_{0,butadiene}/c_{0,acrolein} = 0.91$
b) $c_{0,butadiene} = 200\,mmol\,L^{-1}$, $c_{0,acrolein} = 230\,mmol\,L^{-1}$, $c_{catalyst} = 35\,mmol\,L^{-1}$; $c_{0,butadiene}/c_{0,Acrolein} = 0.87$

For model validation different other either mechanistic based[9] or pure black box models[10] have been tested, but no model could describe the reaction in a more convincing way.

2.7 Summary: The kinetics of the Diels-Alder reaction

An automatised method for the investigation of the kinetic of the polymer supported salen-chromium catalysed Diels-Alder reaction of acrolein and 1-methoxy-1,3-butadiene to form 2-methoxy-cyclohexene-carbaldehyde was successfully developed. The automatised liquid handling facilitated the simultaneous performance of five reactions with an automatised addition of the compounds, sampling and dilution. The scale of the reactions could be reduced to 200 μl saving the cost-intensive catalyst as well as starting materials. The time concentration plots were fitted to a mathematical model (symmetric random Eley-Rideal model). The model was simplified to predict the reaction progress with a single parameter for the rate-determining step of the formation of the product. The parameter k_{+3} was estimated to $2.4 * 10^{-3}\,L\,mmol^{-1}\,h^{-1}$ with a confidence interval of $\pm 1.6 * 10^{-4}\,L\,mmol^{-1}\,h^{-1}$. The model showed a good consistency with the measured data as long as the substrate concentrations were more than ten times higher than the catalyst concentration. At

[9] Langmuir-Hinshelwood kinetic based model as well as different bireaction model know from the enzyme kinetics, c.f. Segler 1993 [117].
[10] The black box model were inspired by the models presented in table 2.1.

higher catalyst to substrate ratios the predicted concentrations differed from the measurements. This could be explained by an unspecific adsorption of compounds onto the polymer. The observed acceleration of the reaction rate during the first hours of the reactoin may be explainable by an unspecific adsorption as well. In general, it could not be clearly stated that the reaction was a real homogeneous reaction. The catalyst was homogeneously soluble in the reaction system, but the reaction kinetics displayed also features of a heterogeneous reaction.

2.8 Continuous synthesis of 2-methoxy-cyclohexene-carbaldehyde

In the following the experimental implementation of the continuous synthesis of 2-methoxy-cyclohexene-carbaldehyde in a membrane reactor is presented. The materials and methods are described in detail in appendix A.

2.8.1 The chemical membrane reactor (CMR)

The reactor system for the performance of the continuous Diels-Alder synthesis must assure the retention of the catalyst as well as sufficient stability against the pressure, solvent and reagents. The reactor system used was a membrane reactor developed for the application of the biotransformation of free enzymes. Enzymes as optimised biocatalysts are retained in nature since its origin by means of membranes [106, 118]. Following the same strategy, the *enzyme membrane reactor (EMR)* was developed by Evonik Industries AG, formerly Degussa AG, and their partners, Wandrey and Kula, in the early 1980s [31]. In this concept, enzymes with a molecular weight in the range of 20000-200000 $g\,mol^{-1}$ are retained by an ultrafiltration membrane in a dead end filtration mode. An internal magnetic stirrer homogenises the reaction volume and reduces the concentration polarisation at the surface of the membrane and the accumulation of retained material on the membrane. This technology was introduced by Degussa AG for acylase process in 1981 and has been in production since then [32, 33]. The schematical drawning of the membrane reactor is shown in figure 2.20: it consists of a housing of steel and internal installations like a stirrer, a Teflon sinter supporting plate and Chemraz® sealings. The reaction volume is 10 ml.

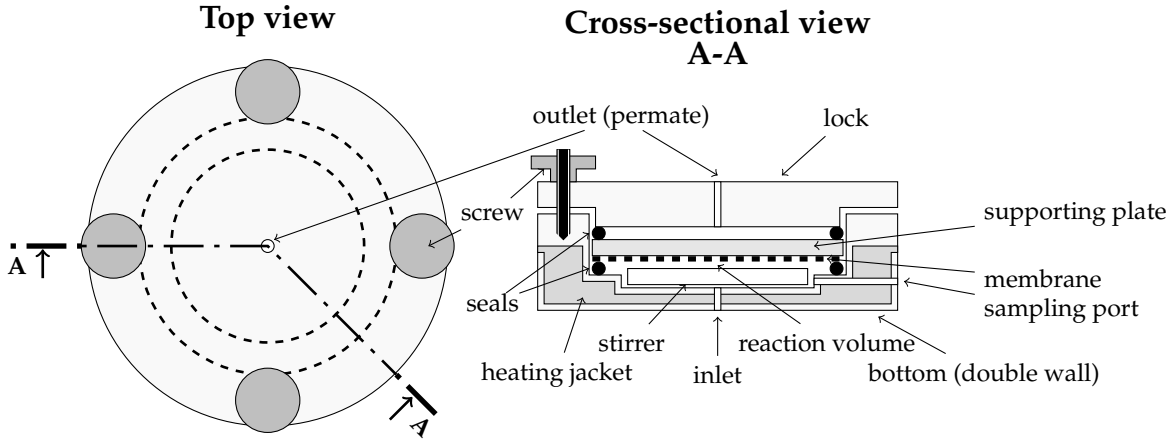

Figure 2.20: The membrane reactor

The EMR was also successfully applied to chemical catalysts bound to a polymeric backbone forming an enlarged molecular weight catalyst, so-called chemzyme (chap-

ter 1.3) [32, 119, 28]. Soon after the first report of binding a catalyst to a homogeneous backbone by Bayer and Mutter in the early 1970s [98], the concept of using soluble polymeric bound catalysts was reported [120]. Bayer and Schurig accomplished the separation of the soluble macro molecular catalyst from low-molecular products [120], which was the first application of the chemzyme-membrane reactor (CMR). But it took more then 20 years until the first successful continuous operation of a membrane reactor for a homogeneous reaction catalysed by a polymer supported chiral catalyst was reported [28]. Since then a growing numbers of illustrative reports [118, 121, 122, 123, 119, 34, 124, 125, 126, 127, 128, 32] related to CMR feature the importance of the topic.

The principle experimental set-up is shown in figure 2.21. The solvent (toluene) and substrates were stored in a fluid container, which was connected with the HPLC-pump to feed the reactor. The pump could be connected directly or via a by-pass with the reactor. The by-pass facilitated the opportunity to add catalyst (volume of 2 ml) during a continuous operation of the system. It was loaded with the help of a syringe and after a switch of the valves the volume of the loop is pumped into the reactor. The by-pass was realised with a manual sample injector of the company Rheodyne, which enables the switching of the valves with only a low pressure drop. The pump operated close to the minimum of its flow rate range ($< 0.6\,ml\,h^{-1}$ Range: $0.06 < flow\,rate < 600\,ml\,h^{-1}$) and only a low back pressure ($< 1\,bar$) could be established. Because of the low flow rates it was difficult to control the rate at its set point and the real residence times differed from the desired times. The calibration of the pump revealed that the real flow differed from the adjusted flow rate with an uncertainty of 10 %. Therefore the actual flow rate had to be verified gravimetrically during operation. The permeate was collected by the liquid handling robot in glass vials. Also the sample preparation for the analysis was performed by the robot. As membrane the membrane Starmem™ 120 of the supplier 'Membrane-Extraction-

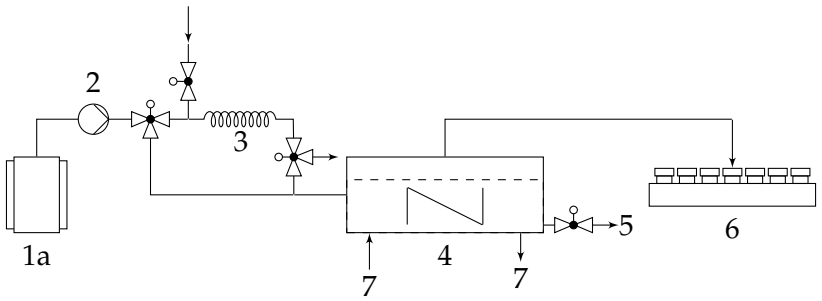

Figure 2.21: Schematically drawing of the membrane reactor set up: 1 thermostated container for toluene and reactants; 2 HPLC pump, 3 by-pass for catalyst injection, 4 membrane reactor, 5 retentate outlet, 6 automated sampling collector, 7 temperature control

Technology' was used. The membrane proved to be suitable for the retention of the polymer bound salen catalyst, while at the same time the solvent, reactants and product can pass the membrane [106, 118]. The cut-off is specified by the supplier with a MWCO of 200 $g\,mol^{-1}$ [11] and the stability of polyimide membrane in solvents like toluene and ethyl acetate is proven [129]. The unsupported salen ligand has a molar mass of around 260 $g\,mol^{-1}$ depending on the side chains. In principle the salen ligand can be retained by the membrane, but as it is visible in figure 1.6, a retention of around 90 % is not feasible for the operation of a continuous membrane reactor. The retention must be higher then 99 %, so that a polymer support is necessary to enlarge the molecule.

2.8.2 The Diels-Alder reaction in a continuously operated membrane reactor

The experimental procedure is described in appendix A.1.11. In this chapter mainly the results are discussed.

Investigated process factors were the reactant concentrations, the amount of catalyst and the residence time, c.f. 2.4. The residence times were estimated using the kinetic model, c.f. chapter 2.8.2. Due to the solubility of the catalyst the maximal concentration was set to 70 $mmol\,L^{-1}$ active centres. The longest residence time was determined by the lowest reasonable pump rate (0.2 $ml\,h^{-1}$). The residence times were chosen to cover the range over approximately 60 % conversion. To keep the number of factors manageable for each parameter – residence time and catalyst concentration – two values were investigated and combined (table 2.4).

The presented residence times are mean values and the total experiment period lasted 71 days, whereas after 43 days the membrane and catalyst were replaced. To increase the catalyst concentration from period **B** to **C** again 300 mg catalyst was added into the reaction during the operation via the by-pass. For the injection the flow rate was increased to reduce the time required to inject the catalyst and reduce the risk of a blockade by possibly precipitated catalyst. The injection of the catalyst was therefore associated with a new start-up phase. Before the experiment period **D** the reactor was flushed with toluene at the maximum pressure of 11 bar for 16 residence times, to remove substrates and product. Then the process was started again with a lower starting material concentration.

Before period **E** the membrane was replaced. The change of the membrane was only a measure of precaution. There existed no experiences in the long term stability of the membrane for this reaction system and the membrane was mounted and operated for more than one month. It was used for the purification of the catalyst as well as for the continuous operated reaction. Therefore it was decided to replace the membrane to reduce the risk of a failure of the second continuous operated mem-

[11] The MWCO is based on rejection of normal alkanes dissolved in toluene defined as MW for 90 % rejection [129].

experiment-period	number of residence times [-]	$c_{reactants}$ $[mmol\ L^{-1}]$	$c_{catalyst}$ $[mmol\ L^{-1}]$	residence time $[h]$	estimated conversion [%]
A	1 - 2	500	35	45	80
B	3 - 21	500	35	16	57
C	22 - 28	500	70	16	73
		flush with toluene			
D	29 - 44	250	70	16	73
		change of the membrane			
E	1 - 6	250	70	25	81
F	7 - 17	250	70	45	88

Table 2.4: Process factors of the continuous operated Diels-Alder reaction in order of application. The residence times are the measured and averaged residence times over the period, temperature 25°C

brane reactor experiment due to a loss of the membrane's integrity.

The total duration of the operation of the membrane reactor was limited by the amount of available butadiene, so that the experiment had to be stopped after 17 residence times in period F.

Estimation of residence times

The mass balance of the continuous operated membrane reactor can be described by the following equation:

$$\frac{d\,n_P}{d\,t} = r\,V_R - \dot{n}_P \tag{2.20}$$

The production of the product P is described by the reaction rate r and the amount of product leaving the reactor is specified in the mass balance by the molar flow of product P, $\dot{n}_P$, out of the reactor. The density can be set as constant and therefore equation 2.20 can be expressed as concentrations. With the introduction of the mean residence time, $\tau = \frac{V_R}{\dot{V}}$, the following equation is obtained:

$$\frac{d\,c_P}{d\,t} = 0 = r\ - \frac{c_P}{\tau} \tag{2.21}$$

When operating the continuously operated reactor at steady state the differential quotient can be set to zero. Introducing the rate equation 2.19 into 2.21 and by the substitution of the concentrations c_B and c_P with the relation in equation 2.22, assuming an initial concentration of P equal to zero and an equimolar ratio of the substrate con-

centrations, the conversion $U = \frac{c_{A,0}-c_A}{c_{A,0}}$ can be calculated as function of the kinetic parameters and the residence time.

$$\begin{array}{ll} (1) & c_B = c_{B,0} - c_{A,0} + c_A \\ (2) & c_P = c_{P,0} + c_{A,0} - c_A \end{array} \tag{2.22}$$

with: $c_{A,0}$, $c_{B,0}$ and $c_{P,0}$ inital concentrations

$$U = \frac{c_{C,0}\, k_3^+\, \tau}{c_{S,0}\, k_3^+\, \tau + 1} \tag{2.23}$$

The conversion as function of the residence time is presented in figure 2.22. The conversion is independent on the starting concentrations, but dependent on the catalyst concentration $c_{C,0}$, the residence time τ and the kinetic parameter k_3^+, while the dependency is equal for both parameters. Doubling the catalyst concentration has the same result as doubling the residence time. From the graph it is clearly visible, that residence times larger 45 h are necessary to yield conversions larger 70% at catalyst concentration of 30 $mmol\ L^{-1}$.

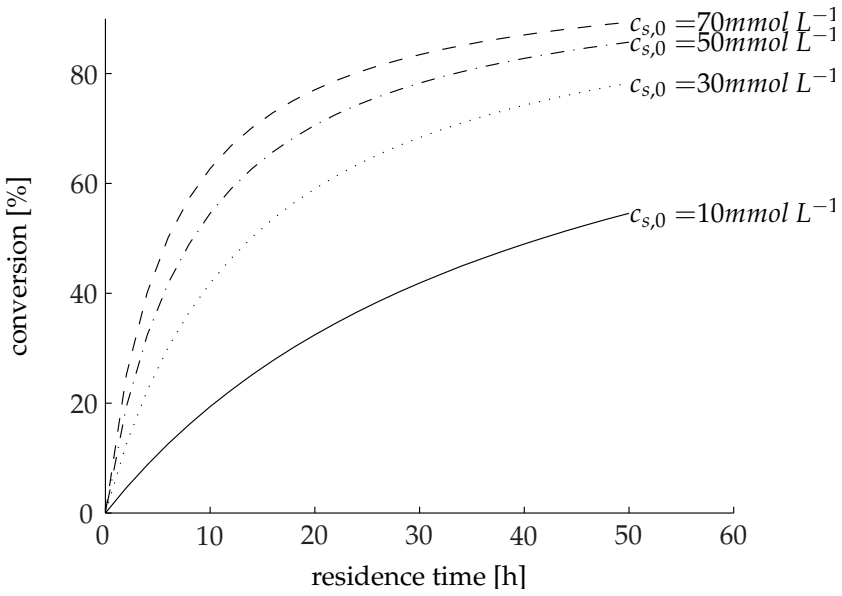

Figure 2.22: Estimation of the conversion as function of the residence time and catalyst concentration in a continously operated membrane reactor

Results: Continuous synthesis of 2-methoxy-cyclohexene-carbaldehyde

The described high retention [106, 118] could be already proven in the process of the catalyst purification. For example the dry mass of the permeate was measured with 0.02 g and the retentat with 0.76 g, consequential an apparent retention of 97 % can be calculated with respect to the fed material. The real retention for the polymer supported catalyst was therefore higher, because the solids in the permeate were mainly low molecular substances like free salen and chromium, which were washed out during purification. A recovery of 100 % of the polymer bound catalyst out of the membrane reactor was also difficult, because of the adhesion of the catalyst to the inner wall and internals of the reactor, so that the measured catalyst weight underestimated the retained catalyst.

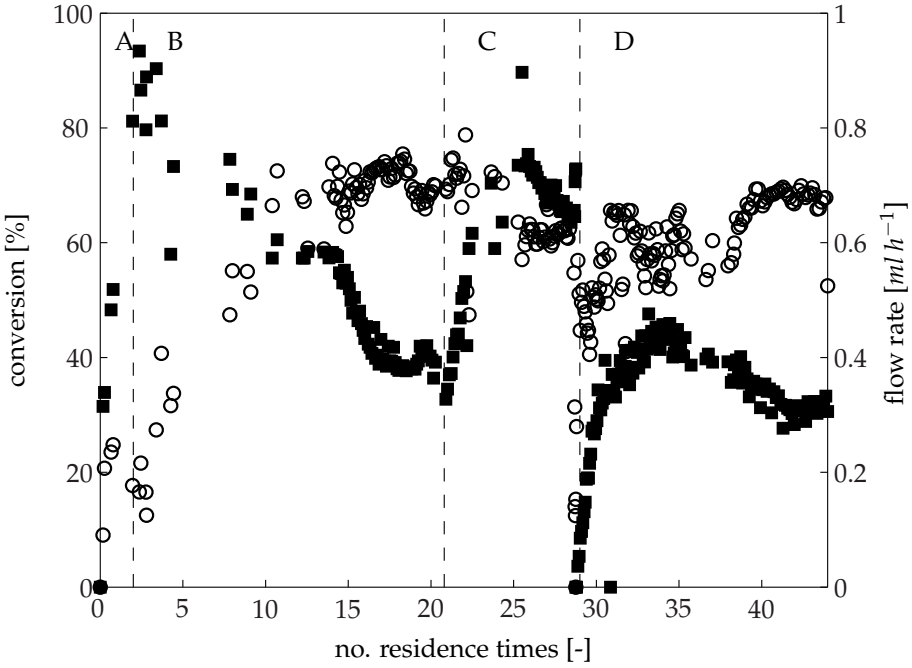

Figure 2.23: Continuous Diels-Alder reaction. Experiment period A to D; reaction conditions c.f. table 2.4; (■): conversion [%], (○): flow rate $[ml\,h^{-1}]$

During the continuous operated Diels-Alder reaction a maximum conversion of 90 % could be reached after only 2.5 residence times at the end of period **A**. c.f. figure 2.23, but this was still the initial phase and a steady state was not reached. It was difficult to controll the flow rate and the flow rate had to be adjusted step wise until the desired flow rate was reached, **B** in figure 2.23. As expected the conversion reduced to 40 %, increasing the flow rate to 0.7 $ml\,h^{-1}$, c.f. section **B**. An injection of 300 mg new catalyst after 22 residence times (**C**) – doubling the catalyst concentration – resulted in a doubling of the conversion to 80 %, which was slightly lower then

the maximum conversion at the doubled residence time in period **A**. At stationary flow rates the conversion decreased with time until the reactor was flushed with pure toluene just before period **D**. After washing with toluene and halving the substrate concentrations the conversion reached a level of 50 % and declined until the flow rate reached a stable value. The adjustment of the flow rate was a difficult task, so that fluctuation of more then 30 % was observed and the conversion followed the trend of the flow rate, but at the same time decreased over the operation time.

The larger variation of the concentrations documented during period **A** and **B** can be attributed to manual sampling, because the liquid handling robot was not available for sampling during that time. Consequently the sampling sequence was lower and the error higher due to, for example, the manual dilution of the samples.

After the membrane change the maximal conversion was reached in period **E** already after approximately three residence times, see figure 2.24. The measured conversion was with 85 % only slightly lower than the maximum conversion obtained during the first run, but in this case the residence was only half of the residence time in run one and the catalyst concentration was doubled.

The system showed only a low response to the reduction of the flow rate (F). The conversion slightly decreased from residence time 4 to 6 and with the flow rate reduction the value of the conversion increased again to the maximum conversion of 80 %. Also during this run the conversion declined with the number of residence times to a value of 65 % and the fluctuation of the flow rate was in the same range as for the first run.

2.8.3 Comparison of simulation and experimental data

The experimental data confirmed the estimated conversions. The conversion at a high residence time and low catalyst concentration, period **A**, was similar to the conversion at halved residence time and doubled catalyst concentration, period **C** and **E**. The lower conversion in period **C** might be caused by a washout of the catalyst. In figure 2.25 two measured conversions are compared with the kinetic model. There is a good consistency between the measurements and the predicton. This figure also offers the reason for the low increase of the conversion from period **E** to **F**: Based on the kinetic model the conversion increases only 8 % with the increasing residence time from 24 to 45 hours.

The determination of the acrolein concentration in the permeate of selected samples is presented in table 2.5. The experimental error in the determination of the acrolein concentration was high, because the acrolein had to be extracted with water before analysis and the extraction step was prone to errors. The error could not be specified more closely, because only a small number of samples was measured and the calibration curve was based only on two samples. But the measurements revealed that no major by-products were formed.

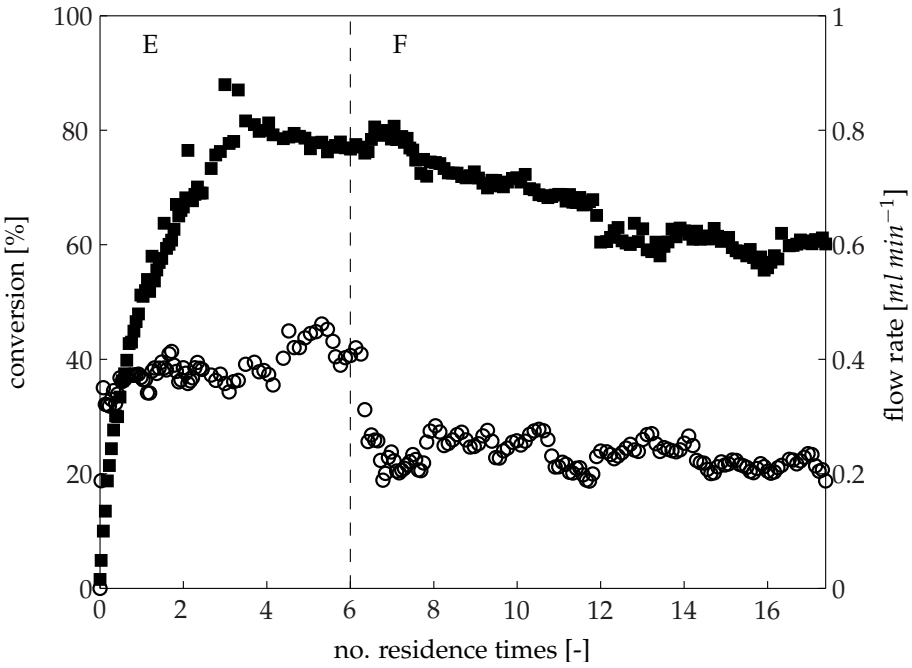

Figure 2.24: Continuous Diels-Alder reaction. Experiment period E and F; reaction conditions c.f. table 2.4; (■): conversion [%], (○): flow rate $[ml\,h^{-1}]$

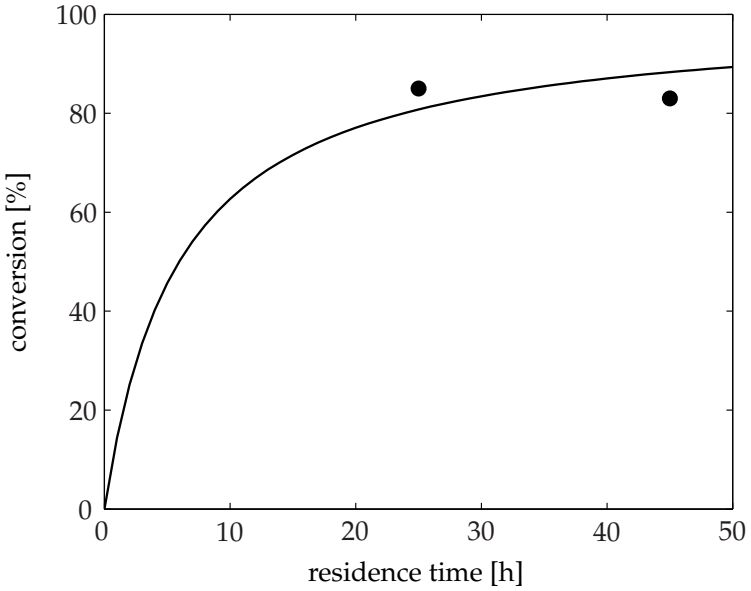

Figure 2.25: Simulation of model and continuous process;
$c_{0,butadiene} = c_{0,acrolein} = 0.25\,mol\,L^{-1}$, $c_{catalyst} = 70\,mmol\,L^{-1}$;
(-): kinetic model, (•): measurements

sampling time $[no.\,residence\,times]$	experimental period	$c_{product}$ $[mmol\,L^{-1}]$	$c_{acrolein}$ $[mmol\,L^{-1}]$
12	B	459	142
17	B	196	459
34	D	115	226
43	D	80	307

Table 2.5: Acrolein concentration in the permeate; feed concentrations: B, 500 $mmol\,L^{-1}$ and D, 250 $mmol\,L^{-1}$

2.8.4 Productivity, stability and retention

The productivity of the tested system was limited. The highest turnover frequency was observed at the 14th residence time in the experimental period **B** and add up to 0.6 h^{-1}, which corresponded to a space time yield of 0.5 $g\,L^{-1}\,d^{-1}$. The averaged turnover frequency for the fist run was 0.165 h^{-1} and for the second run 0.039 h^{-1}.

The total turnover number added up to 174 at the end of period **B**. Because of the increase of the applied catalyst the total turnover number was reduced and added up to 143 prior to the change of the membrane (end period **D**). The optimal catalyst concentration, according to the process condition and most of all according to the total running time of the membrane reactor, was overshoot by the increase of the catalyst concentration. The obtained calculated total turnover number was not the maximum turnover number of the catalyst, because the operation was interrupted. Longer operation times would have resulted in a higher total turnover number. It is to mention, that the interruption of the process was not due to any system based reason, however, the forcus was put on the evaluation of different process conditions. For the second run a total turnover number of 42 was obtained. But here again the process was stopped before the system showed major deficiencies in the activity of the catalyst.

The obtained productivity in the CMR was rather low when compared to the data given in literature. For example the investigation by Kragl et al. [28] showed a total turnover number of 500 and a deactivation of the catalyst could not be observed during the operation of the membrane reactor.

A reason explaining the reduced conversion with the ongoing operation got visible after opening the reactor after 44 residence times. In figure 2.26 a picture of the open reactor shows that considerable amounts of catalyst had accumulated on the membrane, inner walls and on the stirrer. The accessibility of the adhered catalyst for the reaction was reduced and the reaction was limited due to mass transport limitation into the precipitated catalyst. A precipitation of a polymer supported catalyst has been already observed by van Koten, Vogt et al. [130, 131, 132, 122]. In the Pd-catalysed hydrovinylation of styrene, which they performed in a continuous-flow

reactor, precipitation of catalyst in the reactor and on the surface of the membrane took place during the course of the reaction [99].

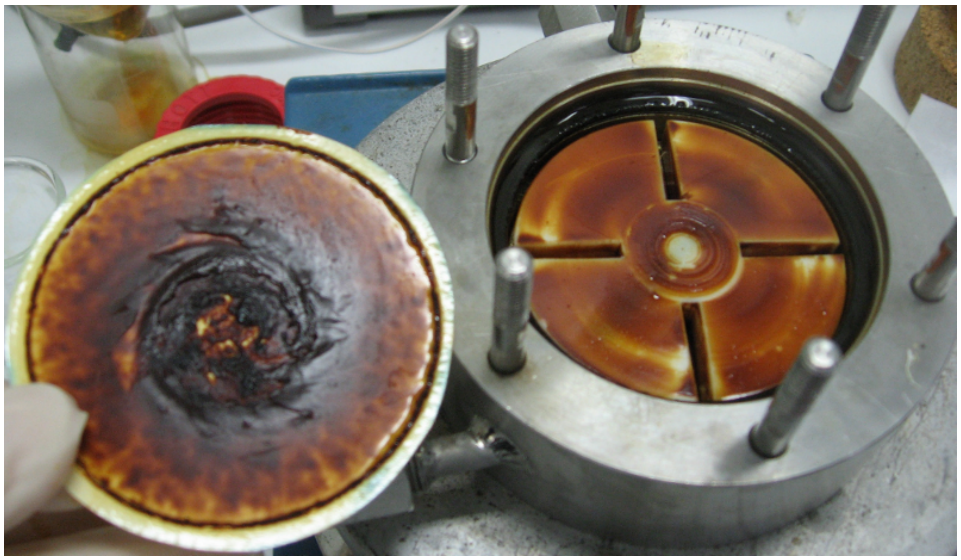

Figure 2.26: Adhesion of the catalyst to the membrane and internals in the membrane reactor after an operation time of 43 days (End period D); $c_{catalysis} = 70\,mmol\,L^{-1}$

Also after the second run precipitated catalyst was found on the membrane and the internals. The residue amount of catalyst could be quantified with 84 mg which was 14 % of the injected catalyst of 600 mg. The real retention of the catalyst under process conditions could not be quantified precisely, because the adhere catalyst could not be removed and collected totally from the membrane and the internals of the reactor so that a precise weighting of the retained catalyst was not possible.

A qualitative statement can be made due to the colouring of the samples. After the injection of purified catalyst after the experiment period **C**, the colour of the permeate changed form slightly yellow to brown (figure 2.27). Attempts to quantify the concentration of the catalyst in the permeates by light absorption were erroneous, so that it could not be used for the determination of the catalyst concentration in the permeate. The yellow colouring of the used diene interfered the measurement and the colouring differed in the different diene batches obtained from the supplier. But a significant influence of the different batches in the kinetic and continuous experiments could not be observed.

The colouring of the permeate especially directly after the injection of the catalyst indicated that the catalyst or chromium was washed out of the reactor. Metal leakage is a known phenomenon of organometallic catalyst and therefore it could be expected that the colouring was caused by the leakage of the chromium rather then the leakage of the polymer. Because the chromium is essential for the catalytic action the catalytic

action was reduced with ongoing metal loss, which could be observed during the experiments.

1 2

Figure 2.27: Colour change of the permeate due to catalyst injection, (1) $c_{catalyst,1} = 35\,mmol\,L^{-1}$ end of period B and (2) $c_{catalyst,1} = 70\,mmol\,L^{-1}$ after catalyst injection beginning of period C

2.8.5 Summary: The continuously operated membrane reactor

A homogeneously catalysed Diels-Alder reaction in a continuously operated membrane reactor could be performed for the first time. A maximum conversion of 80 % was measured and the diastereoselectivity matched the selectivity obtained in batch reactions. The long term stability, which was influenced significantly by the retention of the catalyst complex, was quite good over an operation period of 42 days, whereas the highest turnover frequency of 0.6 h^{-1} represented only a limited productivity. An issue concerning the applicability of the catalyst was the adhesion to surfaces and the precipitation of the catalyst. Also a leakage of metal was observed, which made a chromium capture step essential before further processing.

3 The enzyme catalysed synthesis of cyanohydrins

In the following chapter the investigation of the second reaction – the hydroxynitrile lyase (HNL) catalysed enantioselective hydrogen cyanide (HCN) addition to an aldehyde – is presented. Firstly an introduction about cyanohydrins and their synthesis is given. The focus is here on the enantioselective synthesis catalysed by the enzyme hydroxynitrile lyase. For a better understanding important fuundamentals like the immobilisation of an enzyme and its application in non-conventional reaction media are summarised.

Subsequently the kinetic model of the enzyme catalyse synthesis using the *Hb*HNL is described. The two experimental procedures, the initial rate measurement and the progress curve analysis, are compared. Here a focus is set on the calibration of a multi-wavelength photospectrometric system for the measurement of the concentration of the reactants, deriving a mathematical procedure joining the determination of the kinetic and the calibration parameters simultaneously. After that the immobilisation of the *Hb*HNL on different matrices is described, as well as their application in aqueous and non-conventional media. The question of a suitable organic solvent is tried to be solved. Then follows a discussion about the application of immobilised *Hb*HNL in a continuously operated membrane reactor to synthesise optical enriched cyanohydrins in a membrane reactor.

3.1 The syntheses of cyanohydrins

3.1.1 Syntheses of racemic cyanohydrins

Possible routes of the synthesis of cyanohydrin in the absence of chiral control are shown in figure 3.1. The addition of hydrogen cyanide to aldehydes or ketones produces hydroxy nitriles or cyanohydrins [133, 134, 135]. The actual nucleophile is the cyanide ion, as was demonstrated by Lapworth in 1903, who showed that the addition of bases increases the rate of reactions – one of the first organic mechanism elucidations [136, 45].

Today the direct addition of hydrogen cyanide is commonly used on industrial scale. Due to the high risk potential of pure hydrogen cyanide other methods are popular, particularly in a laboratory environment. A simple and relatively safe procedure is the use of cyanide in an acetic aqueous solution. Also alkali metal cyanides [137], acetone cyanohydrin [138, 139] and organoaluminium cyanides [140] are used in presence of bases or Lewis acids and the employment of trialkylsilyl

cyanides [141, 142], acyl cyanides [143] or alkyl cyanoformates [143, 144, 145] leads to the corresponding O-protected cyanohydrins.

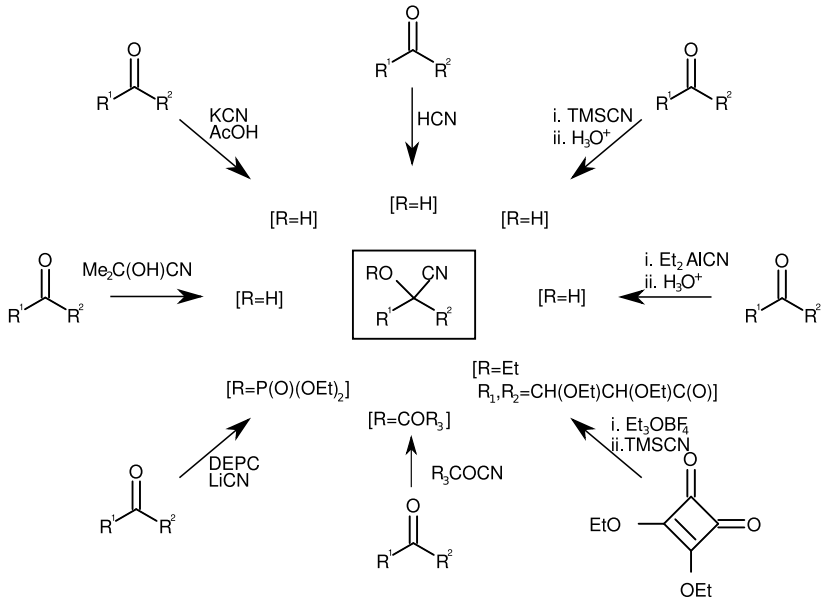

Figure 3.1: Methods of racemic hydrocyanation and cyanation of carbonyl compounds [45]

3.1.2 Enantioselective synthesis of cyanohydrins

As outlined in the introduction the synthesis of chiral cyanohydrins is of remarkable interest. The synthesis of enantiomerically enriched cyanohydrins may be accomplished in the presence of a chiral catalyst [44]. Three classes of chiral catalysts for the asymmetric addition of cyanide to carbonyl compounds are known: cyclic dipeptides, metal complexes and biocatalysts. The asymmetric addition of cyanide to carbonyl compounds catalysed by cyclic dipeptides or metal complexes are described elsewhere, for example [44]. The focus in this study is the biocatalyst approach for the enantioselective synthesis of cyanohydrins.

Enzymes of two different classes and two different reactions are known for the synthesis of non-racemic cyanohydrins:

- Lipase (EC 3.) (racemic cleavage) : *Candida antarctica* lipase A, *Candida antarctica* lipase B, lipase from *Pseudomonas cepacia* and others [44]
- Lyases (hydroxynitrile lyase or oxynitrilase (EC 4.)) (stereoselective synthesis): *Hb*HNL from *Hevea brasiliensis*, *Lu*HNL from *Linum usitatissimum*, *Me*HNL

from *Manihot esculenta*, *Pa*HNL from *Prunus amygdalus*, *Sb*HNL from *Sorghum bicolor* [77]

The use of lipase enzymes for the resolution of racemic cyanohydrins or the corresponding esters or transesterification of the latter with primary alcohols are a well established processes and have been applied to a variety of different α-hydroxy nitriles [44]. The drawback of a classic kinetic resolution strategy is the fact that only 50 % of the theoretical yield of the enantiomer of interest can be achieved, subsequently the target enantiomer has to be separated from the resolution product in a laborious process.

As outlined in the introduction, c.f. chapter 1.2.1, the asymmetric synthesis is the method of choice. No cost intensive separation of a racemate into its enantiomers is required and a low amount of asymmetric information – the asymmetric catalyst – is converted into a large quantity of chiral compounds [8]. Hydroxynitrile lyases are therefore the preferred catalyst, because they catalyse the stereoselective addition of hydrogen cyanide to an aldehyde or a keton. In nature the predominant function of the HNLs is the reverse reaction, the release of HCN as a vegetal defence mechanism against herbivores and microbial attacks. This cyanogenesis defence mechanism is common to higher plants, and enzymes from numerous plant source have been explored for their synthetic applicability, including the hydroxynitriles lyases from the rubber tree, almond, cassava and sorghum [89]. Several different cyanogenic glycosides have been identified, carrying aliphatic or aromatic cyanohydrins [43], that are released by the breakdown of the cyanogenic glycosides into a cyanohydrin and the conversion of cyanohydrin into an aldehyde or ketone hydrogen cyanide. The release of the HCN can occur spontaneously or is catalysed by the hydroxynitrile lyase [45]. The cyanogenic glycosides are used ultimately as a nitrogen source for the amino acid synthesis of young seedling tissues [45].

About 3000 plant species and a small number of other organisms are known to posses these enzymes [89]. Today four different HNLs are available on a large scale via fermentation. The origins, host microorganism and selectivity are presented in table 3.1.

Three different process concepts to perform HNL-catalysed cyanohydrin synthesis are described in literature: one liquid phase [42], organic/aqueous biphasic system [151, 152] and one organic phase with immobilised enzyme [153, 154, 155].

The process concept developed for industrial application is the organic/aqueous biphasic system. The focus of the development was to tailor the process to existing equipment that had been dedicated to the exclusive use with HCN – just a pot and a stirrer [89]. This concept fits better into the plant design for the production of specialities, like pharmaceuticals, fine and argo chemicals. Here multipurpose batch reactors can commonly be found.

From the kinetic point of view, the batch reaction mode is not the preferable mode. HCN and an aldehyde or a ketone react spontaneously uncatalysed in a second-order

natural source		recombinant source	chirality of cyanohydrin
Hevea brasiliensis	rubber tree leaves	*P. pastoris* *E.coli* *S. cerevisiae*	(*S*)
Manihot esculenta	cassava tissue	*E.coli* *P. pastoris*	(*S*)
Baliospermum montanum		*E.coli*	(*S*)
Linum usitatissimum	flax seedings	*P. pastoris*	(*R*)
Prunus amygdalus	almond	*P. pastoris*	(*R*)
Prunus mume	Japanese apricot ume	*P. pastoris*	(*R*)

Table 3.1: Recombinant HNLs, their sources and selectivity [89, 146, 147, 148, 149, 150]

reaction to form racemic cyanohydrin. The spontaneous reaction is slower at low HCN and aldehyde/keton concentrations. Characteristic features of a batch reaction are the high substrate concentrations at the beginning, favouring the formation of a racemic product. The spontaneous reaction can be suppressed when operating the reactor in a semi batch mode feeding the HCN and keeping the HCN concentration at a low level. A requirement for the reliable control of the feed rate is the on-line measurement of one of the reactants to determine the reaction progress. But a reliable measurement is difficult especially in a two phase reaction system. The spontaneous reaction can also be reduced by lowering the pH. The spontaneous reaction stopps at a pH of 3.5, but at such a low pH the enzyme is deactivated. Below pH 5 enzyme activity decreases drastically and at pH 3.5 only about 30 % activity is left after one hour [156]. If the biocatalyst stability is not of immense relevance the enzymes can be discarded after single use, but often the pize of the enzyme has a high impact on the economics of the process. Then a solution can be to uncouple the residence time of the catalyst form the residence time of the reactants. In a continuously operated membrane reactor the concentration of the HCN can be kept low, because the reactor can be operated at high conversions. Also the residence times are uncoupled retaining the catalyst with the membrane. Even though the operation of an organic/aqueous biphasic system in a continuous mode is technically possible the simpler system is an one liquid phase system. Due to the low solubility of the cyanohydrins in an aqueous solution and the required additional downstream process step to extract the cyanohydrins from the aqueous solution to gain the product, the focus in this study is the realisation of the enzyme catalysed synthesis in a purely organic solvent system (non-conventional reaction media). Because enzymes can not be used in purely organic system in their native form the enzymes have to be immobilised on a solid carrier.

3.2 Immobilisation of enzymes

An immobilised enzyme is stationarily bound to a small volume. The size and characteristic of the volume can differ depending on the type and definition of immobilisation. Immobilisation which is achieved by chemical/physical modification can be classified as follows:

- enclosing the enzyme in fibres and (gel)capsule
- covalently, inorganic or absorptive binding to a carrier
- crosslinking of the enzyme or co-crosslinking of the enzyme and a carrier to build a stable enzyme aggregate [157]

The characteristic volume for the immobilisation is small and can be in the case of enzyme aggregates as small as only a few enzyme molecules. Such a chemical/physical modification expands the spectrum of possible applications, because the modification is associated with the enlargement of the mean diameter. The realisation of continuous processes is simplified because of the easier separation of the catalyst. Depending on the size and density of the carriers packed or fluidised bed reactors can be realised. Particles can be suspended in the reaction medium to achieve a quasi homogeneous reaction. In this case the catalyst can be retained in the reactor by filtration or centrifuging.

An enhanced stability of the enzyme is often observed after a chemical/physical modification, but also the kinetic parameters of the enzyme can change. The modification is often accompanied by a loss of specific activity, because the enzyme are damaged during the process of modification. The flexibility of the enzyme is reduced due to forces between the matrix and the enzyme which can result in a higher stability or changed kinetic. Besides the direct impact of the matrix on the enzyme the micro-environment of the enzyme is changed, too. Figure 3.2 illustrates the micro-environment around the enzyme bound to a matrix. The boundary layer covering the surface on which the enzyme is bound has an important influence on the micro-environment. In the boundary layer the physical properties of the reaction media can differ from the bulk phase. For example matrices for binding enzymes have often a highly polar and ionic surface. The polarity and ionogenity of the matrix can lead to a change of pH compared to the bulk phase, it can change the netto-charge of the enzyme as well as the mass transport from the bulk phase thought the boundary layer to the enzyme. The phenomena are quite complex and influence each other so that it is difficult to describe and predict them. Therefore investigation of immobilisation is still a labintensive work. Immobilisation is often necessary for the application of the enzyme in an non-conventional reaction media.

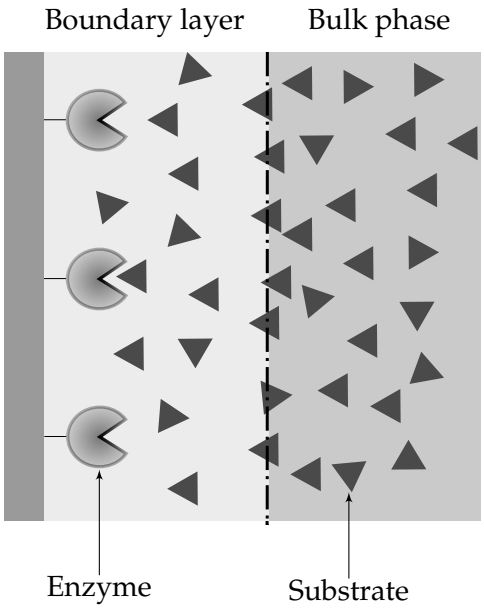

Figure 3.2: Boundary layer Enzyme

3.3 Non-conventional reaction media

When talking about non-conventional reaction media it has to be considered at first how a conventional reaction medium is characterised and which impacts these considerations have on non-conventional reaction media. Enzymes are found in all parts of the cell. Most of them are dissolved in the aqueous environment of which the cell consists, but some are associated to membranes. Amino acids – the protein's buildings blocks – with larger aliphatic side chains are hydrophobic, like methionine. The three-dimensional structure of water-soluble proteins is stabilised by the tendency of hydrophobic groups to cluster together, called the hydrophobic effect [23]. The protein folding proceeds spontaneously under appropriate conditions in the aqueous environment [23]. Hydrophilic amino acids are directed to the surface which is in contact with water, so that the surface of an enzyme is therefore hydrophilic. To some extent membrane associated proteins, like channel proteins, differ from water-soluble proteins because of the feature that the surface which is in contact with a lipid bilayer membrane shows a high distribution of nonpolar and uncharged amino acids. This hydrophobic areas allow the integration into the unpolar region of the bilayer. But all parts directed to the aqueous environment are mainly hydrophilic. Enzymes that are important in the biocatalysis are mainly water-soluble and therefore the natural (conventional) environment can be considered as aqueous and this environment has a big impact on the three-dimensional structures. Most biocatalytical processes are aqueous based processes using natural substrates imitating the natural environment

of the enzyme.

During the last three decades the conversion of unnatural substrates has come more and more in focus of research and industry. One drawback is that water is a poor solvent for nearly all reactants in organic chemistry, because most organic compounds are insoluble in this media [158]. To produce larger quantities of product huge liquid volumes have to be handled, which reduces the space time yield of the reaction and increases the cost and effort of the downstream process. One solution is the application of non-conventional reaction media increasing the solubility of the reactants and simplifying the downstream process, because the removal of water is tedious and expensive due to its high boiling point and high heat of vaporisation [158].

Systems called "non-conventional media" are characterised by the fact, that the major proportion of the reaction mixture is an organic liquid, a gas phase, a high-pressure supercritical fluid or ionic liquid [159, 160]. The common feature of nearly all non-conventional biocatalytic reaction systems is the presence of at least two distinct phases. One phase is usually a nonaqueous fluid. This acts as a reservoir for reactants and/or products but does not contain the biocatalyst [88]. This phase is most often an organic liquid mixture, based on an organic solvent and the reactants, but it may be a gas or a supercritical fluid as well. Another phase contains the biocatalyst. It can be a liquid phase, a dilute aqueous solution (organic/aqueous biphasic system) or a solid support material on which the biocatalyst is immobilised. Between these phases one or more interfaces are located. The properties of these interfaces can be very important for the kinetic behaviour of the system. Substrates and/or products have to cross the interfaces between the reservoir in the nonaqueous phase and the phase containing the catalyst. The contact of the biocatalyst with the interface can be an important mechanism of inactivation [161, 160].

3.3.1 Organic solvent systems

Most of the organic reactants are highly soluble in organic solvents. Thus the use of organic solvents for biocatalytic processes have been investigated for more than two decade [162, 163, 164, 165, 166, 167, 168]. Organic solvent systems can be classified into four groups: pure organic solvents, oil in water emulsions, water in oil emulsions, microemulsions/reverse micells.

Pure organic solvent systems

Due to its hydrophility an enzyme is not soluble in organic solvents. To suspend the enzymes in the organic phase they have to immobilised on a carrier or can be applied in lyophilised form. In the natural environment the hydrophilic groups such as -COOH, -OH, -NH_2, -SH and -$CONH_2$ become hydrated. As a consequence, the surface of an enzyme is covered by a layer of water, which is tightly bound and which

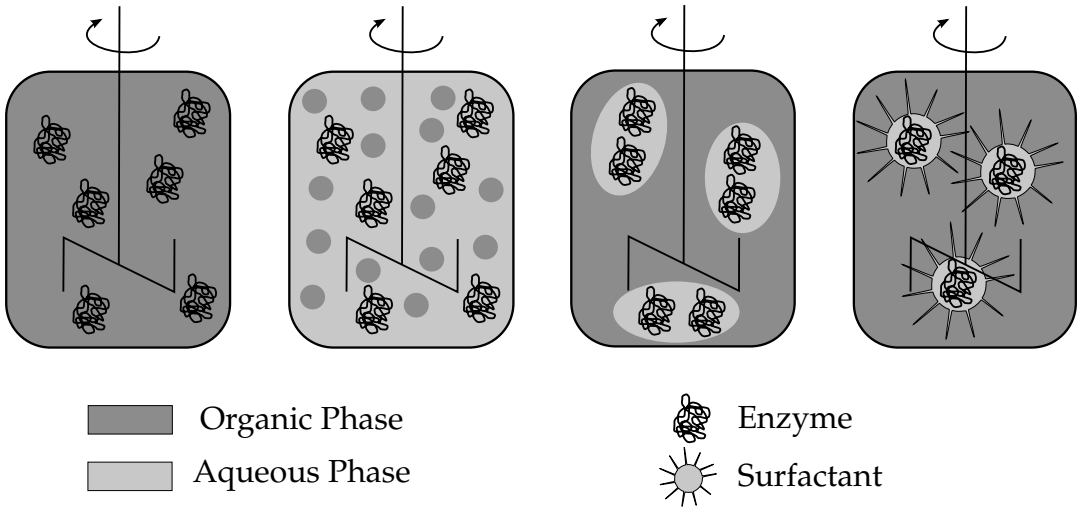

Figure 3.3: Classification of organic/water systems [29]

cannot be removed by lyophilisation [158]. This residual water, accounting for about 5-10 % of the total dry weight of a freeze-dried enzyme, is called *structural water* [169].

In most cases the purely organic solvent systems are not chemically pure. It is generally recognised that the small amount of remaining water is critical to the behaviour of biocatalysts used in mainly non-aqueous (e.g. organic) media [170]. Most biocatalysts are inactive if fully dehydrated, so that a small amount of water has to be present in the organic solvent. Some lipases are active in lyophilised form just containing the structural water, but others need water contents of several percent. The concentration of water in an organic medium should not be neglected, as it can affect both activity and selectivity [171]. The water content which is necessary to maintain the highest activity of the enzyme has to be evaluated independently for each reaction system [29]. The thermodynamic activity of water is probably the most convenient way of characterising the water content of such systems [172]. It differs for each enzyme and is influenced by the solvent and the immobilisation matrix. A systematic approach for the determination of the necessary water content does not yet exists [29]. To complicate matters further, the water content in the organic bulk phase is of less important, but rather the water content in the micro-environment of the enzyme. The hydrophilic structure of common immobilisation matrices bind the water to the surface where the hydrophilic enzyme is located and supplys the catalyst with the essential water. The water content or water activity on the surface is difficult to determine, but an important factor for the activity of the enzyme. Furthermore the water level will also affect the apparent equilibrium of the reaction [170]. Depending on the amount of water in the reaction system the transition of a purely organic solvent to an aqueous/organic two phase system is smoothly. With an increasing amount of water

an aqueous boundary layer is formed until a true aqueous phase emerges.

Aqueous/organic biphasic sytems

The enzyme is located in an aqueous/organic biphasic system in the water phase. The affinity of the product to the organic phase is used to separate the product from the catalyst. Depending on what the continuous (bulk) and the dispersed phase is, it can be distinguished between a water in oil emulsion or an oil in water emulsion, cf. figure 3.3. An emulsion is a mixture of two immiscible (unblendable) substances. To maintain a good distribution of the dispersed phase in the bulk phase high shear forces have to be applied. The mean diameter of the drops of the dispersed phase can be as small as 1 μm, but often the necessary power input to yield such small drops is immense and only a partial dispersion is established. Such emulsions are unstable and they tend to revert to the stable state of oil separated from water over time. The emulsion can be stabilised by the addition of surface active substances (surfactants). Surfactants reduce the surface tension at the phase border. They consist of a hydrophobic tail and a hydrophilic head and orientate according to the inter phase. The hydrophobic tail is in the organic phase and the head in the water phase, stabilising the interfacial area [29].

Special classes of emulsions are the microemulsion and reversible micelles. Microemulsions are emulsions with a very small dropsize diameter. Reversed micells are formed spontaneously when surfactants are dissolved in nonpolar organic solvents. Reversed micells are closed, almost spherical aggregates of surfactant molecules, 15-20 $\AA$ in diameter, the outer shell of which is formed by hydrophobic "tails" of surfactant molecules whereas the inner core is composed of polar heads of these molecules. An important property of reversed micells is their ability to solubilise considerable amounts of water (up to 70 water molecules per surfactant molecule) and other polar compounds [164]. Microemulsion and reverse micells are characterised by the thermodynamical stability of the drops and differing from other two phase systems the drops do not tend to coalescence. The interfacial area can be up to 100 $m^2\,ml^{-1}$ [29], featuring the mass transport over the phase border. The drawback of a stable emulsion is the more complicated downstream process. The separation of the product containing the organic phase from the catalyst containing aqueous phase is difficult. In most caser the complete separation of the two phases is in most cases not possible without damaging the catalyst, due to the small drop diameter. Often the surfactant cannot be separated totally from the product phase [173].

A crucial aspect of the application of purely organic solvents and biphasic systems in the biocatalysis is the selection of the appropriate solvent. As the occurrence of a liquid-liquid interface and the presence of residual amounts of organic solvent in water can lead to the deactivation of the biocatalyst, methods to guide the choice of the proper solvent have been proposed, such as the one reported by Brink and Tram-

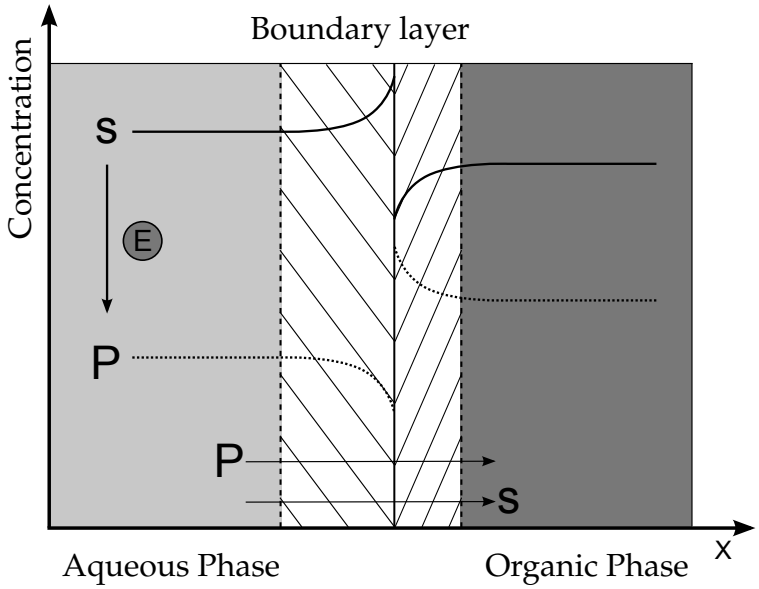

Figure 3.4: Concentration gradient at the phase border of an emulsion with a hydrophilic substrate S and a hydrophobic product P; reaction takes place in the aqueous phase [29]

per [162]. Laane et al. suggested using the polarity of solvents, expressed by the log P value [1], as the main criterion for optimising organic solvents in multi-liquid-phase biocatalysis [174]. This idea had a widespread influence on the choice of organic solvents used as the second phase in enzymatic transformations [156, 175]. An organic solvent with a log P value lower than 2 was considered as not suitable for biotransformation. But this relation cannot be generalised [29]. In other investigations organic solvents with a log P lower than 2 have successfully been used [156, 176, 177, 178]. Also on industrial scale organic solvents with a log P value lower than 2 are used for biocatalytic transformations [49].

The influence of the solvent depends on different factors so that no single factor can be used as decisive criterion. A satisfying systematic does not exist yet, but further investigations have to be undertaken, because the solvent is an important factor for the establishment of enzymatic processes in industry.

3.4 Production of hydrogen cyanide

Cyanides are highly reactive substrates that are used as catalysts in organic chemistry, in pigments, as ligands for transition metal complexes, and are important industrially

[1] The log P value is the logarithmic partition coefficient of a substance in a water/octanol biphasic system.

for extracting precious metals from ores and electroplating baths. [179]

Three different processes for the production of hydrogen cyanide are of industrial relevance:

- the Andrussaw process (equation 3.1)
- the Degussa process (equation 3.2)
- the Shawinigan (BASF) process (equation 3.3)

$$2\,CH_4 + 2\,NH_3 + 3\,O_2 \longrightarrow 2\,HCN + 6\,H_2 \tag{3.1}$$

$$CH_4 + NH_3 \longrightarrow HCN + 3\,H_2 \tag{3.2}$$

$$CH(O)NH_2 \longrightarrow HCN + H_2O \tag{3.3}$$

Small amounts of HCN can be produced by the addition of acids to cyanide salts of alkali metals In the laboratory, small amounts of HCN are produced by the addition of acids to cyanide salts of alkali metals:

$$H^+ + NaCN \longrightarrow HCN + Na^+ \tag{3.4}$$

In this study hydrogen cyanide was produced with the apparatus presented in figure 3.5. As HCN source cyanide salts has been used. A detailed description of the production and all precautions is given in the appendix A.2.4 and appendix C.

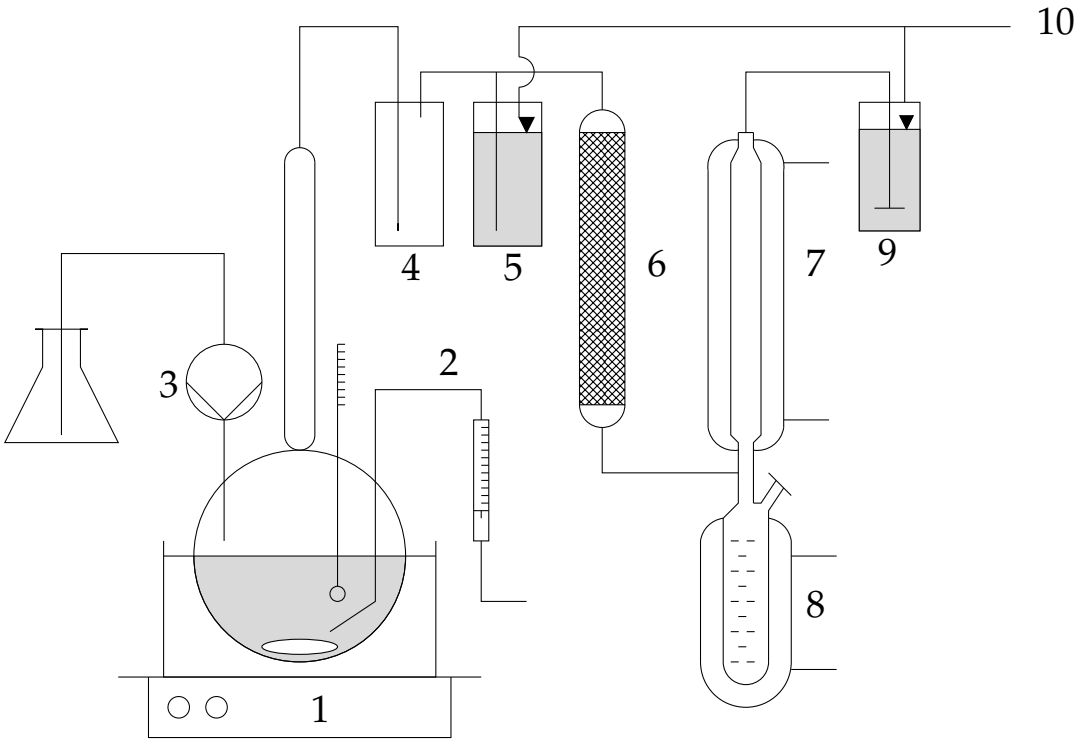

Figure 3.5: HCN production apparatus

No.	Constituents
1	temperature-controlled reaction vessel
2	N_2 gas inlet with pressure control
3	peristaltic pump
4	Gas wash bottle (safety bottle)
5	Pressure control valve
6	Drying column
7	Coil condenser (double walled)
8	Cryo trap
9	$NaOH$ gas wash bottle for HCN containing gases
10	Outlet cleaned gas

Table 3.2: Constituents of the HCN apparatus

3.5 Kinetics of the synthesis of optical active cyanohydrins catalysed by an enzyme

In the beginning of the 20th century the first general rate equation for reactions involving enzymes was derived by Henri [117]. It was based on the observation that the initial rate of an enzymatically catalysed reaction was directly proportional to the concentration of the enzyme, but increased in a non-linear manner with increasing substrate concentration c_S up to a limiting maximum rate v_{max}. Henri assumed a quasi-equilibrium also called rapid equilibrium assumption, of the enzyme, substrate and the enzyme-substrate (ES) complex. The overall rate of the reaction is limited by the breakdown of the ES-complex to the free enzyme and product. With the assumption that the reverse reaction is insignificant, the overall reaction is visualised as equation 3.5.

$$E + S \underset{k_{-1}}{\overset{k_{+1}}{\rightleftharpoons}} ES \overset{k_{+2}}{\rightarrow} E + P \tag{3.5}$$

In the year 1925 Michaelis and Menten confirmed Henri's experimental work and presented the rate equation 3.6 known as "Henri-Michaelis-Menten-equation."

$$\frac{v}{v_{max}} = \frac{c_S}{K_S + c_S} \tag{3.6}$$

here is $K_s = \frac{k_{-1}}{k_{+1}} = \frac{c_E\, c_S}{c_{ES}}$, which is the true dissociation constant of the enzyme-substrate complex. $v_{max} = k_{+2}\, c_{E,total}$ is the limiting maximal velocity, that can be observed, when all enzymes are present as enzyme-substrate complex where $c_{E,total} = c_{ES} + c_E$, the total concentration of the active sites [117].

Briggs and Haldane presented a more general approach in 1925 [180]. They did not assume an equilibrium but stated within a short time after starting the reaction in a batch reactor the enzyme-substrate complex would reach up to a near-constant or "steady-state" level. The concept of the "steady-state" was first proposed by Max Bodenstein in 1914 [25]. Accordimg to this principle ES will be formed after the initial pre-steady-state period at the same rate at which it decomposes. The steady-state level will be very close to the equilibrium level if the rate of equilibration is very rapid compared to the rate at which ES decomposes to E+P [117]. On the other hand if k_2 is comparable to k_{-1} or larger, then the steady-state level will be lower than the equilibrium level. The rate at which P is formed will be proportional to the steady-state concentration of ES.

From the reaction mechanism, equation 3.5, the rate equations derive as follows. The change of the concentrations of the substrate, product, enzyme and enzyme-substrate complex can be defined as the sum of the first or second order micro re-

action steps resulting in a set of differential equations, see equation 3.7 to 3.10

$$\frac{dc_S}{dt} = -k_{+1}\, c_S\, c_E + k_{-1}\, c_{ES} \tag{3.7}$$

$$\frac{dc_E}{dt} = -k_{+1}\, c_S\, c_E + (k_{-1} + k_{+2})\, c_{ES} \tag{3.8}$$

$$\frac{dc_{ES}}{dt} = k_1\, c_S\, c_E - (k_{-1} + k_2)\, c_{ES} \tag{3.9}$$

$$\frac{dc_P}{dt} = k_{+2}\, c_{ES} \tag{3.10}$$

The concentration of the total enzyme (active sites) is described by the relation

$$c_{E,total} = c_{ES} + c_E \tag{3.11}$$

Applying the steady-state concept the differentials of the enzyme-substrate complex, equation 3.9, as well as of the enzyme, equation 3.8, get zero ($\frac{dc_E}{dt} = \frac{dc_{ES}}{dt} = 0$). By the substitution of the unknown concentration c_{ES} and c_E in equation 3.7 or 3.10 the rate equations for the product P and the substrate S can be expressed as:

$$\frac{dc_P}{dt} = -\frac{dc_S}{dt} = k_{+2}\, c_{E,total} \frac{\frac{k_{+1}}{k_{-1}+k_{+2}}\, c_S}{1 + \frac{k_{+1}}{k_{-1}+k_{+2}}\, c_S} \tag{3.12}$$

With $\frac{k_{+1}}{k_{-1}+k_{+2}}$ and v_{max} the equation can be transformed into

$$\frac{v}{v_{max}} = \frac{c_S}{K_m + c_S} \tag{3.13}$$

The equation 3.13 is identical to equation 3.6 only that K_m, also called Michaelis constant, is a dynamic or pseudo-equilibrium expressing the actual steady-state concentration rather than equilibrium concentrations [117]. The equation 3.6 is a special case of the Briggs-Haldane steady-state treatment. When k_{+2} is very small compared to k_{-1} than $K_m \approx \frac{k_{-1}}{k_{+1}} \approx K_s$.

While the Henri-Mechaelis-Menten approach is limited to irreversible reactions the steady-state model can also be applied to a reversible reaction assuming not only an enzyme-substrate but also an enzyme-product complex. Such a reaction scheme is presented in equation 3.14.

$$E + S \underset{k_{-1}}{\overset{k_{+1}}{\rightleftharpoons}} ES \underset{k_{-2}}{\overset{k_{+2}}{\rightleftharpoons}} EP \underset{k_{-3}}{\overset{k_{+3}}{\rightleftharpoons}} E + P \tag{3.14}$$

After defining the integral balances for the concentrations of the components the unknown concentrations of the enzyme, enzyme-substrate and enzyme-product complex can be substituted applying the steady-state assumption and the rate equation can be derived [117].

3.5.1 Kinetic model describing the enzyme catalysed cleavage and synthesis of mandelonitrile

Bauer et al. proposed an ordered-uni-bi mechanism for the description of the *Hb*HNL catalyse cleavage/synthesis of mandelonitrile [176]. Because Bauer et al. did not have access to (*S*)- and (*R*)-mandelonitrile they used racemic mandelonitrile. To investigate the effects of the two enantiomers independently in this study the ordered-uni-bi mechanism was expanded with an additional inhibition by the (*R*)-mandelonitrile. The kinetic model consists of two parts: the enzyme and the uncatalysed reaction.

Kinetics of the enzyme catalyse reaction

The elementary reaction steps of the enzymatically catalysed reaction are shown in figure 3.6. It is assumed, that all reactions are reversible. The enzyme binds the benzaldehyde (BA) and builds the enzyme-benzaldehyde-complex (E-BA). The enzyme catalyses the formation of a C-C bound using hydrogen cyanide (HCN). The HCN is added catalyticly to the aldehyde forming a nitrile, the so called (*S*)-mandelonitrile. The formed enzyme-nitrile-complex (E-(*S*)-MN) decomposes again to the free enzyme and the (*S*)-mandelonitrile. Also (*R*)-mandelonitrile can binde to the catalystic centre forming the enzyme-nitrile-complex (E-(*R*)-MN). The (*R*)-mandelonitrile blocks the centre but is not catalytically cleaved to benzaldehyde and HCN. The mass balances describing the elementary reaction steps are presented in the equations 3.15 to 3.23.

Reactants[2]

$$\frac{dc_{BA}}{dt} = k_5 * c_{E-BA} - k_6 * c_E * c_{BA} \tag{3.15}$$

$$\frac{dc_{HCN}}{dt} = k_3 * c_{E-(S)-MN} - k_4 * c_{E-BA} * c_{HCN} \tag{3.16}$$

$$\frac{dc_{(S)-MN}}{dt} = k_2 * c_{E-(S)-MN} - k_1 * c_E * c_{(S)-MN} \tag{3.17}$$

$$\frac{dc_{(R)-MN}}{dt} = -k_7 * c_{(R)-MN} * c_E + k_8 * c_{E-(R)-MN} \tag{3.18}$$

$$\tag{3.19}$$

[2] Because the presented reaction model is based on the model published by Bauer et al [176] a similar nomenclature for the parameters is used.

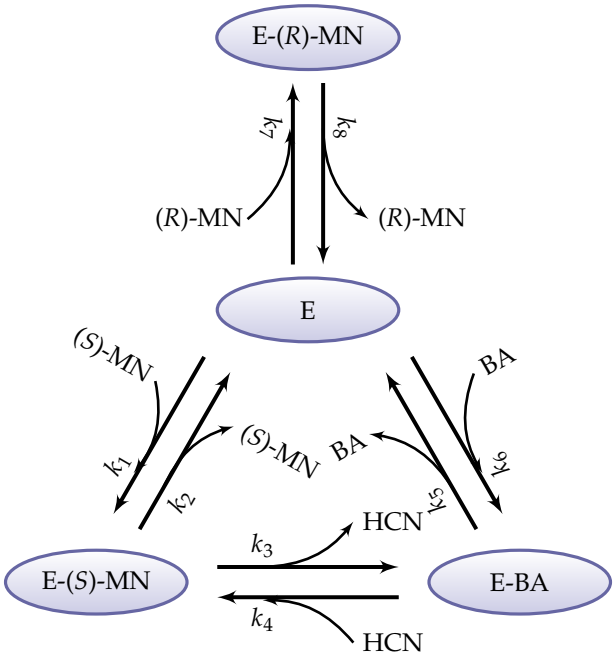

Figure 3.6: ordered-uni-bi mechanism with a competitive inhibition by (*R*)-mandelonitrile

Enzyme complexes

$$\begin{aligned}\frac{dc_E}{dt} =& k_2 * c_{E-(S)-MN} - k_1 * c_E * c_{(S)-MN} \\ & - k_6 * c_E * c_{BA} + k_5 * c_{E-BA} \\ & - k_7 * c_E * c_{(R)-MN} + k_8 * c_{E-(R)-MN}\end{aligned} \tag{3.20}$$

$$\begin{aligned}\frac{dc_{E-BA}}{dt} =& k_3 * c_{E-(S)-MN} - k_4 * c_{E-BA} * c_{HCN} \\ & + k_6 * c_E * c_{BA} - k_5 * c_{E-BA}\end{aligned} \tag{3.21}$$

$$\begin{aligned}\frac{dc_{E-(S)-MN}}{dt} =& - k_2 * c_{E-(S)-MN} + k_1 * c_E * c_{(S)-MN} \\ & + k_4 * c_{E-BA} * c_{HCN} - k_3 * c_{E-(S)-MN}\end{aligned} \tag{3.22}$$

$$\frac{dc_{E-(R)-MN}}{dt} = k_7 * c_E * c_{(R)-MN} - k_8 * c_{E-(R)-MN} \tag{3.23}$$

$$c_{E_0} = c_E + c_{E-BA} + c_{E-(S)-MN} + c_{E-(R)-MN} \tag{3.24}$$

c_{E_0} represents the concentration of catalytic sites. If one enzyme contains only one catalytic site per molecule, c_{E_0} equals the molar concentration of the enzyme.

With equation 3.24 and the steady-state assumption ($\frac{dc_E}{dt} = \frac{dc_{E-BA}}{dt} = \frac{dc_{E-(S)-MN}}{dt} = \frac{dc_{E-(R)-MN}}{dt} = 0$) the unknown concentration of the enzyme complexes in equations 3.15 to 3.18 can be replaced. The parameters k_1 to k_8 can be grouped as follows expressing the familar kinetic parameters according to the "Henri-Michaelis-Menten" equation 3.6 and 3.13, c.f. chapter 3.5.

$$v_{max_{cleavage}} = k_{cat_{cleavage}}\, c_{E_0} = \frac{k_3\, k_5}{(k_5 + k_3)}\, c_{E_0} \tag{3.25}$$

$$K_{m_{BA}} = \frac{k_2}{k_6} \tag{3.26}$$

$$K_{m_{HCN}} = \frac{k_3 + k_2}{k_4} \tag{3.27}$$

$$K_{m_{(S)-MN}} = \frac{(k_3 + k_2)\; k_5}{k_1\,(k_5 + k_3)} \tag{3.28}$$

$$v_{max_{synthesis}} = k_{cat_{synthesis}}\, c_{E_0} = k_2\, c_{E_0} \tag{3.29}$$

$$K_{i_{BA}} = \frac{k_5}{k_6} \tag{3.30}$$

$$K_{i_{HCN}} = \frac{(k_5 + k_3)}{k_4} \tag{3.31}$$

$$K_{i_{(S)-MN}} = \frac{k_2}{k_1} \tag{3.32}$$

$$K_{i_{(R)-MN}} = \frac{k_8}{k_7} \tag{3.33}$$

The rate equation for the change of the benzaldehyde concentration can be expressed according to equation 3.34.

$$v = \frac{d\, c_{BA}}{d\, t} = \frac{v_{max_{synthesis}} \left(\frac{v_{max_{cleavage}}\, K_{m_{HCN}}\, K_{i_{BA}}}{v_{max_{synthesis}}\, K_{m_{(S)-MN}}} c_{(S)-MN} - c_{BA}\, c_{HCN} \right)}{K_{m_{HCN}}\, K_{i_{BA}} + \frac{K_{m_{BA}}}{K_{i_{S-MN}}}\, K_{i_{HCN}}\, c_{(S)-MN} + K_{m_{BA}}\, c_{HCN} + \cdots} \tag{3.34}$$

$$\cdots + K_{m_{HCN}}\, c_{BA} + c_{BA}\, c_{HCN} + \frac{K_{m_{BA}}}{K_{i_{S-MN}}} c_{HCN}\, c_{(S)-MN} + \cdots$$

$$\cdots + \frac{K_{m_{HCN}}\, K_{i_{BA}}}{K_{i_{R-MN}}}\, c_{(R)-MN} + \frac{K_{m_{BA}}}{K_{i_{R-MN}}} c_{HCN}\, c_{(R)-MN}$$

Mathematical analysis

The mathematical analysis of the equation system reveals that the equations for the **four** process variables (equation 3.15 to 3.18) contain **four** unknown enzyme complexes and **eight** unknown kinetic parameters. For the derivation of the rate equation 3.34 **five** equations 3.20 to 3.24 were used.

	4	enzyme complexes		12	unknown parameters
+	8	kinetic parametes	-	5	equations
=	12	unknown parameters	=	7	**independent variables**

Nine parameters are described by the equations 3.25 to 3.33. These nine parameters are therefore not independent and two more dependencies can be formulated: The equilibrium constant K_{eq}, equation 3.35, and the Haldane, equation 3.36, for ordered-uni-bi mechanisms found by Straathof and Heijnen [181].

$$K_{eq} = \frac{k_1\, k_3\, k_5}{k_2\, k_4\, k_6} = \frac{v_{max_{cleavage}}\, K_{m_{BA}}\, K_{i_{HCN}}}{v_{max_{synthesis}}\, K_{i_{(S)-MN}}} = \frac{v_{max_{cleavage}}\, K_{m_{HCN}}\, K_{i_{BA}}}{v_{max_{synthesis}}\, K_{m_{(S)-MN}}} \tag{3.35}$$

$$\frac{K_{m_{(S)-MN}}}{K_{i_{(S)-MN}}} = 1 + \frac{v_{max_{cleavage}}}{v_{max_{synthesis}}} \left(1 - \frac{K_{m_{BA}}}{K_{i_{BA}}}\right) \tag{3.36}$$

The enzyme catalysed reaction can therefore be described by seven kinetic parameters. The parameters can be selected arbitrarily beside one rate determining parameter $v_{max_{synthesis}}$ or $v_{max_{cleavage}}$ and the parameter $K_{i_{(R)-MN}}$ describing the inhibition by (*R*)-mandelonitrile.

Kinetics of the uncatalysed reaction

The reaction rate of the uncatalysed racemic cleavage/synthesis of mandelonitrile can be described with the following reaction scheme:

$$\text{HCN} + \text{Benzaldehyde} \underset{k_{11}}{\overset{k_{10}}{\rightleftharpoons}} (R,S) - \text{Mandelonitrile} \tag{3.37}$$

The reaction rate for the change of the benzaldehyde concentration is described by:

$$r_{uncat} = \frac{d\, c_{BA}}{d\, t} = -v = \frac{d\, c_{MN}}{d\, t} = k_{10}\, c_{MN} - k_{11}\, c_{BA}\, c_{HCN} \tag{3.38}$$

The decomposition of racemic mandelonitrile follows a first order kinetics, whereas the formation obeys a second order kinetics.

The mass balances for the micro reaction steps including the uncatalysed reaction are presented in appendix A: equations A.7 to A.14. During the experiments the sum of the chemical and enzymatic reaction was observed. Hence, the reaction rate of the enzymatic reaction could be calculated according to equation 3.39 while the chemical reaction rate could be calculated according to equation 3.38.

$$r_{enzyme} = \left(\frac{d\, c_{BA}}{d\, t}\right)_{enzyme} = \left(\frac{d\, c_{BA}}{d\, t}\right)_{observed} - \left(\frac{d\, c_{BA}}{d\, t}\right)_{chemical} \tag{3.39}$$

3.6 Determination of the kinetic parameters

In this study the parameter of the elementary reaction steps were not determine, but the kinetic parameters of the rate equation 3.34. Two different strategies are followed for the determination of the kinetic parameters.

1. The initial rate measurements
2. The progress curve analysis

While the first strategy simplifies the reaction, by analysing only a small part of the progress curve, the second method uses the whole information presented in the progress curve.

3.6.1 Initial rate measurements

The classical approach for the determination of the kinetics of an enzymatic catalysed reaction is the measurement of the so called *initial reaction rate*. During an initial rate measurement the concentration of the target substrate is followed during the first course of the reaction. It is assumed that the change of the concentration is linear with the time over the observed measurement time, which means, that the reaction rate is constant. The reaction rate is expressed as the difference quotient:

$$r_{initial} = v_{initial} = \frac{\Delta c_S}{\Delta t} \tag{3.40}$$

Traditionally in enzyme kinetics the symbol v is used rather than the r used in chemical kinetics. In the following the symbol r is used for the reaction rate. The difference quotient is only an approximation of the real reaction rate, because the reaction rate is a function of the substrate concentration and the assumption is only valid under certain reaction conditions. In the case of an enzymatic reaction following the Michaelis-Menten kinetic, the reaction rate is marginally dependent on the substrate concentration if the concentration is much larger then the K_m value, because the reaction is a *zero-order kinetic*, c.f. chapter 3.5. But when the concentration is in the range of the K_m value the reaction rate is described by a *first-order kinetic* [117]. Here small changes in the substrate concentration influence the reaction rate, so that the reaction rate cannot be considered as constant. The initial reaction rate must be extrapolated to the time zero.

The idea of the initial rate measurements was developed in a time when the numerical power of modern computer systems was not yet available. The key feature of the method is the linearisation of the system to facilitate a simple visualisation of the dependency of the reaction rates. The big advantage is, that the influence of each substance can be analysed individually. For example, a reverse reaction can be assumed

as insignificant during the initial rate measurements, because over the observation time insignificant amounts of product are formed. Also different reaction patterns can be simply identified and analysed. For the determination of the kinetic parameters the measured reaction rates are plotted as function of the starting substrate concentration in a double reciprocal plot, the so called Lineweaver-Burk plot. The reaction rates, Michaelis and inhibition constants can be calculated from the slope and the interceptions with the x- and y-axes. Nowadays also determination by nonlinear regression methods are used and the calculated reaction rates are fitted to the rate equation.

Regardless of which method for the determination of the kinetics is used, one of the main drawbacks is the indispensable "human interpretation" of the raw data. The real initial rate of a reaction is often underestimated, because not enough measurement points are available to define the linear range of the reaction. This is especially true for fast reactions investigating them at substrate concentrations close to or lower than the K_m. The operator has to interpret the raw data and only apparent initial rates are measured rather than the real initial rate. If enzyme kinetic data are plotted in one of the linear transformations, drawing a line 'by eye' is necessarily subjective [182]. Also the determination of the kinetic parameter becomes more laborious the more parameters have to be investigated. By the statistic analysis of the significance of the obtained parameters only the variations of the calculated velocities to the linear curve in the Lineweaver-Burk plot are often considered. In the case of the nonlinear regression only the variations of the calculated velocities to the curve of the rate equation are considered. The uncertainty of the determination of the initial rates are excluded. The kinetic parameter presented in literature therefore show often a small confidence interval, which did not include the uncertainty of the experimental determination. The advantage of the initial measurements may be that the inhibition pattern can be evaluated graphically using (double) reciprocal plots (Lineweaver-Burk plot, Eadie-Hofstee-diagram, Hanes-Woolf plot).

The progress curve analysis can be an approach to overcome the limitations of the initial rate measurements using the numerical power of modern computer systems.

3.6.2 The progress curve analysis

Progress curve analysis is another approach for the investigation of enzyme kinetics [183, 184, 185, 186, 187, 188, 189, 182, 190, 191, 192]. In this approach the rate equations are not fitted to the initial rates but the integrated form of the rate equations is used to fit the progress curve. A much more difficult task is, however, the integration of this differential rate equation [189]. For simple kinetics like the Michaelis-Menten kinetics the analytic integrated form can be applied, but for more complex kinetics no analytic integrated form is know. For selected cases integrated equations or aproximation of the integrated equations have been published, but no general equations capable of being tailored to all specific cases have been described [189]. Due

to the computation power, which exists nowadays, the more straightforward procedure is the numerically integration of differential algebraic equations (DAEs) to fit the progress curves to measurements.

While the determination of the kinetics with initial rate measurements is a highly iterative method – step by step measurements under different reaction conditions –, the analysis of the progress curve is more straight forward. The progress curve analysis is initiated by a formulation of a possible model equation. After an experimental design follows the experimental part. The kinetic parameters are determined by an optimisation of the model parameters to find the best fit with the experimental values. Finally the model is validated with the help of statistic tools. In principle, progress curve studies can give the same sort of information as with initial rate measurements although there are some advantages and disadvantages using this method. The advantages can be summarised as follows [184, 193]:

- More of the available information is used, saving substrate, enzyme and time.
- The formation of pure products in the course of the reaction makes it possible to determine product inhibition without adding products, which is especially useful if they are expensive or not easily available.
- The data does not have be transformed (e.g. calculation of the initial rates, plotting the Lineweaver-Burk plot). The original distribution of the error is conserved.
- Additional information about the conversion per time and the enantiomeric excess can be obtained.

The main disadvantages are some error sources which cannot be specified as [193]:

- Inaccurate starting concentrations of enzyme or substrates.
- Enzyme inactivation during the course of the reaction.
- Side reactions may occur, e.g. non-enzymatic substrate conversion.
- Changes in the system properties, e.g. pH, temperature, evaporation of substrates or products.

For initial rate measurements the error sources are identical but with a different weighting. The accuracy of the concentrations of the enzyme and substrate are important for both methods. But the reaction time for initial rate measurements is chosen so short that the inactivation of the catalyst and influences of side reactions as well as changes in the system properties are less likely. A main drawback of the progress curve analysis is that much more mathematics have to be applied.

As a conclusion it can be said that the more straight forward way and the increased use of the power of modern computation systems makes progress curve analysis an effective tool to evaluate enzyme kinetics in shorter time with less experimental effort. But still the uncertainty of the experimental recording of the progress curves, for example the uncertainty of the calibration, is often not included in the statistical evaluation.

3.7 A mathematical procedure joining the determination of the kinetics and the calibration parameters in a simultaneous process

In the following a mathematical procedure is derived to join the determination of the kinetics and the calibration parameters simultaneously.

Calibration involves connecting one (or more) sets of variables with each other. Usually one set is a series of physical measurements, such as some spectra or molecular descriptors, and the other contains one or more parameters such as the concentration of a number of compounds or biological activity [194]. Calibration is an area of chemometrics and chemometrics is defined as:

> The chemical discipline that uses mathematical and statistical methods, (a) to design or select optimal measurement procedures and experiments, and (b) to provide maximum chemical information by analysing chemical data [194].

Calibration belongs to part (b) and is part of daily lab work. To establish the relationship between a measuring device and the units of measure, most of the analytics have to be calibrated, because often the desired unit of measure is not directly measurable. For example, for the measurement of the pH-value an ion-selective glass electrode is used. Depending on the H^+-ion-concentration a voltage emerges from the potential difference between a measurement and a reference electrode and this voltage is to a large extent directly proportional to the pH-value. The proportional factor as well as the point of origin of the voltage/pH-relationship are determined in a calibration measurement of at least two different operation points. For such a calibration precisely defined reference samples must be available The quality of the calibration depends strongly on the quality of the reference samples. Modern analytic methods allow the quantification of, for example, the concentrations of a mixture. The concentration determination of a mixture with chromatographic methods like High Pressure Liquid (HPLC) or Gas Chromatography (GC) is a standard routine in (bio)chemical laboratories and industrial processes. The calibration for such methods becomes more laborious the more compounds are to be analysed simultaneously. All reference samples of the compounds must be available and the peak area to concentration ratio must be determined for each individual compound.

Even more elaborated is the calibration of spectroscopic analytic methods involving multi-wavelength measurements, like UV-VIS-IR[3], Fourier transform infrared spectroscopy (FTIR), fluorescence and nuclear magnetic resonance (NMR) spectroscopy. The measured response of one substance is often not so clearly defined and is often not univariate like the retention time in a chromatographic method. Furthermore, the response can be strongly influenced by the concentrations of the other substances in the mixture. Then a multivariate calibration must be used. Using classical calibration approaches to measure the reference samples one by one at different concentrations and in combination with each other is time consumptive. Therefore new approachs must be developed to reduce the calibration efforts of such multi-dimensional analytic methods.

In the following the attempt to develop a method for a self calibration kinetic parameter determination by combining multi-wavelength UV spectroscopy, chemometrics and advanced optimisation algorithms is outlined. Firstly the theory of uni- and multivariate calibration is described, before the combination with an advanced optimisation algorithm is illustrated. After that the method is applied in different complexities for the determination of kinetic parameters of an enzymatic catalysed reaction of benzaldehyde and hydrogen cyanide forming enantioselective mandelonitrile.

3.7.1 Univariate calibration

Univariate (classical) calibration is the most used calibration approach and involves relating two single variables to each other and is often called linear regression. Such linear relations like the area to concentration relation in HPLC and GC analysis or absorption at a single wavelength to concentration relation in spectroscopic analysis are intensively used in daily lab work. Mathematically the straight-line model can be written as

$$y = b_0 + b_1 x + e \tag{3.41}$$

Here y is the dependent variable (for example the concentration of a single compound) and x the independent variable (for example the absorption at one wavelength), b_0 and b_1 are the model parameters describing the interception and the slope, respectively. The difference between measured and predicted data is the error e. A more generalised presentation is equation 3.42,

$$\boldsymbol{y} = \boldsymbol{X}\boldsymbol{b} + \boldsymbol{e} = \begin{pmatrix} y_1 \\ y_2 \\ \vdots \\ y_n \end{pmatrix} = \begin{pmatrix} 1 & x_1 \\ 1 & x_2 \\ \vdots & \vdots \\ 1 & x_n \end{pmatrix} \begin{pmatrix} b_0 \\ b_1 \end{pmatrix} + \begin{pmatrix} e_1 \\ e_2 \\ \vdots \\ e_n \end{pmatrix} \tag{3.42}$$

[3]UV: ultraviolet, VIS: visible, IR: infrared

where, in the simples case, $\boldsymbol{y}$ is a vector of the dependent variable consisting, for example, of the concentrations of one compound in a number of samples, and $\boldsymbol{X}$ the matrix of the independent variables, for example, the absorption at one specific wavelength. In the present case the parameter vector $\boldsymbol{b}$ consists of the straight-line equation of only two elements. The parameter elements in vector $\boldsymbol{b}$ are estimated on the basis of the *generalised inverse* by [195]:

$$\boldsymbol{b} = (\boldsymbol{X}^T\boldsymbol{X})^{-1}\boldsymbol{X}^T\boldsymbol{y} \tag{3.43}$$

Considering a new set of measurements $\hat{\boldsymbol{X}}$, the dependent variable $\hat{\boldsymbol{y}}$ can be predicted as follows:

$$\hat{\boldsymbol{y}} = \hat{\boldsymbol{X}}\boldsymbol{b} \tag{3.44}$$

The main assumption applying univariate calibration is, that the measured single response, the independent variable, is depending only on one factor, like the concentration of a single compound. Also it is to mention that this method is restricted to the measurement of a single component and, a maybe more important fact, this method does not include extra, and often complementary information, in the measured response. Some individual wavelengths in a spectra may be influenced by noise or unknown interferences. To overcome these drawbacks multivariate calibration methods can be applied.

3.7.2 Multivariate calibration

In the case of multivariate modeling several independent as well as several dependent variables may operate [195]. The three most important regression methods are:

- Multi linear least squares regression (MLR)
- Principal component regression (PCR)
- Partial least squares regression (PLS)

The multi linear least squares regression

Multi linear least squares regression (MLR) is the expansion of the univariate straight-line model, c.f. 3.7.1. The general-least-squares problem that relates a matrix of dependent variable Y to a matrix of independent variables X can be stated as follows:

$$\begin{pmatrix} y_{11} & y_{12} & \cdots & y_{1m} \\ y_{21} & y_{22} & \cdots & y_{2m} \\ \vdots & \vdots & \ddots & \vdots \\ y_{n1} & y_{n1} & \cdots & y_{nm} \end{pmatrix} =$$

$$\begin{pmatrix} x_{11} & x_{12} & \cdots & x_{1m} \\ x_{21} & x_{22} & \cdots & x_{2m} \\ \vdots & \vdots & \ddots & \vdots \\ x_{n1} & x_{n1} & \cdots & x_{nm} \end{pmatrix} \begin{pmatrix} b_{11} & b_{12} & \cdots & b_{1m} \\ b_{21} & b_{22} & \cdots & b_{2m} \\ \vdots & \vdots & \ddots & \vdots \\ b_{n1} & b_{n1} & \cdots & b_{nm} \end{pmatrix} + \begin{pmatrix} e_{11} & e_{12} & \cdots & e_{1m} \\ e_{21} & e_{22} & \cdots & e_{2m} \\ \vdots & \vdots & \ddots & \vdots \\ e_{n1} & e_{n1} & \cdots & e_{nm} \end{pmatrix} \tag{3.45}$$

In matrix notation we get:

$$\boldsymbol{Y} = \boldsymbol{X}\boldsymbol{B} + \boldsymbol{E} \tag{3.46}$$

The error matrix $\boldsymbol{E}$ represents the difference between measured and predicted data. Any estimation of the regression parameters $\boldsymbol{B}$ can be done in the same way as for univariate straight-line model by the *generalized inverse*. $\boldsymbol{B}$ is given by:

$$\boldsymbol{B} = (\boldsymbol{X}^T\boldsymbol{X})^{-1}\boldsymbol{X}^T\boldsymbol{Y} \tag{3.47}$$

Typical procedures to solve the multi linear least squares regression problem, equation 3.46 and 3.47, respectively, are Gaussian elimination or Gauss-Jardan elimination. More efficient solutions are based on the decomposition of the $\boldsymbol{X}$ matrix by algorithms, such as LU decomposition, Householder reduction, or one of the most powerful methods, singular value decomposition (SVD) [195].

For the prediction of a new set of dependent variable $\hat{\boldsymbol{Y}}$ from a measurement $\hat{\boldsymbol{X}}$ equation 3.48 is used.

$$\hat{\boldsymbol{Y}} = \hat{\boldsymbol{X}}\boldsymbol{B} \tag{3.48}$$

MLR based methods have the disadvantage that all significant components must be known [194]. The identification of all significant components can be time-consuming and error-prone. Another important aspect is that MLR based methods are sensitive to noise [195]. A method for multivariate calibration identifying the significant components is the principal component regression.

The principal component regression

Principal component regression (PCR) is best performed by means of singular-value decomposition (SVD). With this method, the matrix $\boldsymbol{X}$ is decomposed into two or-

thonormal matrices $\boldsymbol{U}$ and $\boldsymbol{V}$, that are joined by a diagonal matrix $\boldsymbol{W}$

$$\boldsymbol{X} = \boldsymbol{U}\boldsymbol{W}\boldsymbol{P}^T = \boldsymbol{T}\boldsymbol{P}^T \tag{3.49}$$

where $\boldsymbol{X}$ is the original data matrix consisting of n rows (objects) and p columns (features); The matrix $\boldsymbol{T} = \boldsymbol{U}\boldsymbol{W}$ is called the *score matrix* with n rows and d columns (number of principal components [PCs]) and $\boldsymbol{P}$ is the the *loading matrix* with d columns and p rows [195].

PCA may be considered a tool for discovering structures in multivariate data, in particular for the purpose of reducing the dimensionality. PCA, in effect, takes a cloud of data points and rotates and projects it onto a space of lower dimension, selecting the directions in the data space with maximum variability (highest information). The number of principal components reflects the dimensions of the new subspace. By increasing the dimensions of the subspace more information of the original data is incorporated into the model. The first principal component shows the major variation within the $\boldsymbol{X}$ variables, the second principal component shows the next one in line on the magnitude of variance and so on. For example the first PC is related to the concentration of the main compound. Higher PCs are related to other compounds, temperature, pH shifts or noise, whose can have an impact on the original data .

Now for regression the data set transformed and in dimension reduced (the score matrix $\boldsymbol{T}$) is used and the score matrix $\boldsymbol{T}$ can be related to the dependent variables $\boldsymbol{Y}$ as follows:

$$\boldsymbol{Y} = \boldsymbol{T}\boldsymbol{C} + \boldsymbol{E} \tag{3.50}$$

where $\boldsymbol{C}$ is the matrix of the regression parameters, which can be calculated according to equation 3.51.

$$\boldsymbol{C} = (\boldsymbol{T}^T\boldsymbol{T})^{-1}\boldsymbol{T}^T\boldsymbol{Y} \tag{3.51}$$

The comparison of equations 3.51 and 3.47 shows the similarity between the MLR and PCR method. The main difference is that the MLR method uses the original data matrix $\boldsymbol{X}$ for regression, while the PCR method extracts the underlying effects in the $\boldsymbol{X}$ data for building the $\boldsymbol{T}$ matrix. Using PCR only independent effects are consider and low-variance noise effects can be excluded. This can improve the quality of the model significantly [195]. The prediction of dependent variables $\hat{\boldsymbol{Y}}$ in a new set of measurements is done by equation 3.52. The matrix $\boldsymbol{P}\boldsymbol{C}$ is called the regression matrix and may be compared to the $\boldsymbol{B}$ matrix of MLR.

$$\hat{\boldsymbol{Y}} = \hat{\boldsymbol{X}}\boldsymbol{P}\boldsymbol{C} \tag{3.52}$$

PCR methods only analyse the variance of the $\boldsymbol{X}$ data and rotate and transform the $\boldsymbol{X}$ data to find the major variance in the $\boldsymbol{X}$ data. But the major variance in $\boldsymbol{X}$ does not need to correlate with the dependent variables $\boldsymbol{Y}$. This can be, when the relevant

underlying effects are small in comparison to any irrelevant ones. Then they may not appear among the first few principal components and the selection of the used PC can be difficult.

Partial least squares regression (PLS) solves this problem. Here the covariance between the $\boldsymbol{X}$ data and the dependent variables $\boldsymbol{Y}$ is maximised.

The partial least squares regression (PLS)

While PCR and MLR methods perform the decomposition of the $\boldsymbol{X}$ matrix independently of the dependent variables $\boldsymbol{Y}$, a method using the information from the $\boldsymbol{Y}$ matrix is the Partial Least Squares Regression (PLS) algorithm. Each PLS latent variable direction of the $\boldsymbol{X}$ matrix is modified so that the covariance between itself and the $\boldsymbol{Y}$ matrix is maximised [195]. Both the $\boldsymbol{X}$ and $\boldsymbol{Y}$ matrices are decomposed into smaller matrices according to the equations 3.53 and 3.53.

$$\boldsymbol{X} = \boldsymbol{T}\boldsymbol{P}^T + \boldsymbol{E} \tag{3.53}$$

$$\boldsymbol{Y} = \boldsymbol{U}\boldsymbol{Q}^T + \boldsymbol{F} \tag{3.54}$$

By analogy with PCA the $\boldsymbol{T}$ and $\boldsymbol{U}$ are the score matrices and $\boldsymbol{P}$ the loading matrix of the $\boldsymbol{X}$, $\boldsymbol{E}$ is the error matrix of the $\boldsymbol{X}$ matrix, $\boldsymbol{Q}$ is the loading matrix of the $\boldsymbol{Y}$, and $\boldsymbol{F}$ is the error matrix of the $\boldsymbol{Y}$ matrix. Equations 3.53 and 3.54 are linked by the inner relationship:

$$\boldsymbol{U} = \boldsymbol{T}\boldsymbol{B} \tag{3.55}$$

The matrix $\boldsymbol{B}$ holds the regression coefficients from which the scores in the Y-space ($\boldsymbol{U}$) are estimated from the scores in the X-space ($\boldsymbol{T}$)[4]. A new set of dependent variables $\widehat{\boldsymbol{Y}}$ is estimated by:

$$\widehat{\boldsymbol{Y}} = \widehat{\boldsymbol{T}}\boldsymbol{B}\boldsymbol{Q}^T = \widehat{\boldsymbol{X}}\boldsymbol{R} \tag{3.56}$$

where the regression matrix $\boldsymbol{R}$ is defined as $\boldsymbol{R} = \boldsymbol{W}\left(\boldsymbol{P}^\top\boldsymbol{W}\right)^{-1}\boldsymbol{Q}^\top$. $\boldsymbol{W}$ is the weight matrix of the PLS weights [195].

The *N-Way* toolbox for MATLAB© is a freely available collection of functions and algorithms for modelling multiway data sets by a range of multilinear models. Several types of models are covered: canonical decomposition-parallel factor analysis (CANDECOMP-PARAFAC), multilinear partial least-squares regression (PLSR), generalised rank annihilation method (GRAM), direct trilinear decomposition (DTLD) and the class of Tucker models [196]. Beside this it offers functions for preprocession data like scaling and centering. The multiway regression method called N-way partial least squares (N-PLS) has been developed by Rasmus Bro 1996 [197]. The developed algorithm is superior to unfolding methods, primarily owing to a stabilisation of

[4] c.f. the npls help function of the *N-way* toolbox [196]

the decomposition. This stabilisation potentially leads to an increased interpretability and better predictions and the algorithm is fast compared with e.g. PARAFAC [197].

3.7.3 The optimisation strategies

The second aspect in joining the determination of the kinetics and the calibration parameters, is the determination of the kinetic parameters. The determination of the kinetic parameters to fit a model to experimental data is called *optimisation*. For optimisation different strategies have been developed over the last centuries. Probably the best know strategy is the *least squares regression method*, which Johann Carl Friedrich Gauß published 1809 in the second volume of his publication: *Theoria motus corporum coelestium in sectionibus conicis solem ambientium* [198]. The sum of squared residuals is defined as:

$$\min_{\vec{x}} \sum_{i=1}^{n} (y_m - y_i)^2. \tag{3.57}$$

$y_m - y_i$ describe the difference of the values of the model function y_m and the measured y_i value. The best fit is that instance of the model for which the sum of squared residual has its least value (global minimum).

Well known least squares regression algorithms solving nonlinear data-fitting problems are the interior-reflective Newton, the Levenberg-Marquardt and the Gauss-Newton method [199].

In general it can be distinguished between so called local and global optimisation. Often an optimisation problem has several local minima. A directed search strategy, like the algorithms mentioned, starts at initials values and finds the local minimum close to the initial values rather than the global minimum. Hence the results are strongly dependent on the initial values, which is a common drawback of directed optimisation strategies.

A strategy which enhances the chance to find the global optima are the evolutionary algorithms, the so called genetic algorithms.

The genetic algorithms

Genetic algorithms are a method for solving both constrained and unconstrained optimisation problems. It is based on natural selection, the process that drives biological evolution. The principle of evolution was first transferredto the world of modern computing by Alex S. Fraser [41]. The genetic algorithm repeatedly modifies a population of individual solutions. At each step, the genetic algorithm selects at random individuals from the current population to be parents and uses them to produce the children for the next generation. Over successive generations the population “evolves” towards an optimal solution. One can apply the genetic algorithm to solve a variety of optimisation problems that are not well suited for

standard optimisation algorithms, including problems in which the objective function is discontinuous, non-differentiable, stochastic, or highly nonlinear [200]. The genetic algorithms have become meanwhile an excepted tool in the optimisation of process conditions for example of a fermentative production of different compounds [201, 202, 203, 204, 205, 206, 84, 207, 208].

The optimisation strategy used in this study is always a combination of a genetic algorithm (`ga`) followed by a nonlinear least-squares solver (`lsqnonlin`; interior-reflective Newton method). Combining both optimisation strategies allows to search a huge space of parameters using the genetic algorithm and to refine the solution with the nonlinear least-squares solver in an effective manner.

3.7.4 How to join the determination of the kinetics and the calibration parameters

The calibration of the analytic is a crucial step for the determination of kinetic parameters and the quality of the parameters is strongly influenced by the quality of the calibration. In 2002 Solle and coworkers outlined a strategy to combine the determination of kinetic parameters, describing the growth of a yeast, and the calibration of a 2D-fluorescence measurement [84]. In figure 3.7 the principle program scheme is presented.

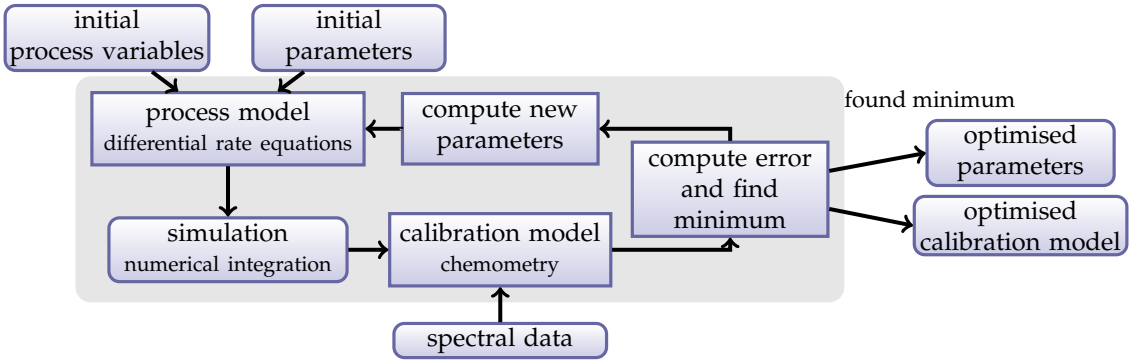

Figure 3.7: The principle program schema combining parameter optimisation and calibration according to Solle and coworkers [84]

The main difference between this strategy to a conventional optimisation is, that the estimation of the parameters for the calibration model is incorporated into optimisation algorithms. This strategy enables the performance of a calibration procedure without any further measurements [84]. The prior knowledge of the process is used and a mathematical differential process model is assumed. This differential model is used to simulate the process and the calibration is performed based on the simulation, correlating the simulation with the raw data (spectral data). Solle and coworkers [84] used the partial least squares regression for correlation, but linear uni- or multivariate calibration models can also be applied, depending on the type of measurement. Then

the calibration is used to predict the variables of the process from the raw data. The quality function – the sum of squared residuals – is calculated as the residual of the predicted and simulated values. The parameter of the simulation is varied, so that the sum of the residuals is minimised, which means, that the calibration correlated with the raw data and the simulation in the best way.

Solle and coworkers [84] showed that they could determine the parameters of a process model describing the glucose, ethanol and the biomass concentration of a yeast fermentation and simultaneously obtain calibration models for a 2D-fluorescence measurement for the measurement of the three concentrations.

As a possible error source the starting concentrations of the reactants have been identified for the fitting the model to a progress curve. When measurements of the initial conditions are available this information can be used for the prediction of accurate starting concentrations. This prediction can also be integrated in the scheme presented in figure 3.7. In figure 3.8 the principle program schema is shown combining parameter optimisation, calibration and estimation of the initial process variables. Supplementary to the inner loop for optimisation of the process parameters the pro-

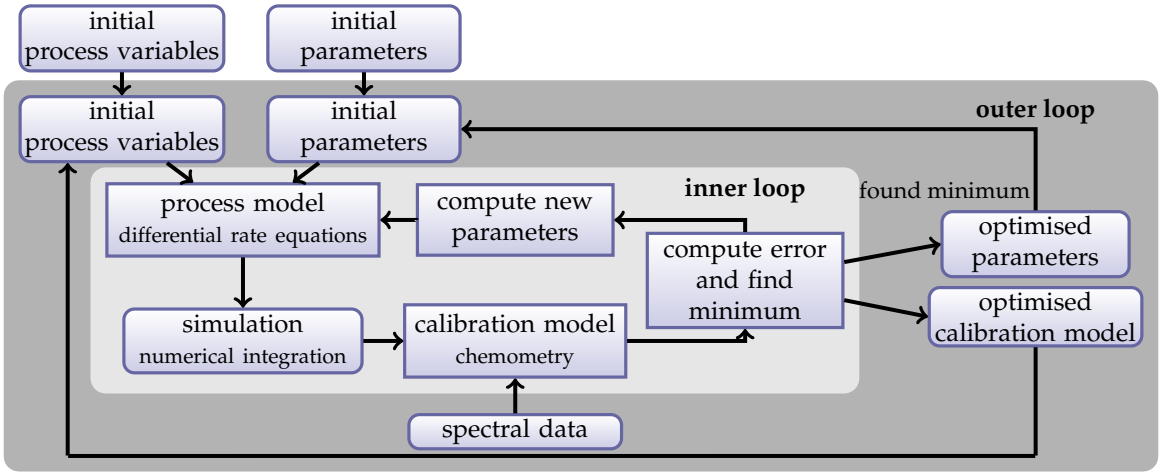

Figure 3.8: The principle program schema combining parameter optimisation, calibration and estimation of the initial process variables

gram is extended with a second outer loop. In this loop the optimised calibration is used to predict the initial process variables. With the new optimised initial process variables a new optimisation is started and after this optimisation the new initial process variables are predicted with the optimised calibration once again. This iterative procedure is continued until a criterion for termination is fulfilled.

In the classical optimisation problem the simulated values are compared with measured values, for examples concentrations are compared, c.f. 3.7.3. In the outlined procedures in figure 3.8 the measured value are spectral data which must be transferred into concentrations or the concentrations predicted by the kinetic model must

be transferred into spectral data by a calibration model (uni- or multivariate). The calibration model is derived during the optimisation procedure automatically. In contrast to the classical optimisation problem in the outline procedure the predicted values by the mathematical model are compared with values calculated with the calibration model. The optimisation and quality function are calculated as follows:

1. Simulation of the concentration time curves with assumed initial process variables and assumed initial kinetic parameters for m individual reactions (experiments).

2. The simulated concentrations are used to derive the calibration model (inner loop).

3. The calibration model is used to predict the concentration time curves from the spectra (inner loop).

4. The predictions and the simulations are compared and the quality function is calculated (inner loop).

$$F = \sqrt{\sum_{j=1}^{m} \sum_{k=1}^{o} \sum_{i=1}^{n} \left(\frac{y_{i,j} - \hat{y}_{i,j}}{\max y_{0,j}} \right)^2} \tag{3.58}$$

   - n is the number of species.
   - o is the number of measurements for each of the species.
   - $y_{i,j}$ are the simulated values of the individual reaction j.
   - $\hat{y}_{i,j}$ are the values predicted by the calibration model of the individual reaction j.
   - $\max y_{0,j}$ is the theoretical maximal value of the individual reaction j.

     The normalisation of the difference of the simulated and predicted value is done to equal the influence of the different individual reactions at different reaction conditions, otherwise reactions at higher concentrations would have a larger influence on the quality function.

5. The kinetic parameters are changed and the next iteration step is started at point 1. The iteration continue until a minimum of the quality function is found (inner loop).

6. The spectrum at time point zero for each individual reaction j and the optimised calibration model are used to calculate new initial process variables (outer loop).

7. The iteration is started again at point 1 with optimised kinetic parameters and initial process variables. To increase the convergence of the algorithm (inner loop) the search space for the genetic algorithm – the range of the population – is reduced according to the following equation:

$$range = parameters \pm \Delta range * f \tag{3.59}$$

$$f = f_\infty + e^{-(n-1)*b} * (1 - f_\infty) \tag{3.60}$$

   - *range*: search space
   - *parameters*: optimised process parameters of the previous optimisation
   - $\Delta range$: specified maximal range of the search space
   - f: decline factor; $f \in \mathbb{R}$ and $1 \geq f \geq f_{end}$
   - f_∞: end value of the factor f after ∞ iterations
   - n: number of iterations; $n \in \mathbb{N}_{>0}$
   - b: declining parameter; $b \in \mathbb{R}$ and $b \geq 0$

   The influence of the declining parameter b on the factor f is illustrated in figure 3.9.

8. If no improvement of the quality function is achieved after evaluating a specified number of populations and generations the optimisation is stopped.

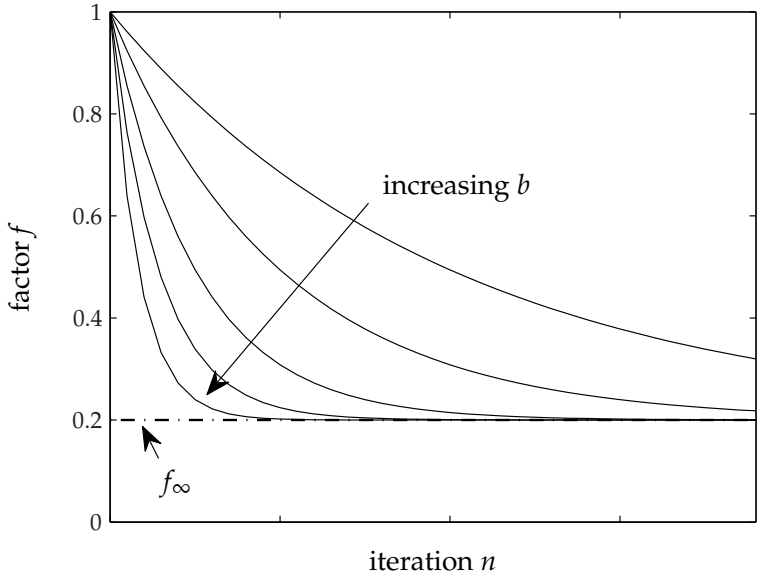

Figure 3.9: Influence of the declining parameter b on the factor f

For the initial optimisation of the kinetic parameters and the calibration model, a real number genetic algorithm is used. For search refinement the initial obtained kinetic parameters and calibration model are optimised by an interior-reflective Newton method using the `lsqnonlin` function. The quality function is vectorised, which allow a simultaneous evaluation of the quality function for each population member as well as the parallel computing on modern multiprocessor or multicore systems.

3.7.5 The measurements

Description of the materials and method, HCN production and precautions, enzyme activity assay, kinetic measurements etc. are given in appendix A.2. In this chapter only the reactor system used in combination with the on-line spectrometric measurement and spectral data collection and data processing is described. The experimental procedure is based on the enzyme activity test developed by Bauer et. al. [209, 156, 176, 177, 177].

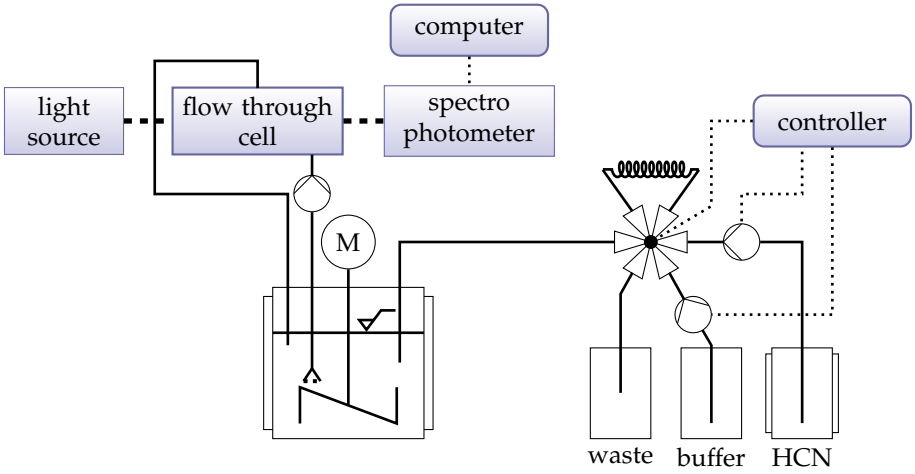

Figure 3.10: Reactor setup for kinetic measurements

The experimental setup for all kinetic measurements is shown in figure 3.10. The main challenge was to facilitate a precise addition of the hydrogen cyanide with its boiling point that is lower than the laboratory room temperature during spring and summer time. The physical properties of hydrogen cyanide are presented in the appendix A.11.

A flow-through cell for light absorption measurements was attached to the double walled and agitated reactor, c.f. chapter 3.7.6. The reaction solution was pumped continuously through the cell at a flow rate of 30 $ml\,min^{-1}$. The volume of the sampling loop – tubing, pump and flow-through cell – was determined gravimetricly and was calculated with 3.5 ml resulting in a mean residence in the sampling loop of 7 s.

The enzyme was not damaged by the pumping, which could be shown in preliminary tests. The enzyme could be pumped through the cell for more then three hours without a significant loss of activity.

The addition of HCN into the reactor turned out to be a difficult task. Due to the high vapour pressure and the low boiling point that is close to room temperature the handling with one-use syringes and standard pipettes was difficult, inexact and risky, because the HCN tended to boil in the syringes and tips of the pipettes especially during the uptake, when the liquid was sucked in. The general procedure of the addition of HCN developed to overcome these difficulties is outlined in figure 3.11. The system consisted of the liquid handling robot described in chapter 2.5 and two valves, the pump valve and the loop valve. The pump valve was controlled by the micro-controller of the liquid handling robot and the loop valve was hand-driven with a position control, enabling the controller to observe the position of the hand valve and using the position change as trigger for the injection. The valves were a six-port HPLC injection valves. A sampling loop (20, 50 and 100 μl) was attached to the loop valve which was filled with HCN from a cooled storage vessel via the dilutor of the liquid handling robot. According to the manual of the liquid handling robot the accuracy of the added volume was better than 4% error. During the filling the outlet was connected with a waste vessel. After switching the valve, the outlet was connected with the reactor and the inlet with the pump valve. Then the content of the sampling loop was pumped into the reactor with a liquid flow. The buffer flow direction was controlled by the pump valve. In the filling position the pump was connected with the waste vessel. After starting the pump the valve was switched after a run-in period of 5 s and was then connected with the loop whose outlet was then connected with the reactor. The run-in period was set to establish a constant flow. After the injection time of 5 s the pump valve was switched back and the pump stopped.

With this procedure 2.8 ml solution (HCN and buffer) could be reproducibl transferred into the reactor. The whole injection system was placed into a cooling chamber. In this chamber the temperature was lowered to ca. 10°C, to facilitate a safe handling of the HCN.

3.7.6 The collection of spectral data

For on-line measurement a multiwavelength high-resolution photospectrometer system of the company *ocean optics* was used. The system consisted of a balanced deuterium tungsten halogen light source (DH-2000-BAL), a flow-cell for absorbency measurements with adjustable path length made of stainless steel (FIA-Z-CELL) and a high-resolution spectrometer (HR2000). The system components were connected via optical fibre (QP1000-2-UV-VIS). Due to the optical range from 200-1100 nm and the flow cell with adjustable path length, the application range of such a system is large. Integration times from 3.8 ms to 10 seconds allowed a good time resolution as well

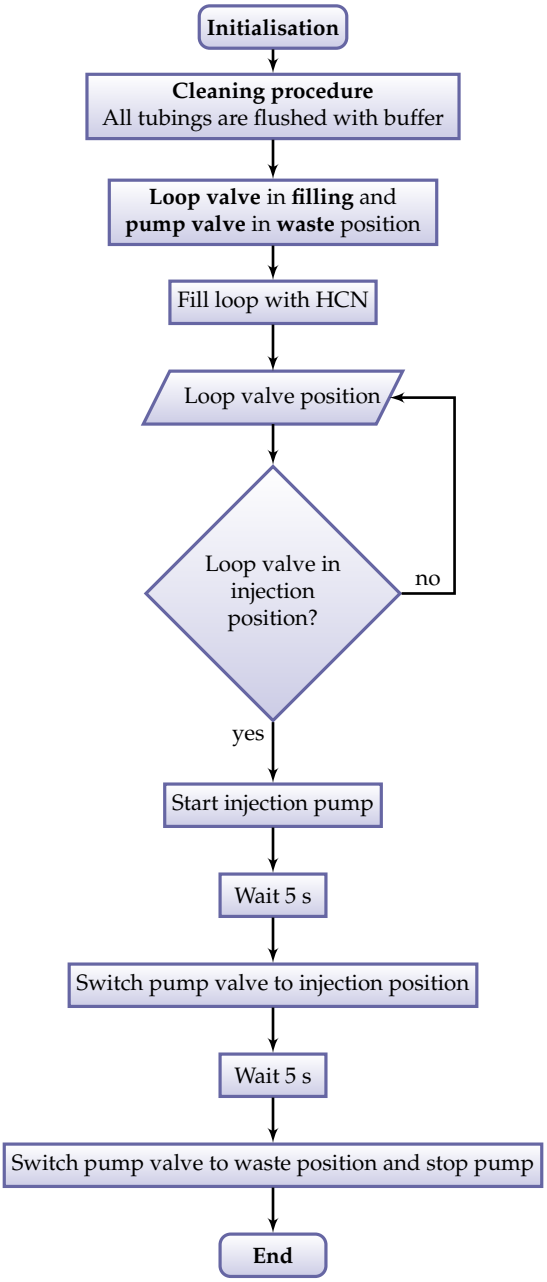

Figure 3.11: Flow chart of the HCN addition program

as the easy adaptation to the measurement task. Because the standard spectrometer operating software could not provide the required specification for the measurement task, especially the time resolved recording of the absorption of a specified spectral range, a new control software had to be developed. The OOILVD LabVIEW drivers (ocean optics, Inc.) features the integration of the spectrometer system into a *National Instruments LabVIEW* environment, which was used as controlling software.

The spectrometer had a 3648-element CCD-array[5] device detector and a grafting diffracted the light. The diffracted light was focused on the one-dimensional CCD-array detector and each element of the CCD-array recorded the intensity of the light beam of a close spectral range of approximately $\Delta\lambda = 0.25nm$.

The control software related each element of the intensity vector $I = [I_{\lambda_1} \cdots I_{\lambda_i} \cdots I_{\lambda_{3648}}]$ of size 3648 to a real wavelength. The relation was determined by the calibration of the spectrometer with light sources of defined spectra. Due to the linearity of the system the relation could be specified with two parameters. To increase the signal to noise ratio the intensities at each wavelength were averaged over a specified time, which can range from the integration time (not averaging) up to several hours (depending on the memory of the computer system). Furthermore a moving average smoothing was performed according equation 3.61.

$$\bar{I}_{\lambda_i} = \frac{1}{2n+1} \sum_{j=-n}^{n} I_{\lambda_{(i+j)}} \tag{3.61}$$

The absorption for each wavelength was calculated according to equation 3.62.

$$A_{\lambda_i} = -log\left(\frac{\bar{I}_{\lambda_i} - \bar{I}_{\lambda_i,dark}}{\bar{I}_{\lambda_i,0} - \bar{I}_{\lambda_i,dark}}\right) \tag{3.62}$$

The intensity I_{λ_i} is the measured intensity, $I_{\lambda_i,0}$ is the reference intensity or background intensity, for example the medium. The intensity $I_{\lambda_i,dark}$ is the measured intensity while the shutter of the lamp is closed and accounts mainly to the electrical noise of the CCD detector.

Figure 3.12 to 3.14 show the three different front panels of the software. In panel 1 the operation mode – intensity or absorption – could be specified and the system could be configured; integration time, average time and smoothing parameters could be set as well as the reference values for $\bar{I}_0$ and $\bar{I}_{dark}$. The readings were presented in an intensity/absorption versus wavelength plot. In panel 2 and 3 the parameters for the time resolved measurements could be set. The control panel 2 configured a single wavelength and panel 3 a multiwavelength measurement. The wavelength or wavelength range could be specified as well as the sampling frequency and the measurement time. The data were stored as ASCII file. The specification of the ASCII-

[5] A charge-coupled image sensor

file is given in appendix A table A.12. All other data processing and analysis has been

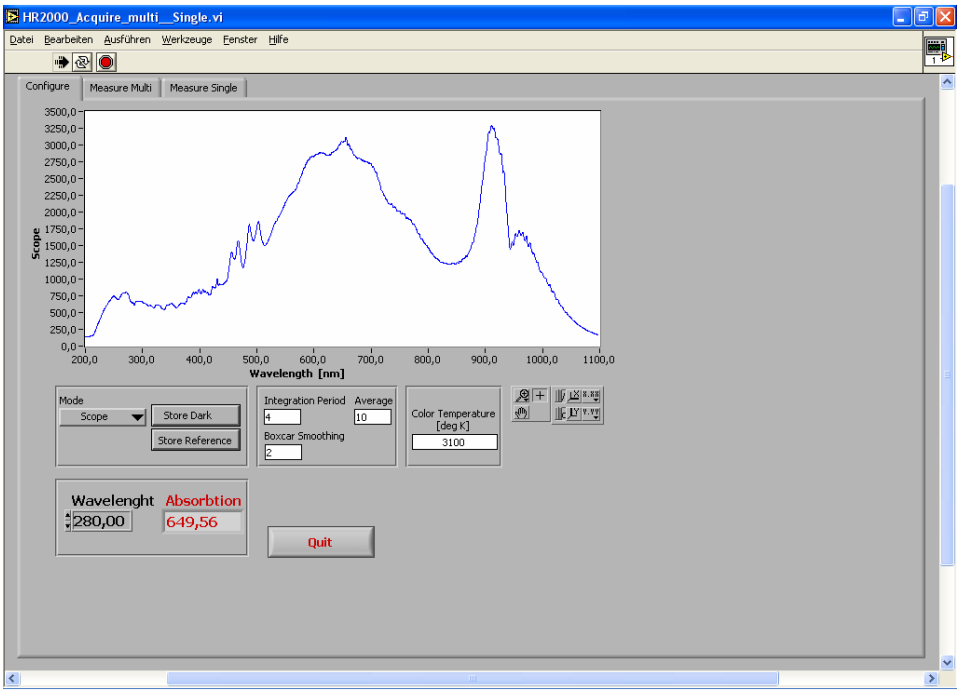

Figure 3.12: The photospectrometer measurement software: configuration panel

done with Matlab™(R2007a).

The data preprocessing

Due to air bubbles in the fluid flow through the cell outliners were visible in the recorded spectra. These outliners could be removed by applying a smoothing function across the time dimension, because the absorption change must be continuous. The smoothing function applied was a function of the Curve Fitting Toolbox™using the methods of local regression, weighted linear least squares and a 2nd degree polynomial model in the robust version that assigns lower weight to outliners in the regression. The method assigns zero weight to data outside six mean absolute deviations. By that the outliners could be removed effectively without loosing spectral information.

For ease of interpretation and for numerical stability of the multivariate calibration model it is recommended to centre the data before the analysis. This was done by subtracting the averages from all variables both in matrices $\boldsymbol{X}$ and $\boldsymbol{Y}$.

In figure 3.15 an example of a typical time course of the spectral data is shown.

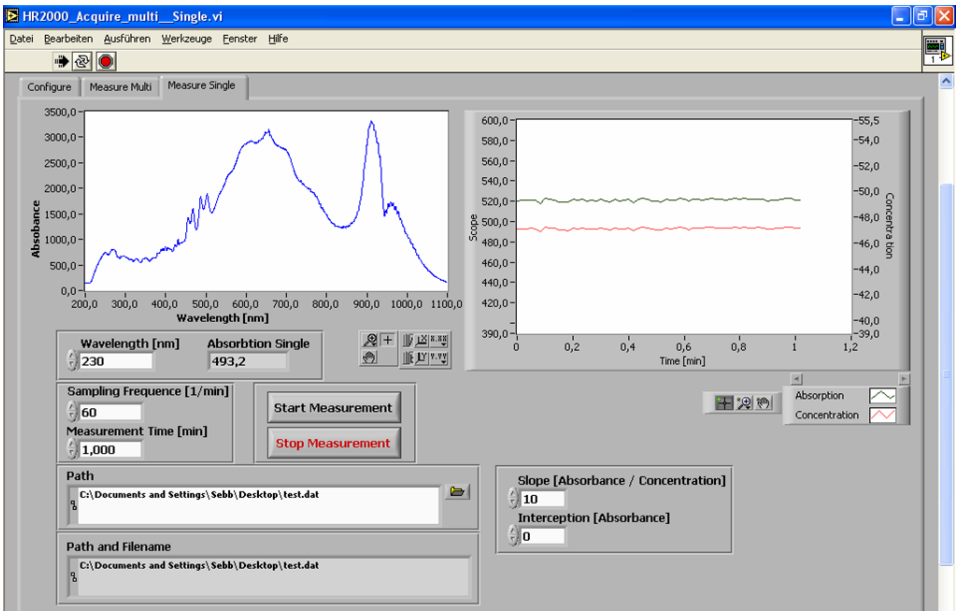

Figure 3.13: The photospectrometer measurement software: single wavelength measurement

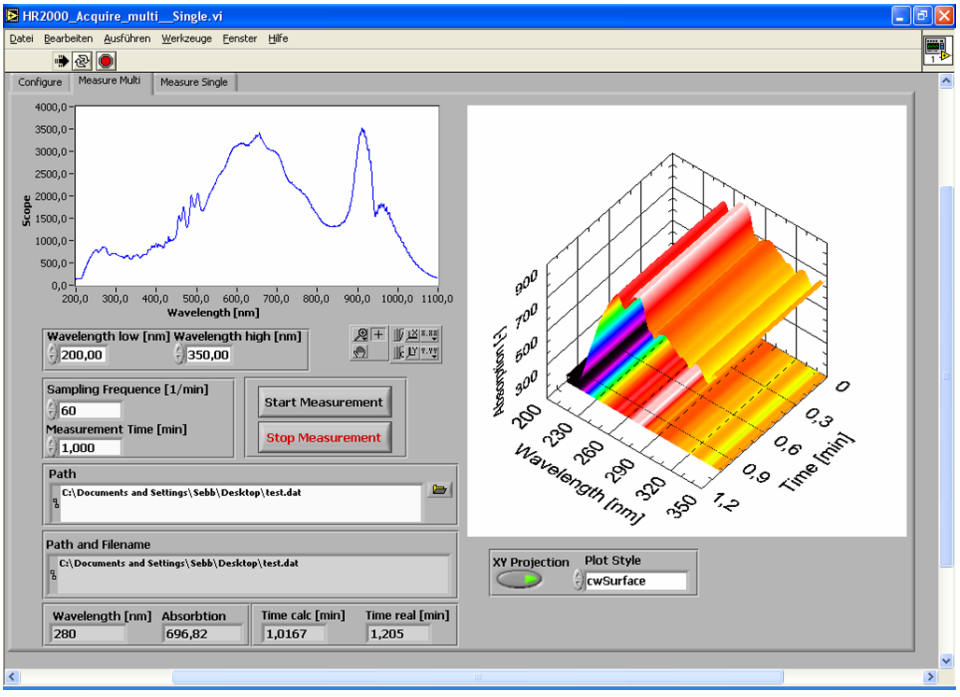

Figure 3.14: The photospectrometer measurement software: multi-wavelength measurement

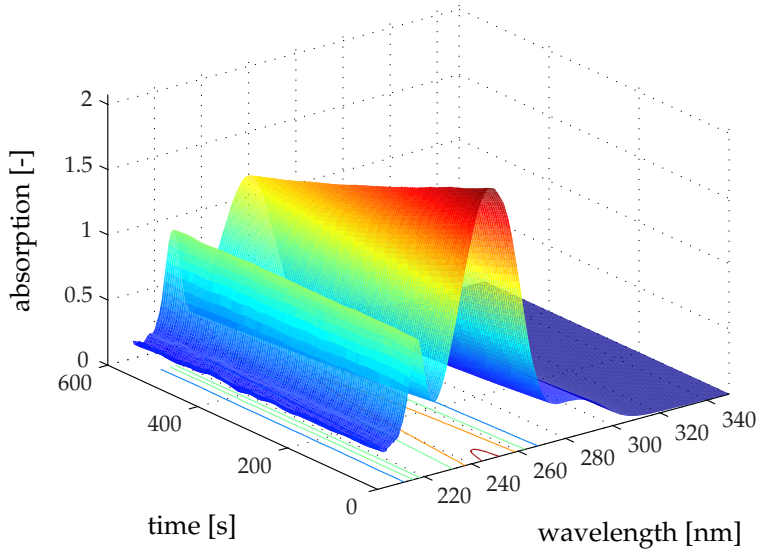

Figure 3.15: An example of a typical time course of the spectral data

3.8 Results and Discussion: joining the determination of the kinetics and the calibration parameters

In this chapter the results of the determination of kinetics and the calibration parameters are presented. Measurements were performed for different substrate and catalyst concentrations and the spectra were recorded. First the calibration and optimisation of the kinetic parameters were performed independently and the kinetic parameters were estimated using the method of initial rate measurements. These results are compared with kinetic parameters obtained by progress curve analysis. Then the calibration is joined with the determination of the kinetic parameters. Two calibration methods are compared, the linear calibration model evaluating the adsorption at one chosen wavelength and the multivariate model applying partial least squares regression at a wavelength range. Finally the optimisation of the initial concentration is incorporated into the optimisation procedure as well.

3.8.1 The linear calibration model: Benzaldehyde

The benzaldehyde concentration was calculated from the light absorption measurements at 280 nm. The calibration is based on 111 independent absorption measurements at benzaldehyde concentrations from 0 to 14 $mmol\,L^{-1}$. Benzaldehyde was dissolved in a citric acid-phosphate buffer (0.1 $mmol\,L^{-1}$, pH 5.0), filled into the reactor and thermostatically controlled to 25°C. The solution was pumped through the flow-through cell and the absorption was measured. The integration time was set

to 4 *ms*, ten measurements were averaged and the moving average smoothing parameter (Boxcar smoothing) was set to 2 (average of three CCD-elements). The path length of the flow-through cell was set manually [6], so that the absorption concentration relation was linear in the concentration range as shown in figure 3.16. The

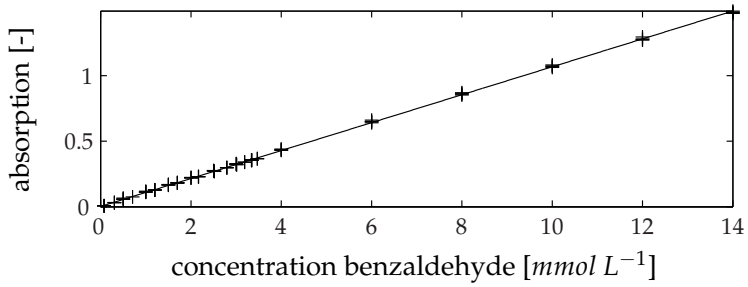

Figure 3.16: Calibration spectrophotometer for benzaldehyde concentration; 111 measurements in the range of 0 to 15 $mmol\ L^{-1}$

proportionality factor could be calculated to 0.1065 $\pm$ 0.003 absorption unit per concentration [$L\,mmol^{-1}$]. The linearity was good with a coefficient of determination (R^2) of 0.998. The relative mean standard deviation could be calculated to 3.7%. The lower detection limit was 0.05 $mmol\ L^{-1}$, which was equal to 0.005 absorption units. Then the signal got close to the noise level and the relative mean standard deviation increased drastically [7].

3.8.2 Kinetics of the uncatalysed reaction

Racemic mandelonitrile is cleaved/synthesised uncatalysed in an aqueous reaction system. The uncatalysed reaction was evaluated under the standard reaction conditions of the kinetic measurements but without enzyme, c.f. appendix A.2.5. For the cleavage reaction the measurement time was set to 30 min and for the synthesis reaction to 10 min. The mandelonitrile and the benzaldehyde concentrations were varied from 1 to 15 $mmol\ L^{-1}$ and the HCN concentration was set to 25 and 50 $mmol\ L^{-1}$, respectively. The measured concentrations are listed in appendix A table A.14. From the recorded absorption spectra the absorption at the wavelength of 280 *nm* were extracted and the curves were smoothed rejecting outliners. The linear calibration model was applied, c.f. chapter 3.8.1 and the concentration curves were calculated.

The optimisation of the model (equation 3.38), fitting the progress curve provided the parameters presentet in table 3.3. The optimised parameters confirmed the published data.

[6] The exacted length was not specified, but it was lower than 1 *mm*.

[7] Because the system can be tuned with different parameters – integration time, averaging and path length – the detection range could be adjusted also in different ranges. Especially the lower detection limit might be reduced by increasing the path length, but at the same time the linear range would also be reduced.

parameter	measured value	literature[176] value	unit
k_{10}	$1.163\,10^{-5} \pm 0.005\,10^{-5}$	$9.34\,10^{-6} \pm 2\,10^{-8}$	$[L\,mmol^{-1}\,s^{-1}]$
k_{11}	$2.063\,10^{-5} \pm 0.117\,10^{-5}$	$2.40\,10^{-5} \pm 5\,10^{-8}$	$[s^{-1}]$

Table 3.3: Kinetic parameters chemical reaction

3.8.3 Initial rate measurements

For the optimisation of the kinetic parameters 80 individual measurements were evaluated. The recorded absorption spectra were processed like described above and only the absorption at a wavelength of 280 nm was evaluated. The linear calibration model was applied, c.f. chapter 3.8.1, and the concentration curves were calculated. The initial rates were calculated by linear regression from the first time range of the recorded concentration progress curves. The time range was set by a visual survey of each individual plot. All initial rates obtained were used simultaneously for the optimisation of the quality function according to equation 3.57 and the measured initial rates were compared with the calculated rates according to equation 3.34. For the optimisation the measured initial benzaldehyde concentrations were used. Mandelonitrile concentrations were corrected as described in appendix A.2.5. The results of the optimisation of the kinetic model assuming a competitive inhibition by the (*R*)-mandelonitrile is shown in table 3.4.

For the verification of the model an independent experiment with a simulation using the optimised kinetic parameters. The comparison with the measured concentrations and the enantiomeric excess is shown in figure 3.17. A good consistency of the simulation and the measurements is visible. The calculated enantiomeric excess differed from the measured one especially during the first 20 minutes. The measurement of the enantiomeric excess is a more sensitive measure than the concentration and due to the low concentrations of the mandelonitrile during that period the measurement error was increased. Small changes in the integration of the peak area measured by the GC can significantly influence the measured enantiomeric excess. The reason for the decrease of the measured enantiomeric excess can also be the inactivation of the enzyme. The inactivation was not included into the mathematical model.

As example, in figures 3.18 and 3.19 the contour plots for the Michaelis Menten parameter for HCN $K_{m,HCN}$ and the reaction rate for synthesis $k_{cat,synthesis}$ and the Michaelis Menten parameter for HCN $K_{m,BA}$ and the reaction rate for cleavage $k_{cat,c}$ are shown. The wide-stretched elliptical-shaped minimum of the quality function with only small changes along the major axis of the ellipse is noteworthy. Such wide-stretched elliptical-shaped minima are often observed fo the type of Michaelis Menten used for the formulation of the rate equation, as for example shown by Lindner and

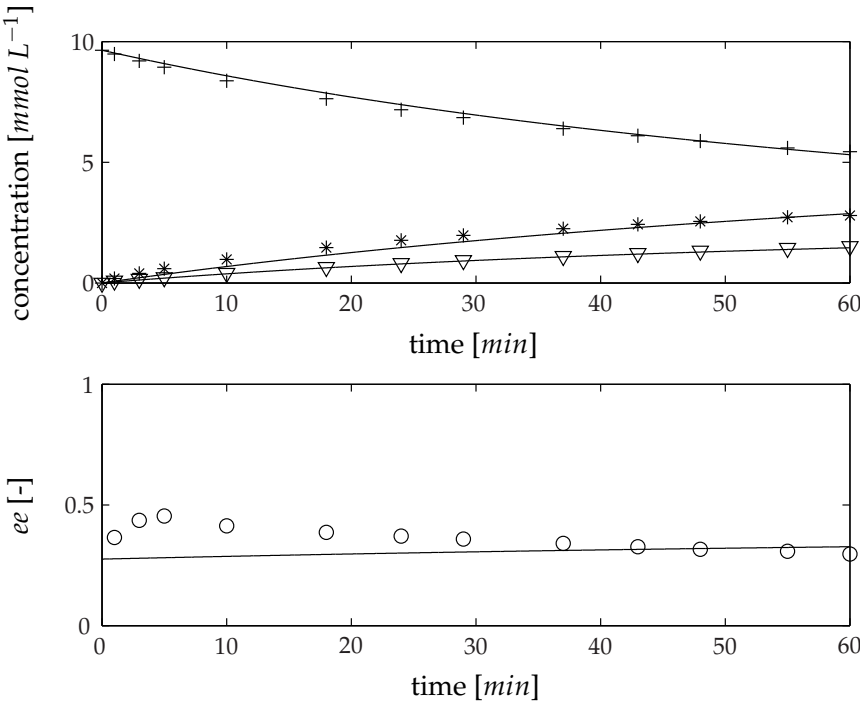

Figure 3.17: Comparison of measurement and simulation of *Hb*HNL synthesis of (*S*)-mandelonitrile $(*)$. 0.05 $mol\,L^{-1}$ citrate phosphate buffer pH 5,0 25°C, *Hb*HNL 0.35 mgL^{-1}, benzaldehyde $(+)$ 10 $mmol\,L^{-1}$, HCN 12.5 $mol\,L^{-1}$, (*R*)-mandelonitrile $(\bigtriangledown)$, enantiomeric excess (O), solid line: simulation with kinetic parameters presented in table 3.4

Parameter	Values		Unit
	(*R*)-MN inhibition	no (*R*)-MN inhibition	
$k_{cat_{cleavage}}$	33 ± 1.8	33 ± 2.7	$[s^{-1}]$
$k_{cat_{synthesis}}$	142 ± 18	132 ± 22	$[s^{-1}]$
$K_{m_{HCN}}$	14.2 ± 5.5	14.4 ± 7.9	$[mmol\ L^{-1}]$
$K_{m_{BA}}$	0.64 ± 0.3	0.45 ± 0.4	$[mmol\ L^{-1}]$
$K_{m_{(S)-MN}}$	1.7 ± 0.2	1.9 ± 0.4	$[mmol\ L^{-1}]$
$K_{i_{BA}}$	0.5 ± 0.1	0.35 ± 0.1	$[mmol\ L^{-1}]$
$K_{i_{(R)-MN}}$	3.7 ± 0.7	-	$[mmol\ L^{-1}]$
$K_{i_{(S)-MN}}$ [1]	1.8 ± 0.3	2.3 ± 0.9	$[mmol\ L^{-1}]$
$K_{i_{HCN}}$ [1]	12.6 ± 3	10.7 ± 3	$[mmol\ L^{-1}]$
Residual sum of squares	$1.6 * 10^{-5}$	$3.3 * 10^{-5}$	-

[1] $K_{i_{(S)-MN}}$ and $K_{i_{HCN}}$ have been calculated according to equations 3.35 and 3.36, the confidence intervals have been calculated according to the Gaussian error propagation law (equation A.1) .

Table 3.4: Kinetic parameters optained by initial rate measurements; with and without inhibition by (*R*)-mandelonitrile

Hitzmann [210] and Zvarel et al. [211]. The angle of the semi-axes of the ellipsoid to the coordinate axes implies a correlation of these two parameters. Thus, they cannot be estimated independently from each other [211]. In contrast to that, the semi-axes of the ellipsoid for the parameters $K_{m,BA}$ and $k_{cat,c}$ are almost parallel to the coordinate axes, which indicates a low correlation of both parameters.

The model can predict the experimental data quite well, but the parameters cannot be estimated with sufficient precision. Two possible reasons for this can be considered: first, the experimental data were insufficient for estimating the parameters precisely. This will be the case especially if the experimentally accessible region is rather limited, as it may happen, for example, due to the low solubility of the reactants [211]. Secondly the model structure is too complex.

To reduce the complexity of the model the competitive inhibition of (*R*)-mandelonitrile was excluded thereby reducing the free parameters to six. The result is also shown in table 3.4. The values of the parameters for the model without inhibition by (*R*)-mandelonitrile were almost identical to the parameters for the model with inhibition by (*R*)-mandelonitrile. The comparison of the simulation with the independent experiment showed also a good consistency (result not shown). Comparing the residual sum of the squares shows that the residual of the more complex model was with $1.62 * 10^{-5}$ about half of the residual of the simplified model and therefore the confidence intervals were smaller. The exclusion of the inhibition decreased the goodness of the optimised parameters and therefore it can be concluded,

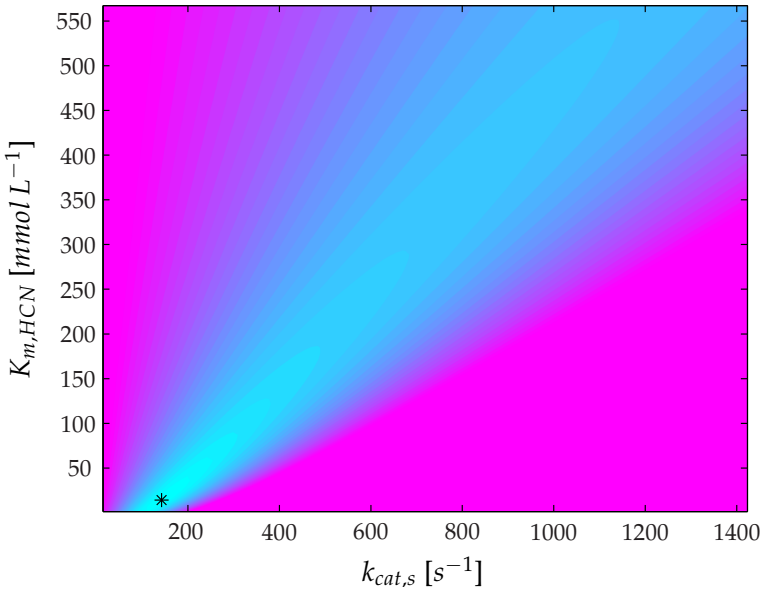

Figure 3.18: Contour plot of the quality function for the reaction rate for synthesis $k_{cat,synthesis}$ and the Michaelis-Menten parameter for HCN $K_{m,HCN}$, initial rate measurements, model with (*R*)-mandelonitrile inhibition. The parameter combination obtained by optimisation is marked with a star.

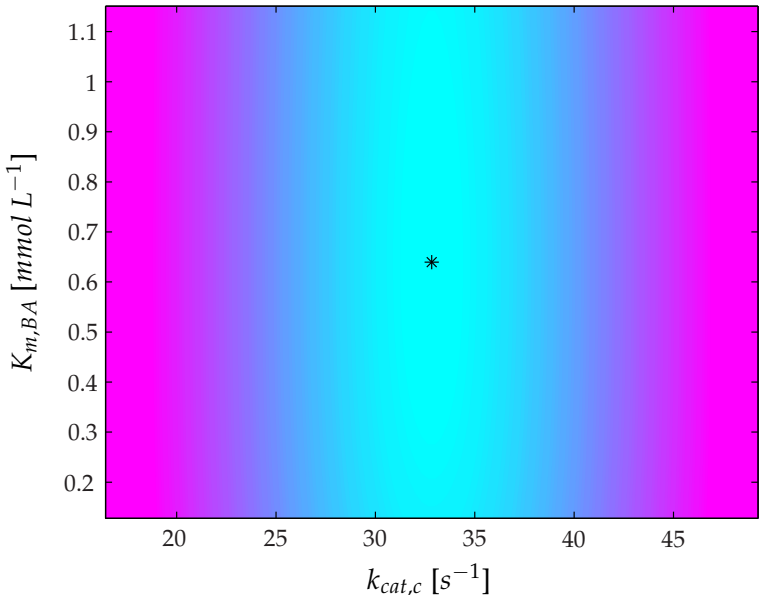

Figure 3.19: Contour plot of the quality function for the reaction rate for cleavage $k_{cat,c}$ and the Michaelis Menten-parameter for Benzaldehyde $K_{m,BA}$, initial rate measurements, model with (*R*)-mandelonitrile inhibition. The parameter combination obtained by optimisation is marked with a star.

that the inhibition was a significant parameter in this model. The low significance was also seen in the broader minima comparing the contour plots for both models (cf. figures 3.18 to 3.21)

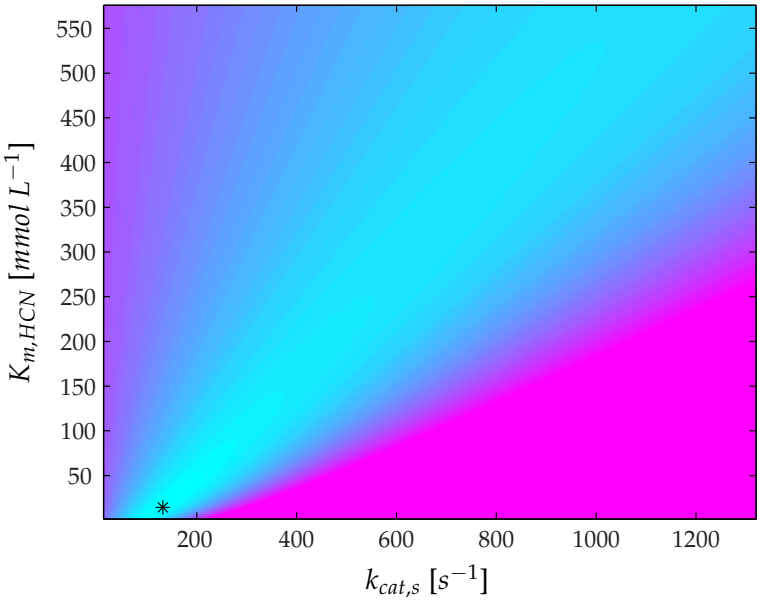

Figure 3.20: Contour plot of the quality function for the reaction rate for synthesis $k_{cat,synthesis}$ and the Michaelis Menten-parameter for HCN $K_{m,HCN}$, initial rate measurements, model without (*R*)-mandelonitrile inhibition. The parameter combination obtained by optimisation is marked with a star.

It can be concluded, that the model could predict the experimental data quite well. The parameters, however, could not be estimated with sufficient precision. A further reduction of the parameters would not reflect the reaction model assumed. Of course the increase of the number of well designed experiments can increase the precision of the optimised parameters. Bauer[88] used, for example, several hundred initial rate measurements. Another possible way is a different optimisation strategy which is not based on the initial rates, but rather the whole reaction curve from the start to the equilibrium.

3.8.4 The progress curve analysis

Two strategies were followed for the progress curve analysis. First the "classical" progress curve analysis where the parameters were optimised fitting the simulation to measured concentration time curves. As the second option the optimisation of the calibration model was included and the model was fitted as described in chapter 3.7.4. In both cases the same six independent reactions were used simultaneously for the optimisation, the initial concentrations were randomly chosen and three syntheses

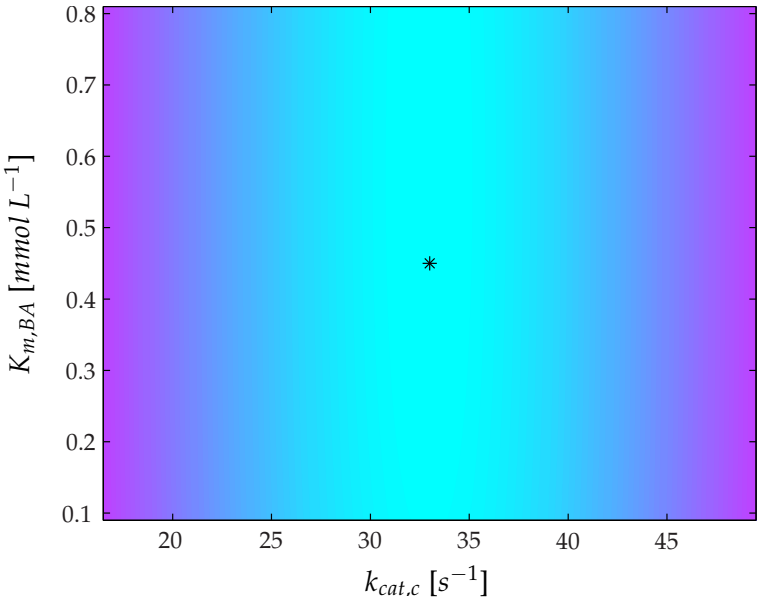

Figure 3.21: Contour plot of the quality function for the reaction rate for cleavage $k_{cat,c}$ and the Michaelis Menten-parameter for benzaldehyde $K_{m,BA}$, initial rate measurements, model without (*R*)-mandelonitrile inhibition. The parameter combination obtained by optimisation is marked with a star.

and three cleavage reactions were considered.

The progress curve analysis with prior calibration

The curves were fitted to the concentration curve for benzaldehyde calculated from the absorption at 280 *nm* with the correlation factor measured beforehand, c.f. chapter 3.8.1. In table 3.4 the results obtained by the progress curve analysis as it is described in chapter 3.6.2 are presented. For the progress curve analysis the inhibition by (*R*)-mandelonitrile was excluded. In contrast to the initial rate measurements the parameter $K_{i_{(R)-MN}}$ could not be obtained with the same precision than the other parameters. The absolute value of the confidence interval for $K_{i_{(R)-MN}}$ were in the range of the value itself. As shown in figure 3.22 the independent experiment could be well predicted with the obtained parameters. The fit was slightly less precise compared to the parameters obtained by initial rate measurements. Especially the predicted enantiomeric excess was lower than the measurement, which was caused by a lower ration of $k_{cat,synthesis}$ to $K_{m,HCN}$ of 6.25 compared to 9.2 for the initial rate measurement. But the statistical significant was much larger and the confidence intervals were significanty smaller compared to the initial rate measurements. This shows that the progress curve analysis could reduce the effort of experimental effort drastically, because only six measurements were considered in contrast to eighty. Also the analysis of the mea-

sured date was less laborious, because no initial rates had to be calculated for each measurement and the progress curve was used directly.

Parameter	Value	Unit
$k_{cat_{cleavage}}$	12 ± 0.3	$[s^{-1}]$
$k_{cat_{synthesis}}$	200 ± 7	$[s^{-1}]$
$K_{m_{HCN}}$	32 ± 2.5	$[mmol\ L^{-1}]$
$K_{m_{BA}}$	1.6 ± 0.15	$[mmol\ L^{-1}]$
$K_{m_{(S)-MN}}$	0.13 ± 0.02	$[mmol\ L^{-1}]$
$K_{i_{BA}}$	0.25 ± 0.07	$[mmol\ L^{-1}]$
$K_{i_{(S)-MN}}$ [1]	0.2 ± 0.006	$[mmol\ L^{-1}]$
$K_{i_{HCN}}$ [1]	7.4 ± 1.2	$[mmol\ L^{-1}]$
Residual sum of squares	$1.5 * 10^{-4}$	$[mmol\ L^{-1}]$

[1] $K_{i_{(S)-MN}}$ and $K_{i_{HCN}}$ have been calculated according to equations 3.35 and 3.36, the confidence intervals have been calculated according to the Gaussian error propagation law (equation A.1) .

Table 3.5: Kinetic parameters progress curve: prior linear calibration

The contour plots for the progress curve analysis for the parameter $k_{cat,synthesis}$, $K_{m,HCN}$ and $k_{cat,f}$, $K_{m,BA}$ are shown in figures 3.23 and 3.24. They were similar to the contour plot for the initial rate measurements and showed the dependency of $k_{cat,synthesis}$ and $K_{m,HCN}$. But the minima were more distinctive and therefore the parameters were optimised with a higher precision.

The confidence intervals included the experimental uncertainties, because the absorption multiplied by the calibration factor was directly used for the optimisation and statistical evaluation. But the uncertainty of the calibration was not included. The calibration of the spectrophotometer was itself a time-consuming procedure and the uncertainty of the calibration was influenced by the purity of the calibration substance, the error of the preparation of the test solution and the number of calibration points. A straightforward time saving solution would have to include the calibration directly in the optimisation of the kinetic parameters.

Progress curve analysis including a linear univariate calibration model

To include the calibration directly into the optimisation procedure the optimisation of the calibration factor was introduced as an additional parameter into the optimisation procedure of the kinetic parameters. The quality function was rewritten, c.f

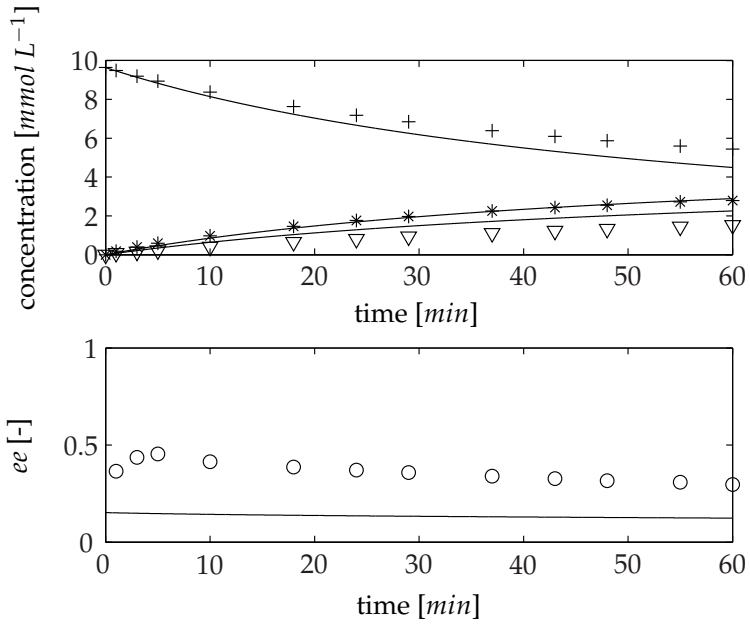

Figure 3.22: Comparison of the measurement and simulation of *Hb*HNL synthesis of (*S*)-mandelonitrile $(*)$, progress curve analysis. 0.05 $mol\,L^{-1}$ citrate phosphate buffer pH 5,0 25°C, *Hb*HNL 0.35 mgL^{-1}, benzaldehyde $(+)$ 10 $mmol\,L^{-1}$, HCN 12.5 $mol\,L^{-1}$, (*R*)-mandelonitrile $(\bigtriangledown)$, enantiomeric excess (O), solid line: simulation with kinetic parameters presented in table 3.5

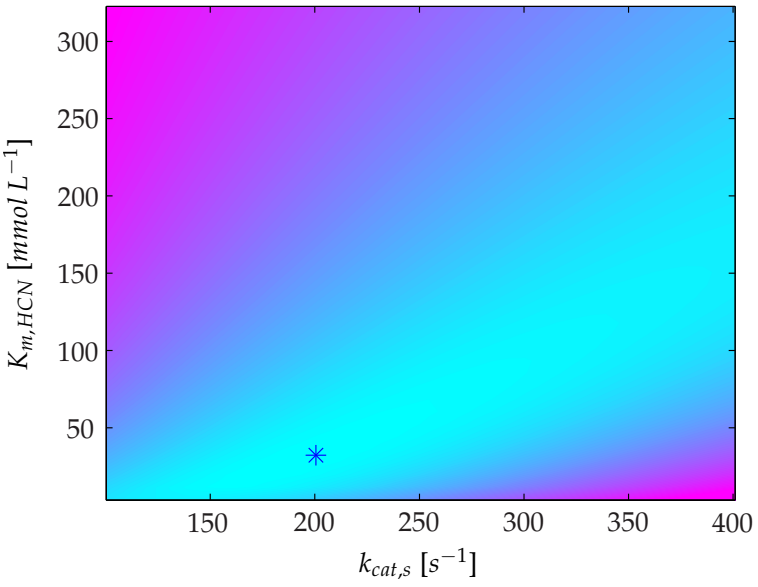

Figure 3.23: Contour plot of the quality function for the reaction rate for synthesis $k_{cat,synthesis}$ and the Michaelis Menten-parameter for HCN $K_{m,HCN}$, progress curve analysis. The parameter combination obtained by optimisation is marked with a star.

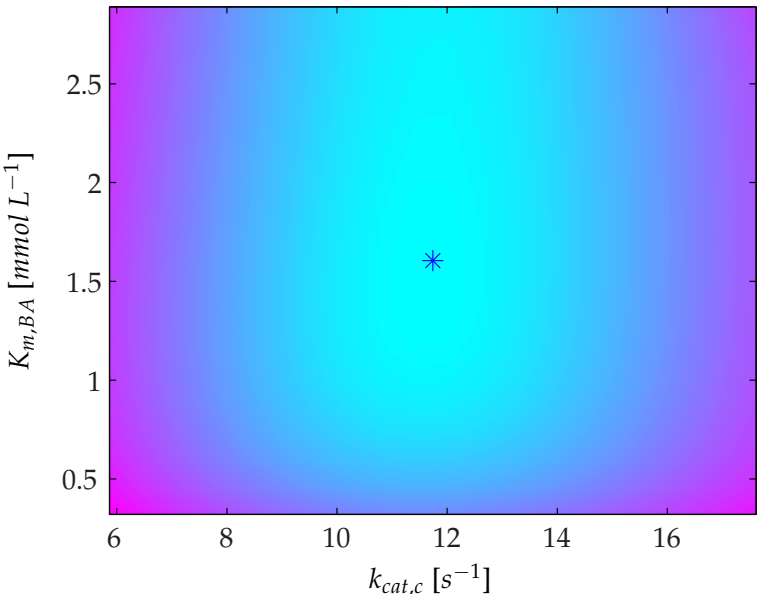

Figure 3.24: Contour plot of the quality function for the reaction rate for cleavage $k_{cat,c}$ and the Michaelis Menten parameter for Benzaldehyde $K_{m,BA}$. The parameter combination obtained by optimisation is marked with a star.

equation 3.58. As initial concentrations the theoretical applied concentrations were assumed.

As seen in figure 3.25 and table 3.6 the inclusion of the calibration into the optimisation of the kinetic parameters led to similar results, compared to the previous results presented. Besides the kinetic parameters the calibration factor could be obtained as well. The residual sum of the squares and the absolute values of the confidence intervals were almost identical. Also the shapes of the minima were very similar as seen in the contour plots in figure 3.26 and 3.27.

A calibration factor for the linear calibration model of 0.1084 ± 0.0002 absorption unit per concentration $[L\,mmol^{-1}]$ was calculated. The linearity was very good with a coefficient of determination (R^2) of 0.999. The obtained calibration factor was identical to the factor obtained by prior calibration (0.1065 ± 0.003), but with a confidence interval teen times smaller.

Because of the decomposition of the mandelonitrile to HCN and benzaldehyde the real initial benzaldehyde and mandelonitrile concentration differ from calculated concentrations. The existing concentrations could be calculated for the recorded spectra. The prediction of the initial concentrations was also included by iterative adaptation of the initial concentrations using the iteratively optimised linear calibration model to predict the initial concentration as described in chapter 3.7.4.

The result is shown in table 3.7. Kinetic parameters were found which could predict the progress curve of an independent experiment. The optimised parameters were

Parameter	Value	Unit
$k_{cat_{cleavage}}$	12 ± 0.26	$[s^{-1}]$
$k_{cat_{synthesis}}$	178 ± 7.2	$[s^{-1}]$
$K_{m_{HCN}}$	14 ± 1.7	$[mmol\ L^{-1}]$
$K_{m_{BA}}$	1.5 ± 0.0004	$[mmol\ L^{-1}]$
$K_{m_{(S)-MN}}$	0.18 ± 0.017	$[mmol\ L^{-1}]$
$K_{i_{BA}}$	0.36 ± 0.087	$[mmol\ L^{-1}]$
$K_{i_{(S)-MN}}$ [1]	0.2 ± 0.0005	$[mmol\ L^{-1}]$
$K_{i_{HCN}}$ [1]	4.3 ± 1.2	$[mmol\ L^{-1}]$
Residual sum of squares	$1.08 * 10^{-4}$	$[mmol\ L^{-1}]$

[1] $K_{i_{(S)-MN}}$ and $K_{i_{HCN}}$ have been calculated according to equations 3.35 and 3.36, the confidence intervals have been calculated according to the Gaussian error propagation law (equation A.1) .

Table 3.6: Kinetic parameters progress curve: including a linear univariate calibration model

Parameter	Value	Unit
$k_{cat_{cleavage}}$	14 ± 0.8	$[s^{-1}]$
$k_{cat_{synthesis}}$	101 ± 7	$[s^{-1}]$
$K_{m_{HCN}}$	20 ± 3.2	$[mmol\ L^{-1}]$
$K_{m_{BA}}$	0.9 ± 0.002	$[mmol\ L^{-1}]$
$K_{m_{(S)-MN}}$	0.3 ± 0.05	$[mmol\ L^{-1}]$
$K_{i_{BA}}$	0.4 ± 0.15	$[mmol\ L^{-1}]$
$K_{i_{(S)-MN}}$ [1]	0.3 ± 0.001	$[mmol\ L^{-1}]$
$K_{i_{HCN}}$ [1]	10.5 ± 4.2	$[mmol\ L^{-1}]$
Residual sum of squares	$3.9 * 10^{-4}$	-

[1] $K_{i_{(S)-MN}}$ and $K_{i_{HCN}}$ have been calculated according to equations 3.35 and 3.36, the confidence intervals have been calculated according to the Gaussian error propagation law (equation A.1) .

Table 3.7: Kinetic parameters progress curve analysis: including a linear univariate calibration model and an approximation of the initial concentrations

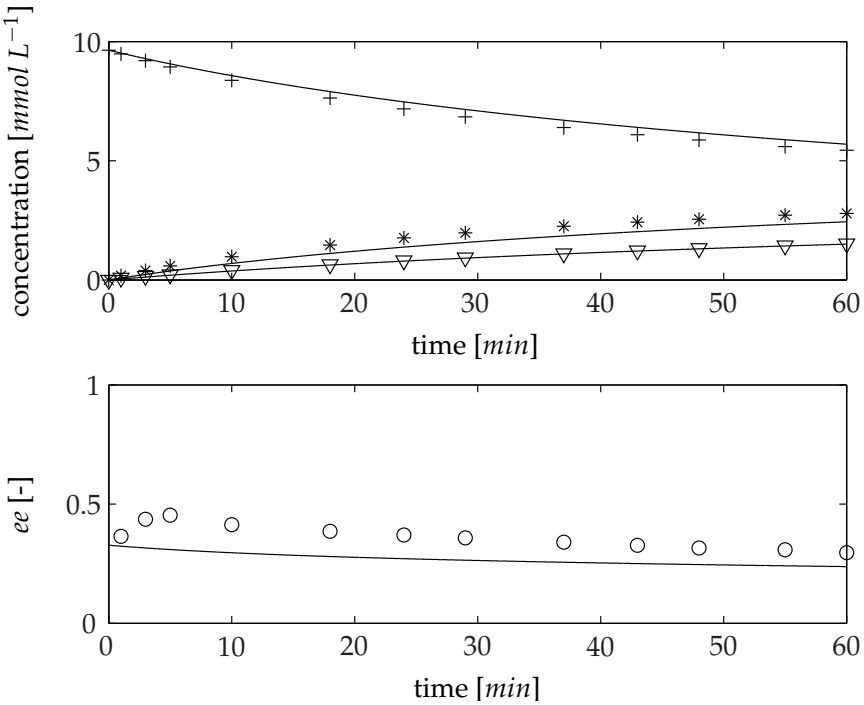

Figure 3.25: Comparison of the measurement and simulation of *Hb*HNL synthesis of (*S*)-mandelonitrile $(*)$, progress curve analysis and linear calibration model. 0.05 $mol\ L^{-1}$ citrate phosphate buffer pH 5,0 25°C, *Hb*HNL 0.35 mgL^{-1}, benzaldehyde $(+)$ 10 $mmol\ L^{-1}$, HCN 12.5 $mol\ L^{-1}$, (*R*)-mandelonitrile $(\bigtriangledown)$, enantiomeric excess (O), solid line: simulation with kinetic parametes presented in table 3.6

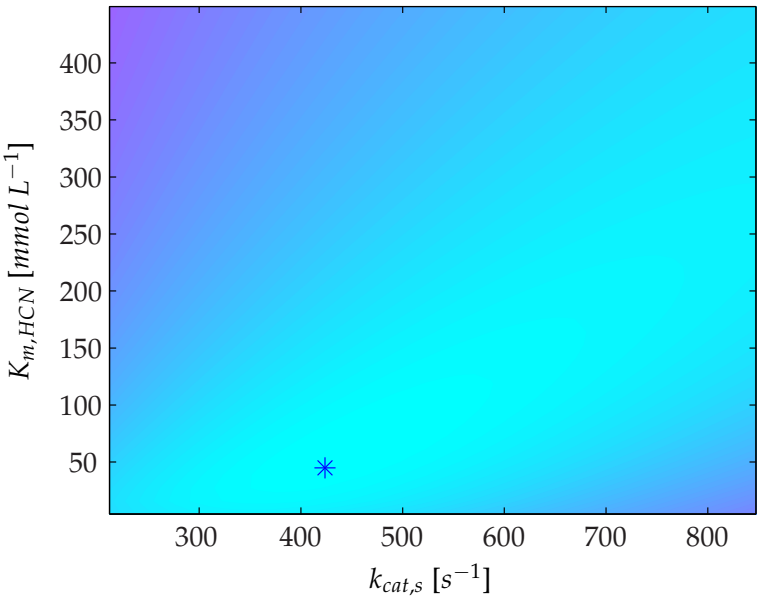

Figure 3.26: Contour plot of the quality function for the reaction rate for synthesis $k_{cat,synthesis}$ and the Michaelis Menten-parameter for HCN $K_{m,HCN}$, progress curve analysis and linear calibration model. The parameter combination obtained by optimisation is marked with a star.

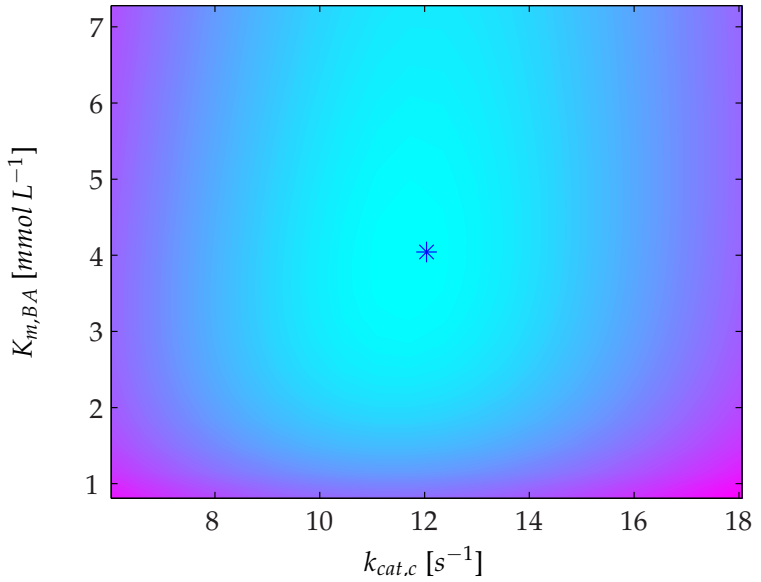

Figure 3.27: Contour plot of the quality function for the reaction rate for cleavage $k_{cat,c}$ and the Michaelis Menten parameter for Benzaldehyde $K_{m,BA}$, progress curve analysis and linear calibration model. The parameter combination obtained by optimisation is marked with a star.

similar to the parameters obtained by progress curve analysis with prior calibration.

The calibration factor was determined with 0.1079 ± 0.0002 absorption unit per concentration $[L\,mmol^{-1}]$. The linearity was very good with a coefficient of determination (R^2) of 0.999. It differed by 0.0005 from the value obtained without any adaptation of the initial concentrations and it is within the confidence interval obtained by prior calibration (0.1065 ± 0.003). This small difference resulted in a difference in the calculated concentration of less then 0.5 %, which is much smaller than the error caused by the handling of the liquid during the experiment. The similar calibration factor obtained in this procedure compared to the prior calibration showed, that the prediction and iterative adaptation of the initial concentration worked well.

The results shows, that the inclusion of the calibration into the optimisation of the kinetic parameter makes – in this case – any calibration prior to the experiment unnecessary. The experimental effort could be reduced drastically and the obtained confidence intervals for all parameter now include the uncertainty of the calibration.

Progress curve analysis including a multivariate partial least squares calibration model

While in the previous chapter the procedure was described using a single linear calibration model that examines only the absorption only at a single wave length, modern spectrophotometric systems measure simultaneously the absorption in a broad wave length range. The spectrophotometer used had a detection range from 200 to 1100 nm. A challenge would be to use the information of such spectra directly for the simultaneous optimisation of the kinetic parameters and a multivariate calibration model, which includes more than one measured substance, without previous knowledge of the adsorption spectra of the investigated reactants.

The partial least squares regression provides a mathematical tool to examine the spectra for such a multivariate calibration. This procedure can be implemented in a similar way as the approach using the linear calibration model. This is done replacing the linear with the partial least squares regression. The optimisation procedure is outlined in chapter 3.7.4. For optimisation the model did not include the competitive inhibition with (*R*)- mandelonitrile. A two substance calibration model was built for benzaldehyde as well as mandelonitrile. The result of the optimisation is presented in table 3.8.

As seen in table 3.8 the optimised parameters are similar to the parameters obtained with all other fitting procedures. The comparison with an independent experiment showed a good consistency, c.f. figure 3.28. The calibration model could be used to calculate the concentration time curves of benzaldehyde and mandelonitrile from the spectral data. The benzaldehyde concentration calculated by the univariate linear and by the multivariate calibration model showed a convincing agreement, too, c.f. figure 3.29. Also the reciprocal operation, the prediction of the adsorption time spectra, is possible. In the figures 3.30 and 3.31 the differences between a recorded and a

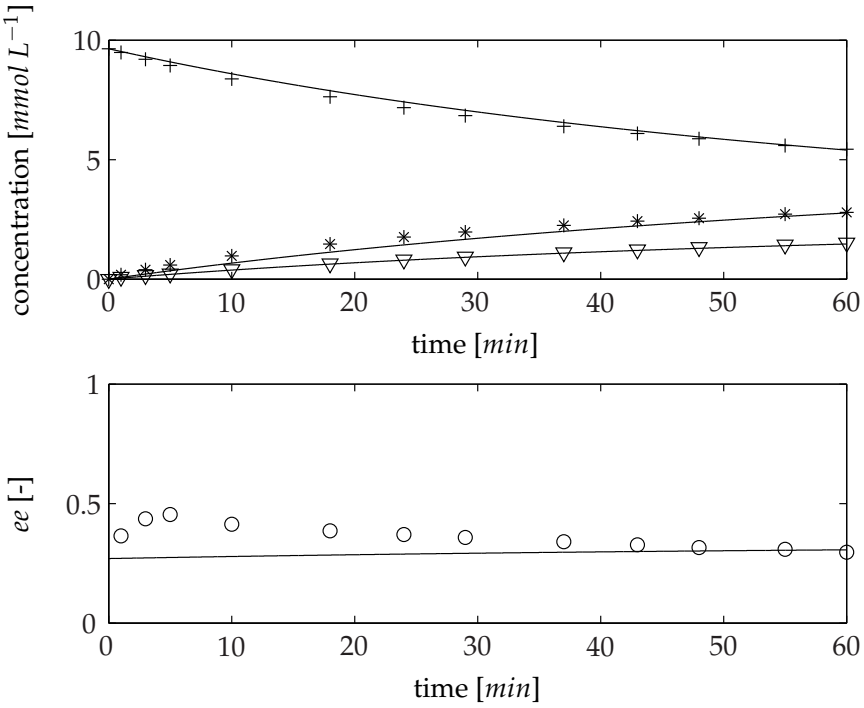

Figure 3.28: Comparison measurement and simulation of *Hb*HNL synthesis of (*S*)-mandelonitrile $(*)$, progress curve analysis and PLS calibration model. 0.05 $mol\ L^{-1}$ citrate phosphate buffer pH 5,0 25°C, *Hb*HNL 0.35 mgL^{-1}, benzaldehyde $(+)$ 10 $mmol\ L^{-1}$, HCN 12.5 $mol\ L^{-1}$, (*R*)-mandelonitrile $(\bigtriangledown)$, enantiomeric excess (O), solid line: simulation with kinetic parameters presented in table 3.8

Parameter	Value	Unit
$k_{cat_{cleavage}}$	28	$[s^{-1}]$
$k_{cat_{synthesis}}$	173	$[s^{-1}]$
$K_{m_{HCN}}$	22	$[mmol\ L^{-1}]$
$K_{m_{BA}}$	0.3	$[mmol\ L^{-1}]$
$K_{m_{(S)-MN}}$	0.8	$[mmol\ L^{-1}]$
$K_{i_{BA}}$	0.4	$[mmol\ L^{-1}]$
$K_{i_{(S)-MN}}$ [1]	0.36	$[mmol\ L^{-1}]$
$K_{i_{HCN}}$ [1]	12.6	$[mmol\ L^{-1}]$

[1] $K_{i_{(S)-MN}}$ and $K_{i_{HCN}}$ have been calculated according to equations 3.35 and 3.36, the confidence intervals have been calculated according to the Gaussian error propagation law (equation A.1) .

Table 3.8: Kinetic parameters progress curve analysis PLS

predicted absorption time curve for two different numbers of principal components are shown. Here the influence of different numbers of principal components became visible. Increasing the number of principal components from two to five halved the root mean squares error from RMSE=0.031 to 0.015.

Due to the influence of the number of principal components, the interpretation of the confidence intervals was complex. They are strongly influenced by the constraints for the optimisation. Because of the enormous number of calculations, which had to be performed during the regression steps optimising the multivariate calibration model, the computation time increased drastically. The increase was caused by the evaluation not only of a single wavelength but rather of up to 3648 for the spectrophotometer. In this study a wavelength range from 210 to 300 nm was evaluated which was equal to 360 individual wavelength. The precision of the calibration model influences the computation time and can be controlled by the numbers of principal components which in this case was set to five. Six experiments were used simultaneously for optimisation resulting in a computation time of several hours up to days on a standard personal computer [6].

It could be shown that the calibration and optimisation of kinetic parameters can be combined using partial least squares regression. The absolute values of the confidence intervals of the kinetic parameter were influenced by the number of principal

[6] Intel Core 2 Duo processor T9400 (2.53 GHz, 10600 MHz FSB, 6 MB L2 chache), 4 GB DDR2, operation system opensuse 11.1, Matlab Release 2007a)

Parameter	Value							Unit
	i	ii	iii	iv	v	vi	vii	
$k_{cat_{cleavage}}$	33 ± 1.8	33 ± 2.7	12 ± 0.3	12 ± 0.26	14 ± 0.8	28	64 ± 1	$[s^{-1}]$
$k_{cat_{synthesis}}$	142 ± 18	132 ± 22	200 ± 7	178 ± 7.2	101 ± 7	173	3436 ± 24	$[s^{-1}]$
$K_{m_{HCN}}$	14.2 ± 5.5	14.4 ± 7.9	32 ± 2.5	14 ± 1.7	20 ± 3.2	22	350 ± 45	$[mmol\ L^{-1}]$
$K_{m_{BA}}$	0.64 ± 0.3	0.45 ± 0.4	1.6 ± 0.15	1.5 ± 0.0004	0.9 ± 0.002	0.3	5.2 ± 0.3	$[mmol\ L^{-1}]$
$K_{m_{(S)-MN}}$	1.7 ± 0.2	1.9 ± 0.4	0.13 ± 0.02	0.18 ± 0.017	0.3 ± 0.05	0.8	3.1 ± 0.1	$[mmol\ L^{-1}]$
$K_{i_{BA}}$	0.5 ± 0.1	0.35 ± 0.1	0.25 ± 0.07	0.36 ± 0.087	0.4 ± 0.15	0.4	1.18 ± 0.02	$[mmol\ L^{-1}]$
$K_{i_{(R)-MN}}$	3.7 ± 0.7	-	-	-	-	-		$[mmol\ L^{-1}]$
$K_{i_{(S)-MN}}$ [1]	1.8 ± 0.3	2.3 ± 0.9	0.2 ± 0.006	0.2 ± 0.0005	0.3 ± 0.001	0.36	3.3 ± 0.2	$[mmol\ L^{-1}]$
$K_{i_{HCN}}$ [1]	12.6 ± 3	10.7 ± 3	7.4 ± 1.2	4.3 ± 1.2	10.5 ± 4.2	12.6	150 ± 14	$[mmol\ L^{-1}]$

[1] $K_{i_{(S)-MN}}$ and $K_{i_{HCN}}$ have been calculated according to equations 3.35 and 3.36, the confidence intervals have been calculated according to the Gaussian error propagation law (equation A.1) .

Table 3.9: Summary of Kinetic parameters:

i intial rate measurement

ii intial rate measurement without inhibition by (*R*)-mandelonitrile

iii progress curve analysis with prior linear calibration

iv progress curve analysis including a linear univariate calibration model

v progress curve analysis including a linear univariate calibration model and an approximation of the initial concentrations

vi progress curve analysis including a PLS calibration model

vii literature values by Bauer [88]

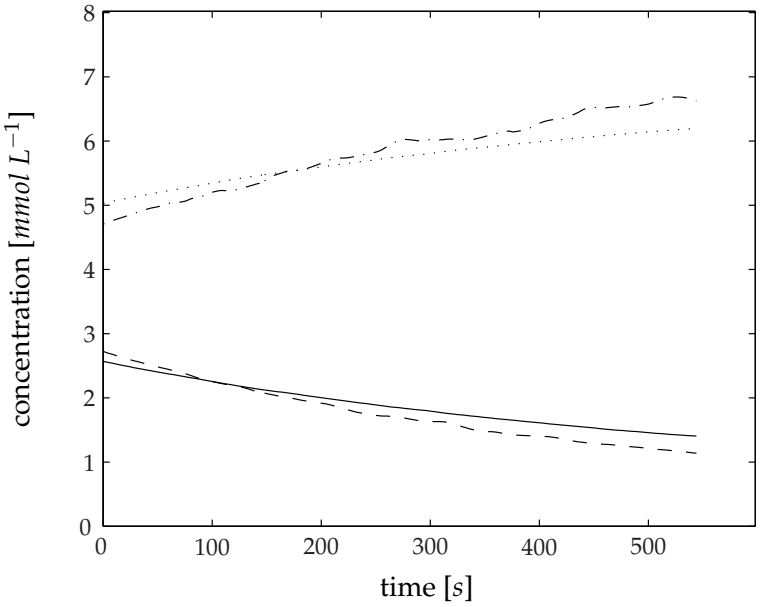

Figure 3.29: Calculated concentrations of benzaldehyde (- -) and mandelonitrile (- . -) by the multivariate calibration model, compared to the concentrations of benzaldehyde (–) and mandelonitrile (:) calculated with the univariate linear model

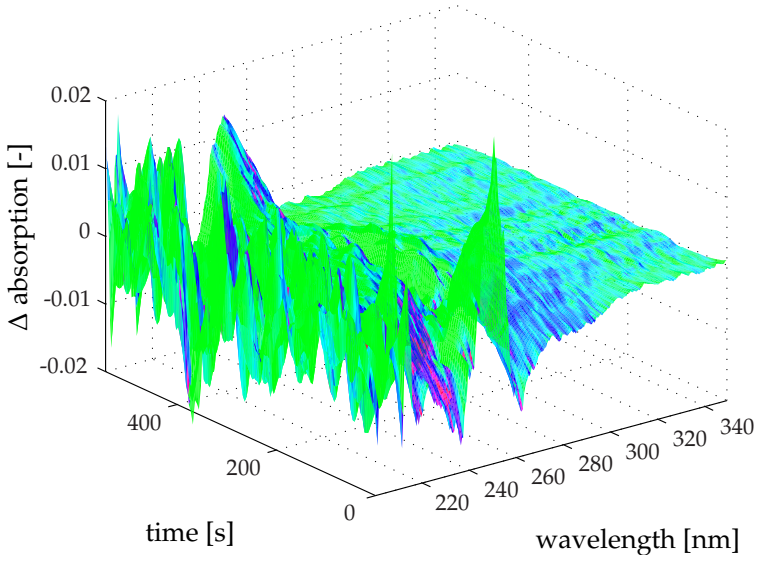

Figure 3.30: Difference between recorded and by the multivariate calibration model predicted absorption-time curve, numbers of principal components = 2, RMSE=0.031

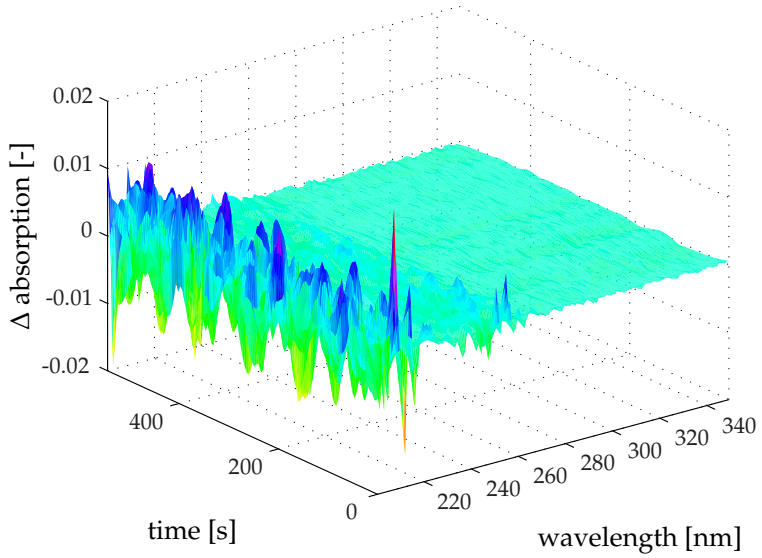

Figure 3.31: Difference between recorded and by the multivariate calibration model predicted absorption-time curve, numbers of principal components = 5, RMSE=0.015

components and could not be directly compared to the intervals presented above. But it can be concluded, that the procedure led to a significant result. The main advantage was, that the experimental effort could be drastically reduced, that no calibration was needed and that the information which could be supplied by a modern spectro photometer could be used in an effective way. No previous knowledge of the adsorption spectra of the investigated reactants was necessary and the adsorption spectra could be predicted from the obtained calibration model. Because the human factor and the subjective interpretation of the experimental data during initial rate measurements could be excluded, these results are generally validat.

3.8.5 Comment on the optimisation procedure

The progress curve analysis optimisation studies showed that it was difficult to find an unique minimum. Here the problem of the parameter determination of such a system became obvious. Due to the number and the dependency of the parameters the optimisation was a challenge and the optimisation algorithm found a local rather than the global minimum. The combination of a genetic algorithm with classical least squares regression increased the chance to find the global minimum in an effective way, because the genetic algorithm is categorised as a global search heuristic, while the algorithms implemented in the `lsqnonlin` function is a local solver. Therefore it was important to start the local optimisation `lsqnonlin` with a suitable set of initial parameters, which could be supplied by the genetic algorithm. The drawback of the genetic algorithm was the low tendency to converge. Therefore a huge number of calculations was necessary, which increased the calculation time. To find the ini-

tial parameter for the `lsqnonlin` was the time-consuming step and could last up to several days. But still the global minima could only be found for the initial rate measurements.

No elaborated experimental design was used in this study. Because the increase of the calculation time is not a "consumer-friendly" approach, the combination of the strategy with a differential model based experimental design would be a straightforward solution, like it is proposed by Zavrel and coworkers [211] or Körkel and Arrellano-Garcia [212]. For example Zavrel and coworkers [211] optimised the experimental procedure in silico and could reduce the absolute value of the confidence intervals by a factor more than 200. This differential model based experimental design offers a tool to plan experiments in an effective way. The experimental procedure, the sampling and the costs[7] of the experiments can be optimised to find optimal reaction conditions. For the determination of the kinetic parameters a minimal number of experiments is design and the significant of the identified parametes is maximised at the same time. This model based experimental design is not limited to batch processes, also semi-batch like fed-batch and semi-continuous processes can be considered as shown by Roeva and coworkers [206]. And especially the fed-batch technique offers opportunities to increase the statistical significance of the obtained parameters, because semi-continuous conditions can be established in areas of the large sensitivity of the system.

3.8.6 Summary and comparision with literature data

The comparison with the literature data in table 3.9 shows a significant difference in the reaction rates and affinity to the substrates for the synthesis reaction benzaldehyde and HCN. The reason for this may be the actual HCN concentration during the measurements. Bauer [88] used HCN dissolved in the reaction buffer, which he stored frozen at -18°C and thawed before reaction. Because of the high vapour pressure of the HCN the preparation of the solution the procedure was prone to errors. Also the small reaction volume, lower the 1 *ml* in a cuvette with 2 *mm* measurement length, and the small volumes of the HCN buffer solution which was added were sources of error. The actual concentration of HCN during the measurements may have been lower than expected. The lower actual concentrations of HCN and the dependency of the different parametes like $K_{m,HCN}$, $k_{cat,synthesis}$ may have caused the deviance.

In table 3.9 the results of the different experimental and optimisation designs – initial rate and progress curve analysis – are summarised. It could be shown, that different experimental and optimisation designs could be used to find convenient kinetic parameter for a given kinetic model. The effort to obtained the experimental basis were by far the largest for the initial rate measurements. The progress curve

[7] For example an artificial cost function can be defined to reduce the costs of the sampling. In this case the cost might be the time for sample preparation and analysis as well as additional cost like auxiliary materials.

analysis especially in combination with the integration of the calibration reduces the experimental work but at the same time increases the computational effort and the need of substantial knowledge about simulation and optimisation procedures. Also the confidence intervals obtained using the progress curve analysis approaches were lower (excluding the PLS calibration model approach). Therefore in the following the parameters iv table 3.9 (progress curve analysis including a linear univariate calibration model) will be used as reference model. Because computing power these days are not the limiting factor any more the progress curve analysis is superior the initial rate measurements. In combination with a non linear experimental design the progress curve analyis would prove its superiority.

3.9 Immobilisation of the *Hb*Hnl

As described in chapter 3.3 for the application of the enzyme in an non-conventional reaction medium the immobilisation of the enzyme is essential. In this section the immobilisation of the *Hb*HNL on different carriers is described as well as the application in an aqueous and pure organic solvent system.

3.9.1 Investigated carriers

The following immobilisation matrices were investigated for the possibility of immobilisation of *Hb*HNL:

- Sepabeads (porous polymer particles, covalent and adsoptive binding)
- Celite (porous diatomaceous earth particles, adsoptive binding)
- Poraver beads (porous glass particles, covalent binding)
- Nano carriers (nano-size detonation diamonds, covalent binding)

Sepabeads

Sepabeads® EC were purchased from Resindion S.R.L., Italy. These carriers were introduced by the company as suitable for many different applications. Like many other immobilisation matricest they are supposed to permit a multiple or repetitive use of a single batch of immobilised enzyme, the ability to rapidly stop the reaction by removing the immobilised enzyme from the reaction solution, the possibility to use a higher enzyme concentration in the reaction milieu and an increasing operational stability [213].

They are stable in water, different organic media and "dry state" [213]. The polymer structure is a physically and chemically stable cross-linked copolymer of methacrylate, which is not degradable by microorganisms and has a high capacity to bind proteins. The Sepabeads EC used had a particle size distribution of 150-300 μm and a specific density of 1.13 $g\,ml^{-1}$. They were available with a wide variety of functional groups for immobilisation (EP, epoxy; EA, amine; HA, hexamethylamino; BU, butyl), table 3.10. Different types of Sepabeads have been successfully applied for the immobilization of different enzymes [214]. On industrial scale Sepabeads are used for the conversion of cephalosporin C into alpha-keto-adipoyl-7-amino-cephalosporanic acid [215] and the production of 6-amino penicillanic acid [216]. Also the application of the beads in a continously operated plug-flow-reactor for the synthesis of acetophenone has been reported [217] as well as the successful use of octadecyl Sepabeads in a repetitive batch mode in the hydrolysis of 6-(5-chloropyridin-2-yl)-5-(O-butyryl)-7-oxo-5,6-dihydropirrolo[3,4b]pyrazine [218].

Sepabeads	Functional Group	Formed bondage	Immobilisation Buffers
EC-EP	epoxy	covalent	1.25 M, pH 7.0
EC-HFA	amino-Epoxy	covalent	20 mM, pH 8.0
EC-EA	ethylamine	covalent	20 mM, pH 8.0
EC-HA	hexamethylamino	covalent	20 mM, pH 8.00
EC-BU	butyl	physical adsorption	5 mM, pH7

Table 3.10: Functional binding sides of Sepabeads

Celite

Celite, also known as diatomaceous earth (Kieselgur) which occurs naturally, is a chalk-like sedimentary rock with a high porosity. It consists of fossilized remains of a hard-shelled algae, the diatom. Due to its inner composition Celite is extremly lightweight and has a high specific inner surface. As powder with a particle size of from 10 to 200 μm made of the desiccated shells of diatoms it is commonly used as a filtering agent, adsorbent, and abrasive in many chemical operations [219]. Its hydrophobicity and high specific inner surface make it an excellent carrier for the immobilisation of enzymes as catalyst in an organic solvent reaction system. The carrier binds the water necessary for the activity of the enzyme to the inner and outer surface of the carrier where also the enzyme is located. So no explicit second bulk liquid phase besides the organic phase is formed and the solid carrier can be applied directly in the non aqueous reaction system (solvent free, organic solvent or ionic liquid). Celite was successfully applied as immobilisation matrix for different enzymes and different reaction systems.

Hydrolases – esterases[8], lipases[9] glycosidase[10], peptidase[11] and other hydrolases[12]– as well as oxidoreductases[13] and lyases[14] could be successfully immobilised on Celite and performance improvements were reported. The stability of the enzymes especially in non aqueous reaction systems as well as the reusability and retention of the catalyst could be enhanced by the immobilisation. Costes et al. reported in 1999 the immobilisation of *Hb*HNL on Celite and its application in a low

[8] examples for esterases [220, 221, 222]
[9] examples for lipases [223, 224, 225, 226, 227, 228, 220, 229, 230, 231, 232, 233, 234, 235, 236, 237, 238, 239, 240, 241, 242, 243, 244, 245, 246, 247, 248, 249, 250, 251, 252, 253, 254, 255, 256, 257, 258, 259, 260, 261, 262, 263, 264, 265, 266, 267, 268, 269, 270, 271, 272, 273, 274, 275, 276, 277]
[10] examples for glycosidases [278, 279, 280, 281, 282, 283, 284]
[11] examples for peptidaes [285, 286, 287, 288, 289, 290, 291, 292, 293, 294, 295, 296, 297, 298, 299, 300, 301, 266, 302, 303, 273, 304]
[12] examples for othe hydrolases [305, 306, 307, 308, 309, 250]
[13] examples for oxidoreductases [310, 311, 312, 313, 314, 315, 316, 317, 318, 319, 320, 321, 322]
[14] example for lyases [323, 324, 325, 257, 273]

water reaction system [323]. They synthesised 2-hydroxy-4-phenyl-butanenitrile in diethylether, dibutylether, diisopropylether or tertbutyl-methylether as organic solvents containing only 1 % water. The mostly used immobilisation procedure for the immobilisation of enzyme on Celite is by adsorption. The enzyme solution is added to the dry carrier and the liquid is removed by freeze-drying.

Poraver Beads

The beads were donated by Dennert Poraver Gmbh, Schluesselfeld, Germany. The Poraver porous glass beads are a recycling product of glass used as for sound proofing, mortar and some other applications.

To produce the beads the recycling glass is cleaned and grounded to a fine glass powder. After the addition of water, binding and expanding agents it is formed into its round shapes in the granulating dish. The granulate is expanded in a rotating furnace at approx. 900°C. The expanding process generates a fine-pored, creamy white, round granulate, entrapping minute air chambers inside. The particle density is $900 \pm 120\, kg\, m^3$ and the apparent density $400 \pm 60\, kg\, m^{-3}$ [326]. After sieving six different particle size distribution are available and a distribution of 0.1 - 0.3 mm was used in our experiments.

Nano Particles

The reduced activity and the changed observed kinetics of immobilised enzymes are often attributed to mass transport hindrance in the capillary tube of the porose carrier. The inner surface of a porose carrier can be the multiple of the outer surface and the enzyme is bound mostly on inner surfaces. The transport of the reactants to the enzyme is dominated by diffusion. If the specific reaction rate is larger than the diffusion rate the overall reaction is diffusion controlled, which results in a lower apparent specific activity as well as a changed apparent kinetics. A solution can be to reduce the diameter of the particles to reduce the length of the diffusion. The lower limit of the reduction are the so called nano particles. The mean diameter of such particles are in the range of the enzyme itself. In this study nano diamods (nano-size detonation diamonds) were used for immobilisation which has been functionalised with amino functions [327, 328, 329, 330, 331]. The nano-diamonds were kindly provided by Prof. Dr. Anke Krueger, Nanocarbon Materials, Otto-Diels-Institut for Organic Chemisty, Christian-Albrechts-University Kiel. The already amino-functionalized particles (agglomerate size 550 nm, prior to chemical functionalization: primary particles of 4-5 nm, agglomerates of $\approx 300\, nm$) [328]. The immobilisation of the enzyme followed the reaction steps presented in figure 3.32.

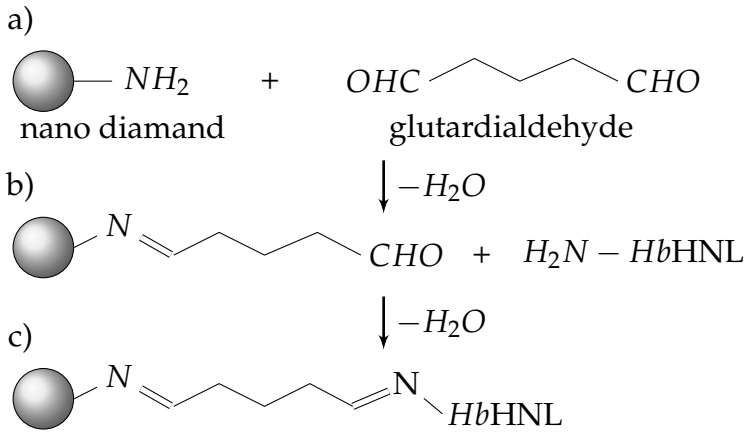

Figure 3.32: Immobilisation of the (*S*)-HNL on nano carriers: a) amino functionalised carries were activated with glutardialdehyde, b) The enzyme was incubated with active nano carriers for 24 hours, c) immobilised HNL on nano carriers.

3.9.2 Results and Discussion: Immobilisation

In the following chapter the results of the immobilisation are discussed. The Materials and Methods are described in appendix A.4. In general the *Hb*HNL was immobilised according standard procedure and in the first comparison study no optimisation of the immobilisation procedure was prepare. All immobilisates were tested in reactions using organic solvents and all carriers were lyophilised before application in the test reaction to remove water. Because the non-immobilised enzyme can not be applied directly in organic solvents, no reverence reaction could be performed so that the activity yield could not be determined. Also a comparison of the immobilisation yield would be incorrect, because for example for the immobilisation on Celite, the carrier were not washed before lyophilisation and 100 % of the applied enzyme were bound to the carrier. Therefore mainly the selectivity in a cleavage reaction of racemic mandelonitrile towards the cleavage of (*S*)-mandelonitrile was used to compare the different carriers.

*Hb*HNL immobilised on Sepabeads

Sepabeads EC were in general not suitable for the application of the synthesis of chiral cyanohydrins, because the carrier itself catalysed the nonselective cleavage of the cyanohydrin. The mandelonitrile was stable in different organic solvents saturated with buffer and no significant cleavage of the nitrile could be observed as shown in figure 3.41 for toluene. For diisopropyl ether the observation was similar (results not shown). But using the *Hb*HNL immobilised on Sepabeads in the cleavage reaction in diisopropyl ether a conversion of over 60 % of (*R*)- as well as (*S*)-mandelonitrile was observed already after less then 10 min but no selectivity was shown. The reason

was the catalytic action of the carrier. The carrier with butyl functionalisation and absorptive binding of the enzyme showed a slightly different picture, figure 3.33. Here the reaction reaction rate was much slower and after 300 min reaction time a conversion of 35 % was measured, with a low enantioselectivity of 1.5 % enantiomeric excess.

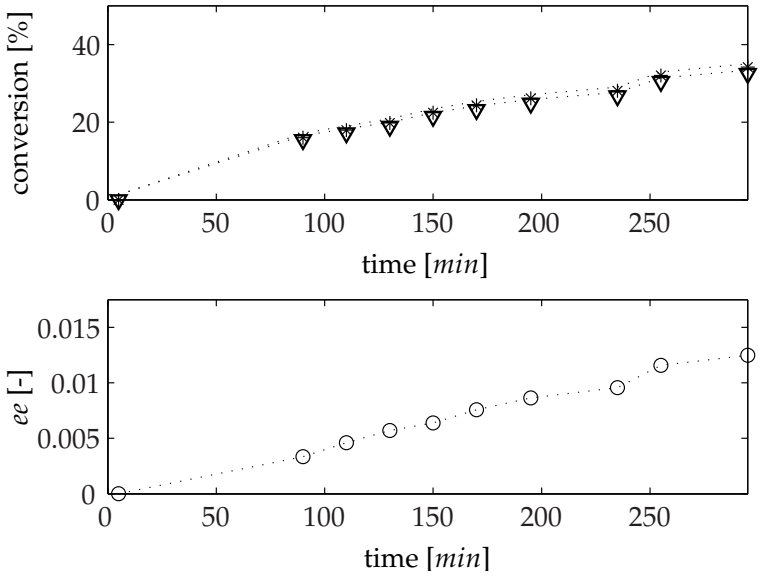

Figure 3.33: *Hb*HNL immobilised on Sepabead EC-BU and its application in diisopropyl ether saturated with citrate phosphate buffer (0.05 $mol\,L^{-1}$, pH 5.0), $c_{MN} = 12\,mmol\,L^{-1}$, $c_{enzyme,immobilised} = 53\,U\,ml^{-1}$, reaction temperatur 25°C; (*S*)-mandelonitrile $(*)$, (*R*)-mandelonitrile $(\bigtriangledown)$, enantiomeric excess (O), dashed line: visual aid

Also the Sepabead EC-BU carrier catalysed the nonselective cleavage of mandelonitrile, but with a lower reaction rate compared to the other investigated Sepabeads. The carrier material itself was catalyticlly active and mandelonitrile was also cleavage using a carrier with not active enzyme immobilsed. In figure 3.34 the time course of the cleavage of mandelonitrile catalysed by the BSA-Sepabeads EP immobilisate is shown. The picture is identical to the time course of the cleavage using a *Hb*HNL-Sepabeads EP immobilisate. So the enzyme was not influencing the reaction but the carrier catalysed it. It could not be determined which chemical group of the carrier was responsible for the catalytic action, but the spacer used for connecting the enzyme to the polymeric support may have been responsible.

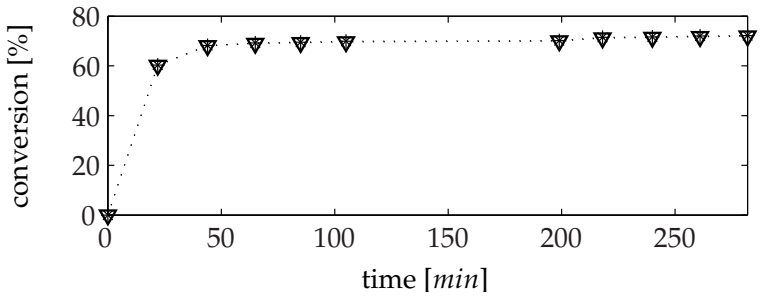

Figure 3.34: BSA immobilised on sepabead EC-EP and application in diisopropyl ether saturated with citrate phosphate buffer (0.05 $molL^{-1}$, pH 5.0), $c_{MN} = 12\,mmol\,L^{-1}$, $c_{enzyme,immobilised}$ = saturated, reaction temperatur 25°C; (*S*)-mandelonitrile $(*)$, (*R*)-mandelonitrile $(\bigtriangledown)$, dashed line: visual aid

*Hb*HNL immobilised on Poraver beads

*Hb*HNL could be successfully immobilised on the poraver beads. In figure 3.35 the conversion time plot of the enatioselective cleavage of racemic mandelonitrile in buffer saturated diisopropyl ether is shown. The catalyst was selective for the cleavage of the (*S*)-mandelonitrile and the concentration of the (*S*)-mandelonitrile mandelonitrile was almost constant over the whole reaction time. After an acceleration phase of approximately 1 hour the enatiomeric excess was increasing constantly until the reaction was stopped at 45 %. The linear increase of the enantiomeric excess was the result of a linear decrease of the (*S*)-mandelonitrile concentration (conversion up to 66 %) and a constant concentration of the (*R*)-isomere. When processing the reaction for longer time even higher enantiomeric excesses would be possible. Despite the successfull application the immobilisation procedure was quite work intensive. Therefore the immobilisation on Poraver beads was not further investigated, because an easier and less work intensive immobilisation procedure turned out to be feasible, cf. chapter 3.9.2.

*Hb*HNL immobilised on Celite

The procedure of the immobilisation of the enzyme on Celite was the least complicated of the procedures. For the immobilisation of the enzyme the mass ratio of 2 parts enzyme solution to 1 part carrier proved to be suitable due to the fact that Celite can take up water of the amount of 100 % of its weight. Because the water evaporated during lyophilisation, an adsorption efficienty could not be specified, because all enzyme was bound to the carrier. The enzyme immobilised on Celite could not be applied in an aqueous reaction system, because in water the enzyme was partly released from the carrier. In the activity test it could not be differentiated between the activity of the resolubilised or the adsorped enzyme, therefore the activity of the

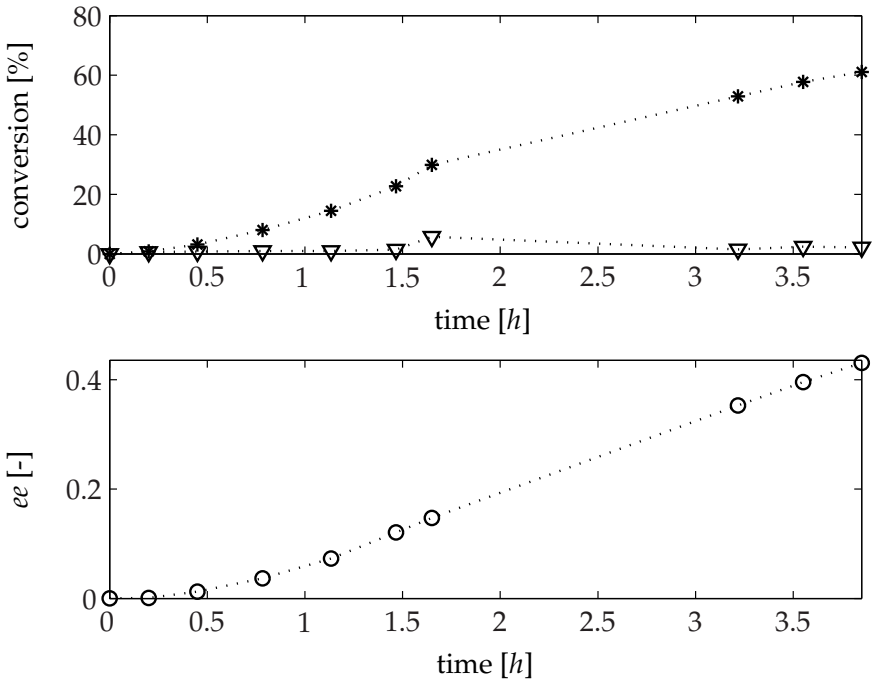

Figure 3.35: *Hb*HNL immobilised on poraver beads and its application in diisopropyl ether saturated with citrate phosphate buffer (0.05 $mol L^{-1}$, pH 5.0), $c_{MN} = 12\,mmol\,L^{-1}$, $c_{enzyme,immobilised} = 53\,U\,ml^{-1}$, reaction temperatur 25°C; (*S*)-mandelonitrile $(*)$, (*R*)-mandelonitrile $(\bigtriangledown)$, enantiomeric excess (O), dashed line: visual aid

immobilisate could not be measured. The carrier could be successfully applied in an non-conventional reaction media for the synthesis of chiral mandelonitrile as shown in figure 3.36. The reaction progress was similar to the reaction catalysed with the

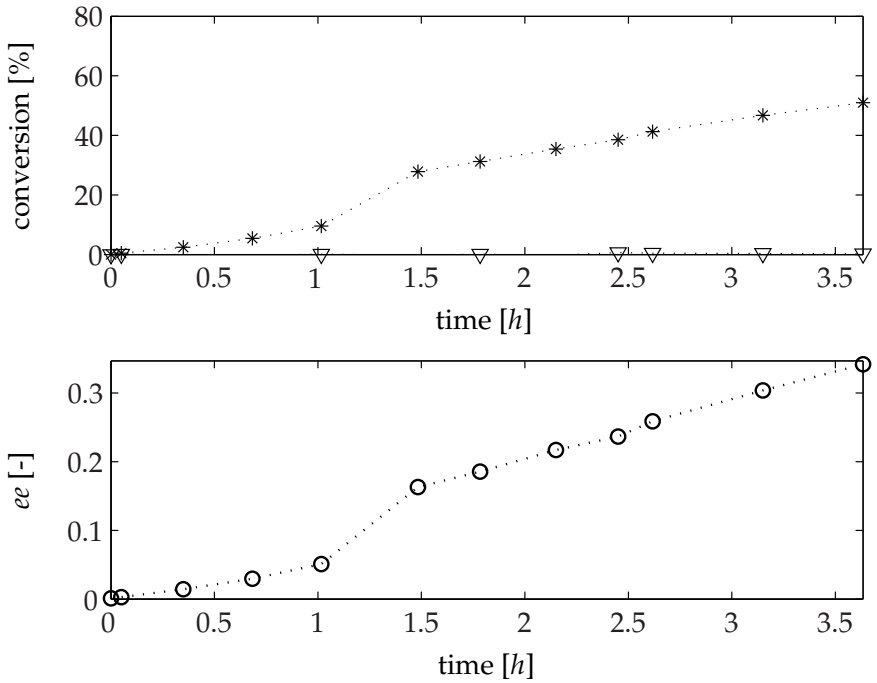

Figure 3.36: *Hb*HNL immobilised on Celite and its application in diisopropyl ether saturated with citrate phosphate buffer (0.05 $mol L^{-1}$, pH 5.0), $c_{MN} = 12\,mmol\,L^{-1}$, $c_{enzyme,immobilised} = 600\,U\,g^{-1}_{celite}$, reaction temperatur 25°C; (*S*)-mandelonitrile $(*)$, (*R*)-mandelonitrile $(\bigtriangledown)$, enantiomeric excess (O), dashed line: visual aid

Poraver immobilisate. After an acceleration phase of 1 hour the enantiomeric excess increased in a linear process until a value of 35 %. Almost no (*R*)-mandelonitrile was cleaved and the conversion of the (*S*)-mandelonitrile went up to 55 %. With longer reaction time higher enantiomeric excess might be reached with this method, too. The selectivity of the Poraver and Celite immobilisat are similar as seen in figure 3.37. The plot of the enantiomeric excess of the remaining substrate as a function of its conversion almost coincided with the theoretical curve constructed for the enantiomeric ratio E=inf, that is, for the case when exclusively the (*S*)-enantiomer is cleaved [332].

*Hb*HNL immobilised on nano carriers

The residual activity and protein concentrations of the supernatant, the washing solution and the enzyme that was immobilisedon nano carriers are presented in table 3.11. During the immobilisation procedure 1.035 *U* of activity (38 %) were lost. The loss

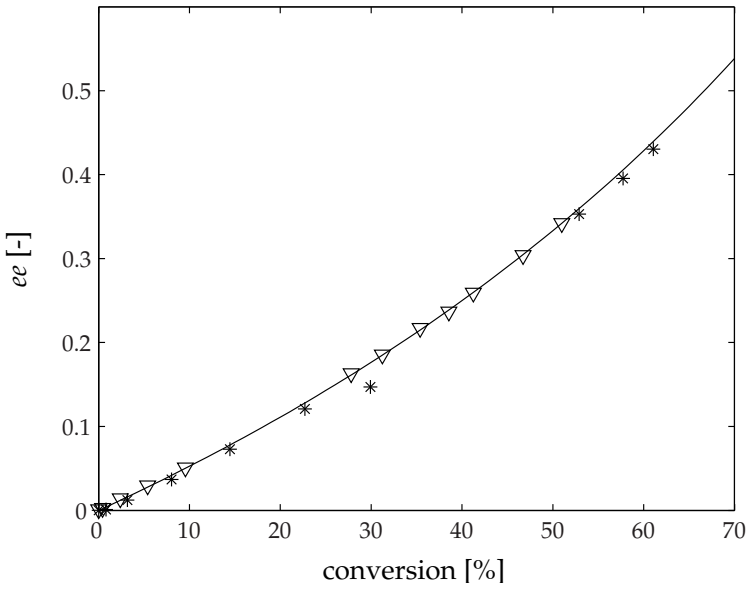

Figure 3.37: Comparison of *Hb*HNL immobilised on Celite $(\bigtriangledown)$ and poraver beads $(*)$ and its application in diisopropyl ether saturated with citrate phosphate buffer; solid line corresponds to the enantiomeric ratio E=inf [333, 332]

Solution	Activity $[U]$	Protein concentration $[mg]$
supernatant	1.45	58.5
sum washing fraction	0.08	1.95
washing fraction + supernatant	1.53	60.5
immobilised enzyme on carrier	0.17	3.8[1]
added enzyme	2.74	60
difference	1.04	0

[1] The concentration of the immobilised enzyme was not measured, because the nano diamonds disturbed the absorption measurement due to the clouding of the solution. The value is calculated on the basis of the activity measurements. It was assumed, that all immobilised enzyme on the carrier surface is active.

Table 3.11: Activity and protein concentrations of the nano carrier immobilisation procedure

of activity might be caused by the inactivation of the enzyme during the incubation period. 0.173 U enzyme could be bound on 15 μg of the carrier (11.5 $U\,mg^{-1}$), which corresponded to 6 % of the added enzyme activity. The activity of the different fractions is illustrated in figure 3.38. Almost all unbound enzyme was removed from the carriers after the second washing. Then the activity in the washing fraction was almost constant with less than 5 $U\,ml^{-1}$. The measurement of the protein concentrations showed the same picture. Almost all protein was found in the supernatant. The amount of immobilised protein was in the range of the measurement error (ca. 10 %) of the assay and could therefore not be detected. After the second washing the detected concentrations in the washing fractions were lower than 0.1 $mg\,ml^{-1}$ (results not shown).

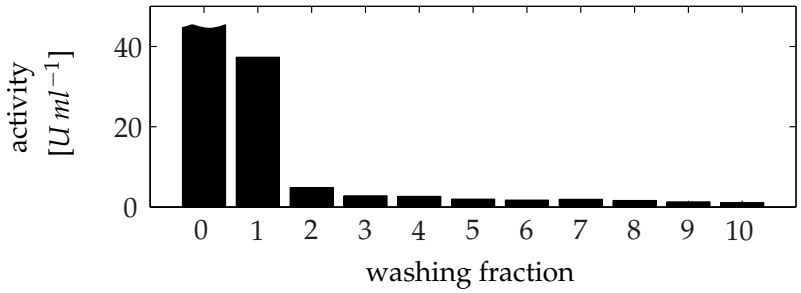

Figure 3.38: Activity in the supernatant and washing fraction of the immobilisation on nano diamonds; 0. Supernatant, activity: 964 Uml^{-1}, 1 to 11. washing fraction

The immobilisation could be performed successfully. A problem during the immobilisation procedure was, however, the separation of the nano particles from the solution. Most of the particles could be removed by centrifugation, but a small amount of the immobilisate stayed in the liquid. The measured activity in the washing fraction can therefore to accrue from suspended immobilisate in the washing fraction.

Cleavage and synthesis of mandelonitrile using *Hb*HNL immobilisied on nanocarriers

The *Hb*HNL that had been immobilised on on nano diamonds could be successfully used for the synthesis of enantioenriched (*S*)-mandelonitrile. As written in appendix A.4.1 the reactions was performend in the aqueous reaction system and the benzaldehyde concentration was varied from 1 to 10 $mmol\,L^{-1}$. To avoid damages on the online analytic due to sediments of the carrier the reaction progress was tracked by GC measurements. A typical reaction progress is presented in figure 3.39. The amount of nano carriers applied was so low that no clouding in the reaction vessel could be observed. But the addition of a precise amount of carriers turned out to be difficult, because the nano carriers tend to agglomerate in the stock solution and these

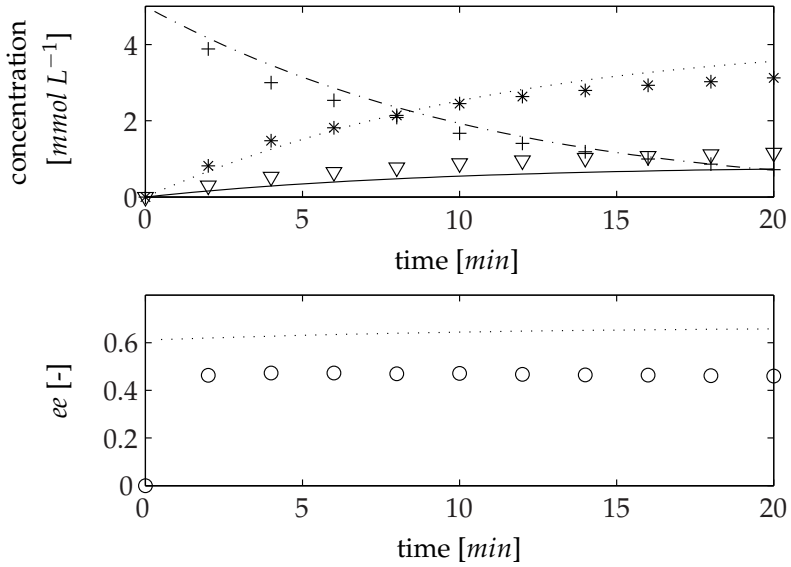

Figure 3.39: Synthesis of enantioenriched mandelonitrile with immobilised *Hb*HNL on nano diamonds, 0.05 $mol\,L^{-1}$ citrate-phosphat buffer, pH 5.0, 25°C, hydrogen cyanid (not shown) $c_{HCN,0} = 50\,mmol\,L^{-1}$, benzaldehyde $(+)$ $c_{BA,0} = 5\,mmol\,L^{-1}$, (*S*)-mandelonitrile $(*)$, (*R*)-mandelonitrile $(\bigtriangledown)$, enantiomeric excess (O); The lines present the simulation with the kinetic model, cf. chapter 3.5, table 3.4:iv

agglomerations were difficult to break in the highly concentrated solution. The agglomerations dissolved in lower concentrated solutions, but the dilution steps were prone to errors due to the agglomerations in the stock solution.

The reaction progress could be simulated with the kinetic model and the kinetic parameters presented in chapter 3.5. Only the applied enzyme activity had to be adjusted. For the simulation an enzyme amount corresponding to 1.2 mgL^{-1} was assumend, but 0.71 mgL^{-1} should have been added. This adjustment of the enzyme concentrations in the simulation stressed the observation made during the experiments, that the agglomeration of the nano diamonds in the stock solution made it difficult to add a precise amount of the catalyst.

Another observation was the reduced enantiomeric excess when using nano diamonds, as visible for example in figure 3.39. Here the measurement of the enantiomeric excess is compared to the simulation: the excess calculated differed significantly from the excess measured. According to the simulation with the substrate and enzyme concentrations outlined the enantiomeric excess should reach a value of 70 %. Instead a value of approximately 50 % was measured. It can be supposed that the carrier material itself catalysed the synthesis of the racemic product.

On the surface of the nano diamonds exist several functional groups, which can also be crosslinked. Due to an incomplete amino functionalisation of the groups on the surface residuals like carboxyl function may have catalysed the unselective syn-

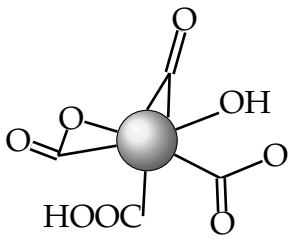

Figure 3.40: Supposted schematische drawing of the Nano diamond surface prior to amino fuctionalisation

thesis and cleavage of mandelonitrile. As a result, the additional chemocatalysed reaction synthesised unselective racemic mandelonitrile and lowered the observed enantiomeric excess, differing from a reaction with non immobilised free enzyme. This assumption could be confirmed in a synthesis reaction containing only non functionalised nano carrier. Here the reaction rate of the synthesis was enhanced compared to the blank reaction (results not shown).

The same autocatalytic effect observed in an aqueous reaction system was also seen in a purely organic system. As it is visible in figur 3.41, mandelonitrile was stable in buffer saturated toluene and the nitrile was cleaved as soon as nano particles were added into the solution.

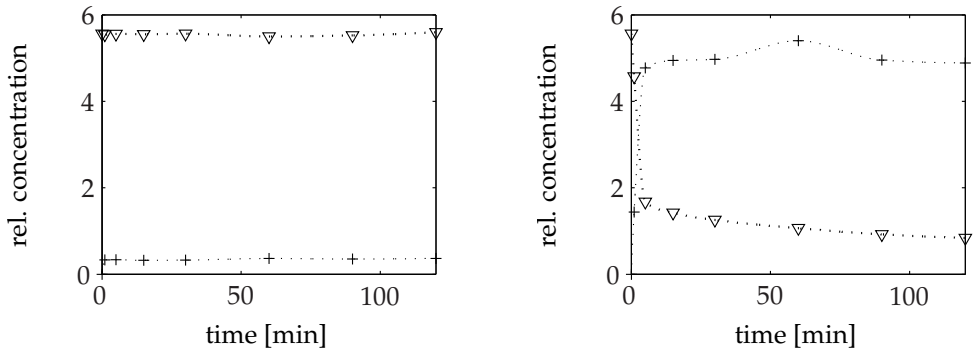

Figure 3.41: Stability of mandelonitrile in toluene saturated with citrate phospate buffer (0.05 $mol L^{-1}$, pH 5.0), reaction temperatur 25°C; $(\bigtriangledown)$ mandelonitrile: $c_{MN,0} = 25\,mmol\,L^{-1}$, $(+)$ benzaldehyde, dashed line: visual aid; concentrations are expressed as peak area of the substance divided by the peak area of the internal standard (normalised peak area).
left: only saturated tolunene
right: catalysing effect of nano diamonds, $c_{nanodiamonds} = 1\,g\,L^{-1}$

[14]The concentration is express as peak area of the substance divided by the peak area of the internal standard (normalised peak area). Im principle due to the linear correlation of the normalised peak

It could be shown that *Hb*HNL can be immobilised on nano diamonds. But such carriers were not suitable for the enantioselective synthesis, because they showed a catalytic activity for the nonselective synthesis of mandelonitrile. The catalytic activity was attributed to different functional groups on the surface of the carriers.

3.10 The application of *Hb*HNL in non-conventional reaction media

3.10.1 Solvent screening

After the successful investigation of the immobilisation of the *Hb*HNL the question of a suitable organic solvent had to be solved. The selection of the solvents was geared towards the task to combine the Diels-Alder reaction with the stereoselective addition of HCN. For the solvent screening the effect of the solvent on the enantioselective cleavage of racemic mandelonitrile with *Hb*HNL immobilised on Celite was investigated, performing the reaction in different solvents. The tested solvents are presented in table 3.12. The solvents were choosen to cover a wide range of polar (low log P values) to unpolar (high log P values) solvents. Laane et al. suggested using the polarity of solvents, expressed by the log P value[15], as the main criterion for optimising organic solvents in multiliquid-phase biocatalysis [174]. This concept has gained a widespread influence on the choice of organic solvents used as the second phase in enzymatic transformations. But often the log P value cannot be correlated to the activity and stability of enzymes applied in biphasic systems. For example the activity and stability of the *Hb*HNL showed no correlation with log P values in a biphasic system [156]. Filho et al. proposed the idea of the functionality of the solvent [178]. They argue that the activity and stability depends on the functionality of the solvent, like esters, cyclic alkenes, etc. rather than the polarity. And the chosen solvents (table 3.12) cover also some of the possible functionalities of organic solvents.

Costest et al. investigated the optimum amount of water for the production of (*S*)-2-hydroxy-4-phenyl-butanenitrile with *Hb*HNL immobilised on celite [323] in different solvents (dibutylether, diethylether, *tert*-butyl-methylether, and diisopropylether). They found out that the optimum water content was between 1 and 1.5 % (v/v), depending on the solvent. Therefore the water content was set to 1 % (v/v).

In the system with the best performance, the conversion of the (*S*)-stereoisomer reached a high level in short time but the conversion of the (*R*)-stereoisomer remained at a low level at the same time. The difference in the conversion of both stereoisomers has to be maximised in a short time. Simultaneously a high conversion must be attained to simplify the downstream process. For the evaluation of the solvents

area to concentration, the concentration could have be direcly calculated by a proportion factor, which was not determained.

[15] Logarithm of the partition coefficient of a given compound in the standard n-octanol/water two-phase system.

Solvent	**log P**	solubility in water	functionality
cyclohexane	3.4	0.05 $g\,L^{-1}$	cyclic alkane
toluene	2.5	0.52 $g\,L^{-1}$	aromatic compound
tert-butyl methyl ether (MTBE)	1.06	42 $g\,L^{-1}$	ether
dichloro methane	1.3	20 $g\,L^{-1}$	halogenated solvent
diisopropyl ether	1.52	12 $g\,L^{-1}$	ether
ethyl acetate	0.68	85.3 $g\,L^{-1}$	ester

Table 3.12: Selected for screening

the reaction progress was measured and the conversions of both stereoisomers were measured independently. For the comparison of the solvents a performance factor was calculated according to equation 3.63, which express the prefomance criteria. The performance factor describes the apparent reaction rate of the cleavage of (*S*)-mandelonitrile minus the apparent reaction rate of the cleavage of (*R*)-mandelonitrile.

$$f = \left(\frac{c_{S,0} - c_S(t)}{c_{S,0}} - \frac{c_{R,0} - c_R(t)}{c_{R,0}} \right) \frac{1}{t - t_0} \tag{3.63}$$

In figures 3.42 to 3.47 the performence factors measured for the different solvents system are compared. In the upper plots the conversions of (*S*)- and (*R*)-mandelonitrile are shown, in the mid plots the enantiiomeric excesses are presented and the performance factors are shown in the lower plots. In table 3.13 the results

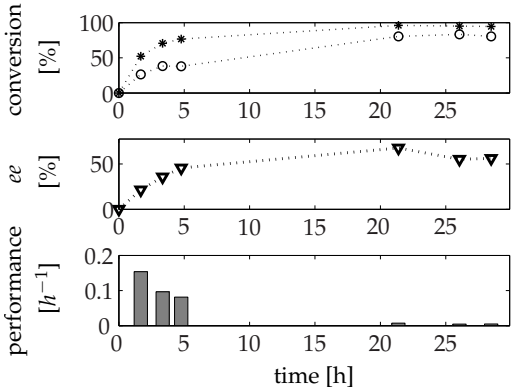

Figure 3.42: *Hb*HNL immobilised on Celite and application in cyclohexane

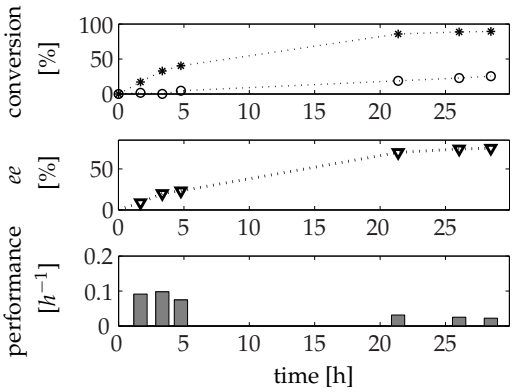

Figure 3.43: *Hb*HNL immobilised on Celite and application in dichloro methane

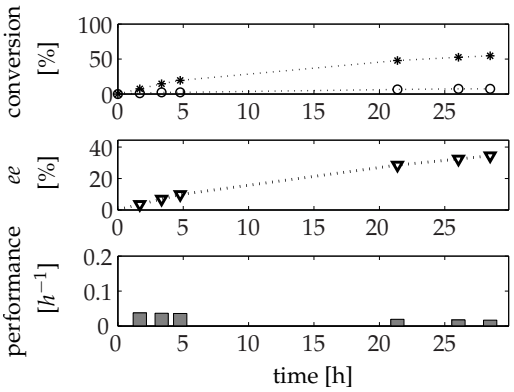

Figure 3.44: *Hb*HNL immobilised on Celite and application in toluol

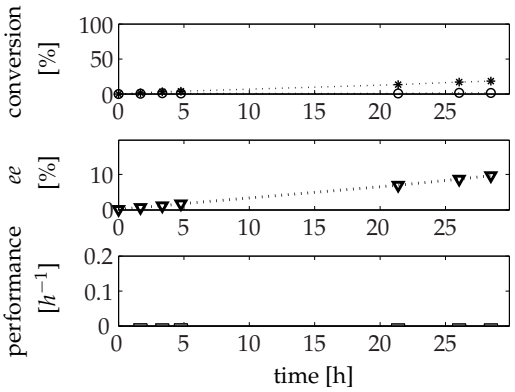

Figure 3.45: *Hb*HNL immobilised on Celite and application in ethyl acetate

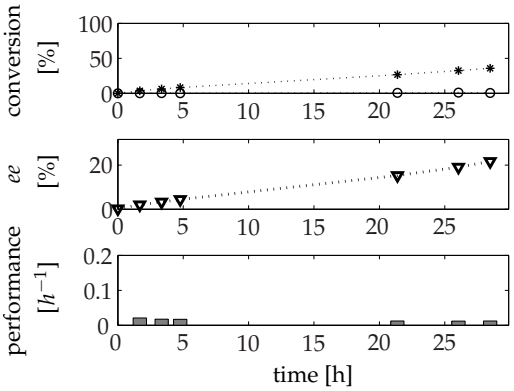

Figure 3.46: *Hb*HNL immobilised on Celite and application in *tert*-Butyl methyl ether

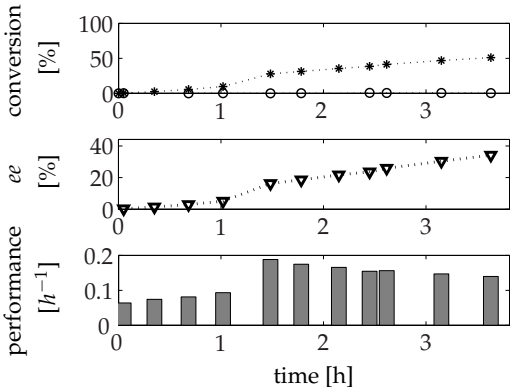

Figure 3.47: *Hb*HNL immobilised on Celite and application in diisopropyl ether

are summarised. Cyclohexane turned out to be not suitable. The performance factor was high at the beginning due to a fast total reaction rate, but it dropped drastically to only 3 % of the maximum with longer reaction times (figure 3.42 and 3.13). The reason for this was a quite fast non selective cleavage of the mandelonitrile, which resulted in a high conversion of the (*R*)-stereoisomer with up to 83.3 %.

Solvent	$U_{S,end}$[1]	$U_{R,end}$[1]	f_{max}	f_{end}
Cyclohexane	96.2 %	83.3 %	15.4	0.5
Dichloro methane	89.4 %	25.4 %	9.8	2.2
Toluene	54.7 %	7.3 %	3.7	1.7
Ethyl acetate	18.5 %	1.6 %	0.7	0.6
tert-Butyl methyl ether	35.7 %	1 %	2.1	1.2
Diisopropyl ether	51 %[1]	0.7 %[1]	18.8	14

[1] The reaction performed in diisopropyl ether was already stopp after 3.6 *h*, all other were stoped after 28.5 *h*

Table 3.13: *Hb*HNL immobilised on Celite and application in different solvents: results

With less reservations dichloro methane and ethyl acetate turned out to be applicable. Dichloro methane had also a high performance factor at the beginning, but it dropped only to 22 % of the maximum. The enzymatic reaction had a higher contribution to the total reaction rate due to a lower nonselective reaction rate, but still the nonselective cleavage reacton was high leading to a conversion of 25.4 % for the (*R*)-stereoisomer. The picture for ethyl acetate was different. Here the performance factor was rather low at 0.7 and almost constant over the whole reaction time. The (*R*)-stereoisomer was cleaved with a low rate and only 1.6 % conversion was reached after 30 hours reaction time. The enzyme cleaved the nitrile selective, but also with a low rate, so that the conversion reached 18.5 % at the end. Toluene and MTBE were feasible too, and the observations were quite similar for these solvents. A moderate performance factor was observed at the beginning which dropped to the half at the end. The performance at its maximum for MTBE was about 56 % of the performance in toluene and at the end the performace in MTBE picked up and was 70 % of the performance in toluene. The reason for the catchup was a lower nonselective reaction rate, which resulted in a lower conversion of the (*R*)-mandelonitrile with only 1 % to 7.3 %.

The outstanding winner of the tests was diisopropyl ether. The performance factor was highest with 18.8 at its maximum and dercreased only with 22 % to 14. This can be explained by a high enzymatic activity and a low nonselective side reaction rate. The enzymatic activity was so high, that already after 3.5 hours a conversion of more the 50 % of the (*S*)-mandelonitrile was observed ((*R*)-mandelonitrile only 0.7 %).

In general, the results could not be correlated to the log P value. The functionality of the solvent played a major role and with some reservations all esters were suitable. The results agreed with the observations made by Bauer et. al. They observed in a two phase system the highest activity using diisopropyl ether and the activity was more than two time higher in comparison to the activity for MTBE. The activity for ethyl acetate was only two thirds of the activity obtained with MTBE [156]. For toluene and cyclohexane no data for comparison are available.

3.10.2 Optimisation of the enzyme loading

For the investigation of influences of the enzyme loading the solvent toluene was chosen. The aromatic solvent showed a good performance and enzyme stability and was a suitable solvent for the application of the chemzyme catalysed Diels-Alder reaction, which diisopropyl ether was not, cf. chapter 4.

A common feature is that there is for each enzyme and matrix an optimal enzyme/carrier ratio for the expression of activity [85]. Barros et al. investigated the influence of the enzyme loading on catalytic activity for the application of α-chymotrypsin immobilised on different carriers for the synthesis of dipeptides *N*-acetyl-L-phenylalanyl-L-alanylamide, *N*-benzoyl-L-tyrosyl-L-alanylamide, and *N*-benzoyl-L-alanyl-L-alanylamide in acetonitrile [305]. They showed, that the specific activity ($\mu mol\, min^{-1}\, g^{-1}_{enzyme}$) they observed passed a maximum with increasing enzyme loading for the immobilisation on celite. Also Costes et al. observed a similar behaviour for the enzyme loading [323].

In figure 3.48 the reaction rates observed in this study are shown as a function of the substrate concentrations and enzyme loading. For all loadings the reaction rate showed a saturation kinetic with increasing concentration and the reaction rate approached a maximum rate whose value was specific for each loading. The highest reaction rates where observed at the highest enzyme loading of 6.8 $mg_{enzyme}\, ml^{-1}_{\text{reaction volume}}$ (114 $mg_{enzyme}\, g^{-1}_{\text{celite}}$) at substrate concentrations of 500 $mmol\, L^{-1}$. At concentrations lower than 100 $mmol\, L^{-1}$ the carrier showed the highest conversion rates with a four times lower loading. The lowest rates were obtained with a loading of 19 $mg_{enzyme}\, g^{-1}_{\text{celite}}$.

A detailed account of the results gives figures 3.49 and 3.50. The apparent activity, reaction rate normalised by the applied enzyme concentration [$mmol\, min^{-1}\, mg^{-1}_{enzyme}$] is plotted both for different substrate concentrations and at a constant substrate concentration of 50 $mmol\, L^{-1}$ and for different enzyme loadings.

The apparent activities reflected the amount of active enzyme on the carrier. The activity crossed a maximum at a loading of 28.5 $mg_{enzyme}\, g^{-1}_{\text{celite}}$. Carriers with higher loadings as well as the carrier with the lowest loading were less active. As previously mentioned such a profile has been observed for different enzymes immobilised on different types of porous carriers. The activity was lower at lower enzyme load-

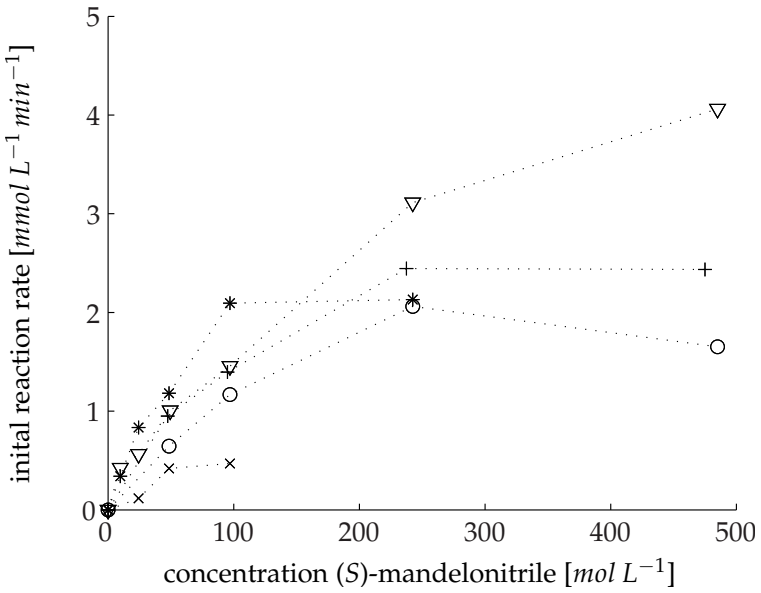

Figure 3.48: Influence of the enzyme loading on the observed reaction rate. *Hb*HNL immobilised on Celite and application in toluene (1 % (v/v) buffer citrate phosphate buffer 0.05 $mol L^{-1}$, pH 5.0), reaction temperatur 25°C, dashed line: visual aid; for the assignment of symbols cf. table 3.14.

Symbol	Spec. activity		Spec. mass	
	$[U\ ml^{-1}_{\text{reaction volume}}]$	$[U\ g^{-1}_{\text{celite}}]$	$[mg_{\text{enzym}}\ ml^{-1}_{\text{reaction volume}}]$	$[mg_{\text{enzyme}}\ g^{-1}_{\text{celite}}]$
$\bigtriangledown$	300	5000	6.8	114
O	150	5000	3.4	114
$+$	150	2500	3.4	57
$*$	75	1250	1.7	28.5
$\times$	50	833	1.1	19

Table 3.14: Assignment of symbols of figure 3.48 and 3.49

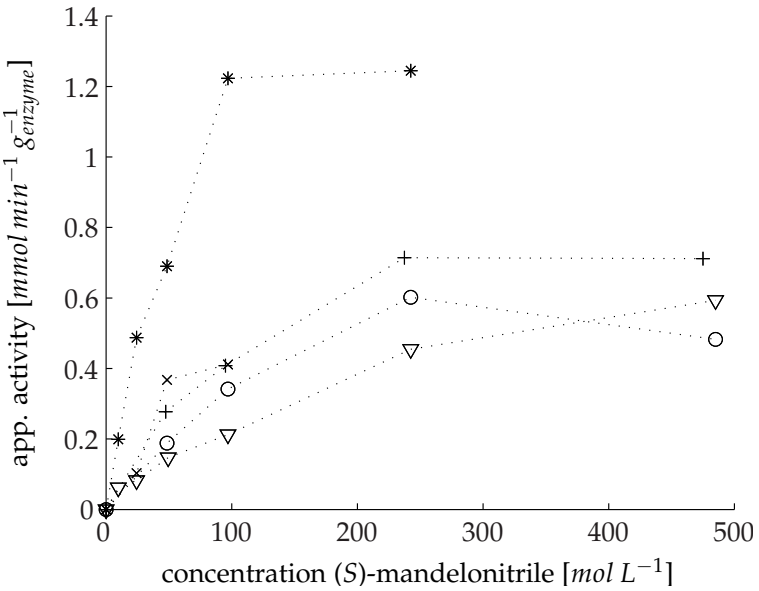

Figure 3.49: Influence of the enzyme loading on the apparent activity rate [$mmol\,min^{-1}\,mg^{-1}_{enzyme}$]. *Hb*HNL immobilised on Celite and application in toluene (1 % (v/v) buffer, citrate phosphate buffer 0.05 $mol\,L^{-1}$, pH 5.0), reaction temperatur 25°C, dashed line: visual aid; for the assignment of symbols cf. table 3.14.

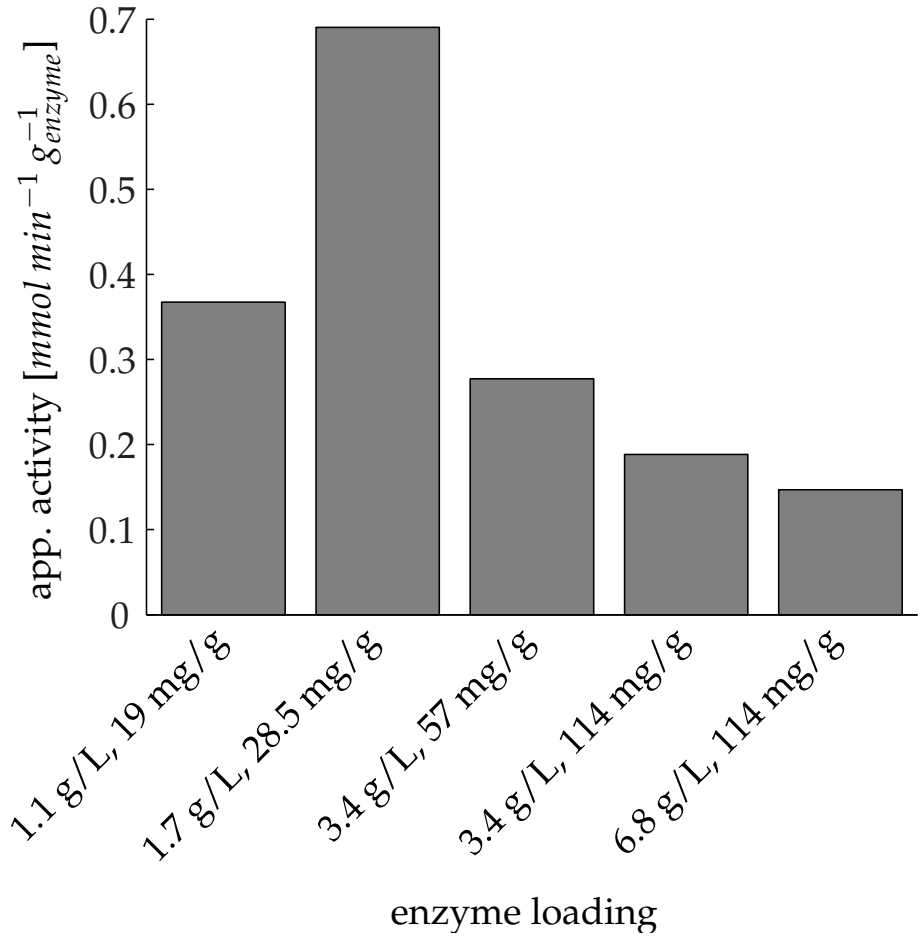

Figure 3.50: Comparison of the apparent activity at 50 $mmol\,L^{-1}$ substrate concentration as function of the enzyme loading on. *Hb*HNL immobilised on Celite and application in toluene (1 % (v/v) buffer citrate phosphate buffer 0.05 mol, L^{-1} , pH 5.0), reaction temperatur 25°C.

ings due to the direct inactivation of the enzyme by the support. This occurs probably because enzyme conformational change/unfolding happens at the support surface [334]. At higher enzyme loading the onset of mass transfer limitations poses another difficulty, that prevents the enzyme from exerting its activity at a higher rate. There are several reasons for these limitations. First, the area for the reaction to take place may have been be reduced due to closed pores, cf. 3.51. Maybe the high loading

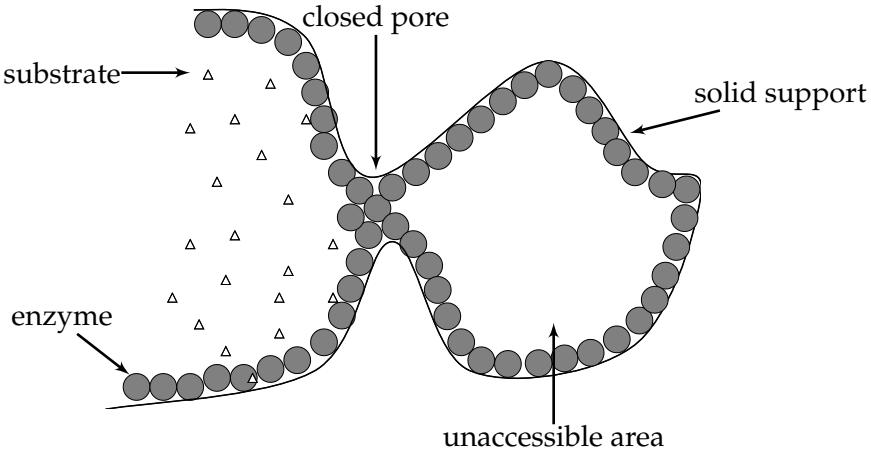

Figure 3.51: Schematic drawing of closed pores and reduced effective area due to overloading

led to a closing of cavitys, so that the surface in the cavities was not longer accessible for the substrate. The effective area for reaction was reduced causing a lower observed reaction rate. A second phenomenon could be the build up of enzyme multilayers, which is illustrated in figure 3.52. The substrate had to be transported through the layer by diffusion and a substrate gradient was build up. The enzymes in the lower layers catalysed the reaction with a lower rate, because the substrate concentration was reduced to a range where the reaction rate follows a kinetic with a reaction order larger than zero. The effect was a lower apparent specific activity. Both effects can occur simultaneously. From an observation of the reaction rate no proper conclusions could be drawn which effect dominated.

Despite the disadvantage of transport limitation a multimolecular enyzme layer can also have positive effects on the long term stability. The outer layers shield the enzymes of the lower layer from the direct contact to, for example, organic solvents. The substrate concentration is reduced over the thickness of the layer, which can reduce the deactivating effects of a substrate. The stabilising effect could also be observed at low enzyme loading by carrying out the immobilisation in the presence of extraneous proteins (albumin, gelatin, casein) or polyethylene glycol [273].

Up to now only the cleavage of racemic mandelonitrile was investigated. During the next experiments the synthesis of enantioenriched (*S*)-mandelonitrile in a purely organic solvent system using *Hb*HNL immobilised on Celite was tested. Following

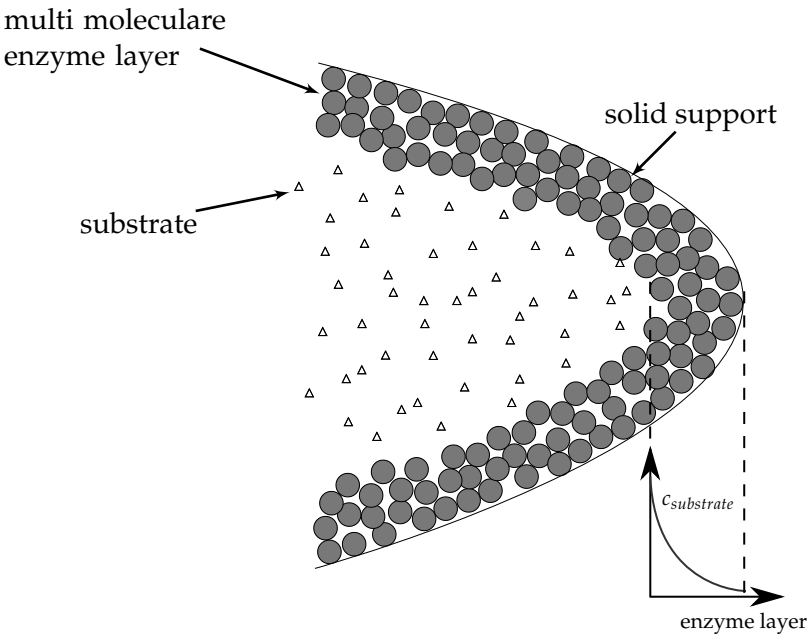

Figure 3.52: Schematic drawing of an multi moleculare enzyme layer and the concentration gradien over the layer

from the results of the solvent screening diisopropyl ether was used with a water content of 1 % (v/v) and starting concentrations of up to 1064 $mmol\,L^{-1}$ for HCN and 412 $mmol\,L^{-1}$ for benzaldehyde, which was 13 times higher than the maximum solubility in water. The results of the enzyme loading presented in chapter 3.10.2 were not known at this point in time. Therefore the higher loading of 6.8 $mg_{enzyme}\,ml^{-1}_{\text{reaction volume}}$, 114 $mg_{enzyme}\,g^{-1}_{\text{celite}}$ was used.

In figures 3.53 to 3.54 the typical time courses of the conversion, enantiomeric excess and apparent reaction rates are shown. In all cases a conversion of over 98 % and enantiomeric excess over 99 % were reached. The time courses of the apparent reaction rates were similar in all examples. At the beginning the apparent reaction rates were about 0.25 $mmol\,L^{-1}\,s^{-1}$. After 50 % conversion the reaction rates were reduced to a half. The reaction rates decreased further more until the reaction reached an equilibrium after 40 min in figure 3.53 and after 60 min in figures 3.55 and 3.54. In the latter cases the HCN concentration was doubled in comparison to the first example. It seemed that the high HCN concentration inhibited the reaction from reaction time 20 to 60 minutes (conversion 60 % to 100 %). Characteristic was the increase of the enantiomeric excess until 90 % conversion.

The reaction progress could be simulated approximately supposing the ordered-uni-bi mechanism, presented in chapter 3.5. In table 3.15 the apparent kinetic parameters are presented. The parameters were obtained by progress curve analysis. The

kinetic parameters were similar to the parameters obtained in the aqueous system. Only the apparent rate parameters $k_{cat_{cleavage}}$ and $k_{cat_{synthesis}}$ are significantly lower in the organic system.

Parameter	Diisopropyl ether	Toluene	Citrate buffer	Unit
$k_{cat_{cleavage,app.}}$	$3.1 * 10^{-4}$	0.0022	33	$[s^{-1}]$
$k_{cat_{synthesis,app.}}$	0.0015	$6.4 * 10^{-4}$	132	$[s^{-1}]$
$\left(\frac{k_{cat_{synthesis,app.}}}{k_{cat_{cleavage,app.}}}\right)$	4.7	0.3	4	[-]
$K_{m_{HCN,app.}}$	14.7	14.7	14.4	$[mmol\ L^{-1}]$
$K_{m_{BA,app.}}$	2	0.8	0.45	$[mmol\ L^{-1}]$
$K_{m_{(S)-MN,app.}}$	1.2	1.2	1.9	$[mmol\ L^{-1}]$
$K_{i_{BA,app.}}$	1.5	1.5	0.35	$[mmol\ L^{-1}]$

Table 3.15: Comparision of the apparent kinetic parameters, progressc curve analysis, solvents: diisopopyl ether, toluene and citrate buffer

The reason for the drastically reduced activity in the organic system was the inactivation during the immobilisation on the one side. On the other hand the reaction was not a homogeneous but a heterogeneous reaction. The relevant concentrations for the kinetics of the enzyme were not the bulk concentrations, but rather the concentrations in the boundary layer around the enzyme on the surface of the carrier. These concentrations were influenced by the rate of diffusion through the pores to the surface of the carrier and by the reaction rate. In the case investigated the situation was even more complicated by the possible existence of a second liquid phase. The enzyme needs a low amount of water to be active [323]. And due to the high hydrophobicity of the Celite most of the water was bound to the Celite where also the enzyme was located, the enzyme was probably surrounded by a water layer. The components had to pass the solvent/water border before they could react at the surface of the carrier where the enzyme was bound. At the solvent/water border the concentrations changed discontinuously and, depending on the properties of the organic solvent, the concentrations in the organic phase differed from the concentrations in the water phase. By only measuring the concentrations in the organic bulk phase it was difficult to determine the concentrations at the location of the enzyme, especially because of the unknown partitioning coefficients for all components. Therefore it could not be distinguished between the different effects and the kinetic parameters were only apparent kinetic parameters, because only the dynamic in the bulk phase was used for their determiation.

As seen in the figures the characteristic increase of the enantiomeric excess at the beginning could not be explained by the kinetic model. It was to be expected, that

the enantiomeric excess started at values close to 100 % and decreased over time. The lower *ee* at the beginning might be the result of local high HCN concentrations directly after the addition. Because HCN is a polar molecule it seeks to the surface of the Celite which was hydrophobic and seeks to the aqueous layer. Shortly after injection the concentration of HCN in the aqueous layer raised high, larger than the calculated concentration in the bulk phase. The less polar and larger molecule benzaldehyde diffused with a lower rate to the surface and at the organic/water border the concentration dropped due to the solubility of benzaldehyde which is lower in water than in the organic phase. At the border the benzaldehyde reacted directly with the HCN to racemic mandelonitrile. Because the enzyme was located at the surface of the carrier the reaction could be selectivly catalysed only if the benzaldehyde concentration was larger than zero at the carriern surface. The benzaldehyde had first to diffuse through the layers to the surface, which caused a delay in the production of (*S*)-mandelonitrile.

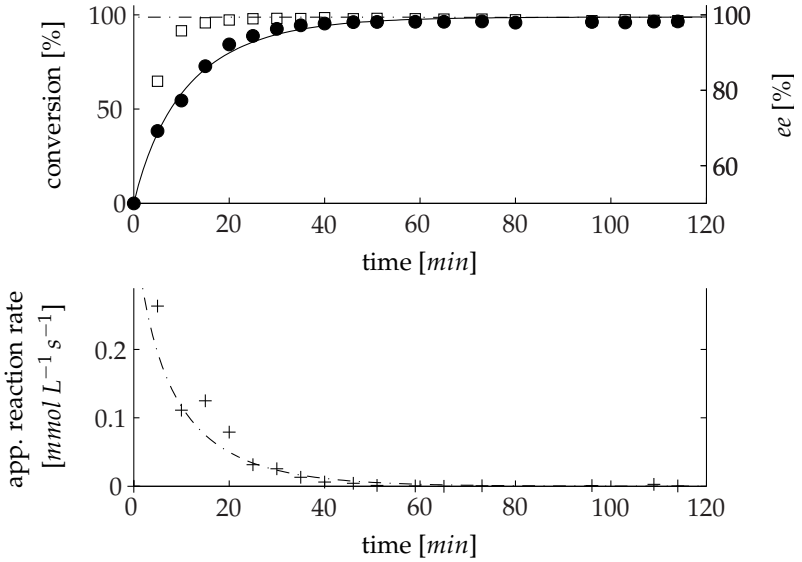

Figure 3.53: Enantioselective synthesis on (*S*)-mandelonitrile in diisopropyl ether. *Hb*HNL immobilised on celite, 6.8 $mg_{enzyme}\, ml^{-1}_{\text{reaction volume}}$, 114 $mg_{enzyme}\, g^{-1}_{\text{celite}}$, HCN 530 $mmol\ L^{-1}$, benzaldehyde 206 $mmol\ L^{-1}$, 1 % buffer;
(• conversion; □ *ee*; **lines** simulations),

Comparison of diisopropyl ether and toluene for the enantioselective synthesis of mandelonitrile

The existence of an aqueous layer, and by that a second water phase, was confirmed by an observation made by comparing the results to a reaction performed in a different solvent than diisopopyl ether. In figures 3.56 and 3.57 the enzymatic catalysed

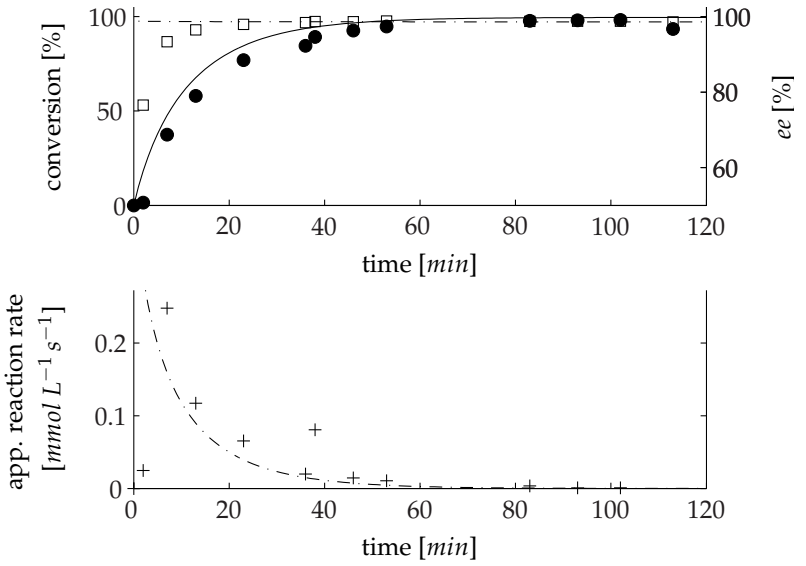

Figure 3.54: Enantioselective synthesis on (*S*)-mandelonitrile in diisopropyl ether. *Hb*HNL immobilised on celite, 6.8 $mg_{enzyme}\, ml^{-1}_{\text{reaction volume}}$, 114 $mg_{enzyme}\, g^{-1}_{\text{celite}}$, HCN 1064 $mmol\, L^{-1}$, benzaldehyde 206 $mmol\, L^{-1}$, 1 % buffer;
(• conversion; □ *ee*; **lines** simulations)

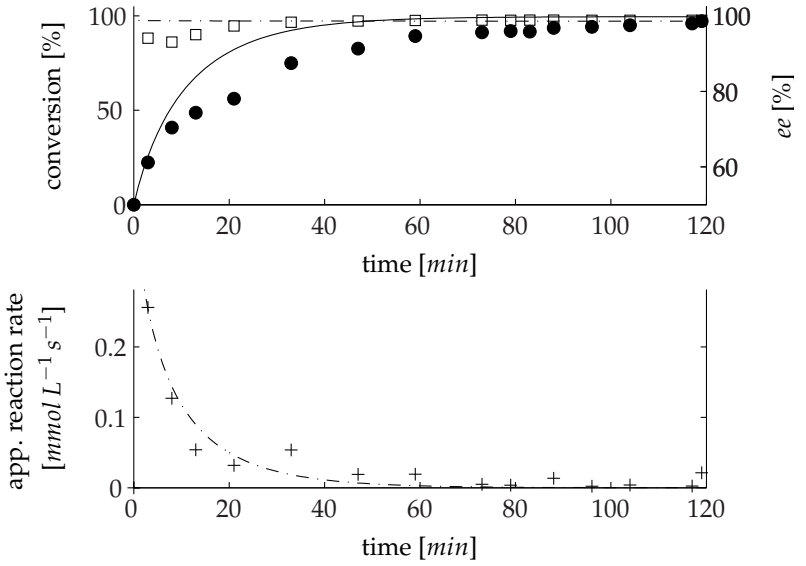

Figure 3.55: Enantioselective synthesis on (*S*)-mandelonitrile in diisopropyl ether. *Hb*HNL immobilised on celite, 6.8 $mg_{enzyme}\, ml^{-1}_{\text{reaction volume}}$, 114 $mg_{enzyme}\, g^{-1}_{\text{Celite}}$, HCN 1064 $mmol\, L^{-1}$, benzaldehyde 412 $mmol\, L^{-1}$, 1 % buffer;
(• conversion; □ *ee*; **lines** simulations)

syntheses of (*S*)-mandelonitrile performed in diisopropyl ether and toluene are compared. In contrast to the previous reactions the benzaldehyde concentration was reduced to 80 $mol\,L^{-1}$. For experimental reasons also the enzyme concentration was reduced to one third to decrease the reaction speed, so that a proper sampling was possible. The reaction carried out in diisopropylether showed the already known characteristics and after 20 minutes a conversion of more than 95 % and an enantiomeric excess of over 99 % was reached. When using toluene as organic solvent only a conversion of about 65 % was observed. The significantly lower apparent equilibrium conversion was caused by the different partition coefficient for mandelonitrile, benzaldehyde and HCN in toluene in comparison to diisopropyl ether. In the equilibrium different concentrations will be reached in the organic bulk phase depending on the different partition coefficients. In this investigated example, mandelonitrile was a polar molecule and therefore the concentration of mandelonitrile in the water phase in the equilibrium with the organic phase was lower in the polar diisopropyl ether than in the unpolar toluene. The mandelonitrile was pushed more into the water phase. In the equilibrium the concentrations in the water phase were similar for both solvents, but due to the different partitioning coefficients the measured concentrations in the bulk phase differed. A lower concentration of mandelonitrile in the equilibrium was observed in the less polar solvent toluene. An indication for the changed partition coefficients were the reduced ratio $k_{cat_{synthesis}}/k_{cat_{cleavage}}$, cf. table 3.15. In toluene the apparent reaction rate of the cleavage reaction war higher than the rate for synthesis and the higher mandelic acid concentration in the aqueous layer could be the reason for this observation.

The benzaldehyde concentrations in the experiments presented in figures 3.56 and 3.56 were significantly lower than in the figures 3.53 to 3.54. Thus also the synthesis of (*S*)- mandelonitrile in toluene was tested with a benzaldehyde starting concentration of 206 $mmol\,L^{-1}$. In figure 3.58 the result is shown. The time curve differed not significantly from the previous results. Only the apparent equilibrium concentration of 88 % was higher than in figure 3.57.

3.10.3 The enantioselective synthesis of (*R*)-mandelonitrile

The hydroxynitrile lyase isolated form *Prunus amygdalus* catalyse the cleavage and synthesis of (*R*)-mandelonitrile enantioselectively. For comparison the same procedure, developed for the *Hb*HNL, was applied also for the synthesis of (*R*)-mandelonitrile using the (*R*)-selective enzyme. The conversion, enantiomeric excess and the reaction rate observed are presented in figure 3.59. Because of a lower volumetric activity only 700 $U\,g^{-1}_{\text{celite}}$ could be applied, and because of the 2.6 times higher specific activity of 51.9 $U\,mg^{-1}$ in comparison to the *Hb*HNL solution the enzyme loading was only 5 $mg_{enzyme}\,g^{-1}_{\text{celite}}$, which was 22.8 times lower.

The reaction progress was similar to the results obtained with *Hb*HNL. After 20

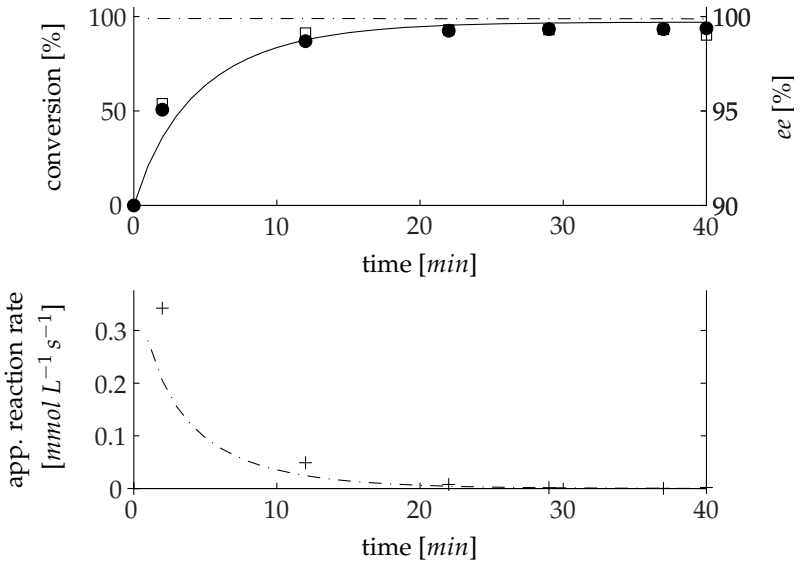

Figure 3.56: Enantioselective synthesis on (*S*)-mandelonitrile in diisopropyl ether. *Hb*HNL immobilised on celite, 2.3 $mg_{enzyme}\, ml^{-1}_{\text{reaction volume}}$, 114 $mg_{enzyme}\, g^{-1}_{\text{Celite}}$, HCN 209 $mmol\, L^{-1}$, benzaldehyde 81 $mmol\, L^{-1}$, 1 % buffer;
(• conversion; □ *ee*; **lines** simulations)

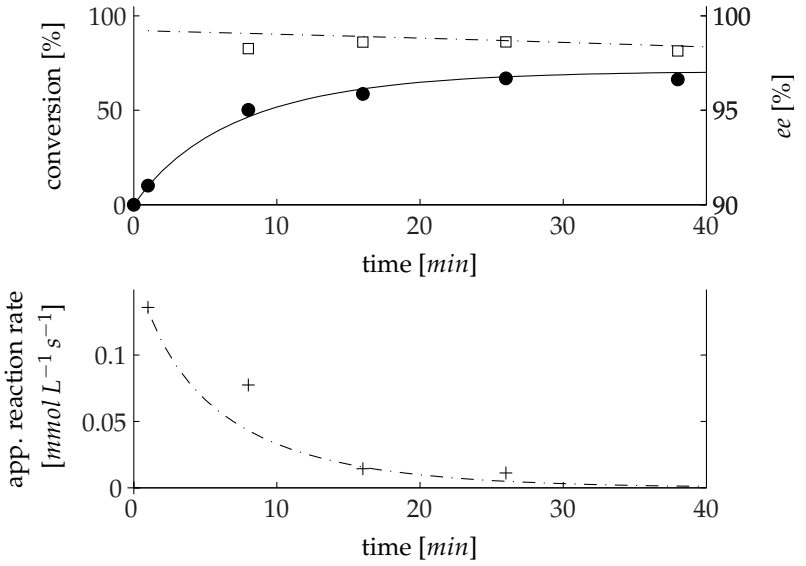

Figure 3.57: Enantioselective synthesis on (*S*)-mandelonitrile in toluene. *Hb*HNL immobilised on celite, 2.3 $mg_{enzyme}\, ml^{-1}_{\text{reaction volume}}$, 114 $mg_{enzyme}\, g^{-1}_{\text{celite}}$, HCN 206 $mmol\, L^{-1}$, benzaldehyde 81 $mmol\, L^{-1}$, 1 % buffer;
(• conversion; □ *ee*; **lines** simulations)

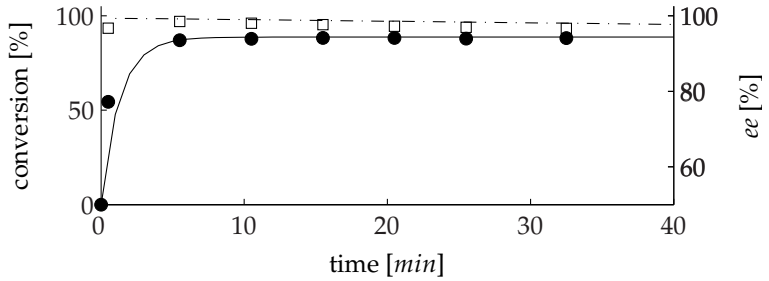

Figure 3.58: Enantioselective synthesis on (*S*)-mandelonitrile in toluene. *Hb*HNL immobilised on celite, 6.8 $mg_{enzyme}\ ml^{-1}_{\text{reaction volume}}$, 114 $mg_{enzyme}\ g^{-1}_{\text{celite}}$, HCN 530 $mmol\ L^{-1}$, benzaldehyde 206 $mmol\ L^{-1}$, 1 % buffer;
(• conversion; □ *ee*; **lines** simulations)

minutes the maximum conversion of roughly 80 % was reached, the enantiomeric excess increased in that time from 85 % to more 99 %. The maximum reaction rate observed was about two times higher than the rates in the experiments using *Hb*HNL.

The unpolar toluene maybe accounted for the apparent equilibrium conversion of 88 % and a more polar solvent would possible lead to a higher conversion. The higher reaction rate and the high enantiomeric excess supposedly originated from a more stable enzyme especially during the immobilisation procedure. The lower specific enzyme loading favoured also an enhanced reaction rate, because no pores were blocked and all enzyme was easily accessible for the substrates. Because the synthesis of (*R*)-mandelonitrile was not in the focus of this work and the experiments were mainly executed to produce enantioenriched (*R*)-mandelonitrile, no further experiments were conducted.

3.10.4 Summary: the enantioselective synthesis of mandelonitrile

(*S*)- as well as (*R*)-mandelonitrile could be successfully synthesised in a purely organic solvent system. The process was strongly influenced by the choice of the immobilisation matrix, because some of the tested matrices showed an unselected catalytic activity for the investigated reaction, for example cf. figure 3.34. Immobilisation matrices which could be used for enantioselective synthesis were Poraver beads and Celite.

With some reservations also nano diamonds could be applied. It could be shown, that *Hb*HNL could be immobilised on the functionalised carbon particles, but the nanoparticles itself catalysed the reaction unselectively. But still in the aqueous system a conversion was reached of around 84 %, with an enantiomeric excess of 45 % (over 60 % using free enzyme).

Also on porous glass beads – Poraver beads – *Hb*HNL was immobilised successfully and a selective cleavage of racemic mandelonitrile in buffer saturated diiso-

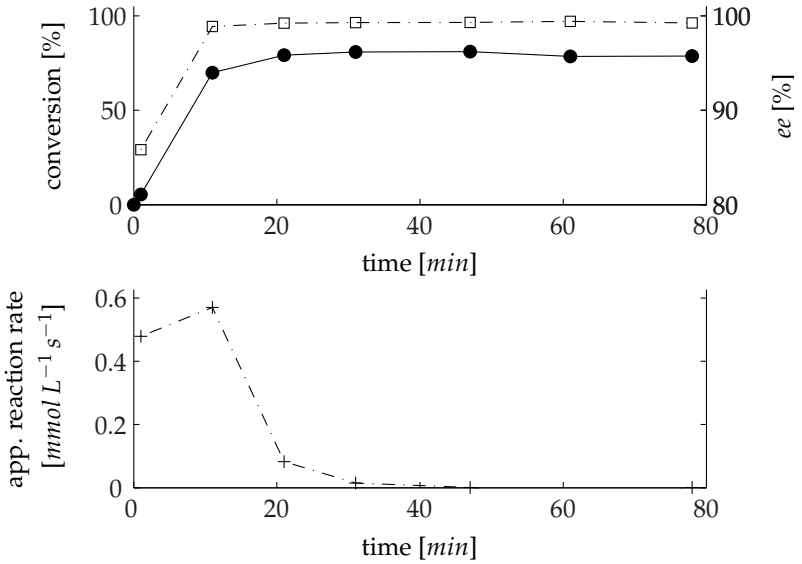

Figure 3.59: Enantioselective synthesis on (*R*)-mandelonitrile in toluene. *R*-HNL immobilised on celite, 0.3 $mg_{enzyme}\, ml^{-1}_{\text{reaction volume}}$, 5 $mg_{enzyme}\, g^{-1}_{\text{celite}}$, HCN 530 $mmol\, L^{-1}$, benzaldehyde 206 $mmol\, L^{-1}$, 1 % buffer; (• conversion; □ *ee*; **lines** visual aids)

propyl ether could be observed. The Poraver beads immobilisate was not used for further investigations, because the immobilisation procedure was work intensive. For certain applications, when special properties like mean diameter, porosity and density are important, the poraver beads may be an interesting matrix.

Of the tested carriers Celite was the one with the best properties. The immobilisation procedure was by far the simplest. The carrier enzyme construct could successfully be used to cleave enantioselective racemic mandelonitrile and to synthesise enantioenriched (*S*)- and (*R*)-mandelonitrile as well. High enantiomeric excesses of more than 99 % could be reached as well as high conversions of over 95 %. The observed equilibrium conversion was influenced by the choice of the organic solvent. In the polar solvent diisopropyl ether the maximum conversion was about 10 % higher than using the unpolar solvent toluene. When immobilised enzymes are used in hydrophobic media partition of hydrophilic components onto hydrophilic carriers may severely affect the reaction [335] and the differents partition coefficients in the two different solvents can explain the different observed maximal conversions.

The time curves of the reactions using Celite as immobilisation matrix could be simulated assuming an ordered-uni-bi mechanism. However, this simulation described not the real mechanism. The reaction was influenced by the diffusion through the pores, by the mass transport through the solvent/water border and the diffusion through the boundary layer to the enzyme at the surface of the carrier. These phenomena were not mapped by the kinetic model.

3.11 Continuous enantioselective synthesis of (*S*)-mandelonitrile

In this chapter the continuous enzymatic synthesis and cleavage of (*S*)-mandelonitrile in an organic solvent is discussed. The schema of the reactor is shown in figure 3.60. The reactor consisted of a Membralox T1-70 Modules, Fa. Pall, with a mono channel ceramic nanofiltration membrane with a cut of of 1000 *Da*. The inner channel diameter was 7 *mm* with a length of 250 *mm* and a surface area of 5.5 cm^2. All piping was realised as stainless steel tubes with an outer diameter of 6 mm and a wall thickness of 1 mm. As circling pump a Watson–Marlow 500R peristaltic pump was used. The two feed solutions were filled in closed glass bottles which were stored on ice. For the synthesis reaction the first feed solution contained toluene and benzaldehyde and was pumped with a HPLC-pump Merck L-6000A. The second solution contained a toluene HCN mixture, 8 volumes toluene and 1 volume HCN. Due to the low viscosity of the HCN and toluene mixture of less than 0.6 $mPa\,s$ the tested micro gear pump (HNP high performance pump mzr-2905) and piston pump (HPLC-Pump Merck L-6000A) were not suitable for pumping the fluid. The solution could be pumped with a syringe pump Gibson Dilutor 401. For the investigation of the cleavage reaction only the first feed vessel was filled with a toluene and racemic or (*S*)-mandelonitrile solution. All used toluene was saturated with phosphate buffer 500 $mmol\,L^{-1}$, pH 5.0 and 2 $mmol\ L^{-1}$ 2-phenylethanol was added as internal standard. The permeate was collected with an autosampler (FRAC-100, Fa. Amersham Biosciences) in glass tubes.

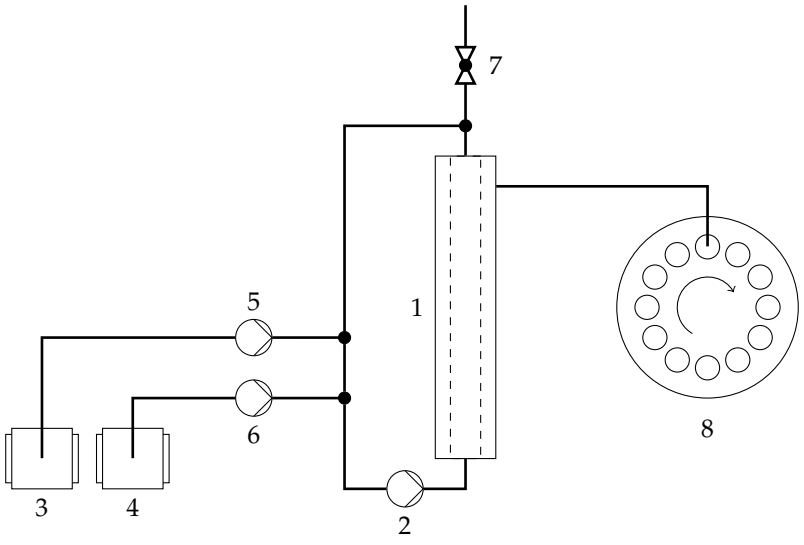

Figure 3.60: Reactor setup for continuous synthesis of mandelonitrile: 1 membrane reactor, 2 circulation pump, 3 container benzaldehyde and toluene, 4 container HCN and toluene, 5 feed pump benzaldehyde and toluene, 6 feed pump HCN and toluene, 7 valve for filling, 8 autosampler retentat.

A crucial question was the choice of a suitable pumping tube for the peristaltic

pump (2). The tubing had to withstand the organic solvent, benzaldehyde, HCN and mandelic acid nitrile as a mixture. The tubings listed in table 3.16 were tested. Samples of the tubing were stored for 48 h in toluene containing 200 $mmol\,L^{-1}$ racemic mandelonitrile and the swelling of the tubing was observed. As example in figure 3.61 two different types of tubing are compared. The Viton-Fluron tubing showed no swelling, but the Neoprene's outer diameter showed an increase of about 30 %. Only two tubings tested showed no swelling: the Viton-Fluron, Ismatec and Viton, Watson-Marlow. Unfortunately, both tubings failed in a test under real conditions. Already after about 1 hour of circling the toluene mandelonitrile mixture in the membrane reactor the tubing formed cracks and started leaking. Using an standard laboratory PCV tubing with an inner diameter of 6.4 mm and a wall thickness of 1.6 mm turned out to be suitable at low pressures[14] and changing the tube after each run.

No.	Name	Company
1	Viton-Fluron	Ismatec
2	Viton	Watson-Marlow
3	Tygon	Watson-Marlow
4	Neoprene	Watson-Marlow
5	Butyl	Watson-Marlow
6	Silicone	Watson-Marlow
7	Marprene/Bioprene	Watson-Marlow
8	Peristaltic	W.L. Gore Associates

Table 3.16: Tested tubing materials

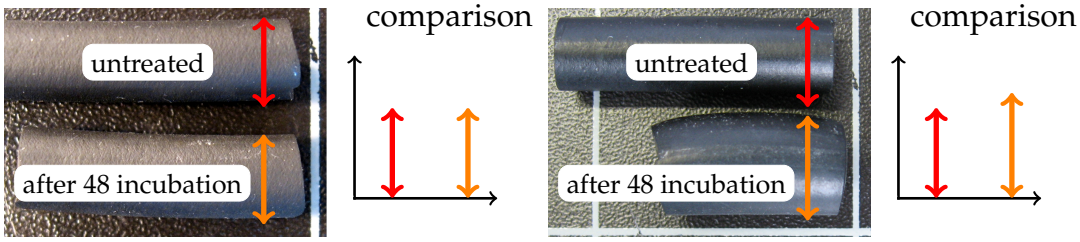

Figure 3.61: Stability of the tubings for the peristaltic pump; left: Viton Fluron, right: Neopren

Using the PVC tubing the volume of the reactor without the ceramic membrane was measured volumetrically to 56.2 $\pm 0.5\,ml$. The membrane reduced the reaction volume by 28.9 ml and a final reaction volume of 27.34 $\pm 0.5\,ml$ could be calculated.

[14]The back pressure was lower than 0.2 bar, which was the lowest accuracy of the pressure gauge of the HPLC-Pumpe Merck L-6000A.

3.11.1 Flow regime and minimum flow velocity

The mean volumetric flow and flow velocity depend on the inner tube diameter and the revolution speed of the pump. According to the manual the mean volumetric flow could be approximately calculated for the given tubing by equation 3.64.

$$w_r = 0,1064 \cdot n - 0,067 \tag{3.64}$$

with

- w_r: mean volumetric flow $[ml\,s^{-1}]$
- n: revolution speed of the pump $[min^{-1}]$

The flow conditions at different positions in the loop of the reactor at a revolution speed of 30 min^{-1} were calculated in table 3.18. Because the diameters differed the Reynolds number had to be calculated for each segment. The Reynolds number was calculated according to equation 3.65. The physical parameters of the main substances are presented in table 3.17.

$$Re = \frac{\rho \cdot v \cdot L}{\eta} \tag{3.65}$$

with:

- L: characteristic length (tubing diameter) $[m]$
- ρ: density $[kg\,m^{-3}]$
- v: flow velocity $[m\,s^{-1}]$
- η: dynamic viscosity $[kg\,s^{-1}\,m^{-1}]$

toluene	density ρ	0.87 $kg\,L^{-1}$
	dynamic viscosity η	0.609 $kg\,m^{-1}\,s^{-1}$
celite	density ρ	1.45 $kg\,L^{-1}$
	mean particle diameter according to the supplier d_p	73 μm

Table 3.17: Physical data of toluene and celite

The flow regimes in all segments were clearly laminar with $Re << Re_{crit}$ ($Re_{cit} = 2300$)[15] and also with the maximum revolving speed of the pump no turbulent flow regime could be established.

[15] laminar flow occurs when $Re < 2300$, Re_{crit}

component	diameter [mm]	v [$cm\,s^{-1}$]	flow w [$cm^3\,s^{-1}$]	Reynolds number
peristaltic pump Tubing	6.4	10.13	3.26	0.93
membrane	7	8.5	3.26	0.85
Steel tubings and fittings	6	11.5	3.26	0.99

Table 3.18: Flow velocity and Reynolds number in the different segments of the reactor at a speed of 30 min^{-1}

The minimum applicable flow velocity is in theory the velocity at which the celite particle are transported vertically against the force of gravity. According to Stokes, for a laminar flow regime the minimum flow velocity v_{min} had to be larger than the velocity of descent $v_{descent}$ of the particles, equation 3.66.

$$v_{descent} = \frac{(\rho_s - \rho_f) \cdot {d_p}^2 \cdot g}{18 \cdot \eta_f} \tag{3.66}$$

With the physical parameters of table 3.17 the velocity of descent could be calculated to $v_{descent} = 2.8 \cdot 10^{-3} m\,s^{-1}$. This value was just a theoretical value, because due to agglomeration of the celite particle the mean diameter was increased. The maximal theoretical diameter of the particles at which the velocity of descent equals the flow velocity vertically against the force of gravity (v_{min}=$v_{descent}$) could be calculated to $d_p = 1.28\,cm$, which was larger then the tubing diameter. Therefore it could be excluded that at 30 rpm revolving speed the particles descent in the vertical membrane.

Catalyst preparation

As catalyst *Hb*HNL was used. Because the enzyme solution used for all foregone experiments was exhausted, all experiments in the continuously operated reactor were performed with the second enzyme preparation. This enzyme solution had a much lower volumetric enzyme activity and the solution turned out to be much less stable compared to the enzyme preparation used beforehand. Especially the freeze-drying process was disadvantageous for the enzyme activity and the immobilised enzyme could not successfully be applied in a continuous process. Because the specific activity of the second solution was much higher than that of the first solution the assumption is that the impurities – inactive *Hb*HNL as well as other proteins – had a stabilising effect. Therefore it was decided to apply a non dried enzyme carrier. Due to the lower volumetric activity of the used solution in comparison the the first solution only 460 $U\,g^{-1}_{celite}$ were applied in comparison to up to 5000 $U\,g^{-1}_{celite}$ in the batch reactions.

3.11.2 The continuous enantioselective cleavage of mandelonitrile

The principle application of the continuously operated membrane reactor using *Hb*HNL immobilised on Celite as catalyst was tested in the cleavage of mandelonitrile. Two different feed solutions were used. Until operation time 11 h the reactor was fed with a (*S*)-mandelonitrile solution ($ee < 99$ %) with a concentration of 25 $mmol\,L^{-1}$. After the use of this solution it was exchanged to a racemic mandelonitrile solution with a concentration of 50 $mmol\,L^{-1}$. Because of the HCN release during the cleavage of the mandelonitrile the reactor was only operated during day time. Over night the feed as well as the circling pump were stopped. In figure 3.62 the time course of the conversion calculated for the cleavage of (*S*)-mandelonitrile and the relative concentration of the internal standard is shown. The relative concentration of the internal standard was an indication of the replacement of the initial solvent and as expected after 6 residence times the initial solvent was replaced, a steady state was reached and the relative concentration kept at a constant level within the measurement error.

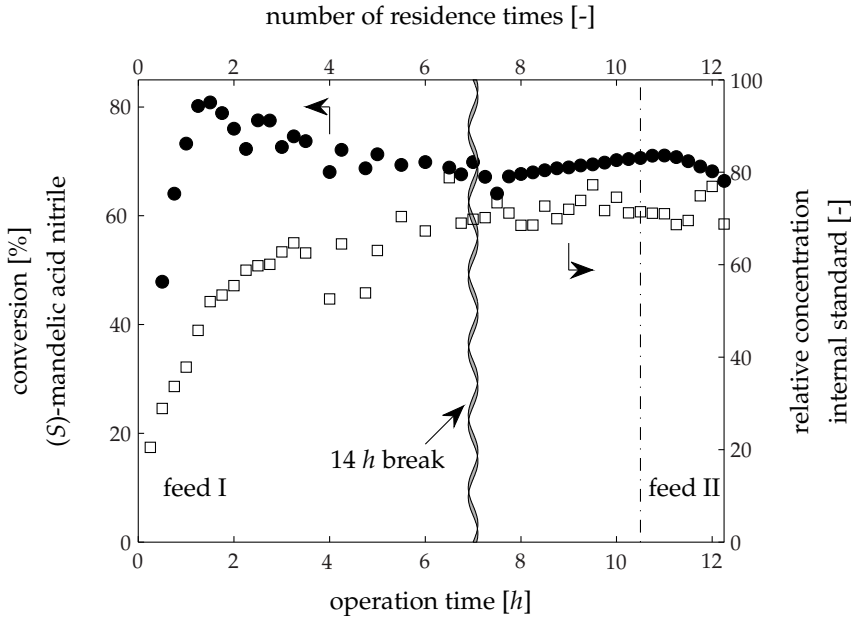

Figure 3.62: Enantioselective cleavage of (*S*)-mandelonitrile in toluene in a continuously operated membrane reactor, *Hb*HNL immobilised on celite, 50 $g_{celite}\,L^{-1}_{\text{reaction volume}}$, 460 $U\,g^{-1}_{celite}$, Feed I: 25 $mmol\,L^{-1}$ (*S*)–mandelonitrile; Feed II: 50 $mmol\,L^{-1}$ racemic mandelonitrile; 14 hour break after 7 hour operation, •: conversion of (*S*)-mandelic acid calculated on the feed concentration; □: relative concentration of the internal standard

The same is true for the conversion. After 6 residence times a constant conver-

sion was reached, which was only slightly influenced by the 14h break during night time. After the break the conversion increased slowly until the feed solution was changed. The distribution of the measurements was tighter the second day, which was the result of a more uniform operation during this day. The enantiomeric excess is presented in figure 3.63. During the first two hours the enantiomeric excess decreased from the initial value of over 99 % down to a value of 20 % which is the result of a selective cleavage of the (*S*)-mandelonitrile, as well as the formation of (*R*)-mandelonitrile in a non selective reaction, due to the strong increase of the HCN and benzaldehyde in the aqueous boundary layer covering the surface of the carrier. After six hours operation a conversion and an enantiomeric excess of 70 % was reached which is 30 % lower than when assuming a 100 % selective reaction. During the 14 hours break in which the feed and the circulation were stopped the conversion kept almost constant, which was seen in the first sample after the operation was started again. The enantiomeric excess fell with 30 % down to 40 %, because of an increase of the (*R*)-mandelonitrile concentration. After three hours operation the same values were reached as at the end of the day before. The feed was changed to racemic mandelonitrile after eleven hours operation time to evaluate if the enzyme was still active. If the enzyme is active and the (*S*)-enantiomer is selectively cleaved, the enantiomeric excess will become negative, because the concentration of the (*S*)- decreases below the concentration of the (*R*)-enantiomer. And as seen in figure 3.63 the enantiomeric excess decreased to a value lower than -20 %, before the operation had to be stopped at the end of the day, proving that the enzyme was still active after being incubated in organic solvent more then 26 hours (twelve hours operation and 14 hour break).

The continuously operation of the membrane reactor for the application of immobilised *Hb*HNL in buffer saturated toluene could be shown. The next step was the investigation of the enzymatically catalysed synthesis of (*S*)-mandelonitrile with the same reactor setup.

3.11.3 The continuous enantioselective synthesis of mandelonitrile

For the synthesis reaction two different feed solutions were prepared in buffer saturated toluene containing 2 $mmol\,L^{-1}$ 2-phenyl ethanol as internal standard. The first solution contained 50 $mmol\,L^{-1}$ benzaldehyde and the second solution 3 $mol\,L^{-1}$ HCN. The feed rates were adjusted in such a way that the molar ratio of HCN to benzaldehyde was two at all flow rates. Two residence times were tested 1.2 and 2.4 h. During the first run it was detected that the actual flow rate did not match the set point of pump control [16]. Therefore the flow rate had to be adjusted during the operation to match the targeted flow rate. This can be seen in figures 3.64 and 3.66, the measured flow rates are plotted. In the same plots also the relative concentration of the internal standard is shown. The relative concentration of the internal standard

[16] The flow rate was checked before the reactor was set up

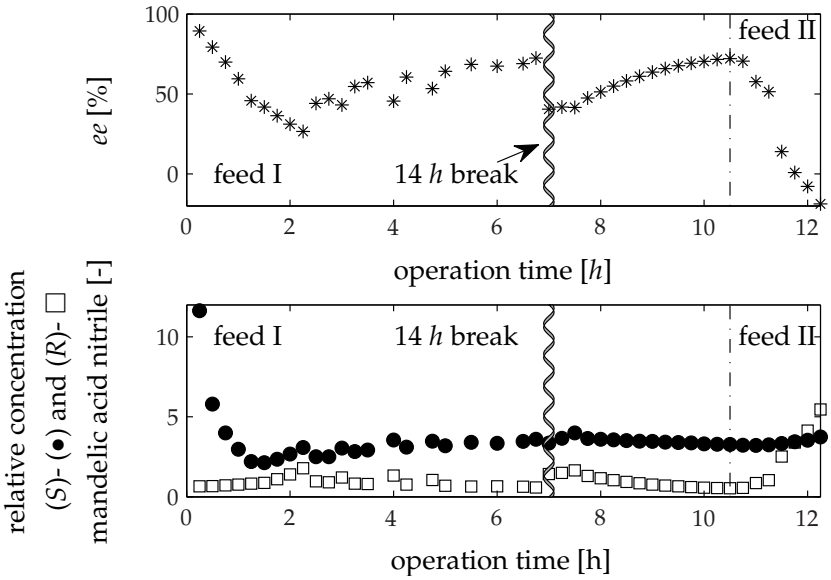

Figure 3.63: Enantioselective cleavage of (*S*)-mandelonitrile in toluene in a continuously operated membrane reactor, *Hb*HNL immobilised on celite, 50 $g_{celite}\, L^{-1}_{\text{reaction volume}}$, 460 $U\, g^{-1}_{celite}$, Feed I: 25 $mmol\, L^{-1}$ (*S*)–mandelonitrile; Feed II: 50 $mmol\, L^{-1}$ racemic mandelonitrile; 14 hour break after 7 hour operation, $*$: enantiomeric excess, •: concentration (*S*)-mandelonitrile; □:concentration (*R*)-mandelonitrile

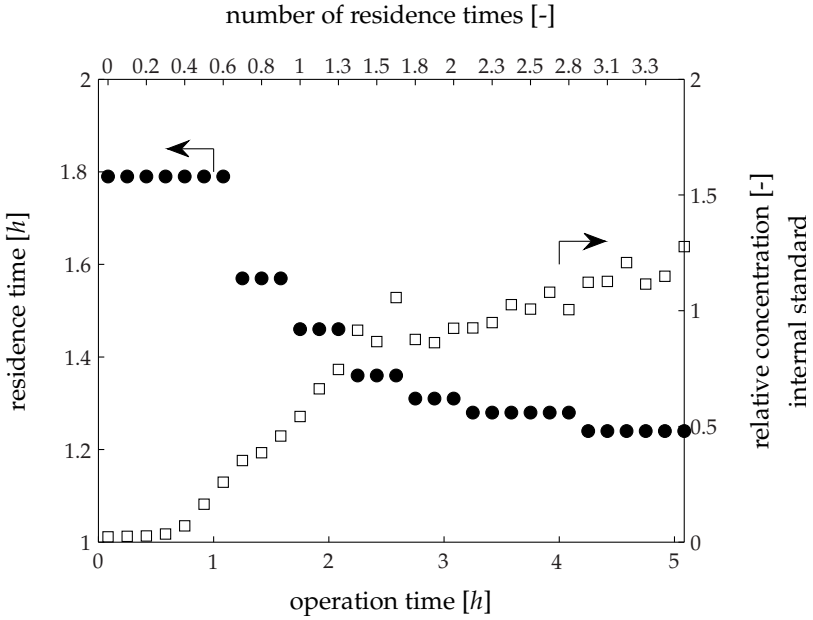

Figure 3.64: Enantioselective synthesis of (*S*)-mandelonitrile in toluene in a continuous operated membrane reactor, set-point residence time 1.2 *h*; *Hb*HNL immobilised on celite, 50 $g_{celite}\, L^{-1}_{\text{reaction volume}}$, 460 $U\, g^{-1}_{celite}$, Feed I: 50 $mmol\, L^{-1}$ benzaldehyde; Feed II: 3 $mol\, L^{-1}$ HCN; •: measures residence times [h]; □: internal standard, relative concentration

was calculated by dividing the measured peak areas of the samples by the peak area of the feed solution. The broad distribution was based on the fact, that the samples were measured in a random order and that the time span between the measurement of two sequentially taken samples could be more than a week. During storage and handling solvent evaporated and the concentrations of the components were changed in the vial. Therefore relative concentrations larger than one were measured. The distribution of the internal standard was eliminated by normalising the measured peak areas of one component with the peak area of the internal standard in the same sample.

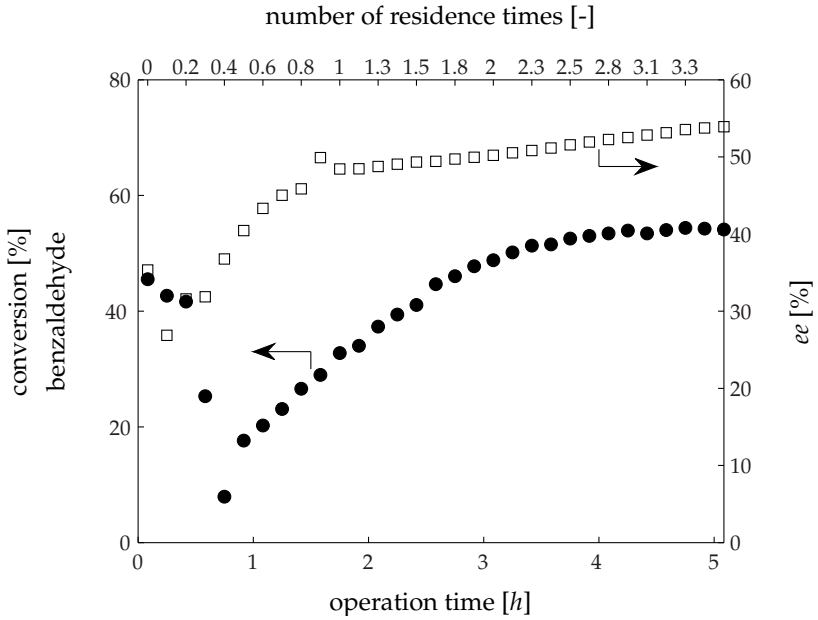

Figure 3.65: Enantioselective synthesis of (*S*)-mandelonitrile in toluene in a continuous operated membrane reactor, set point residence time 1.2 *h*; *Hb*HNL immobilised on celite, 50 $g_{celite}\, L^{-1}_{\text{reaction volume}}$, 460 $U\, g^{-1}_{celite}$, Feed I: 50 $mmol\, L^{-1}$ benzaldehyde; Feed II: 3 $mol\, L^{-1}$ HCN; ●: conversion; □: enantiomeric excess *ee*

Unfortunately, the reactor could not be operated in steady state conditions. Because of the toxicity of the HCN the reactor could be operated only during daytime, reaching only 3.5 numbers of residence during the first experiment. In the second experiment with lower residence time of 2.4 *h* only 2.5 numbers of residence could be realised during day time. To prolong the operation of the reactor the feed and circling was stopped over night and started again on the next day. As seen in figures 3.64 to 3.67 neither the relative concentration of the internal standard nor the conversion or the enantiomeric excess reached a constant level.

The operation of the continuously operated membrane reactor for the enantioselective synthesis of (*S*)–mandelonitrile could be shown. In the first experiments

a conversion of 54 % could be reached with an enantiomeric excess of also 54 %. The maximum enantiomeric excess was much lower compared to the excess obtained in the batch reactions. The main difference in the preparation of the catalyst was that the catalyst in the membrane reactor was not dried before application. As mentioned above the drying process was not applicable for the enzyme solution used. The aqueous layer around the enzyme was therfore much thicker and the ratio of the water to the enzyme was much higher, so that the volume in which the noncatalysed racemic formation of mandelonitrile could take place was larger. The second run showed that at longer residence times a slightly larger conversion could be reached with at maximum 60 %, with a decrease consequent of the enantiomeric excess to 42 %. The low increase of the conversion at a doubling of the residence time indicated that the reached concentrations were close to the equilibration concentrations of the system. The concentrations measured in the organic phase were a function of a multiplicity of parameters: the thermodynamical equilibrium of the reactions itself, the ratio of the water to bulk phase, the ratio of the water to the enzyme and the solubility of the different components in the water and organic phase, which determine the distribution of the components in the two layers. From the batch experiments it can be concluded, that the water content played an important role for a high enantiomeric excess, which follows also from the observation, that the non catalysed racemic formation does not take place in the organic but in the water phase. In figure 3.65 the enantiomeric excess increased linear from 49 % to 54 % during the last 3 hours of the operation. The reason may has been the water have been removed constantly from the system. The solubility of water in the organic phase changed with in creasing mandelonitrile concentration, because benzaldehyde has a different polarity than mandelonitrile. Although the feed solutions were saturated with phosphate buffer the water may have been removed due to the changed water solubility.

The enzyme was stable at least for days of operation. During the break over night in the second run the enzyme was stored under reaction conditions. The conversion increased from 63 % to 74 % and the enantiomeric excess dropped from 40 % to 31 % during the 16 hours break. After starting the feed again the enantiomeric excess increased again over 40 % which indicated that the enzyme had a similar activity than the day before.

Because a steady state operation could not be reached due to the short operation times more insights into the process could not be gained. The feasibility of a continuously operated membrane reactor for the enzymatically catalysed synthesis of (*S*)-mandelonitrile operation of such a reactor was proven in principle. An important role plays the immobilisation of the enzyme and a low water content. The optimal enzyme loading for batch reactions must to be ideal. At an optimised loading all enzyme is accessible for the reaction and no cavities are block. Then the necessary residence time is minimised. A stabilising effect might have the co–immobilisation of a non catalytic enzyme or crosslinking agent. If the process will be profitable a high enantiomeric excess must be realised with a high stability of the enzyme.

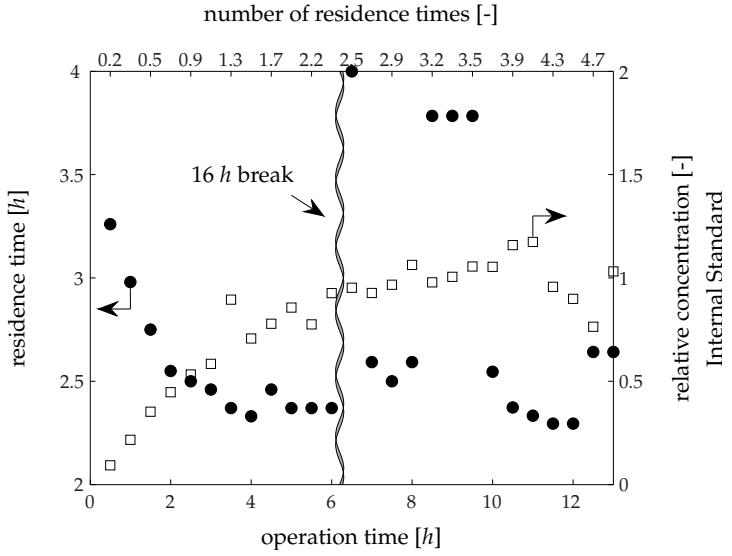

Figure 3.66: Enantioselective synthesis of (*S*)-mandelonitrile in toluene in a continuous operated membrane reactor, set point residence time 2.4 h; *Hb*HNL immobilised on celite, 50 $g_{celite}\, L^{-1}_{\text{reaction volume}}$, 460 $U\, g^{-1}_{celite}$, Feed I: 50 $mmol\, L^{-1}$ benzaldehyde; Feed II: 3 $mol\, L^{-1}$ HCN; •: measures residence times [h]; □: internal standard, relative concentration

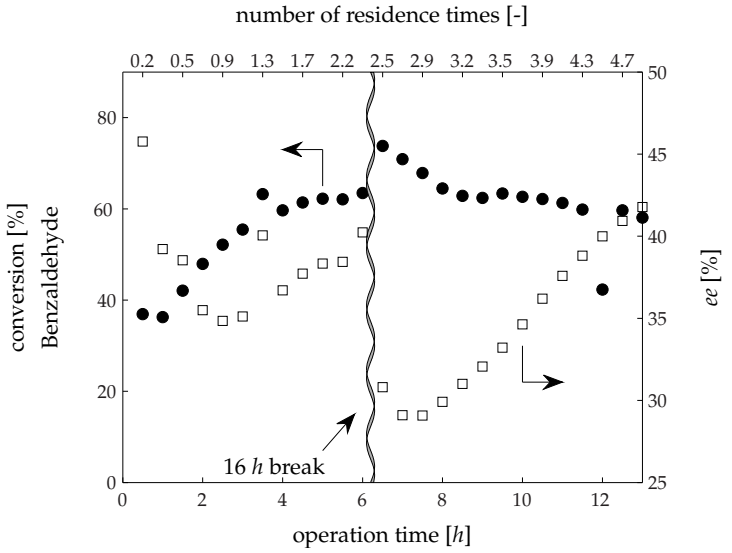

Figure 3.67: Enantioselective synthesis of (*S*)-mandelonitrile in toluene in a continuous operated membrane reactor, set point residence time 2.4 h; *Hb*HNL immobilised on celite, 50 $g_{celite}\, L^{-1}_{\text{reaction volume}}$, 460 $U\, g^{-1}_{celite}$, Feed I: 50 $mmol\, L^{-1}$ benzaldehyde; Feed II: 3 $mol\, L^{-1}$ HCN; •: conversion; □: enantiomeric excess *ee*

For the laboratory process a more robust and automised reactor setup must be used, so that the reactor can also be operated over night. About half of the working time was necessary for the production of hydrogen cyanide and a safe shutdown of the process, including the cleaning procedures. Decreasing the time of production of HCN by the development of an automised, continuous production of hydrogen cyanide in small quantities, which can be directly coupled to the continuously operated membrane reactor, would enable the process development in the laboratory. A crucial question for a safe operation is the choice of the cycling and feeding pumps. The peristaltic pump worked not satisfyingly, because no tubing material was found which showed an adequate durability without any tendency for swelling. The feeding pumps assure a constant flow also at low pressure. All pumps have to be explosion proofed, because the organic solvent and especially the hydrogen cyanide can form explosive atmospheres.

4 The combination of the Diels-Alder reaction and the enantioselective addition of HCN

The main objective of this study was to show the feasibility of a continuous production of cyanohydrin according to the reaction sequence presented in figure 1.10, whereas the first reaction is catalysed by a chemzyme and the second one by an enzyme. Avi and coworkers showed that employing *Hb*HNL in the reaction of HCN and 2-methoxy-cyclohexene-carbaldehyde the formation of the (*S*)-configured centre is preferred [336], so the principle function has been proved. As solvent for the combination of both reactions toluene was chosen, because both reactions can be performed in toluene, so that a solvent change is not necessary. The ethers, like diisopropyl or *tert*-butyl methyl ether, were not considered, because they tend to form explosive peroxides. As described in the previous chapters the continuously production of the carbaldehyde as well as the enantioselective synthesis of the cyanohydrin could be shown. In first tests to establish the linkage of both continuously operated reactions different fractions of the output stream of the continuously operated chemzyme membrane reactor were used test the enzyme catalysed addition of HCN in a batch reaction. The same reaction condtions were applied as described in chapter 3.10. Because only the less stable enzyme solution II was at hand,c.f. table A.7, for these batch reactions the catalyst was prepared as described in chapter 3.11.1. The HCN was added in a twofold excess calculated on the concentration of the 2-methoxy-cyclohexene-carbaldehyde measured.

Unfortunately no selective reaction could be observed, only the non-selective addition of HCN. The reason for this was the low stability of the enzyme in the presence of acrolein. The time curve of the enzyme activity was measured incubating an enzyme buffer solution with the different substances added, which were in the output stream of the continuously operated chemzyme membrane reactor. The enzyme was diluted to an activity of 10 $U\,ml^{-1}$ in a 0.05 molar citrate-phosphate buffer (pH 5.0) and the different substrates were added. The solutions were incubated at 20°C in a thermostatically controlled water bath and the time curve of the enzyme activity was measured up to 14 d. The half lifes of the enzyme were calculated, which is defined

as the loss of activity according to a first order kinetics:

$$\begin{aligned} \frac{d\,A}{dt} &= -k_d\,t \\ \Longrightarrow \quad ln\left(\frac{A}{A_0}\right) &= -k_d\,(t) \\ \overset{A=0.5\,A_0}{\Longrightarrow} \quad t_{\frac{1}{2}} &= \frac{ln(2)}{k_d} \end{aligned} \tag{4.1}$$

substance	concentration $[mmol\,L^{-1}]$	measured half live time $t_{\frac{1}{2}}$ $[d]$
buffer	–	60
toluene	saturated buffer	∞
diisopropyl ether	saturated buffer	36
benzaldehyde	10	54
1-methoxy-1,3-butadiene	10	36
acrolein	10	2.9 (0.8)
2-methoxycyclohex-3-enecarbaldehyde	10	60

Table 4.1: The half life times of *Hb*HNL in a citrate phosphate buffer pH 5.0 in the presence of different substances

In the reaction procedure applying immobilised enzyme on celite the surface of the carrier where the enzyme is located, is covered with a buffer layer and the stability in the aqueous layer is of importance. Hence the half life time was measured in the buffer system. The effects of the adsorption on the stability could not be mapped in this assay, but the results give a first indication. The substances and measured half life time are shown in table 4.1.

The half life times for all substances except acrolein were in the range of the untreated sample. Only in the presence of acrolein the half life time was drastically reduced. In figure 4.1 the logarithmic activity as function of time is compared for acrolein and toluene. The activity of the sample incubated with toluene did not decrease over the measurement time of 14 d. In comparison, the half life time with acrolein was reduced to 2.9 d evaluating only the first eight activity measurements the time was reduced even more to 0.8 d. In the solutions tested from the reactor the acrolein concentration was at its minimum 50 $mmol\,L^{-1}$, five times higher than in the activity tests, which decreased the half life time even more. Hence the enzyme was deactivated to fast.

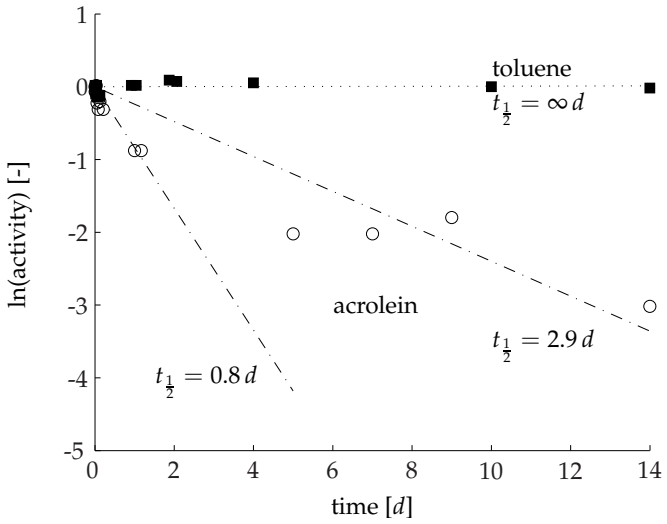

Figure 4.1: Half life of the *Hb*HNL in a citrate phosphate buffer pH 5.0 in presence of toluene and acrolein, respectively

4.1 Discussion and outlook

Unfortunately, the main objective of this study to show the feasibility of a continuous production of the cyanohydrin according to the reaction sequence presented in figure 1.10 was not achieved. However several steps on the path to a continuous production of the cyanohydrin could be taken.

The automated experimental procedure using a robotic liquid handling system provided the basis for the investigation of the salen catalysed reaction kinetics. For the kinetic investigation samples had to be taken repeatedly over a reaction time of more than 12 hours for a larger number of experiments, which was only possible with such an automated system. Because small reaction volumes of only 200 μl could be established the consumption of the value catalyst and substrates could be minimised. The time concentration plots could be fitted to a mathematical model (symmetric random Eley-Rideal model). The model was simplified to predict the reaction progress with a single parameter for the rate-determining step of the formation of the product (range of the substrate concentrations $200 < c_{substate} < 1000\, mol\, L^{-1}$, catalyst concentrations $0 < c_{catalyst} < 70\, mol\, L^{-1}$ of active centres). The parameter k_{+3} was estimated to $2.4 * 10^{-3}\, L\, mmol^{-1}\, h^{-1} \pm 1.6 * 10^{-4}$ and showed the low activity of the catalyst. The experimental deviation of about 16 % was satisfying for the evaluation of major effects, but not for the evaluation of the assumed adsorption phenomenons. In general, it could not be clearly stated that the reaction was a real homogeneous reaction. The catalyst appeared to be homogeneously soluble in the reaction system, but the reaction kinetics displayed also features of a heterogeneous reaction.

The low activity was confirmed in the continuously operated membrane reactor experiments. The membrane reactor could be operated for longer than 44 days. Also the reported high retention of the catalyst of over 99 % could be confirmed and the kinetic model could be used to predict the conversion as function of the catalyst and residence time within the evaluated concentration range, c.f. figure 2.25. The model showed, that due to the low specific activity of the catalyst high conversions of over 90 % could only be reached, when the residence times were larger than 50 hours at a maximum catalyst concentration of $70\,mol\,L^{-1}$. Beside the low activity, the low solubility of the catalyst was the limiting factor for the increase of the space time yield. In all reaction vessels precipitation and adhesion of the catalyst to the walls were observed. The solubility of the catalyst was higher in more polar solvents than toluene – like for example acetone –, but acetone is not a suitable solvent for the enzymatic catalysed follow up reaction. Diisopropyl ether is maybe a suitable solvent as long as the peroxide formation can be excluded.

Catalyst engineering could be a tool to increase the activity as well as the solubility in polar solvents of the salen catalyst. The specific activity can be increased by increasing the number of active centres on each polymer molecule. The structure of the active centre can be optimised to increase activity and reduce the metal leakage which can be a large problem in industrial scale. In particular, molecular modelling maybe helps to improve the structure of the active centre and maybe the enantioselectivity as well as the diastereoselectivity can be improved too. But also the dendrimer can be optimised to increase the solubility of the catalyst, by changing the chemical structure of the dendrimer. For commercial success also the production process for the catalyst must be optimised, because up to now the catalyst was only be prepared in small lab quantities, including washing steps using large volumes of solvents.

The investigation of the enzymatic catalysed addition of HCN showed, that the synthesis of cyanohydrins is possible with an enantiomeric excess of larger 99 % in batch reaction with enzyme immobilised on Celite and aldehyde starting concentrations of up to 1000 $mmol\,L^{-1}$ and a space–time–yield larger $1\,mmol\,L^{-1}\,s^{-1}$. The immobilisation on Celite is a simple procedure, but a drying procedure of the enzyme–celite preparation must be developed for larger application. Maybe washing of the enzyme–celite immobilisate with a suitable polar solvent followed by an evaporation of the organic solvent/water-organic solvent azeotrope is a feasible procedure for water removal in larger scale. Also the immobilisation of the *Hb*HNL on porous glass beads (Poraver glass beads) can be used for immobilisation, but this procedure is much more labour intensive. If the immobilisation on Poraver beads can be a competitive immobilisation process must be investigated in future studies.

The observation that different apparent equilibrium concentrations were measured using different solvents (toluene and diisopropyl ether) and that the different levels of the apparent equilibrium concentrations could be explained by different partition coefficients of substrates and products showed that a closer look into the microenvironment surrounding the enzyme is important. The micro environment close to

the enzyme is of importance for the stability as well as the activity of the enzyme. While in aqueous reaction systems often the bulk phase represents also the condition close to the enzyme, this is different for the application of immobilised enzyme especially in non-conventional media. In general the use of enzymes in non-conventional media is a not well-understood area of application. In particular, the conditions in the micro environment are often not known, which is also true for this investigation. Especially the stability of the (immobilised) enzyme and the influences on the stability under reaction condition must be evaluated more deeply, because the low stability of enzymes is often the greatest challenge for the application of enzymes in industrial scale especially for mid and low cost products.

The experimental implementation of the continuously operated enzyme reactor using toluene as solvent and HCN as substrate was complex. The stability of the ceramic membrane was given but a suitable tube for the peristaltic pump could not be found. Also the high toxicity of the HCN was a challenge. The operation of HCN experiments was limited to day time. The needed HCN hat be produced and destroyed within this time, so that no operation over night were possible. The production of HCN lasted up to four hours until the operation of the membrane reactor could be started. The shutdown of the membrane reactor inclusive HCN destruction and cleaning lasted two hours. Therefore only a limited time frame for the operation of the continuously operated membrane reactor was given. A steady state operation could not be established, so that only limited results could be obtained. But it could be shown that the enantioselective synthesis of (*S*)-mandelonitrile can be performed in a continuously operated enzyme-membrane-reactor.

Due to the competition of the non catalysed unselective and the enzymatically selective reaction and the toxicity of the HCN, low substrate concentrations are preferred, which was the case in the membrane reactor operated as a CSTR. A plug-flow reactor would favour not a high enantiomeric excess, because at the entrance of the fixed bed the substrate concentrations are high and decrease with the length of the bed. A fluidised bed reactor with a large degree of back mixing would require high strength of the particles. A fixed bed operated in the mode of a continuous operated stirred tank – multiple passage of the reactants over the catalytic bed– is a compromise between a particle suspension, fixed bed with a single passage of the reactants or a fluidised bed. For the design the fixed bed would need a high permeability to reduce pressure drop over the packed bed. The drawback of a fixed bed is, that the inactivated catalyst can not be replaced easily and a special focus must be again the stability of the catalyst.

As shown, impurities – like acrolein – deactivated the enzyme rapidly. To overcome this problem, the conversion of acrolein in the first reaction must be close to 100 % or the acrolein must be removed before entering the enzyme membrane reactor. The first solution would result in a drastic increase of the catalyst concentration, which was limited due to the solubility of the catalyst or the drastically increase of the residence time. But the dependency of the conversion on the residence time was

rather insignificant, as shown in figure 2.25, and the residence time must be increased at least fourfold. The result would be a larger reaction volume of a factor of four to maintain the same production level (product per time). In both cases the concentration of the expensive catalyst must also be increased at least by four.

The acrolein can be removed by distillation, because acrolein has the highest vapour pressure in the reaction mixture. Also an extraction with water would be possible. The water extraction step would also enable the saturation of the reaction mixture with water, which is essential for the enzyme catalysed reaction, but probably a single extraction step would be less selective compared to a single-stage distillation. Both solutions would be contradictory to the objectives of this study. But for an economical process the different options must be considered and weighted. At this stage of the investigation a final judgement if the direct coupling of the process or an intermediate separation of the acrolein is the most promising process cannot be given.

For the implementation of the direct coupling of both reactions in a continuous process a more efficient catalyst for the Diels-Alder reaction must be developed. Also the influences on the stability of the enzyme in the reaction system must be understood better. The handling of HCN in a research laboratory is labour intensive and it requires an intensive and detailed organisation of the laboratory. Investigating a continuous process is time intensive and the investigation of the stability of a catalyst in a continuous operation maybe requires an operation over several days and nights. This is only possible if the process of HCN production and the membrane reactors are much more automated to meet the challenges of the toxicity of hydrocyanic acid.

The model driven calibration approach for the investigation of the kinetics of a catalysed reaction by progress curve analysis including the optimisation of a multivariate calibration model directly into the parameter fitting showed, that the number of experiments could be reduced drastically, without losing significance. The experimental design using 80 individual initial rate measurements were compared to six measurements evaluated using progress curve analysis. The comparison showed good agreement between the different experimental designs. The reduction of the number of necessary experiments is particularly of interest, when hazardous or high-price substances are involved. The model driven calibration approach was successfully tested analysing the kinetics of the *Hb*HNL catalysed reaction of benzaldehyde, hydrogen cyanide and mandelonitrile using a linear and a PLS regression calibration model for the calibration of a multiwavelength photo-spectrometer. In principle this approach can be used for any multivariate measurement like other spectrometric (FTIR, NMR etc.) or GC and HPLC measurements. In combination with a robotic liquid handling system and a non-linear experimental design the investigation of the kinetics of very diverse reactions can be automated and accelerated.

4.2 Summary

In this study a two step reaction sequence has been studied to synthesise stereoselective cyanohydrins starting with simple, commercially available building blocks. The first step was a Diels-Alder reaction catalysed by a chemzyme and the second a *Hb*HNL catalysed, enantioselective addition of hydrogen cyanide to the aldehyde formed in the first reaction. Both reaction kinetics were studied. For the kinetic studies of the Diels-Alder reaction a robotic liquid handling procedure was developed. The reaction volume could be minimised down to only 200 μl saving the high-value catalyst and the experiments could be carried out automated, including the sampling and sample preparation. The experimental data could be fitted to a developed kinetic model and the model could be used to predict the time courses of the product concentration. On the basis of the kinetic model a continuous process was designed using a membrane reactor. The membrane reactor was operated longer than 40 days. Due to the limited solubility and the low specific activity of the catalyst only a space-time-yield could be achieved of $0.5\, g\, L^{-1} d^{-1}$.

Because both reactions should be coupled without an intermediate purification step, the enzymatically catalysed reaction had to be carried out in the same organic solvent as used in the first reacton step. For the application of the *Hb*HNL in such a one liquid phase organic solvent reaction system it had to be immobilised. Different carriers were tested: Sepabeads, nano diamonds, Poraver glass beads and Celite. The enzyme could be successfully immobilised on nano diamonds, glass beads and Celite. Because of the simple immobilisation procedure, the immobilisation on Celite was chosen for further experiments. As suitable solvent toluene and diisopropyl ether were found. A conversion of more than 95 % and an enantiomeric excess of over 99 % was reached and the space time yield of $1\, mmol\, L^{-1}\, s^{-1}$ was measured.

The enantioselective synthesis of (*S*)-mandelonitrile could be carried out in a continuously operated membrane reactor, too. Because of the toxicity of *HCN* the membrane reactor could be operated only for six hours and no steady state operation could be established, so that only rudimentary results were achieved.

The Diels-Alder reaction and the *Hb*HNL catalysed reaction could not be coupled directly, because the remaining acrolein of the uncompleted Diels-Alder reaction inactivated the enzyme too fast. In the continuously operated chemzyme membrane reactor only a conversion of maximal 80 % was measured.

A model driven calibration approach for the investigation of the kinetics of a catalysed reaction by progress curve analysis including the optimisation of a multivariate calibration model for the measurement devices directly into the parameter fitting procedure was developed. The comparison of different experimental designs – inital rate measurements und progess curve analysis in combination with an uni- or multivariate calibration model – showed, that the number of experiments could drastically be reduced from 80 to six measurements without losing the significance of the model parameter.

A Appendix: Materials and Methods

A.1 Synthesis of functionalised cyclohexenyl structures

A.1.1 Experimental procedure

The procedure of the addition of compounds and the probing is illustrated in figure 2.7. Prior to reaction start, the rack of the robot was loaded with vials. In all vials, except the compound vials, micro inserts were placed to reduce the inner volume to 300 μl and to increase the filling level for a proper volume handling. The sampling vials were filled with 100 μl toluene containing 1 M TFA. The starting material acrolein and butadiene were provided undiluted while the 40 mg of catalyst was dissolved in 1 ml toluene. To enhance solubility of the catalyst the filled vial was treated in an ultrasonic water bath for several minutes and vortexed intensively. With each sampling a volume of 20 μl was taken from the reactors and diluted in 300 μl toluene. After mixing, three times aspirating and dispensing fast a volume of 100 μl, 100 μl were transferred into the sampling vial containing 100 μl with 1 M TFA. The filling of the reactors and the probing were totally automated and controlled by the micro controller of the liquid handling robot. The program code is presented in chapter B.1.

The program started with a sequence of prompts in which the attribute of the new reaction procedure were defined. Parameters like volumes of the reactions (100 μl - 1.5 ml), volumes of the stating materials and catalyst, numbers of samples as well as time points of the probing could be entered. The flow chart of the liquid handling program is shown in figure A.1 and it can bee seen, that the program consist of different time–controlled loop structures. To speed up the filling procedure the three different compounds – acrolein, butadiene and catalyst solution – were not transferred one by one. First the tube connecting the dilutor with the needle was fill with toluene. Then 3 μl air was aspired and after that exact volume of the catalyst solution was aspirated, separated by the bubble form the solvent. Then again a 3 μl air bubble was intaken separating now the catalyst from the first starting material solution. In the same way it was continued until all compounds were aspirated in the tube. An important aspect was the pressure difference in the vials and the environments. All vials were sealed with caps and when a solution was aspirated in a vial the pressure was reduced, which was enforced during the pull out of the needle out of the vial, because the rubber cap was bulged in direction of the needle movement. Further more due to the mass inertia the liquid in the tube moved with an offset compared to the needle movement along the Z–plan. This could lead to a loss of liquid at the top of the needle, when the needle was moved directly after an intake of a liquid.

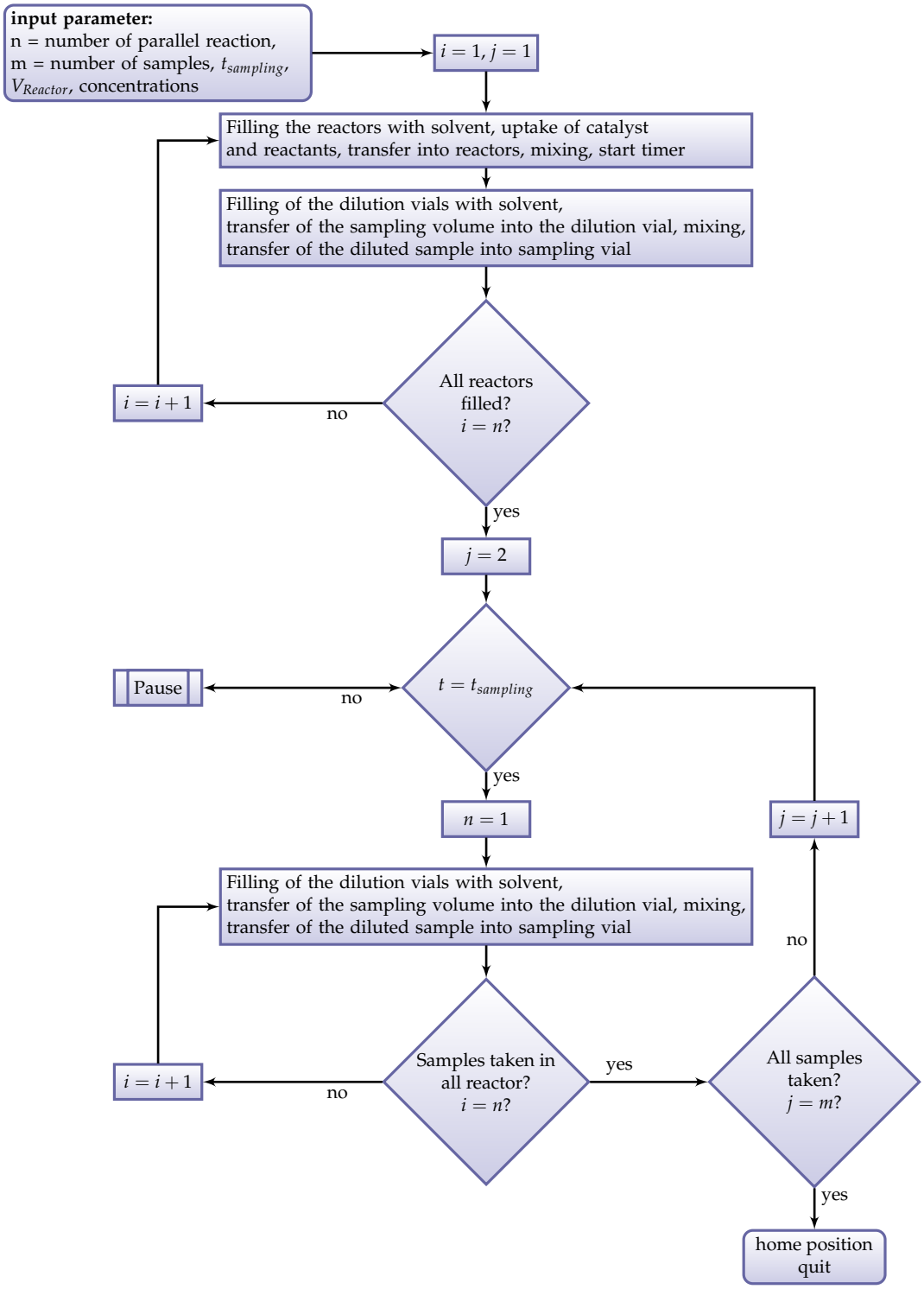

Figure A.1: Flow chart of the liquid handling program

The speed of the Z–plan movement was not controllable, hence the systematical error could only be prevented by the following procedure: Before the needle was pulled out of a sealed vial after an intake of a liquid, the tip of the needle was moved shortly over the surface of the liquid and a bubble of the gas phase in the vial was aspirated. Experiments showed, that a volume of 3 μl (approximately 1.5 cm tube length) was enough to prevent the loss of liquid. Therefore after any intake of a liquid the outline procedure was applied. With this procedure the accuracy of the liquid transfer could be increased and volumes of minimum 1 μl could be transferred with a small error averaged of only 4%, cf. chapter A.1.2

For the kinetic measurements the temperature is a parameter which has to be controlled. For the control of the temperature in the vials, thermostat-controlled liquid could be pumped through the double–walled rack. The rack temperature rang which could be realised was from 0 to <100°C. A temperature below 0°C would cause icing of the rack while the upper temperature is limited by the boiling points of the liquids. But a high rack temperature might led to malfunction of the robot, because the environmental conditions for operation the robot was given by 5 to 40°C. For the investigated catalyst it is reported that lower temperature favour the enantioselectivity as well as lower temperature reduces the reaction time. The investigated reaction is not particular sensitive to temperature [106] and first results from reactions at room temperature existed, so that the temperature has been set to the typical lab temperature of 25°C. The samples were analysed after the completed run of the reactions. The dilution of the samples were chosen in that way that, the expected concentrations were in the range of the linear slope of the calibration (0 to 37 $mmol\,L^{-1}$). Due to the dilution also the concentration of the catalyst was reduced to a value that it did not interfere with the analytic.

A.1.2 Error of liquid transfer

The determination of the error of liquid transfer with the robot is important, to exclude systematical errors because of a malfunction of the dispenser and to get information of the accuracy of the liquid transfer. The error was determined gravimetricaly. For that purpose a fixed volume of water had been transferred form one vial into a new vial. The transfer had been repeated 20 times and the transferred mass had been determined on an analytical balances. The results are presented in table A.1. The error was calculated as mean values of all 20 repetitions of the same volume. Especially small volumes, in the range of the sample volume as well as the volumes of the added starting material, have been examined. The results show a small error averaged of only 4%. The accuracy was independent of the transferred volume, but the difference was directed. In general the transferred volume had been to low. The systematical error could be included into the calculation by reducing the volumes with 2%. Then the error was normal distributed and only 2%.

single transfer volume $[\mu l]$	repetition	$V_{theoretical}$ $[\mu l]$	$V_{measured}$ $[\mu l]$	error absolute $[\mu l]$	error relative [%]
2	20	40	37.024	2.976	7
5	20	100	99.193	0.807	1
10	20	200	189.850	10.150	5
20	20	400	386.159	13.841	3

Table A.1: Error of liquid transfer; 20 times repetition

A.1.3 Gas chromatographic measurement of 2-methoxy-cyclohexen-carbaldehyde

The parameters of the gas chromatographic method for the measurement of 2-methoxy-cyclohexen-carbaldehyde is shown in table A.2 and in figure A.2 a typical chromatogram is presented. With this method a separation of diastereomers as well as enantiomers was possible. The diastereomers could be identified comparing nuclear magnetic resonance spectroscopy (NMR) measurements of the used 2-methoxy-cyclohexen-carbaldehyde with the gas chromatographic measurements[1]. But the enantiomers could not be identified, because reference substances have not been available. The determined *cis*:*trans* ratio of 1:10 could be confirmed in the gas chromatographic measurements and The diastereomeric excess in the calibration sample could be calculated to $de = 93\%$ with a standard deviation of 3%. To get an indication of a possible drift of the GC measurements all samples of the different experiments and calibration were measured in a random order.

Calibration: 2-methoxy-cyclohexen-carbaldehyde

In figure A.3 the calibration curve for the 2-methoxy-cyclohexen-carbaldehyde is shown. A linear correlation of the total product concentration and total peak area could be observed. The reference sample was supplied by the cooperation partner Dendritic Polymer Research Group, Prof. Dr. Rainer Haag, Institute of Chemistry and Biochemistry - Organic Chemistry, Freie Universität Berlin. The synthesis was performed in g scale with the free salen catalyst with a chromium transition metal. To a solution of 0.1 *mmol* (R,R)-catalyst Cr(III) Cl in 2 *ml* dry dichloromethane, stirred under nitrogen, was added 1.6 *g* molecular sieves 4 Å. The reaction was started by adding 2 *mmol* 1-methoxy-1,3-butadiene and acrolein and proceeded over night. The next day the reaction was stopped adding TFA into the reaction mixture. The solvent

[1] The NMR measurements of the reference sample were carried out at the Institute of Chemistry and Biochemistry - Organic Chemistry, Freie Universität Berlin, Dendritic Polymer Research Group, Prof. Dr. Rainer Haag.

GC	
GC	Hewlett Peackard Agilent 6890
Column	Varian 9082217
	CP-Chirasil-Dex CB
	Capillary 25 m x 320 μm x 0.25 μm nominal
Carrier gas	Hydrogen
	2.7 $ml\ min^{-1}$
	0.45 bar
Detector	flame ionisation detector (FID)
Detector temperature	250°C
Injection volume	1 μl
Split factor	10:1
Injector temperature	220°C
Temperature profile	isothermal 20 min 90°C
Retention times	*cis* I: 14.6 min
	cis II: 14.8 min
	trans I: 17.4 min
	trans II: 18.1 min
Integration parameter	Slope Sensitivity: 1
	Peak Width: 0.1
	Area Reject: 0.5
	Height Reject: 0.05
	Shoulders: off

Table A.2: Gas chromatographic method for the measurement of 2-methoxy-cyclohexencarbaldehyd

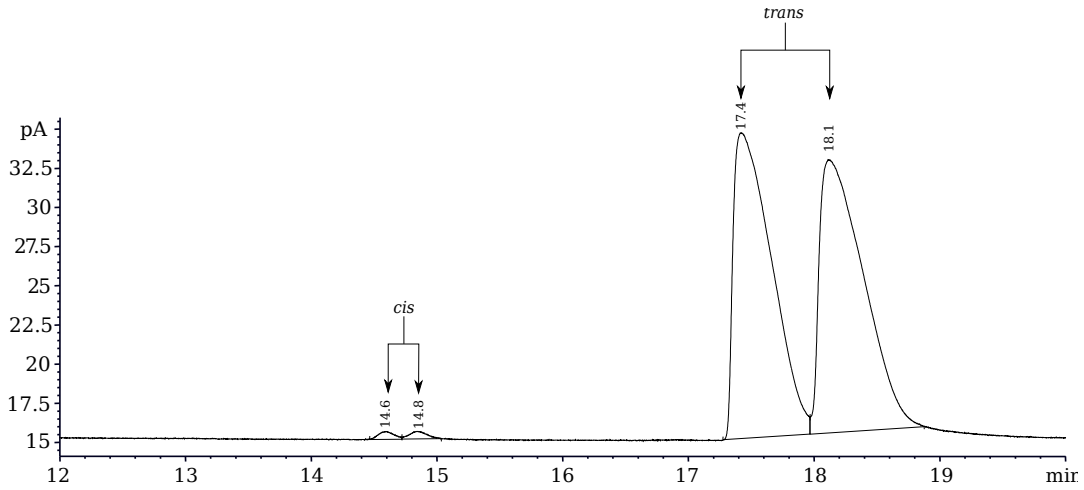

Figure A.2: Typical chromatogram of the measurement of 2-methoxy-cyclohexen-carbaldehyde

was removed in vacuum and the product purified by column chromatography of silica gel using n-hexane/EtOAc in a volume ratio of 9 to 1. The purity and configuration of product was determined by NMR spectroscopy. In the range of the measuring accuracy the product was pure with a *trans*/*cis* ratio of 9 to 1.

For the calibration solution of 0 to 71.3 $mmol\,L^{-1}$ in toluene has been prepared. A saturation of the GC column could be observed for samples with a concentration of higher then 36 $mmol\,L^{-1}$, therefore only concentrations up to 36 $mmol\,L^{-1}$ where included in the calibration. The density of 2-methoxy-cyclohexen-carbaldehyde has been assumed with 1 $g\,ml^{-1}$, whereas the density of cyclohexen carbaldehyde is known with 0.94 $g\,ml^{-1}$. Due to the low amount of the reference sample available a more precise determination of the density could not be performed. The linear correlation can be specified with $c_{Prod} = m \cdot Area$, $m = 0.0173 \pm 0.0011\ mmol\,pA^{-1}s^{-1}$. A recalibration has been performed at different time points during the work and a significant change could not be observed.

Uncertainty of the gas chromatographic measurement of 2-methoxy-cyclohexen-carbaldehyde

To quantify the uncertainty of the gas chromatographic measurement of 2-methoxy-cyclohexen-carbaldehyde a stock solution was prepared, stored at -18°C and measured as reference for each experimental run. All samples were measured within three months and the results are shown in table A.3.

The relative standard deviation was calculated to 5.1 %, which was in an acceptable range.

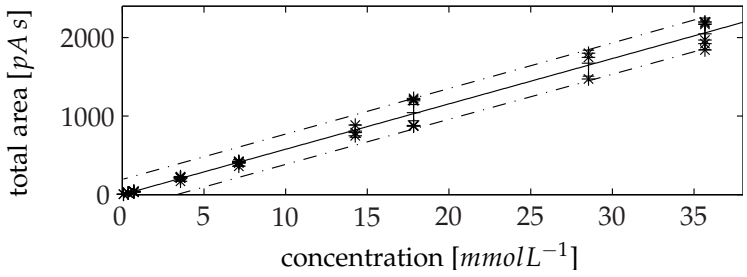

Figure A.3: GC calibration 2-methoxy-cyclohexen-carbaldehyde; $c_{Prod} = m * totalarea$, $m = 0.0173 \pm 0.0011\, mmol\, pA^{-1}s^{-1}$, dashed lines: upper and lower 95% prediction bounds of observation

Run	measured concentration $[mmol\, L^{-1}]$
1	216.9
2	213.4
3	215.2
4	218.6
5	217.2
6	210.5
7	232.7
8	220.0
9	218.8
10	235.1
11	236.9
12	240.3
13	219.4
14	246.1

Table A.3: Uncertainty of the gas chromatographic measurement of 2-methoxy-cyclohexen-carbaldehyd; mean value: 224.4 $mmol\, L^{-1}$; standard deviation: 11.4 $mmol\, L^{-1}$, 5.1 %

A.1.4 Error propagation: liquid handling

For the interpretation of the measurement the uncertainty of a measurement is an important factor. The uncertainty of a single measurement of an unprocessed sample can be calculated from a series of closely defined repetitive measurements. But for a processed sample, like the samples of the automated kinetic measurement, in the calculation of the uncertainty the error propagation of sampling processing has to be included. The investigation of the error propagation give also information about possible targets for an optimisation.

The error propagation of an uncertainty of a measurement can be calculated in case of several independent input parameter with the Gaussian law of error propagation, equation A.1

$$u_y = \sqrt{\sum_{i=1}^{n} \left(\frac{\partial y}{\partial x_i} \cdot u_i \right)^2} \tag{A.1}$$

u_y is here the propagated error. As it can be seen from equation A.1 the partial derivatives of the model function $y = y(x_1\,,\ x_2\,,\ \cdots)$ are needed. In the case of the automated addition of the compounds S into the reaction vial the model function is given with:

$$c_S = \frac{V_S\,\rho_S}{M_S\,V_R} \tag{A.2}$$

c_S is the concentration, V_S the added volume, ρ_S the density of the added substance, M_S the molar mass and V_R the final volume. With the assumption that only V_S and V_R have relative uncertainty of u_S and u_R the uncertainty of the concentration is given with:

$$u_y = \sqrt{\left(\rho_S/(M_S\,V_R)\cdot u_S\,V_S\right)^2 + \left(V_S\,\rho_S/(M_S\,V_R^2)\cdot u_R\,V_R\right)^2} \tag{A.3}$$

In that way the uncertainty at each step of the procedure could be calculated and in table A.4 the relative uncertainties of the different steps were calculated on the basis of concentrations. As simplification it was assumed, that the relative uncertainty was not depending on the magnitude of the parameter. For all calculations the systematic error corrected uncertainty of the liquid transfer was used, cf. chapter A.1.2. While the uncertainties of the liquid handling steps were quite low, seen in the low increase of uncertainty from step to step, the GC–analysis was a crucial step. The uncertainty of the GC measurment was of the same size as the liquid handling. Therefore the GC–analysis is a good target to increase the reliability of this procedure. This can be done by optimisation of the GC method as well as the optimisation of analysis of the chromatograms, which can be work intensive and the chance of success is low. A repetitive measurement of one sample followed by an averaging would increase also the reliability, but this would also increase dramatically the time for analysis, which was not possible in this case, because the utilised capacity of the GC was already up to 100 %.

Step	error propagation [%]
Addition of compounds into the reactor	2.8
Dilution step I	3.8
Dilution step II	4.1
GC–analysis	5.1

Table A.4: Error propagation of the relative uncertainties at different steps in the automated reaction system

A.1.5 Determination of acrolein

The concentration has been determined by a HPLC method[2]. A Beckmann Ultrasphere ODS 4.6 X 25 *cm* column has been used with a mobile phase of a methanol water mixture with a volume ratio of 1:4. The flow rate was 1 $ml\,min^{-1}$ and acrolein has been detected with UV absorbance at a wavelength of 220 *nm*. Prior to the HPLC analysis at room temperature the samples had to be extracted with deionised water and had to be diluted. Due to the extraction step the accuracy was very low and only samples from the continuous operated membrane reactor have been analysed.

A.1.6 Analysis of the salen transition metal catalyst

The direct determination of the concentration of the catalyst in solution was not know. The amount of active centres where determined by Inductively Coupled Plasma Optical Emission Spectrometry. The measurements were performed at the Zentrallabor Chemische Analytik, Hamburg University of Technology.

A.1.7 Sample stabilisation with TFA

The stability of the sample is a significant factor and the reaction must be stopped directly after the probing. Tests failed to develop an automated absorption of the catalyst on silica gel. The catalyst could be bound effectively to the matrix but a reproducible elution of the product could not be permitted. Therefore the catalysed reaction has been stopped, by adding trifluoro acetic acid (TFA) to the diluted samples. The functionality of this procedure could be proved by storing the reaction samples in one case in toluene and in the other case in a 0.5 $mol\,L^{-1}$ TFA solution. The samples were analysed directly ofter the sampling and after 24 hours of storage at room temperature. The results are shown in figure A.4 and A.5. All variations of

[2]The measurements has been done by the Zentrallabor Chemische Analytik, Technische Universität Hamburg-Harburg.

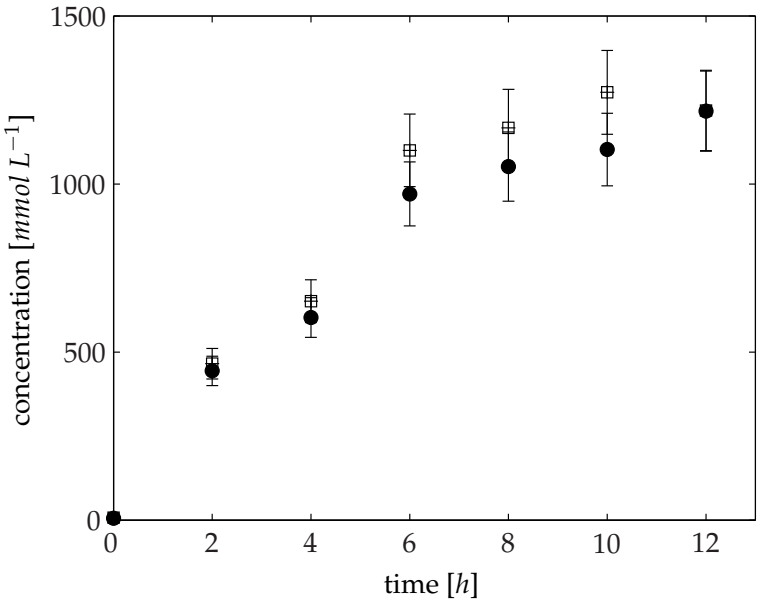

Figure A.4: Sample stability without TFA directly after sampling (■) and after 24 h (□)

the measured concentrations were in the range of the measurement error of the GC, cf. chapter A.1.3. But in figure A.4 a systematical increase of the measured concentration was observable compared to the averaged concentrations. Therefore it could be concluded that the addition of TFA stabilises the samples and inhibits the catalyst. In kinetic measurements the samples were stabilised by the addition of TFA to enhance the accuracy of the measurements, because the time offset between the probing and the GC analysis could be up to 56 hours.

A.1.8 Kinetic investigation of a homogeneously catalysed Diels–Alder reaction

The investigated reaction was performed in a batch reactor with different initial concentrations of the participating compounds, cf. table A.5. The catalyst loading is expressed as ration of the active sides, the chromium content, to the amount of the lower concentrated starting material. The reactions had been performed using a liquid handling robot, cf. chapter 2.5. The lowest precision of this robot was 1 μl. To adjust precisely the concentrations presented in table A.5 volumes of a fraction of the precision of the robot had been added. For example 1000 $mmol\ L^{-1}$ ($c_{intended}$) of butadiene was equal to a butadiene volume of 20.2 μl, due to the rounding to the next integer 20 μl was applied resulting in a concentration of 990 $mmol\ L^{-1}$ (c_{real}). In table A.6 the error due to rounding is presented. An equimolar addition of the to starting materials was not possible, because of their different densities. For clarity's sake in the following the initial concentrations are denoted by $c_{intended}$, but for all cal-

No.	$c_{butadiene}$ $[mmol\ L^{-1}]$	$c_{acrolein}$ $[mmol\ L^{-1}]$	$m_{catalyst}$ $[mg/Reactor]$	$c_{catalyst}$ $[mmol\ L^{-1}]$	*catalyst loading* $[mol\%]$
1	200	1000	6	35	17.89
2	200	200	6	35	17.89
3	1000	200	6	35	15.59
4	350	350	7.5	44	12.74
5	300	300	6	35	11.93
6	1000	350	6	35	9.35
7	400	350	6	35	9.35
8	400	1000	6	35	8.94
9	500	500	6	35	7.16
10	700	700	7	41	6.06
11	600	1000	6	35	5.96
12	600	600	6	35	5.96
13	1000	600	6	35	5.84
14	800	1000	6	35	4.47
15	800	800	6	35	4.47
16	1000	800	6	35	4.25
17	1000	1000	6.5	38	3.91
18	1000	1000	6	35	3.60
19	1200	1200	6	35	2.98
20	1000	1000	4.5	27	2.71
21	1400	1400	6	35	2.56
22	1600	1600	5.5	32	2.04
23	1000	1000	3	18	1.80
24	1000	1000	1.5	9	0.91
25	1000	1000	0	0	0.00

Table A.5: Initial conditions in the batch reactions

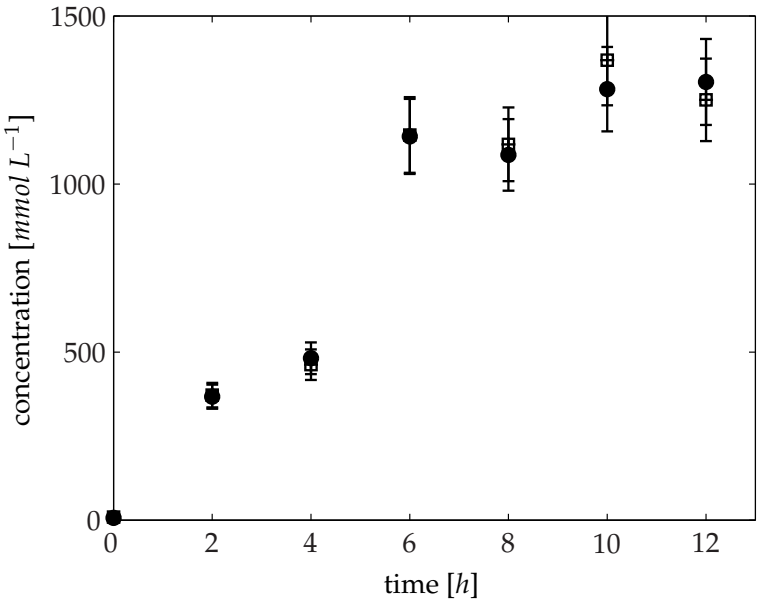

Figure A.5: Sample stability with 0.5 $mmol\ L^{-1}$ TFA directly after sampling (•) and after 24 h (○)

culation were used the exact concentrations c_{real}. The reaction volume has been set to 200 μL, so that the starting material and catalyst consumption could be minimised. To get information about the reproducibility, experiment 12 had been performed two times and experiment 18 seven times.

A.1.9 Reversibility the Diels–Alder reaction

For the mathematical description of the kinetics a fundamental assumption was made, that a reverse reaction is negligible. To prove this assumption experimentally to 100 μl of a product solution with a concentration of 70 $mmol\ L^{-1}$ in toluene 100 μl of a catalyst solution with a concentration of 47.2 $mmol\ L^{-1}$ also in toluene was added. The reaction course was followed for 12 hours and each second hour a sample was taken. As blank reaction of a product solution with 35 $mmol\ L^{-1}$ without catalyst each second hour samples were taken. The reactions and sampling were performed automated with the liquid handling robot.

A.1.10 Purification of the chemzyme

The purity of the polymeric supported catalyst was not known and it was expected, that beside the desired macro molecule also free Salen as well as not complex bound

$c_{intended}$ $[mmol\ L^{-1}]$	$c_{butadiene,real}$ $[mmol\ L^{-1}]$	$c_{acrolein,real}$ $[mmol\ L^{-1}]$
200	198	227
300	297	303
350	347	379
400	396	379
500	495	530
600	594	606
800	792	833
1000	990	985
1200	1188	1212
1400	1386	1364
1600	1584	1590

Table A.6: Intended and real concentrations in batch reaction

free chromium were in the catalyst preparation [3]. These low molecular weight compounds could be separated form the polymeric bound catalyst by means of ultrafiltration. For this purpose also the membrane reactor was used (Starmem™ 120 of the supplier 'Membrane-Extraction-Technology'). The principle set up is described in chapter 2.8.1.

For operation the membrane was preconditioned and mounted into the reactor. The reactor was operated at a constant pressure of 10 *bar* for at least one hour pumping toluene through the reactor with a closed retentat outlet. Before each experiment the integrity of the membrane was test, by pumping toluene through the reactor with a pump rate of 0.35 $ml\ min^{-1}$. With full integrity the pressure increased to more the 8 *bar* within several minutes. Toluene was pumped continuously through the reactor for catalyst preparation. To apply a concentrated solution of catalyst, 5 *ml* ethyl acetate was added to the dry row catalyst preparation and the solution was shaken by 20°C for several hours. Two times 2 *ml* of the concentrated row catalyst solution has added into the by–pass and flushed into the reactor. The catalyst was dissolved in ethyl acetate, because of the higher solubility of the catalyst in this solvent. For washing the pump was controlled at constant pressure at 11 *bar*, which was the maximum operation pressure of the reactor. About 0.5 *g* catalyst could be loaded and after about 20 residence times the purified catalyst could be harvested via the retentat outlet. The mean flow rate over the entire operation time was 0.2 $ml\ min^{-1}$ and

[3] The catalyst had been synthesised by our cooperation partner, Dendritic Polymer Research Group, Prof. Dr. Rainer Haag, Institute of Chemistry and Biochemistry - Organic Chemistry, Freie Universität Berlin.

started with a higher flow rate at the beginning and was reduced with operation time due to the concentration polarisation at the membrane. For the clean in place procedure the reactor was flushed with ethyl acetate at least 2 residence times. The filtrate and retentat was collected and the solvents removed in vacuum and the mass of the remaining solids was measured. The purified catalyst was used for all experiments, for the kinetic measurements, cf. chapter A.1.8, as well as for the continuous operated membrane reactor.

The yield in a single purification step was averaged 89%. All residues in all used vessels were collected and purified later, so that the overall yield could even be increased.

A.1.11 Diels–Alder reaction in a continuous operated membrane reactor

The reactor setup is displayed in figure 2.21. For conditioning of the reactor system, the reactor was washed with toluene for 20 hours at a controlled pressure of 11 *bar*. 300 and 600 *mg* catalyst were dissolved in 2 and 4 *ml* ethyl acetate, respectively. To mediate the dissolving of the catalyst the solution was treated for 3 minutes in an ultra sonic bath. The catalyst solution was injected into the by–pass and transferred into the reactor with the toluene flow. Again the system was operated 20 hours pumping toluene through the system to remove the ethyl acetate. Then low had been switched form the toluene to the substrate fluid container. Here the starting material had been dissolved in an equimolar ratio in toluene with a concentration of 250 and 500 $mmol\,L^{-1}$, respectively. The storage container was cooled to 4°C to reduce the evaporation of the toluene as well as increase the stability of the acrolein and butadiene. The colling was important, because the prepared solution was used up to one week. After switching to the reaction compounds the system was operated for one residence time at maximal flow rate, for a fast filling of tubing and the reactor with the reactant solution. Then the flow rate was reduced to the intended rate. The influence of the pressure on the reaction rate could be neglected, because the reaction take place in a one-phase, liquid medium. The flow rate was limited by the maximal transmembrane pressure of 11 *bar*, which was the constructive limit. Theoretically it would preferable to operate the reactor at the maximum transmembrane pressure to establish a high flow rate and by that high throughput, but due to the findings from the kinetic investigations the reactor was operated at much lower flow rates.

The samples were collected in sampling vial sealed with a septum. When available the sampling was done with the liquid handling robot, cf. figure 2.6, and about 1.5 *ml* were collected per vial. The vials were cooled to 4°C in the rack and weighed before and after sampling to calculate the real flow rate. For GC analysis the samples had to be diluted, which were also automated with the liquid handling robot, samples with a feed concentration of 500 $mmol\,L^{-1}$ were diluted 20 times and with a concentration of 250 $mmol\,L^{-1}$ ten times. Samples were collected for several days and stored at -18°C. To detected fluctuation in the GC analysis a reference sample were analysed at

regular intervals and the samples were measured randomised. For the experiment period A to C 141 samples were analysed and for the period D further 133 samples. The reaction progress of the period E and F was followed with 199 samples and in two of these samples the acrolein concentration was measured.

The duration of the operation of the membrane reactor was limited by the amount of available butadiene so that the experiment had to be stop after 17 residence times in period F. After the experiment the reactor was flushed with toluene for 20 hours at maximum transmembrane pressure to remove low molecule material, like remaining substrates and product. Then the catalyst solution was collected via the retentat outlet and dried in vacuo. The amount of recovered catalyst amount was measured gravimetrically. Then the reactor was opened and cleaned with acetone. The catalyst adhered in the reactor was collected and the amount also determined gravimetrically.

A.2 Enzyme catalysed synthesis of cyanohydrins

A.2.1 The *Hb*hydroxynitrile lyase

The recombinant *Hb*HNL from *Hevea brasiliensis* expressed in *Pichia pastoris* was kindly provided by Institute of Organic Chemistry, TU Graz, Austria. Two different production batches were used. The clear yellow enzyme solutions were stored at 4°C (25 mM potassium phosphate, pH 7.45). The activity was checked on a regularly basis, cf. table A.7 and no significant loss of activity over the time was observed. For

enzyme	protein concentration $[mg\,mL^{-1}]$	volumetric activity $[U\,mL^{-1}]$	specific activity $[U\,mg^{-1}]$
*Hb*HNL (Batch I)	103.9	5400	51.9
*Hb*HNL (Batch II)	0.4	460	1150
*Pa*HNL	1.01	141	139.6

Table A.7: Protein concentration and activity of the HNL stock solutions

the synthesis of enantiopure (*R*)-mandelonitrile the (*R*)-selective hydroxynitrile lyase form *Prunus amygdalus* was used. The enzyme was expressed heterogeneously in *Saccharomyces cervisiae* and also kindly provided by the Institute of Organic Chemistry, TU Graz, Austria. The enzyme was stored at +4°C in a Na_3PO_4-buffer. The activity was checked on a regularly basis, cf. table A.7 and no significant inactivation could be observed over the period of the project.

A.2.2 HNL activity test

The activity test is based on the cleavage of mandelonitrile into benzaldehyde and HCN. The chance of the benzaldehyde concentration is monitored by UV absorption

(UvikonXL, Bio–Tek Instruments) at a wavelength at 280 nm at 25°C [4]. All determinations were executed at least threefold. The composition of the buffers used for the test

	Components	Concentration $[mol\ L^{-1}]$	pH
assay buffer:	citrate– phosphate buffer	0.05	5.0
enzyme buffer:	phosphate buffer	0.005	6.5
substrate buffer:	citrate– phosphate buffer	0.06	3.5
substrate solution:	80 $\mu\ l$ racemic mandelonitrile were dissolved in 10 ml substrate buffer		

Table A.8: Solutions for the Activity test

are listed in table A.8. The enzyme solution was prepared in a dilution series with the Enzyme buffer to 0.4 - 1 $U\ ml^{-1}$, so that the change of absorbancy ($\Delta A\ min^{-1}$) was between 0.06 to 0.14 after subtraction of the blank reaction. Enzyme and substrate solutions were stored on ice and prepared daily.

The test reaction

The rate of the chemical reaction and the rate of both – the chemical and the enzymatic reaction – was measured separately. The following procedure was performed: The

To pipette into a cuvette	blank $[\mu l]$	sample [5] $[\mu l]$
Assay buffer	700	700
Enzyme solution	–	100
Enzyme buffer	100	–
Start reaction with		
Substrate solution	200	200

Table A.9: Activity test procedure

absorbance was measured and the reaction was observed for five minutes. From the linear part of the absorbance time measurement, the absorbance change per time unit

[4] The temperature had to be controlled properly because 1°C deviation let to more then 10 % error

[5] The blank value corresponds to the chemical reaction, the sample to the sum of chemical and enzymatic reaction

(slope) was calculated using linear regression and the slope was used to calculate the activity according the equations A.4 and A.5

$$\left(\frac{\Delta A}{\Delta t}\right)_{enzymatic} = \left(\frac{\Delta A}{\Delta t}\right)_{sample} - \left(\frac{\Delta A}{\Delta t}\right)_{chemical} \tag{A.4}$$

The activity is determined by:

$$activity = \frac{V_{total}}{(\varepsilon_{280} * l * V_{enzyme})} * \frac{\Delta A}{\Delta t} = \frac{1}{(1.376 * 1 * 0.1)} * \frac{\Delta A}{\Delta t} \; [U\, ml^{-1}] \tag{A.5}$$

ε is the molar absorption coefficient of benzaldehyde and l the thickness of the cuvette. As the molar absorption coefficient ε of benzaldehyde is about 100 times larger then the one of mandelonitrile the absorption coefficient of mandelonitrile can be neglected [337].

$$\begin{aligned} \varepsilon_{BA,280nm} &= \quad 1376 \quad [L\, mol^{-1}\, cm^{-1}] \\ \varepsilon_{MN,280nm} &= \quad 16 \quad\;\; [L\, mol^{-1}\, cm^{-1}] \end{aligned}$$

The activity is expressed in *units* [U] and one unit is defined as the amount of enzyme which cleaves 1 μmol of (*S*)-mandelonitrile per minute.

Determination of the protein content of the enzyme solution

The protein content in the enzyme solution as well as in the washing solution of the immobilisation were determined with the BioRad protein assay using bovine serum albumin (BSA) as a standard protein. The micro titer plate assay was used according to the manual. For the calibration six dilution of the protein standard in the range of zero to 0.5 $mg\, ml^{-1}$ were prepared. The enzyme stock solution were diluted with water and the dilution series and standards were assayed in duplicates. After incubation of the samples with the dying solution for 5 minutes at room temperature the absorbance was measured with a microtiter plate reader at 595 nm.

A.2.3 Gas chromatic determination of benzaldehyde and mandelonitrile

The measurement of enantiomeric distribution of the enantioenriched mandelonitrile was done by GC measurements. Beside the distribution also the benzaldehyde and (*S*) and (*R*)- mandelonitrile concentration could be determined. While benzaldehyde could be measured directly, the mandelonitrile could only detected in an acetylated form, due to the polarity of the *HO*-group of the nitrile. The acetylation was done with acetic acid anhydrite in an organic solvent and in the presence of pyridine. Acetic acid anhydrite and pyridine were added into the organic solvent in which the nitrile was dissolved in the ratio 1:1:5. The reaction time were at least 12 hours. After that time no further reaction could be observed and the samples were stable

for several weeks stored at -18°C. The parameters for the GC are listed in table A.10. Samples from aqueous solutions were extracted with one part organic solvent (MTBE) and one part aqueous buffer. The enantiomeric excess (*ee*) of *S*- and *R*- mandelonitrile

gas chromatography	Hewlett Peackard Agilent 6890
column	Chiraldex FS 50m (Chromatographie service Juelich)
carrier gas	hydrogen, 3.1 $mL\,min^{-1}$
detector	flame-ionisation-detector (FID)
injector volume	1 μl
injector temperature	250°C
detector temperature	250°C
temperature program	14 min 115°C, ramp 15°C min^{-1} to 160°C
total run time	35 min
internal standard	2-phenyl ethanol
retention time	benzaldehyde 12.4 min
	2-phenyl ethanol 21.3 min
	(*R*)-mandelonitrile 28.4 min
	(*S*)-mandelonitrile 29.1 min

Table A.10: GC Parameters

was determined from the ratio of the peak areas of the acetylated derivatives and the *ee* was calculated with equation 1.1.

A.2.4 HCN production and precautions

Hydrogen cyanide was produced with the apparatus presented in figure 3.5. As HCN source cyanide salts has been used. The chemical equation of the HCN production is presented in equation A.6. The required amount of HCN was freshly prepared by adding drop wise a 30% NaCN solution to aqueous sulphuric acid (60%) at 80°C with a peristaltic pump (3). HCN was transferred in a nitrogen stream (2) through a drying column (6) and collected in a cooling trap (8) at -13°C, cf. figure 3.5 and table 3.2. The gas outlet was washed in a gas washer containing NaOH/water solution pH 11 and 25% hydrogen peroxides in a ratio of one to three.

$$\underbrace{H_2SO_4}_{60\%H_2SO_4} + \underbrace{2NaCN}_{30\%aqu.} \rightarrow 2HCN + Na_2SO_4 \tag{A.6}$$

The production and handling of pure hydrogen cyanide bear a high risk potential. The production followed a given protocol, the protocol is shown in the appendix C. The physical and toxic properties are presented in table A.11. Special attention must

be turned to the low boiling point of HCN which is close to or even below the room temperature. Due to the high vapour pressure of 0.816 *hPa* at 20°C the risk to get a toxic concentration in the air is high, so that the HCN must be handled in closed vessels. All reaction equipment, in which HCN or cyanides were involved, was placed in a well ventilated hood. Beside an air flow control three hoods were connected by pass-through door, so that the cyanide contaminated material could be transferred within the ventilated hoods. The ventilation system of the three hoods was equipped with a four redundant ventilators and by a fault of one ventilator the fourth ventilator takes over. The power supply of the ventilation system and the power plugs in the hoods were backuped by a two stage backup system, an uninterruptible power supply which takes over the power supply at a break down of the main line until the diesel fuel driven emergency power generator takes over. By that a power supply was assure, especially for the colling devises keeping the HCN in a liquid phase. The air in the hoods were continuously monitored by two electrochemical sensor for HCN (Pac III, Dräger Safety AG). At the entrances to the HCN lab warning signs were pleased, cf. figure 3.5. All HCN working were carrying out under supervision of a second trained person.

In case of emergency gas masks were located near by the hood and in an emergency locker outside the laboratory. Also an artificial respiratory equipment (Dräger Safety AG, emergency oxygen systems Akut 2001) as well as antidots (4-DMAP) and infusions (Natriumthiosulfat) were stored in the locker. All employee were trained in Fist aid and especially in emergency measures in case of a HCN accident including the handling of the artificial respiratory equipment and using gas masks. All employes were medically examined whether there were personal risks for handling HCN, like allergies to the antidot.

All waste containing cyanide was collected. The pH of the waste solution was adjusted to pH 11 with sodium hydroxide and hydrogen peroxide was added to decompose HCN to carbon dioxide and gaseous nitrogen.

Warning sign and physical and safety data of hydrogen cyanide

density	0.69 $g\,ml^{-1}$
molecular weight	27.03 $g\,mol^{-1}$
melting point	- 13.3°C
boiling point	25.7°C
R-phrases	12-26-50/53
S-phrases	1/2-7/9-16-36/37-38-45-60-61
Threshold Limit Value	10 $ml\,m^{-3}$ = 11 $mg\,m^{-3}$
TD_{Lo}[1](human, peroral)	1.471 $mg\,kg^{-1}$ [338]
TD_{Lo} (human,intravenous)	0.055 $mg\,kg^{-1}$ [338]
LC_{50}[2](human, inhalativ)	3030 ppm after 1 min [339]
	270 ppm after 6-8 min [339]
	181 ppm after 10 min [339]
	135 ppm after 30 min [339]

T+ F+ N

[1] Lowest published toxic dose (Toxic Dose Low, TD_{Lo}) is the lowest dosage per unit of body weight of a substance known to have produced signs of toxicity in a particular animal species.

[2] A dose at which 50% of subjects will die.

Table A.11: Conversion as function of the catalyst concentration; $c_{0,butadiene} = c_{0,acrolein} = 1\,mol\,L^{-1}$

Figure A.6: Warning sign: experiments HCN

A.2.5 Specification of the ASCII-file recording the spectral data

In the first row of the data file the configuration information like integration time, average time and smoothing parameters and in the second row the recorded wavelength range are presented. In the first column the relative time in minutes of the measurements are shown.

No. raw						
1	integration time	average time	smoothing parameter parameter	9999	$\cdots$	9999
2	9999	λ_1	λ_2	λ_3	$\cdots$	λ_{end}
3	t_1	I_{λ_1,t_1}	I_{λ_2,t_1}	I_{λ_3,t_1}	$\cdots$	I_{λ_{end},t_1}
4	t_2	I_{λ_1,t_2}	I_{λ_2,t_2}	I_{λ_3,t_2}	$\cdots$	I_{λ_{end},t_2}
:	:	:	:	:	$\ddots$	:
end	t_{end}	$I_{\lambda_1,t_{end}}$	$I_{\lambda_2,t_{end}}$	$I_{\lambda_3,t_{end}}$	$\cdots$	$I_{\lambda_{end},t_{end}}$

Table A.12: Schema of the data file, 9999 is a spacer

Kinetic measurements of *Hb*HNL catalysed reaction

All reactions have been performed in a 0.05 $mol\ L^{-1}$ citrate–phosphate buffer, pH 5.0. The total reaction volume was 20 ml and temperature-controlled at 25°C. The enzyme concentration for the cleavage reaction was 7.13 $\mu g\ ml^{-1}$ and for the synthesis reaction 0.713 $\mu g\ ml^{-1}$[6]. The measurement time was set to 480 seconds and the absorption was measured at the wavelength range 200 to 350 nm. For the measurements the enantiopure mandelonitrile was used and the concentration range was 0.5 to 15 $mmol\ L^{-1}$. Also the benzaldehyde concentration reached form 0.5 to 15 $mmol\ L^{-1}$ and the HCN concentration was adjusted to 25, 50 and 100 $mmol\ L^{-1}$, respectively. The different reaction conditions are shown in table A.13.

No.	intended				recalculated			
	BA [$mmol\ l^{-1}$]	HCN [$mmol\ l^{-1}$]	(*S*)-MN [$mmol\ l^{-1}$]	(*R*)-MN [$mmol\ l^{-1}$]	BA [$mmol\ l^{-1}$]	HCN [$mmol\ l^{-1}$]	(*S*)-MN [$mmol\ l^{-1}$]	(*R*)-MN [$mmol\ l^{-1}$]
1	0	0	0.5	0	0.01	0	0.49	0
2	0	0	1	0	0.02	0	0.98	0
3	0	0	2	0	0.06	0	1.94	0
4	0	0	3	0	0.11	0	2.89	0
5	0	0	6	0	0.09	0	5.91	0

[6]The synthesis reaction was considerable catalysed faster then the cleavage reaction, therefor a lower enzyme concentration was used.

6	0	0	10	0	0.31	0	9.69	0
7	0	0	12	0	0.55	0	11.45	0
8	0	0	1	10	0.6	0	0.94	9.47
9	0	0	2	10	0.21	0	1.88	9.91
10	0	0	3	10	0.43	0	2.82	9.76
11	0	0	6	10	0.24	0	5.91	9.75
12	0	0	10	10	0.5	0	9.75	9.75
13	0	0	12	10	0.5	0	11.73	9.77
14	0	0	0.5	0	0.05	0	0.45	0
15	0	0	2.5	0	0.24	0	2.26	0
16	0	0	5	0	0.52	0	4.48	0
17	0	0	7.5	0	0.64	0	7.36	0
18	0	0	12	0	0.03	0	11.97	0
19	0	0	15	0	1.04	0	13.96	0
20	0	0	20	0	2.02	0	17.98	0
21	0	0	1	0	0.06	0	0.94	0
22	0	0	2	0	0.1	0	1.9	0
23	0	0	3	0	0.34	0	2.66	0
24	0	0	5	0	0.78	0	4.22	0
25	0	0	7.5	0	0.35	0	7.15	0
26	0	0	1	3	0.11	0	0.94	2.96
29	0	0	10	3	0.59	0	9.39	3.00
30	0	0	15	3	0.97	0	14.08	2.95
31	0	0	1	10	0.16	0	0.94	9.9
32	0	0	3	10	0.35	0	2.82	9.83
33	0	0	6	10	0.83	0	5.63	9.54
34	0	0	10	10	1.0	0	9.39	9.62
35	0	0	15	10	1.54	0	14.08	9.38
36	0	0	0.5	0	0.08 0	0.422	0	
37	0	0	1	0	0.162	0	0.838	0
38	0	0	2	0	0.28	0	1.72	0
39	0	0	3	0	0.23	0	2.77	0
40	0	0	5	0	0.19	0	4.81	0
41	0.5	25	0	0	0.52	25	0	0
42	1	25	0	0	1.03	25	0	0
43	1.5	25	0	0	1.55	25	0	0
44	2	25	0	0	2.14	25	0	0
45	2.5	25	0	0	2.41	25	0	0
46	3	25	0	0	3.28	25	0	0
47	5	25	0	0	5.25	25	0	0
48	6	25	0	0	6.32	25	0	0

49	0.5	50	0	0	0.5	50	0	0
50	1	50	0	0	1.01	50	0	0
51	1.5	50	0	0	1.75	50	0	0
52	2	50	0	0	2.09	50	0	0
53	3	50	0	0	3	50	0	0
54	5	50	0	0	5.21	50	0	0
55	1	50	0	5	1.11	50	0	4.89
56	2.5	50	0	5	2.63	50	0	4.87
57	5	50	0	5	5.3	50	0	4.70
58	7.5	50	0	5	8.17	50	0	4.33
59	10	50	0	5	10.89	50	0	4.11
60	15	50	0	5	15.66	50	0	4.34
61	1	25	0	5	1.86	50	0	4.14
62	2.5	25	0	5	3.29	50	0	4.21
63	5	25	0	5	6.06	25	0	3.94
64	7.5	25	0	5	8.36	25	0	4.14
65	10	25	0	5	10.66	25	0	4.34
66	12.5	25	0	5	13.35	25	0	4.15
67	5	25	0	10	6.70	25	0	8.30
68	7.5	25	0	10	10.02	25	0	7.48
69	10	25	0	10	11.63	25	0	8.37
70	12.5	25	0	10	13.94	25	0	8.56
71	4	25	0	0	3.96	25	0	0
72	5	25	0	0	5.07	25	0	0
73	6	25	0	0	5.76	25	0	0
74	7	25	0	0	7.02	25	0	0
75	5	100	0	0	4.99	100	0	0
76	6	100	0	0	5.80	100	0	0
77	7	100	0	0	6.93	100	0	0
78	8	100	0	0	7.99	100	0	0
79	5	100	0	5	5.48	100	0	4.52
80	5	100	0	10	5.65	100	0	9.35

Table A.13: Reaction conditions for the kinetic measurements of *Hb*HNL catalysed reaction

The benzaldehyde concentrations have been calculated from the measured absorption at 280 *nm* at time point zero. The mandelonitrile concentration was corrected by the subtraction of the difference of the measured and intended benzaldehyde concentration, because the higher measured concentration in present of mandelonitrile was caused by a purity of the samples of 95% – the remaining 5% were benzaldehyde– and the uncatalysed cleavage of the mandelonitrile in the reaction buffer prior to the reaction start. In case of different concentration of (*R*)- and (*S*)-mandelonitrile the

concentrations were corrected proportional to their concentrations.

No.	intended			recalculated		
	BA $[mmol\,l^{-1}]$	HCN $[mmol\,l^{-1}]$	MN $[mmol\,l^{-1}]$	BA $[mmol\,l^{-1}]$	HCN $[mmol\,l^{-1}]$	MN $[mmol\,l^{-1}]$
1	10	25	0	10.3	25	0
2	15	25	0	13.9	25	0
3	5	25	0	5.42	25	0
4	5	25	0	5.42	25	0
5	0.5	50	0	0.53	50	0
6	1.5	50	0	1.6	50	0
7	1	50	0	1.04	50	0
8	2	50	0	2.22	50	0
9	3	50	0	3.04	50	0
10	5	50	0	5.37	50	0
11	0	0	10	0.014	0	9.99
12	0	0	20	0.024	0	19.98
13	0	0	0.5	0.007	0	4.99

Table A.14: Reaction conditions for the kinetic measurements of the uncatalysed reaction

A.3 Mass balances of the *Hb*HNL catalysed reaction including uncatalysed reaction

Substrates

$$\frac{dc_{BA}}{dt} = k_5 * c_{E-BA} - k_6 * c_E * c_{BA} + k_{10} * c_{(S)-MN} + k_{10} * c_{(R)-MN} - k_{11} * c_{BA} * c_{HCN} \tag{A.7}$$

$$\frac{dc_{HCN}}{dt} = k_3 * c_{E-(S)-MN} - k_4 * c_{E-BA} * c_{HCN} + k_{10} * c_{(S)-MN} + k_{10} * c_{(R)-MN} - k_{11} * c_{BA} * c_{HCN} \tag{A.8}$$

$$\frac{dc_{(S)-MN}}{dt} = k_2 * c_{E-(S)-MN} - k_1 * c_E * c_{(S)-MN} - k_{10} * c_{(S)-MN} + 0.5 * k_{11} * c_{BA} * c_{HCN} \tag{A.9}$$

$$\frac{dc_{(R)-MN}}{dt} = -k_{10} * c_{(R)-MN} + 0.5 * k_{11} * c_{BA} * c_{HCN} - k_7 * c_{(R)-MN} * c_E + k_8 * c_{E-(R)-MN} \tag{A.10}$$

Enzyme complexes

$$\begin{aligned}\frac{dc_E}{dt} &= k_2 * c_{E-(S)-MN} - k_1 * c_E * c_{(S)-MN} \\ &\quad - k_6 * c_E * c_{BA} + k_5 * c_{E-BA} \\ &\quad - k_7 * c_E * c_{(R)-MN} + k_8 * c_{E-(R)-MN}\end{aligned} \tag{A.11}$$

$$\begin{aligned}\frac{dc_{E-BA}}{dt} &= k_3 * c_{E-(S)-MN} - k_4 * c_{E-BA} * c_{HCN} \\ &\quad + k_6 * c_E * c_{BA} - k_5 * c_{E-BA}\end{aligned} \tag{A.12}$$

$$\begin{aligned}\frac{dc_{E-(S)-MN}}{dt} &= -k_2 * c_{E-(S)-MN} + k_1 * c_E * c_{(S)-MN} \\ &\quad + k_4 * c_{E-BA} * c_{HCN} - k_3 * c_{E-(S)-MN}\end{aligned} \tag{A.13}$$

$$\frac{dc_{E-(R)-MN}}{dt} = k_7 * c_E * c_{(R)-MN} - k_8 * c_{E-(R)-MN} \tag{A.14}$$

The factor of 0.5 in equation A.9 and A.10 describes that in the unselective chemical reaction 50 % (*S*)- and 50 % (*R*)-mandelonitrile is synthesised.

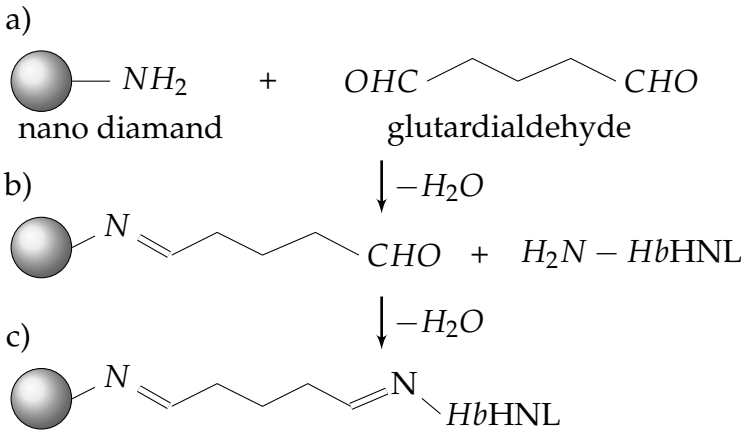

Figure A.7: Immobilisation of the (*S*)-HNL on nano carriers: a) amino functionalised carries were activated with glutardialdehyde, b) The enzyme was incubated with active nano carriers for 24 hours, c) immobilised HNL on nano carriers.

A.4 Immobilisation: Materials and Methods

A.4.1 Immobilisation of the *Hb*HNL on a nano carries

The nano carriers were nano diamonds which have been functionalisiered with amino functions. This was done by reacting the surface with trimethoxy-(3-Aminopropyl)-silan by which free primary amino functions occur. The immobilisation of the enzyme followed the reaction steps presented in figure A.7. 15 mg carrier were washed three times with 1.5 ml 20 $mmol\,L^{-1}$ potassium-phosphate buffer. Between every washing step the carrier were separated by centrifugation (Eppendorf AG, Centrifuge 5415 D) at 13000 rpm for 5 min. Then the carrier were activated in 1.5 ml the potassium-phosphate buffer and 2% glutardialdehyde for 12 hours mixed on a shaker at 150 rpm at room temperature. After the addition of the glutardialdehyde to the buffer the pH was adjusted with to pH 8.0.

After the washing of the immobilisate with the buffer to remove the glutardialdehyde, the enzyme was immobilised on the carrier. For immobilisation the *Hb*HNL enzyme stock solution (5300 $U\,ml^{-1}$) was diluted with the potassium-phosphate buffer in the ratio 1:3. To the carrier 1.5 ml of this solution was added, shaken and incubated for 12 hours at +4°C. After the incubation the carriers were washed with 1.5 ml buffer several times and the wash solution was collected. The activity and protein content in the wash solution were measured to determine the efficiency of the immobilisation.

Activity test of the immobilised *Hb*HNL on nano carriers

For the activity of the immobilised (*S*)-HNL on nano carriers the standard activity test was used. The clouding due to the carries were negligible and did not influence the

test. Also a sedimentation of the carriers could not be observed. Because the covalent bounds are unstable under acid conditions as the enzyme buffer, cf. table A.8, the 20 $mmol\,L^{-1}$ potassium phosphate buffer, pH 8.0 was used. All washing fraction which contained enzyme as well as the supernatant of the immobilisation procedure had been analysed.

Synthesis of (*S*)-mandelonitrile with *Hb*HNL immobilised on nano carriers

The application of the immobilised enzyme for the synthesis of chiral mandelonitrile were in the aqueous reaction system, cf. chapter kinetic). As reaction medium the 50 $mmol\,L^{-1}$ citrate–phosphate buffer, pH 5.0, has been used and all reaction were performed at 25°C. The benzaldehyde concentration was set to $c_{BA} = 1$, 5, 7.5 and 10 $mmol\,L^{-1}$. As internal standard 1 $mmol\,L^{-1}$ 2-phenyl ethanol was added. The reaction was started by the addition of HCN with the automated procedure and a HCN concentration of 50 $mmol\,L^{-1}$ was applied. The amount of nano carries added into the reactor were calculated on the basis of the activity measurements and the amount corresponding to 0.713 $ml\,L^{-1}$ of the enzyme stock solution were applied. The reaction time were set to 20 min and the benzaldehyde concentration. The reaction progress was followed by GC measurements, cf. chapter A.2.3. Every second minute 750 μl sample was taken and extracted with *tert*-butyl-methy ether in the ratio 1:1. After intensive mixing and phase separation 500 μl of the organic phase were transferred into a GC-vial and derivatised with 100 μl acetic acid anhydrite and 100 μl pyridine. After 24 hours reaction the samples were analysed on the GC.

Cleavage of (*S*)-mandelonitrile with *Hb*HNL immobilised on nano carriers

Three cleavage reactions had been performed. The same reaction conditions were used as for the kinetic measurements in aqueous medium. The substrate concentrations applied are presented in table A.15. Also the internal standard of 1 $mmol\,L^{-1}$ 2-phenyl ethanol was added. The reaction was started by the addition of the immo-

Experiment	(*S*)-MN [$mmol\,L^{-1}$]	(*R*)-MN [$mmol\,L^{-1}$]
1	10	0
2	5	5
3	10	10

Table A.15: Cleavage of (*S*)-mandelonitrile with *Hb*HNL immobilised on nano carriers

bilised enzyme and the amount of carrier corresponded to an enzyme concentration

of 7.13 $mg\,L^{-1}$ of the stock solution. The reaction time were 20 minutes and the same sampling procedure as for the synthesis reaction, cf. chapter A.4.1.

Synthesis of (*S*)-mandelonitrile with *Hb*HNL immobilised on nano carriers in toluene

Also the application of the nano carriers for the stereoselective cleavage and synthesis of mandelonitrile in toluene was tested. The organic solvent has been saturated with 0.05 $mol\,L^{-1}$ citrate-phosphate buffer, pH 5.0. The nano carrier has been washed three times with distilled water and tried at 60°C. 10 mg carrier has been suspended in 1 ml saturated solvent containing 25 $mmol\,L^{-1}$ (*S*)-mandelonitrile. The glass reaction vessels were shaken and the reaction progress were followed for 120 min taking 50 μl samples on regular basis. The samples were acetylated according to the method described in chapter A.2.3. During acetylation the particles sedimented and just before the GC measurement the supernatant was transferred into new vials. Then the concentrations of the benzaldehyde and mandelonitrile were determined by gas chromatographic measurement.

A.4.2 Immobilisation of the *Hb*HNL on Sepabeads

The immobilisation of the *Hb*HNL on the carriers was done according to the manual and the immobilisation was performed in 50 ml Schott flasks.

The enzyme stock solution were diluted with the corresponding phosphate buffer (EC-EP: 1.25 $mol\,L^{-1}$, pH 7.0; EC-HFA, EC-EA and EC-HA: 20 $mmol\,L^{-1}$, pH 8.00; EC-BU: 5 $mmol\,L^{-1}$, pH 7.0) and to 1 g carriers 4 ml of the diluted enzyme solution was added. The amount of enzyme were calculated to 300 $U\,g_{carrier}$ according to the manual.

Sepabeads EC-EA and EC-HA were activated adding 4 ml glutardialdehyde 2% solution diluted in the corresponding buffer to 1 g carrier. After adjusting the pH to 8 the suspension was agitated at 300 rpm on a rotary shaker for one hour. Afterwards the supernatant were eliminated and the resin rinsed with water.

For immobilisation the enzyme solution were added to the (activated) carriers, agitated at 300 rpm. The immobilisation were processed for up to 72 hours depending on the type of carrier at room temperature and +4°C, respectively. After incubation the supernatant was removed and the resin rinsed with water. For the application in organic solvent the carrier were freeze dried for 16 hours.

Immobilisation of Bovine Serum Albumin on Sepabeads

To determine the catalytic efficiency for cleaving the racemic mandelonitrile of the carriers an unspecific non active enzyme solution was immobilised on the carrier. The functional groups for binding were blocked by binding Bovine serum albumin (BSA)

to the carrier. As result just the material for the polymeric carrier could influence the reaction catalytically. The amount of BSA was equal to the amount of immobilised *Hb*HNL. The Immobilisation was done as described previously in chapter A.4.2.

A.4.3 Immobilisation of the *Hb*HNL on celite

The enzyme stock solution was sterile filtered to remove precipitated enzyme and solids, because they would block the small channels of the carrier. The solution has been diluted to the corresponding concentration with a 0.05 $mmol\,L^{-1}$ citrate phosphate buffer, pH 5.0. The pH value of the dilution was adjusted to pH 5.0 with a citric acid solution. For immobilisation 2 ml enzyme solution were added to 1 g celite. The ratios were chosen so that the celite could be suspended in the liquid, but the liquid volume was as low as possible. After mixing of the solution for several minutes the solution was placed in the freezer for at least 1 hour until the liquid was frozen. Then the carrier were freeze dried for 16 hours.

A.4.4 Immobilisation of the *Hb*HNL on porous glass beads

For immobilisation a procedure for the immobilisation of cells was adapted published by Shiver-Lake et al. 2002 [340]. The glass beads were acid washed by immersion in HCl/MeOH (1:1) for 30 min, then rinsed thoroughly with water until the pH was neutral. Next the beads were incubated in concentrated H_2SO_4 for 30 min. Again, the beads were rinsed thoroughly with water to a neutral pH and dried over night at 60°C.

The functionalisation with 3-aminopropyltriethoxy silane, shortly APTS, was accomplished by giving a 8% solution APTS in anhydrous toluene to the beads. This was mixed on a shaker overnight. Next the beads were rinsed with 96% ethanol and washed with water. The aminosilane treated beads were placed in a solution containing 12.5% glutaraldehyde in water for 2 h with gentle agitation followed by several rinse cycle with water.

The enzyme solution was diluted with 0.05 $mmol\,L^{-1}$ citrate phosphate buffer to 600 $U\,g^{-1}_{carrier}$ and 5 ml were added to 2 g carrier. After incubation over night at 4°C the unbound enzyme was removed washing the carrier repeatedly with water. The carrier was freeze dried over night and until use stored at 4°C.

B Appendix: Program codes

B.1 The liquid handling robot procedure: program code

```
No.  Code                      Comment
1    Rack code 0               initialisation
2    a= 0
3    a1= 0
4    a2= 0
5    a3= 0
6    a4= 0
7    a5= 0
8    a6= 0
9    a7= 0
10   a8= 0
11   a9= 0
12   a10= 0
13   a11= 0
14   a12= 0
15   a13= 0
16   a14= 0
17   b3= 10                    volume air bubble
18   input b1/0/1/5            input:  no.  of parallel reactions
     No.  Reaction
19   c8= 450                   time lag of parallel reactions
20   c1= b1*c8                 time lag between samples of of
                               parallel reactions
21   input b8/1/1/7            input:  no.  of samples for each
                               reaction
     No.  Sample
22   input b9/40/c1            input:  time lag between samples for
                               each reaction
     Sample Time
23   input a19/23/0/1500       input:  reaction volumes
     Reaction Volume
24   input a/33/0/400          input:  first reaction:  volume of
                               catalyst solution
     Volume A1
25   input a1/34/0/400         input:  first reaction:  volume of
                               reactant B
     Volume B1
26   input a2/35/0/400         input:  first reaction:  volume of
                               reactant C
     Volume C1
27   c4= a+a1+a2
28   if c4>a19                 volume consistency check:  reactor
29   home                      program termination
30   c4= a+a1+a2+4*b3
31   if c4>500                 volume consistency check:  dilutor
32   home                      program termination
33   if b1>1
34   input a3/33/0/400         input:  second reaction:  volume of
                               catalyst solution
     Volume A2
35   if b1>1
36   input a4/34/0/400         input:  second reacting:  volume of
                               reactant B
     Volume B2
37   if b1>1
38   input a5/35/0/400         input:  second reaction:  volume of
                               reactant C
     Volume C2
39   c4= a3+a4+a5
```

```
40   if c4>a19              volume consistency check:  reactor
41   home                   program termination
42   c4= a3+a4+a5+4*b3
43   if c4>500              volume consistency check:  dilutor
44   home                   program termination
45   if b1>2
46   input a6/33/0/400      input:  third reaction:  volume of
                            catalyst solution
     Volume A3
47   if b1>2
48   input a7/34/0/400      input:  third reacting:  volume of
                            reactant B
     Volume B3
49   if b1>2
50   input a8/35/0/400      input:  third reacting:  volume of
                            reactant C
     Volume C3
51   c4= a6+a7+a8
52   if c4>a19              volume consistency check:  reactor
53   home                   program termination
54   c4= a6+a7+a8+4*b3
55   if c4>500              Abfrage, da Spritzenvolumen limitierend
56   home                   program termination
57   if b1>3
58   input a9/33/0/400      input:  fourth reaction:  volume of
                            catalyst solution
     Volume A4
59   if b1>3
60   input a10/34/0/400     input:  fourth reaction:  volume of
                            reactant B
     Volume B4
61   if b1>3
62   input a11/35/0/400     input:  fourt reaction:  volume of
                            reactant C
     Volume C4
63   c4= a9+a10+a11
64   if c4>a19              volume consistency check:  reactor
65   home                   program termination
66   c4= a9+a10+a11+4*b3
67   if c4>500              volume consistency check:  dilutor
68   home                   program termination
69   if b1>4
70   input a12/33/0/400     input:  fifth reaction:  volume of
                            catalyst solution
     Volume A5
71   if b1>4
72   input a13/34/0/400     input:  fifth reacting:  volume of
                            reactant B
     Volume B5
73   if b1>4
74   input a14/35/0/400     input:  fifth reaction:  volume of
                            reactant C
     Volume C5
75   c4= a12+a13+a14
76   if c4>a19              volume consistency check:  reactor
77   home                   program termination
78   c4= a12+a13+a14+4*b3
79   if c4>500              volume consistency check:  dilutor
80   home                   program termination
81   b4= 16                 configuration row storage tank catalyst
                            solution, reactants
82   b5= 15                 configuration row reactors
83   b6= 300                configuration dilution volume
84   b7= 20                 configuration sample volume
85   b10= 100               configuration volume for analysis
86   c1= 3                  configuration no.  washing circles
87   rinse                  washing position needle
88   for c2=1/c1            washing start
89   Print c2/14
90   Disp 0/500/9
91   next c2                washing end
92   for c3=1/b1            loop filling reactors
93   print c3/14
94   wait                   start timer
```

```
95   c4=a19-a-a1-a2          solvent volume
96   tube b5/c3              reaction vessel
97   height 3                position in z-plane
98   Disp 0/c4/2             addition solvent
99   height                  highest position z-plane
100  aspir 0/b3/1            air bubble for liquid separation in tubing
101  aspir 0/b3/1            air bubble for liquid separation in tubing
102  aspir 0/b3/1            air bubble for liquid separation in tubing
103  tube b4/1               catalyst storage vessel
104  aspir 0/a/1             aspirate catalyst
105  height 28               position in z-plane (tip in gas-phase in
                             the storage vessel)
106  aspir 0/b3/1            air bubble for liquid separation in tubing
107  tube b4/2               storage vessel reactant B
108  height 0                lowest position z-plane
109  aspir 0/a1/0            aspirate reactant B
110  height 28               position in z-plane (tip in gas-phase in
                             the storage vessel)
111  aspir 0/b3/1            air bubble for liquid separation in tubing
112  tube b4/3               storage vessel reactant C
113  height 0                lowest position z-plane
114  aspir 0/a2/0            aspirate reactant C
115  height 28               position in z-plane (tip in gas-phase in
                             the storage vessel)
116  aspir 0/b3/1            air bubble for liquid separation in tubing
117  tube b5/c3              reaction vessel n
118  height 3                position in z-plane (micro insert)
119  c4=a+b3+a1+b3+a2+b3+b3
120  disp 0/c4/1             filling reactor
121  aspir 0/100/4           mixing
122  disp 0/100/4            mixing
123  rinse                   washing position needle
124  disp 0/500/9            washing needle
125  c4=b5-1
126  tube c4/c3              position dilution vial
127  height 8                position in z-plane (micro insert)
128  disp 0/b6/2             dispense solvent
129  height
130  aspir 0/b3/1            air bubble for liquid separation in tubing
131  aspir 0/b3/1            air bubble for liquid separation in tubing
132  tube b5/c3              position reaction vessel
133  height 3                position in z-plane (micro insert)
134  aspir 0/b7/1            aspirate sample
135  height 28               position in z-plane (tip in gas-phase in
                             the reactor)
136  aspir 0/b3/1            air bubble for liquid separation in tubing
137  tube c4/c3              position dilution vial
138  height 3                position in z-plane (micro insert)
139  disp 0/b7/1             dispense sample
140  disp 0/b3/2             dispense air bubble
141  disp 0/b3/2             dispense air bubble
142  height
143  aspir 0/b3/1            air bubble for liquid separation in tubing
144  aspir 0/b3/1            air bubble for liquid separation in tubing
145  height 0                lowest position z-plane
146  aspir 0/150/3           mixing dilution
147  disp 0/150/4            mixing dilution
148  aspir 0/b10/1           aspirate diluted sample
149  height 28               position in z-plane (tip in gas-phase in
                             the dilution vessel)
150  aspir 0/b3/1            air bubble for liquid separation in tubing
151  c4=b5-8
152  tube c4/c3              position diluted sample for analysis
153  height 3                position in z-plane (micro insert)
154  disp 0/b10/1            dispense diluted sample
155  disp 0/b3/2             dispense air bubble
156  Disp 0/b3/2             dispense air bubble
157  height
158  aspir 0/b3/1            air bubble for liquid separation in tubing
159  aspir 0/b3/1            air bubble for liquid separation in tubing
160  height 3
161  aspir 0/100/3           mixing
162  height 6
```

```
163  disp 0/100/4            mixing
164  disp 0/b3/3             dispense air bubble
165  rinse                   washing position needle
166  for c2=1/c1             washing start
167  Disp 0/500/9
168  next c2                 washing end
169  if c3=1                 hand over new variables for next reactor
170  a=a3
171  if c3=1
172  a1=a4
173  if c3=1
174  a2=a5
175  if c3=2
176  a=a6
177  if c3=2
178  a1=a7
179  if c3=2
180  a2=a8
181  if c3=3
182  a=a9
183  if c3=3
184  a1=a10
185  if c3=3
186  a2=a11
187  if c3=4
188  a=a12
189  if c3=4
190  a1=a13
191  if c3=4
192  a2=a14
193  tube b4/4               waiting position
194  height
195  wait c8                 pause till next reactor to keep definite times
196  next c3                 end loop filling reactors
197  if b8<2
198  home                    program termination
199  for c4=2/b8             start loop samples
200  print c4/14
201  wait                    start timer
202  c5=b9-c8*b1             calculation of sample time lag
203  print c5
204  wait c5                 waiting sample time lag
205  for c3=1/b1             start sampling
206  print c3/14
207  wait                    start timer
208  c5=b5-c4
209  tube c5/c3              position dilution vessel
210  height 8
211  disp 0/b6/2             dispense solvent
212  height
213  aspir 0/b3/1            air bubble for liquid separation in tubing
214  aspir 0/b3/1            air bubble for liquid separation in tubing
215  tube b5/c3              position reaction vessel
216  aspir 0/b7/1            aspirate sample
217  height 28               position in z-plane (tip in gas-phase in
                             the reactor)
218  aspir 0/b3/1            air bubble for liquid separation in tubing
219  tube c5/c3              position dilution vial
220  height 3                position in z-plane (micro insert)
221  disp 0/b7/1             dispense sample
222  disp 0/b3/2             dispense air bubble
223  disp 0/b3/2             dispense air bubble
224  height
225  aspir 0/b3/3            air bubble for liquid separation in tubing
226  aspir 0/b3/3            air bubble for liquid separation in tubing
227  height 0                lowest position z-plane
228  aspir 0/150/3           mixing
229  disp 0/150/4            mixing
230  aspir 0/b10/1           aspirate diluted sample
231  height 28               position in z-plane (tip in gas-phase in
                             the dilution vessel)
232  aspir 0/b3/1            air bubble for liquid separation in tubing
233  c5=b5-7-c4
```

```
234  tube c5/c3              position diluted sample for analysis
235  height 3                position in z-plane (micro insert)
236  disp 0/b10/1            dispense diluted sample
237  disp 0/b3/2             dispense air bubble
238  disp 0/b3/2             dispense air bubble
239  height
240  aspir 0/b3/1            air bubble for liquid separation in tubing
241  aspir 0/b3/1            air bubble for liquid separation in tubing
242  height 3
243  aspir 0/100/3           mixing
244  height 6
245  disp 0/100/5            mixing
246  disp 0/b3/3             mixing
247  rinse                   washing position needle
248  for c2=1/c1             start washing
249  Disp 0/500/9
250  next c2                 end washing
251  tube b4/4               waiting position
252  height
253  wait c8
254  next c3                 start sampling
255  next c4                 start loop samples
256  home                    program termination
```

B.2 How to join kinetics and the calibration parameters: example code

B.2.1 Main program

```
%-------------------------------------------------------
% Author: Sebastian Briechle
% Date: 12.06.2010
% Titel: Joining determination of kinetic and calibration
%
% Main Program
%
% Dependencies: Genetic Algorithm and Direct Search Toolboox
%               Optimization Toolbox
%               Statistics Toolbox
%               The N-way Toolbox for MATLAB Rasmus Bro & Claus Andersson
%               Copenhagen University, DK-1958 Frederiksberg, Denmark,
%               rb@life.ku.dk (http://www.models.life.ku.dk/nwaytoolbox/)
%               For speed reasons: use N-way functions without outputs!
%-------------------------------------------------------

clear all
global Parameter_Chem DataSet SimFun Fac

load('./DataSet'); %Processed Data

%--Structure
%
%    DataSet(i)__             i Number of experiments
%                |
%                |_Time       Vector sampling times
%                |_Spectra    Maxtrix Absorption at sampling times
%                |
%                |_c_BA_0     Theoretical initial concentration Benzaldehyde
%                |_c_HCN_0    Theoretical initial concentration HCN
%                |_c_S_MN_0   Theoretical initial concentration ...
%                                        ... (S)-Mandelonitrile
%                |_c_R_MN_0   Theoretical initial concentration ...
%                                        ... (R)-Mandelonitrile
%                |_c_E_0      Theoretical enzyme concentration
%                |_c_BA_0_c   Corrected initial concentration ...
%                                        ... Benzaldehyde
%                |_c_HCN_0_c  Corrected initial concentration ...
%                                        ... HCN
%                |_c_S_MN_0_c Corrected initial concentration ...
%                                        ... (S)-Mandelonitrile
%                |_c_R_MN_0_c Corrected initial concentration ...
%                                        ... (R)-Mandelonitrile
%
%-------Parameters-noncatalysed reaction

k11= 1.163e-05; %[L/s mmol]
k10= 2.063e-05; %[1/s]

Parameter_Chem=[k11 k10];

%--Simulation function kinetic model
SimFun=@ordered_uni_bi;

%--Options Genetic Allgorithm

PopulationSize=120;
Generations=10;
NumberInteration=5;

%%Fitness function
fitnessFunction = @lse_res_ga;

%%Number of Variables
nvars =7 ;
```

```
%%Linear inequality constraints
Aineq = [];
Bineq = [];
%%Linear equality constraints
Aeq = [];
Beq = [];
%%Bounds
UB =[100 2000 100   10   40   40 ];
LB =[10   10  1   0.001 0.001 0.001];
deltaL=(UB+LB)./2;
UB_anf=UB;
LB_anf=LB;
%%Nonlinear constraints
nonlconFunction = [];
%%Start with default options
options = gaoptimset;
%%Modify some parameters
options = gaoptimset(options,'MutationFcn' ,{@mutationadaptfeasible});
options = gaoptimset(options,'PopInitRange' ,[ LB ;  UB ]);
options = gaoptimset(options,'PopulationSize' ,PopulationSize*2);
options = gaoptimset(options,'Generations' ,Generations*1);
options = gaoptimset(options,'StallTimeLimit',inf);
options = gaoptimset(options,'StallGenLimit' ,inf);
options = gaoptimset(options,'Display' ,'iter');
options = gaoptimset(options,'Vectorized' ,'on');
%-------------------------------------
Fac=5; %principal components
%---------------------------------

%-------Calibration with initial Concentrations
cBA_0=[];
Numerator=1;
for i=1:length(DataSet)
    c_BA_0(Numerator)=DataSet(i).c_BA_0;
    Spectra_c_BA_0(Numerator,:)=DataSet(i).Spectra(1:1,1:end);
    Numerator=Numerator+1;
end;
CenterX=[1 0];
ScaleX=[0 0];
CenterY=[1 0];
ScaleY=[0 0 ];
%-- Centering and Scaling
[Xnew,mX,sX]=nprocess(Spectra_c_BA_0,CenterX,ScaleX);
[Ynew,mY,sY]=nprocess(c_BA_0',CenterY, ScaleY);
%---nPLS- Calibration
[Xfactors,Yfactors,Core,B,ypred] = npls(Xnew,Ynew,Fac);
cut_start=1;
Numerator=1;
%---correction of initial concentrations
for i=1:length(DataSet)
     DataSet(i).ypred=nprocess(ypred(Numerator,Fac),CenterY,ScaleY,...
                               mY,sY,-1);
     %Prediciton of concentration by nPLS-model
    if DataSet(i).c_S_MN_0==0 & DataSet(i).c_R_MN_0==0
          DataSet(i).c_R_MN_0_c=0;
          DataSet(i).c_S_MN_0_c=0;
    else
```

```
        if DataSet(i).c_S_MN_c==0 & DataSet(i).c_R_MN~=0
          DataSet(i).c_R_MN_0_c=DataSet(i).c_R_MN_0- ...
                              (DataSet(i).ypred(1)-DataSet(i).c_BA_0);
          DataSet(i).c_S_MN_0_c=0;
           if DataSet(i).c_R_MN_0_c<0
              DataSet(i).c_R_MN_0_c=0;
           end;
        else
                DataSet(i).c_S_MN_0_c= ...
            if DataSet(i).c_S_MN_0~=0 & DataSet(i).c_R_MN_0==0
                   DataSet(i).c_S_MN_0-(DataSet(i).ypred(1)-...
                                        DataSet(i).c_BA_0);
               DataSet(i).c_R_MN_0_c=0;
             if DataSet(i).c_S_MN_0<0
               DataSet(i).c_S_MN_0=0;
             end;
         end;
      end;
           DataSet(i).cBA_0_c=DataSet(i).ypred(1);
      end;
    Numerator=Numerator+1;
end;
%----first Optimisation GA
[X,FVAL,REASON,OUTPUT,POPULATION,SCORES]= ...
ga(fitnessFunction,nvars,Aineq,Bineq,Aeq,Beq,LB,UB,...
   nonlconFunction,options);
Parameter_Enzym=X
[DataSet]=approx_c0_pls_example(DataSet,SimFun,Parameter_Enzym,...
                                Parameter_Chem,Fac);
X_1=X;
for k=1:NumberInteration
%
%-------reduction search space
%
    fend=0.5;
    b=5/NumberInteration
    f=1-(1-fend)*(1-exp(-(k-1)*b))
    UB =X+deltaL*f;
    LB =X-deltaL*f;
        for i=1:length(LB)
            if UB(i)>UB_anf(i)
            UB(i)=UB_anf(i);
            end;
            if LB(i)<LB_anf(i)
            LB(i)=LB_anf(i);
            end;
        end;
    UB
    LB
    options = gaoptimset(options,'PopulationSize' ,PopulationSize);
    options = gaoptimset(options,'Generations' ,Generations);
    options = gaoptimset(options,'PopInitRange' ,[ LB ;  UB ]);
    options = gaoptimset(options,'InitialPopulation' ,[X_1]);
    options = gaoptimset(options,'InitialScores' ,[]);
    [X_1,FVAL_1,REASON,OUTPUT,POPULATION,SCORES] = ...
    ga(fitnessFunction,nvars,Aineq,Bineq,Aeq,Beq,LB,UB,...
       nonlconFunction,options);
```

```
    PopulationSize_a=PopulationSize;
    gen=1;
    while FVAL_1 >=FVAL
        PopulationSize_a=PopulationSize_a+20
        options = gaoptimset(options,'Generations',Generations+1*gen);
        options = gaoptimset(options,'PopulationSize' ,PopulationSize_a);
        options = gaoptimset(options,'PopInitRange' ,[ LB ;  UB ]);
        options = gaoptimset(options,'InitialPopulation' ,[X_1]);
        options = gaoptimset(options,'InitialScores' ,[]);
        [X_1,FVAL_1,REASON,OUTPUT,POPULATION,SCORES] = ...
        ga(fitnessFunction,nvars,Aineq,Bineq,Aeq,Beq,LB,UB,...
           nonlconFunction,options);
        gen=gen+1
        if gen>6
             break
        end;
    end;
    if FVAL<FVAL_1;
        disp('No improvement in this loop')
    else
        disp('Parameter_Enzym')
        FVAL=FVAL_1;
        X=X_1
        Parameter_Enzym=X
        [DataSet]=approx_c0_pls_example(DataSet,SimFun,Parameter_Enzym,...
                                        Parameter_Chem,Fac);
    end;
end;
X
FVAL
REASON
%---------Refine Optimisation (trust region algorithm)
x0=X
LB=0.3*X;
UB=1.3*X;
fitnessFunction=@lse_res_lsqnonlin;
optslsqnonlin=optimset('TolFun',1e-10,'TolX',1e-10,...
                       'MaxFunEvals',100000,'MaxIter',100000);
[optparam,resnorm,residual,EXITFLAG,OUTPUT,LAMBDA,Jacobian]= ...
lsqnonlin(fitnessFunction,x0,LB,UB,optslsqnonlin);
EXITFLAG
optparam
resnorm
%---------Confidential intervalls
cip = nlparci(optparam,residual,'jacobian');
deltaoptparam=cip(:,2)-optparam'
```

B.2.2 Subroutine: calculation of initial concentrations

```
%-------------------------------------------------------
% Author: Sebastian Briechle
% Date: 12.06.2010
% Titel: Joining determination of kinetic and calibration
%
% Sub routing: calculation of initial concentrations
%
% Dependencies: Genetic Algorithm and Direct Search Toolboox
```

```
%               Optimization Toolbox
%               Statistics Toolbox
%               The N-way Toolbox for MATLAB Rasmus Bro & Claus Andersson
%               Copenhagen University, DK-1958 Frederiksberg, Denmark,
%               rb@life.ku.dk (http://www.models.life.ku.dk/nwaytoolbox/)
%               For speed reasons: use N-way functions without outputs!
%-----------------------------------------------------

function [DataSet]=approx_c0_pls(DataSet,SimFun,Parameter_Enzym,...
                                 Parameter_Chem,Fac)

spectra=[];
odesolv=[];

CenterX=[1 0];
ScaleX=[0 0];
CenterY=[1 0];
ScaleY=[0 0 ];

  for i=1:length(DataSet)
    t=[];
    odesolv_a=[];

    y_0=[DataSet(i).c_BA_0_c DataSet(i).c_HCN_0...
         DataSet(i).c_S_MN_0_c DataSet(i).c_R_MN_0_c];
    t,odesolv_i]=ode45(SimFun,DataSet(i).Time,y_0,[],...
              Parameter_Enzym,Parameter_Chem,DataSet(i).cE);

    spectra=[spectra; DataSet(i).Spectra];
    odesolv=[odesolv;odesolv_i];

  end;

[Xnew,mX,sX]=nprocess(spectra,CenterY, ScaleY);
[Ynew,mY,sY]=nprocess([odesolv(:,1)],CenterX, ScaleX);
[Xfactors,Yfactors,Core,B,ypred] = npls(Xnew,Ynew,Fac);

%---correction of initial concentrations

for i=1:length(DataSet)

DataSet(i).ypred=nprocess(ypred(Numerator,Fac),CenterY,ScaleY,...
                                  mY,sY,-1);
        %Prediciton of concentration by nPLS-model

    if DataSet(i).c_S_MN_0==0 & DataSet(i).c_R_MN_0==0
          DataSet(i).c_R_MN_0_c=0;
          DataSet(i).c_S_MN_0_c=0;
    else
        if DataSet(i).c_S_MN_c==0 & DataSet(i).c_R_MN~=0

          DataSet(i).c_R_MN_0_c=DataSet(i).c_R_MN_0-...
                               (DataSet(i).ypred(1)-DataSet(i).c_BA_0);
          DataSet(i).c_S_MN_0_c=0;

           if DataSet(i).c_R_MN_0_c<0
              DataSet(i).c_R_MN_0_c=0;
           end;

        else
            if DataSet(i).c_S_MN_0~=0 & DataSet(i).c_R_MN_0==0

                DataSet(i).c_S_MN_0_c=DataSet(i).c_S_MN_0-...
                                      (DataSet(i).ypred(1)-DataSet(i).c_BA_0);
                DataSet(i).c_R_MN_0_c=0;

             if DataSet(i).c_S_MN_0<0
               DataSet(i).c_S_MN_0=0;
             end;

   end;
      end;

          DataSet(i).cBA_0_c=DataSet(i).ypred(1);
```

```
      end;
    Numerator=Numerator+1;
end;
```

B.2.3 Subroutine: fitness function GA

```
%-----------------------------------------------------
% Author: Sebastian Briechle
% Date: 12.06.2010
% Titel: Joining determination of kinetic and calibration
%
% Sub routing: fitnessFunction GA
%
% Dependencies: Genetic Algorithm and Direct Search Toolboox
%               Optimization Toolbox
%               Statistics Toolbox
%               The N-way Toolbox for MATLAB Rasmus Bro & Claus Andersson
%               Copenhagen University, DK-1958 Frederiksberg, Denmark,
%               rb@life.ku.dk (http://www.models.life.ku.dk/nwaytoolbox/)
%               For speed reasons: use N-way functions without outputs!
%-----------------------------------------------------
function residual=lse_res_ga(Parameter_Enzym)

global Parameter_Chem DataSet SimFun Fac

CenterX=[1 0];
ScaleX=[0 0];
CenterY=[1 0];
ScaleY=[0 0];

residual=[];

[n]=size(Parameter_Enzym,1);

for j=1:n ;

vmax_Spalt=Parameter_Enzym(j,1);
vmax_Synth=Parameter_Enzym(j,2);
KmHCN=Parameter_Enzym(j,3);
KmBA=Parameter_Enzym(j,4);
KmS_MN=Parameter_Enzym(j,5);
KiBA=Parameter_Enzym(j,6);

KiS_MN=KmS_MN/(1+vmax_Spalt/vmax_Synth*(1-KmBA/KiBA));
KiHCN=KiBA*KmHCN*KiS_MN/(KmS_MN*KmBA);

residual_a=[];
Xnew=[];
Ynew=[];
spectra=[];
odesolv=[];
y_0_all=[];
size_odesolve=[];

if KiS_MN>0 % excluding unrealistic parameters

    for i=1:length(DataSet)

        t=[];
        odesolv_a=[];

        y_0=[DataSet(i).cBA_0 DataSet(i).cHCN ...
             DataSet(i).c_S_MN_0 DataSet(i).c_R_MN_0];

        options=odeset('RelTol',0.1);
        [t,odesolv_a]=ode113(SimFun,DataSet(i).Time,y_0,options,...
                             Parameter_Enzym(j,:), Parameter_Chem,DataSet(i).cE);

        spectra=[spectra; DataSet(i).Spectra_Start_Splitt_Reduction];
        odesolv=[odesolv;odesolv_a];
        y_0_all=[y_0_all;y_0];
        size_odesolve=[size_odesolve; size(odesolv_a)];
```

```
    end;
    [Xnew,mX,sX]=nprocess(spectra,CenterY, ScaleY);
    [Ynew,mY,sY]=nprocess([odesolv(:,1) odesolv(:,3)+odesolv(:,4)],...
                          CenterX, ScaleX);
    [Xfactors,Yfactors,Core,B,ypred] = npls(Xnew,Ynew,Fac);
        if Fac<2;
            diff_1=(ypred(:,1)-Ynew(:,1));
            diff_2=(ypred(:,2)-Ynew(:,2));
        else;
            diff_1=(ypred(:,1,Fac)-Ynew(:,1));
            diff_2=(ypred(:,2,Fac)-Ynew(:,2));
        end;
    n=1;
    o=0;
        for m=1:size(size_odesolve,1)
            o=o+size_odesolve(m,1) ;
            diff_norm_1(n:o)= diff_1(n:o)./(y_0_all(m,1)+y_0_all(m,3));
            diff_norm_2(n:o)= diff_2(n:o)./(y_0_all(m,1)+y_0_all(m,3));
            n=o+1;
        end;
 residual=[residual;sqrt(sum((diff_norm_1).^2))+sqrt(sum((diff_norm_2).^2))];
else
    residual=[residual;999999999999999]; % excluding unrealistic parameters
end;
end;
```

B.2.4 Subroutine: fitness function lsqnonlin

```
%-------------------------------------------------------
% Author: Sebastian Briechle
% Date: 12.06.2010
% Titel: Joining determination of kinetic and calibration
%
% Sub routing: fitnessFunction lsqnonlin
%
% Dependencies: Genetic Algorithm and Direct Search Toolboox
%               Optimization Toolbox
%               Statistics Toolbox
%               The N-way Toolbox for MATLAB Rasmus Bro & Claus Andersson
%               Copenhagen University, DK-1958 Frederiksberg, Denmark,
%               rb@life.ku.dk (http://www.models.life.ku.dk/nwaytoolbox/)
%               For speed reasons: use N-way functions without outputs!
%-------------------------------------------------------

function residual=lse_res_lsqnonlin(Parameter_Enzym)

global Parameter_Chem DataSet SimFun Fac

CenterX=[1 0];
ScaleX=[0 0];
CenterY=[1 0];
ScaleY=[0 0];

residual=[];

[n]=size(Parameter_Enzym,1);

for j=1:n ;

  residual_a=[];
  Xnew=[];
  Ynew=[];
  spectra=[];
  odesolv=[];
  y_0_all=[];
```

```
  size_odesolve=[];
    for i=1:length(DataSet)
        t=[];
        odesolv_a=[];
        y_0=[DataSet(i).cBA_0 DataSet(i).cHCN ...
             DataSet(i).c_S_MN_0 DataSet(i).c_R_MN_0];
        options=odeset('RelTol',0.1);
        [t,odesolv_a]=ode113(SimFun,DataSet(i).Time,y_0,options,...
                      Parameter_Enzym(j,:), Parameter_Chem,DataSet(i).cE);
        spectra=[spectra; DataSet(i).Spectra_Start_Splitt_Reduction];
        odesolv=[odesolv;odesolv_a];
        y_0_all=[y_0_all;y_0];
        size_odesolve=[size_odesolve; size(odesolv_a)];
    end;
    [Xnew,mX,sX]=nprocess(spectra,CenterY, ScaleY);
    [Ynew,mY,sY]=nprocess([odesolv(:,1) odesolv(:,3)+odesolv(:,4)],...
                          CenterX, ScaleX);
    [Xfactors,Yfactors,Core,B,ypred] = npls(Xnew,Ynew,Fac);
        if Fac<2;
            diff_1=(ypred(:,1)-Ynew(:,1));
            diff_2=(ypred(:,2)-Ynew(:,2));
        else;
            diff_1=(ypred(:,1,Fac)-Ynew(:,1));
            diff_2=(ypred(:,2,Fac)-Ynew(:,2));
        end;
     n=1;
     o=0;
        for m=1:size(size_odesolve,1)
            o=o+size_odesolve(m,1) ;
            diff_norm_1(n:o)= diff_1(n:o)./(y_0_all(m,1)+y_0_all(m,3));
            diff_norm_2(n:o)= diff_2(n:o)./(y_0_all(m,1)+y_0_all(m,3));
            n=o+1;
        end;
      residual=[residual; (diff_norm_1).^2 ; (diff_norm_2).^2];
end;
```

B.2.5 Subroutine: kinetic model

```
function dy = ordered_uni_bi(t,y,Parameter_Enzym,Parameter_Chem,cE)
dy = zeros(4,1);
%Enzymatic reaction
vmax_Spalt=Parameter_Enzym(1);
vmax_Synth=Parameter_Enzym(2);
KmHCN=Parameter_Enzym(3);
KmBA=Parameter_Enzym(4);
KmS_MN=Parameter_Enzym(5);
KiBA=Parameter_Enzym(6);
KiS_MN=KmS_MN/(1+vmax_Spalt/vmax_Synth*(1-KmBA/KiBA));
KiHCN=KiBA*KmHCN*KiS_MN/(KmS_MN*KmBA);
%Chemical reaction
k11=Parameter_Chem(1);
k10=Parameter_Chem(2);
cBA = y(1);
cHCN =y(2);
cS_MN = y(3);
cR_MN = y(4);
```

```
v=vmax_Synth*(vmax_Spalt*KmHCN*KiBA*cS_MN/(vmax_Synth*KmS_MN)-...
              cBA*cHCN)/(KmHCN*KiBA + KmBA/KiS_MN*KiHCN*cS_MN +...
              KmBA*cHCN + KmHCN*cBA + cBA*cHCN + KmBA/KiS_MN*cHCN*cS_MN);

dy(1) = v*cE + k10*cS_MN + k10*cR_MN - k11*cBA*cHCN; %Benzaldehyd
dy(2) = v*cE + k10*cS_MN + k10*cR_MN - k11*cBA*cHCN; %HCN
dy(3) = -v*cE- k10*cS_MN + 0.5*k11*cBA*cHCN;  %S-Mandelonitrile
dy(4) = -k10*cR_MN + 0.5*k11*cBA*cHCN; %R-Mandelonitrile
```

C Appendix: Batch protocol HCN production

Bach-Protokoll für die Blausäureproduktion

Erstellt von Sebastian Briechle
Seiten: 7
Version: 1.4

Person:_____ Versuch:_____
Datum:_____

C.1 Präambel

Die Herstellung von Blausäure (HCN) birgt ein hohes Potential an Risiken für alle sich im Einzugsbereich befindlichen Personen. Daher sollten alle Arbeiten zur Herstellung und Handhabung von HCN mit größter Sorgfalt und Vorsicht ausgeführt werden. Alle Personen die sich im Einzugsbereich befinden, sind vor den Arbeiten zu informieren und Vorkehrungen sind zu treffen, dass Außenstehende nicht in den Gefahrenbereich eintreten. Dieses Batch-Protokoll soll dazu dienen, zum einen einen sicheren Ablauf der Arbeiten zu gewährleisten und zum anderen aller Arbeiten mit HCN zu dokumentieren. Alle Arbeitsschritte sind zu dokumentieren so wie alle Beobachtungen.

Präambel gelesen:_____

C.2 Vorkehrungen

C.2.1 Gasversorgung

Vor dem Beginn der Arbeiten ist die Versorgung mit Stickstoff und Druckluft zu überprüfen.

C.2.2 Stickstoff

Stickstoff, der Flaschendruck muss größer 70 bar sein

	Flaschendruck [bar]	Signatur
Flasche 1:	_____	_____
Flasche 2:	_____	_____

C.2.3 Abzug

				Signatur
Optische Kontrolle des Abzuges				
und der näheren Umgebung:				_____
Abluftüberwachung eingeschaltet:				_____
Thermostat Füllstand:				_____
Thermostat eingeschaltet:	_____Uhr	_____Datum		_____

C.3 Vorbereitung

C.3.1 Warnschilder

Die *HCN* Warnschilder müssen vor dem Beginn der Arbeiten mit *HCN* klar von aussen sichtbar an den Eingangstüren zum Labor angebracht werden.

	Signatur
Warnschilder aufgehängt:	_____

C.3.2 Trockenturm

	Signatur
Trockenturm befüllt mit $CaCl_2$:	_____

C.3.3 HCN-Vernichtung

Sicherheitsventil

Sicherheitsventil, auffüllen mit

	Signatur
1/3 H_2O_2 siehe Markierungen	_____
2/3 $NaOH$ siehe Markierungen	_____

HCN-Vernichtung

HCN-Vernichtung, auffüllen mit

	Signatur
1/3 H_2O_2 siehe Markierungen	_____
2/3 $NaOH$ siehe Markierungen	_____

C.3.4 Schwefelsäure

Befüllen des Reaktionskolbens

		Signatur
mit 60%iger Schwefelsäure:	_____ml	_____
Badtemperierung anstellen: 80°C	_____°C	_____
Magnetrührer anstellen:		_____

C.3.5 NaCN-Lösung 30%

		Signatur
Eingewogene Masse $NaCN$:	_____g	_____
Eintrag der entnommen Masse $NaCN$ ins $NaCN$-Lagerbuch:	Nr._____	_____
Eingewogene Masse H_2O:	_____g	_____

C.4 Beobachtung durch eine Zweite Person

Alle Arbeitsschritte mit freier HCN oder bei denen freie HCN entstehen kann, sind durch eine zweite, geschulte Person zu überwachen.

		Signatur
Name der Überwachungsperson:	_____	_____

Sgn 1 steht für die Signatur der durchführenden Person
Sgn 2 steht für die beobachtende Person

C.5 Produktionsanlage

	Sgn 1	Sgn 2
Zutropfpumpe kontrollieren und auf 50% einstellen	_____	_____
Drucktest durchgeführt	_____	_____
Kontrolle der Badtemperatur: 80°C_____°C	_____	_____
Kontrolle der Thermostattemperatur: -12.0°C_____ °C	_____	_____
Einstellung des N_2Flow:	_____	_____
Befüllung der Vorlage mit $NaCN$-Lösung	_____	_____

C.6 Produktion

Nach nochmaliger Kontrolle aller Temperaturen, N2flow und Zustand der Anlage kann die Produktion beginnen.

		Sgn 1	Sgn 2
Anschalten der NaCN-Zutropfpumpe:	_____Uhr	_____	_____
Erhöhen der Pumprate auf 100%:	_____Uhr	_____	_____
Erster kondensierter Tropfen *HCN*:	_____Uhr	_____	_____
Ende der Produktion:_____ml *HCN*	_____Uhr	_____	_____

C.7 Postproduktion

	Sgn 1	Sgn 2
Kontrolle der Kühlttemperatur:		
-12.0 °C_____ °C	_____	_____
Abstellen der Wasserbadtemperierung und Rührer:	_____	_____
Absenken des Wasserbades:	_____	_____
Abstellen des N_2flow:	_____	_____

C.8 Durchführung der Versuche

	Sgn 1	Sgn 2
Siehe Laborbuch:_____ Seite.	_____	_____
oder separates Protokoll:_____	_____	_____

C.9 HCN-Vernichtung

	Sgn 1	Sgn 2
Volumen der *HCN* zur Vernichtung: _____ml	_____	_____

C.9.1 Volumen kleiner 2 ml:

Mit N_2 wird die *HCN* in die *HCN*-Vernichtung am Ende der Anlage getrieben

	Sgn 1	Sgn 2
Kühlthermostat abstellen:	_____	_____
Flüssigkeitsstand in der *HCN*-Vernichtung kontrollieren	_____	_____
N_2 vorsichtig öffnen: _____Uhr	_____	_____
Kein *HCN* sichtbar in der Kühlfalle: _____Uhr	_____	_____

Abstellen der N_2 und verschließen	Sgn 1	Sgn 2
der Kühlfalle mit einem Stopfen:	_____	_____

Überprüfen der *CN* Konzentration mit Teststäbchen:	Sgn 1	Sgn 2
Negative:_____ Positiv:_____	_____	_____

Wenn der Test positiv ist:		
H_2O_2 und *NaOH*-Lösung nachfüllen:	_____	_____
Nach 15 min erneuter Test:		
Negative: _____ Positiv:_____	_____	_____

C.9.2 Volumen größer 2 ml:

	Sgn 1	Sgn 2
1L Schottflasche mit H_2O_2: _____ml H_2O_2	_____	_____
und NaOH-Lösung befüllen: _____ml *NaOH*-Lösung	_____	_____
Vorsichtig *HCN* mit einer Spritze aus		
der Kühlfalle in die Schottflache überführen:	_____	_____
!!!Nicht zuschrauben!!!	_____	_____
Nach 15 min Test: Negativ _____ Positiv:_____	_____	_____
Wenn der Test positiv ist:		
H_2O_2 nachfüllen:	_____	_____
Nach 15 min Test: Negativ _____ Positiv:_____	_____	_____
Reste der *HCN* in der Kühlfalle gemäß C.9.1 entsorgen	_____	_____

H2O2 /NaOH-Lösung im Abzug sammeln und Vorschriftsmäßig entsorgen

Abbreviations, symbols and definitions

List of abbreviations

Abbreviation	Meaning
CERC	Chairman of the European Research Councils Chemistry Committees
HCN	hydrogen cyanide
MTBE	Methyl *tert*-butyl ether
HNL	hydroxynitril lyase
*Hb*HNL	hydroxynitril lyase from *Hevea bransiliensis*
*Pa*HNL	hydroxynitril lyase from *Prunus amygdalus*
PCA	principal component analysis
PLS(R)	partial least squares (regression)
EMR	Enzyme Membrane reactor
CMR	Chemzyme Membrane reactor
salen	(*N,N'*-bis(salicylaldehyde)ethylenediamaine)
NMR	Nuclear magnetic resonance spectroscopy
RMSE	root mean square error
UV	ultraviolet range
VIS	visible range
IR	infrared range
FTIR	Fourier transform infrared spectroscopy
HPLC	high performance liquid chromatography
GC	gas chromatography
MLR	Multi linear least squares regression
PCR	Principal component regression
SVD	singular-value decomposition
N-PLS	N-way partial least squares
EP	epoxy
HFA	amino-Epoxy
EA	ethylamine
HA	hexamethylamino
BU	butyl

List of symbols

Symbol	Meaning	Unit
A	Activity	
E_a	activation energy	$[J\,mol^{-1}]$
$\Delta_r H$	enthalpy of reaction	$[J\,mol^{-1}]$
k, v	reaction rate	$[s^{-1}]$
ee	enantiomeric excess	[-]
de	diastereomeric excess	[-]
t	time	[s]
K	equilibrium constant	[-]
k	elementary reaction steps reaction rate coefficients	$[s^{-1}]$ $[L\,mol^{-1}\,s^{-1}]$ $[L^2\,mol^{-2}\,s^{-1}]$
p	partial pressure	$[Pa]$
θ_R	fraction of occupied sites occupied by species R	[-]
RMSE	root mean square error	
r	reaction rate	$[mol\,L^{-1}\,s^{-1}]$
$Re = \frac{\rho \cdot v \cdot L}{\eta}$	Reynolds number	[-]
L	characteristic length	$[m]$
ρ	density	$[kg\,m^{-3}]$
v	flow velocity	$[m\,s^{-1}]$
η	dynamic viscosity	$[kg\,s^{-1}\,m^{-1}]$
n	revolution speed	$[min^{-1}]$
w_r	mean volumetric flow	$[ml\,s^{-1}]$
τ	mean residence time	$[s]$
U	conversion	[-]
I	intensity	[-]
A	absorption	[-]
c_A	concentration of component A	$[molm^{-3}]$
n_P	amount of component P	$[mol]$
$\dot{n}_P$	molar flow of product out of the reactor	$[mol\,s^{-1}]$
V_R	reaction volume	$[m^3]$
$range$	search space	[-]
$parameters$	optimised process parameters of the previous optimisation	[-]
$\Delta range$	specified maximal range of the search space	[-]
f	decline factor; $f \in \mathbb{R}$ and $1 \geq f \geq f_{end}$	[-]
f_∞	end value of the factor f after ∞ iterations	[-]
n	number of iterations; $n \in \mathbb{N}_{>0}$	[-]

b	declining parameter; $b \in \mathbb{R}$ and $b \geq 0$	[-]
$y_{11}...y_{nm}$	dependent variables	e.g. $[mmol\ L^{-1}]$
$x_{11}...x_{nm}$	independent variable	e.g. [-]
$b_{11}...b_{nm}$	regression model parameter	e.g.$[m^3\ mol^{-1}]$
$\boldsymbol{Y}$	matrix of dependent variables	e.g. $[mmol\ L^{-1}]$
$\boldsymbol{X}$	matrix of independent variables	[-]
$\boldsymbol{E}$	error Matrix	e.g. $[mmol\ L^{-1}]$
$\boldsymbol{B}$	matrix of regression parameters (MLR)	e.g.$[m^3\ mol^{-1}]$
$\hat{\boldsymbol{y}}$	matrix of predicted dependent variables	e.g. $[mmol\ L^{-1}]$
$\hat{\boldsymbol{X}}$	matrix of measured independent variables	e.g. [-]
$\boldsymbol{T} = \boldsymbol{UW}$	score matrix	[-]
$\boldsymbol{P}$, bmQ	loading matrix	[-]
$\boldsymbol{C}$	matrix of regression parameters (PCR)	[-]
$\boldsymbol{R}$	regression matrix (PLS)	[-]
$\boldsymbol{W}$	weight matrix of the PLS weights	[-]
n	number of species.	[-]
o	number of measurements for each of the species	[-]
$y_{i,j}$	simulated values of the individual reaction j	e.g. $[mmol\ L^{-1}]$
$\hat{y}_{i,j}$	predicted values of the individual reaction j	e.g. $[mmol\ L^{-1}]$
$\max y_{0,j}$	theoretical maximal value of the individual reaction j	e.g. $[mmol\ L^{-1}]$
F	fitness function	[-]
U	catalytic activity	$[\mu mol\ min^{-1}]$
$v_{descent}$	sedimentation velocity	$[m\ s^{-1}]$
ρ_s	Densitiy solid	$[kg\ m^{-3}]$
ρ_f	Density fluid	$[kg\ m^{-3}]$
d_p	Diameter particle	$[m]$
η_f	dynamic viscosity fluid	$[kg\ s^{-1}\ m^{-1}]$
k_d	inactivation constant	$[s^{-1}]$
λ_i	wavelength i	$[nm]$

List of indices

Index	Meaning
1...11	number of the elemetary reaction step
$+, -$	forward and backward reaction
m	Michaelis constant
i	Inhibition constant
E	Enzyme
C	Catalyst
A	Substrate A
B	Substrate B
AC	A-catalyst complex
BC	B-catalyst complex
P	Product
S	Substrate
ES	Enzyme Substrate complex
BA	Benzaldehyde
HCN	hydrogen cyanide
$(S) - MN$	(*S*)-mandelonitrile
$(R) - MN$	(*R*)-mandelonitrile
max	maximal reaction rate
0	initial contitions $t = 0$
$E - (S) - MN$	enzyme (*S*)-mandelonitrile complex
$E - (R) - MN$	enzyme (*R*)-mandelonitrile complex
$E - BA$	enzyme benzaldehyde complex
cleavage	cleavage reaction of mandelonitirle
synthesis	synthesis reaction of mandelonitirle
eq	equilibrium
dark	intensity in the dark
app	apparent parameter

Bibliography

[1] OECD. Statistical definition of biotechnology (2005). Available online at http://www.oecd.org/document/42/0,3343,en_2649_34537_1933994_1_1_1_1,00.html visited July 12th 2008.

[2] Ostwald, W. über katalysatoren. *Angewandte Chemie* **20**, 2113–21211 (1907).

[3] Blumenthal, G. *Chemie: Grundwissen für Ingenieure* (Teubner Verlag, Wiesbaden, 2007).

[4] Hagen, J. *Industrial catalysis* (Wiley-VCH Weinheim, 2006).

[5] Hädener, A. & Kaufmann, H. *Grundlagen der organischen Chemie* (Birkhäuser Verlag Basel, 2006).

[6] Cahn, R., Ingold, C. & Prelog, V. Specification of molecular chirality. *Angewandte Chemie International Edition in English* **5**, 385–415 (1966).

[7] Hellwich, K. *Stereochemie Grundbegriffe* (Springer Verlag Berlin, 2002).

[8] Shibasaki, M. & Matsunaga, S. *Asymmetric synthesis - The essentials*, chap. Metal-catalyzed asymmetric synthesis, 47–51 (Wiley-VCH GmbH&Co. KGaA, Weinheim, 2007).

[9] Gasser, T. Medikamentöse behandlung von morbus parkinson. *Arzneiverordnung in der Praxis* **3**, 2–4 (1999).

[10] für Arbeitsschutz und Arbeitsmedizin, B. Directive 98/8/ec concerning the placing of biocidal products on the market. inclusion of active substances in annex i or ia to directive 98/8/ec. assessment report: Indoxacarb product-type 18 (insecticide). Tech. Rep., Bundesanstalt für Arbeitsschutz und Arbeitsmedizin (2008).

[11] Neumann, M. *Synthese und Charakterisierung neuartiger Liganden auf [3]Ferrocenophan-Basis*. Ph.D. thesis, Westfälische Wilhelms-Universität Münster (2007).

[12] Lütz, S., Kragl, U., Liese, A. & Wandrey, C. *Asymmetric synthesis with chemical and biological methods*, chap. 3.1 Reaction engineering in asymmetric synthesis, 415–426 (WILEY-VCH Verlag GmbH&Co.KGaA, Weinheim, 2007).

[13] Noyori, R. Asymmetric catalysis: Science and opportunities (nobel lecture). *Angewandte Chemie International Edition* **41**, 2008–2022 (2002).

[14] Nozaki, H., Moriuti, S., Takaya, H. & Noyori, R. Asymmetric induction in carbenoid reaction by means of a dissymmetric copper chelate. *Tetrahedron Letters* **7**, 5239–5244 (1966).

[15] Knowles, W. & Sabacky, M. Catalytic asymmetric hydrogenation employing a soluble, optically active, rhodium complex. *Chemical Communications (London)* 1445 – 1446 (1968).

[16] Katsuki, T. & Sharpless, K. The first practical method for asymmetric epoxidation. *Journal of the American Chemical Society* **102**, 5974–5976 (1980).

[17] Jacobsen, E., Zhang, W., Muci, A., Ecker, J. & Deng, L. Highly enantioselective epoxidation catalysts derived from 1,2-diaminocyclohexane. *Journal of the American Chemical Society* **113**, 7063–7064 (1991).

[18] Ojima, I. (ed.) *Catalytic asymmetric synthesis* (Wiley, New York, 2000).

[19] Blaser, H. *et al.* The chiral switch of metolachlor. the development of a large-scale enentioselective catalytic process. *Chimia* **53**, 275–280 (1999).

[20] Behr, A. *Angewandte homogene Katalyse* (Wiley-VCH, Weinheim, 2008).

[21] Blaser, H., Pugin, B., Spindler, F. & Thommen, M. From a chiral switch to a ligand portfolio for asymmetric catalysis. *Accounts of Chemical Research* **40**, 1240–1250 (2007).

[22] Hugl, H. *Asymmetric synthesis - The essentials*, chap. Asymmetric synthesis in industry, 291–295 (Wiley-VCH GmbH&Co.KGaA, Weinheim, 2007).

[23] Berg, J., Tymoczko, J. & Stryer, L. *Biochemistry, Fifth Edition* (W. H. Freeman & Co Ltd, 2002), fifth edition edn.

[24] Liese, A. Technical application of biological principles in asymmetric catalysis. *Advances in Biochmical Engineering* **92**, 197–224 (2005).

[25] Hilterhaus, L., Howaldt, M., Liese, A. & Chmiel, H. Enzymkinetic. In Chmiel, H. (ed.) *Bioprozesstechnik*, chap. 3, 67–97 (Spektrum Akademischer Verlag, 2006).

[26] Laue, S. *Asymmetrische Transferhydrierung im chemischen Membranreaktor*. Ph.D. thesis, Forschungszentrum Jülich - Institut für Biotechnologie (2002).

[27] Giffels, G., Beliczey, J., Felder, M. & Kragl, U. Polymer enlarged oxazaborolidines in a membrane reactor: enhancing effectivity by retention of the homogeneous catalyst. *Tetrahedron: Asymmetry* **9**, 691–696 (1998).

[28] Kragl, U. & Dreisbach, C. Continuous asymmetric synthesis in a membrane reactor. *Angewandte Chemie International Edition in English* **35**, 642–644 (1996).

[29] Briechle, S., Howaldt, M., Röthig, T. & Liese, A. Enzymatische prozesse. In Chmiel, H. (ed.) *Bioprozesstechnik*, chap. 12, 361–408 (Spektrum Akademischer Verlag, 2006), 2. edn.

[30] Luetz, S., Rao, N. & Wandrey, C. Membranen in der biotechnologie. *Chemie Ingenieur Technik* **77**, 1669–1682 (2005).

[31] Wandrey, C., Wichmann, R., Leuchtenberger, W. & Kula, M. United States Patent US 4304858 "Process for the continuous enzymatic change of water soluble α-ketocarboxylic acids into the corresponding amino acids" (1981).

[32] Wöltinger, J., Karau, A., Leuchtenberger, W. & Drauz, K. *Advances in biochemical engineering/biotechnology*, chap. Membrane Reactors at Degussa, 289–316 (Springer Verlag Berlin Heidelberg, 2005).

[33] Gygax, D. & Kragl, U. Enzymatic two-step synthesis of *N*-acetyl-neuraminic acid in the enzyme membrane reactor. *Angewandte Chemie International Edition in English* **30**, 827–828 (1991).

[34] Nijkamp, M. & Müller, C. Continuous homogeneous catalysis. *European Journal of Inorganic Chemistry* **2005**, 4011–4021 (2005).

[35] Cole-Hamilton, D. & Tooze, R. (eds.) *Catalyst separation, recovery and recycling - Chemistry and process design* (Springer, Dordrecht, 2006).

[36] Chmiel, H. Aufarbeitung. In Chmiel, H. (ed.) *Bioprozesstechnik*, chap. 10, 260–322 (Spektrum Akademischer Verlag, 2006).

[37] Baier, C. & Stimming, U. Imaging single enzyme molecules under in situ conditions. *Angewandte Chemie - international Edition* **48**, 5542–5544 (2009).

[38] Gruber, K., Gugganig, M., Wagner, U. & Kratky, C. Atomic resolution crystal structure of hydroxynitrile lyase from *Hevea brasiliensis*. *Biological Chemistry* **380**, 993–1000 (1999).

[39] Tillyer, R., Boudreau, C., Tschaen, D., Dolling, U. & Reider, P. Asymmetric reduction of keto oxime ethers using oxazaborolidine reagents. the enantioselective synthesis of cyclic amino alcohols. *Tetrahedron Letters* **36**, 4337–4340 (1995).

[40] Bruggink, A., Schoevaart, R. & Kieboom, T. Concepts of nature in organic synthesis: Cascade catalysis and multistep conversions in concert. *Organic Process Research & Development* **7**, 622–640 (2003).

[41] Fogel, D. In memoriam alex s. fraser 1923-200. *IEEE Transactions on Evolutionary Computation* **6**, 429–430 (2002).

[42] Klempier, N., Pichler, U. & Griengl, H. Synthesis of α, β–unsaturated (*S*)–cyanohydrins using the oxynitrilase from hevea brasiliensis. *Tetrahedron: Asymmetry* **6**, 845–848 (1995).

[43] Avi, M. *Enzyme Catalysed Cyanohydrin Reaction on Diels-Alder Adducts: Complex Molecules from Simple Building Blocks*. Ph.D. thesis, Graz University of Technology (2007).

[44] Purkarthofer, T. *Extending the Synthetic Potential of Hydroxynitrile Lyases*. Ph.D. thesis, Graz University of Technology between (2004).

[45] Gregory, R. Cyanohydrins in nature and the laboratory: biology, preparations, and synthetic applications. *Chemical reviews* **99**, 3649–3682 (1999).

[46] Purkarthofer, T., Skranc, W., Schuster, C. & Griengl, H. Potential and capabilities of hydroxynitrile lyases as biocatalysts in the chemical industry. *Applied Microbiology And Biotechnology* **76**, 309–320 (2007).

[47] Holt, J. & Hanefeld, U. Enantioselective enzyme-catalysed synthesis of cyanohydrins. *Current Organic Synthesis* **6**, 15–37 (2009).

[48] Krieble, V. & Wieland, W. The properties of oxynitrilase. *Journal of the American Chemical Society* **43**, 164–175 (1921).

[49] Gröger, H. Enzymatic routes to enantiomerically pure aromatic α-hydroxy carboxylic acids: A further example for the diversity of biocatalysis. *Advanced Synthesis & Catalysis* **343**, 547–558 (2001).

[50] Monterde, M., Nazabadioko, S., Rebolledo, F., Brieva, R. & Gotor, V. Chemoenzymatic synthesis of azacycloalkan-3-ols. *Tetrahedron: Asymmetry* **10**, 3449–3455 (1999).

[51] Zandbergen, P., Brussee, J., van der Gen, A. & Kruse, C. Stereoselective synthesis of β–hydroxy–α–amino acids from chiral cyanohydrins. *Tetrahedron: Asymmetry* **3**, 769–774 (1992).

[52] Effenberger, F., Gutterer, B. & Jäger, J. Stereoselective synthesis of (1r)- and (1r,2s)-1-aryl-2-alkylamino alcohols from (*R*)-cyanohydrins. *Tetrahedron: Asymmetry* **8**, 459–467 (1997).

[53] Effenberger, U., F.and Stelzer. A convenient preparation of 2-substituted (*S*)-aziridines. *Tetrahedron: Asymmetry* **6**, 283–286 (1995).

[54] Effenberger, F. & Stelzer, U. Synthesis and stereoselective reactions of (*R*)-α-sulfonyloxynitriles. *Angewandte Chemie International Edition in English* **30**, 873–874 (1991).

[55] Gaucher, A., Ollivier, J. & Salaün, J. Diastereoselective preparation of cyclopropane amino acids: Synthesis of norcoronamic acid. *Synlett* **3**, 151–153 (1991).

[56] Effenberger, F., Kremser, A. & Stelzer, U. A convenient synthesis of (*S*)-2-azidonitriles, (*S*)-2-aminonitriles and (*S*)-1,2-diamines. *Tetrahedron: Asymmetry* **7**, 607–618 (1996).

[57] Stelzer, U. & Effenberger, F. Preparation of (*S*)-fluoronitriles. *Tetrahedron: Asymmetry* **4**, 161–164 (1993).

[58] Brussee, J., Roos, E. & Van Der Gen, A. Bio-organic synthesis of optically active cyanohydrins and acyloins. *Tetrahedron Letters* **29**, 4485–4488 (1988).

[59] Menendez, E., Brieva, R., Rebolledo, F. & Gotor, V. Optically active (*S*)-ketone- and (*R*)-aldehyde-cyanohydrins via an (*R*)-oxynitrifase-catalysed transcyanation. chemoenzymatic syntheses of 2-cyanotetrahydrofuran and 2-cyanotetrahydropyran. *Chemical Communications* **10**, 989–990 (1995).

[60] Monterde, M., Brieva, R. & Gotor, V. Stereocontrolled chemoenzymatic synthesis of 2,3-disubstituted piperidines. *Tetrahedron: Asymmetry* **12**, 525–528 (2001).

[61] Mandai, T., Hashio, S., Goto, J. & Kawada, M. Palladium-catalyzed rearrangement of α-cyanoallylic acetates application to a new synthetic method for furans. *Tetrahedron Letters* **22**, 2187–2190 (1981).

[62] Schmidt, M., Herve, S., Klempier, N. & Griengl, H. Preparation of optically active cyanohydrins using the (S)-hydroxynitrile lyase from Hevea brasiliensis. *Tetrahedron* **52**, 7833–7840 (1996).

[63] Hamilton, J., Ibbotson, H., Hooper, A. & Pickett, J. 9-methylgermacrene-b is confirmed as the sex pheromone of the sandfly lutzomyia longipalpis from lapinha, brazil, and the absolute stereochemistry defined as s. *Chemical Communications* 2335–2336 (1999).

[64] Fukuda, Y. & Okamoto, Y. First total synthesis of (+/-)-am6898a and (+/-)-am6898d. *Tetrahedron* **58**, 2513–2521 (2002).

[65] Brussee, J., Loos, W., Kruse, C. & Van Der Gen, A. Synthesis of optically active silyl protected cyanohydrins. *Tetrahedron* **46**, 979–986 (1990).

[66] Roos, J. & Effenberger, F. Stereoselective synthesis of β–amino–γ–butyrolactones. *Tetrahedron: Asymmetry* **13**, 1855–1862 (2002).

[67] Johnson, D., Felfer, U. & Griengl, H. A chemoenzymatic access to d- and l-sphingosines employing hydroxynitrile lyases. *Tetrahedron* **56**, 781–790 (2000).

[68] Johnson, D. & Griengl, H. The chemoenzymatic synthesis of (*S*)-13-hydroxyoctadeca-(9z, 11e)-dienoic acid using the hydroxynitrile lyase from hevea brasiliensis. *Tetrahedron* **53**, 617–624 (1997).

[69] Duffield, J. & Regan, A. Asymmetric synthesis of tetronic acids by blaise reaction of protected optically active cyanohydrins. *Tetrahedron: Asymmetry* **7**, 663–666 (1996).

[70] Effenberger, F. & S., J. Stereoselective synthesis of biologically active tetronic acids. *Tetrahedron: Asymmetry* **9**, 817–825 (1998).

[71] Bühler, H., Bayer, A. & Effenberger, F. A convenient synthesis of optically active 5,5-disubstituted 4-amino- and 4-hydroxy-2(5 h)-furanones from (*S*)-ketone cyanohydrins. *Chemistry - A European Journal* **6**, 2564–2571 (2000).

[72] Effenberger, F., Roos, J., Kobler, C. & Bühler, H. Hydroxynitrile lyase-catalyzed addition of hcn to 4-substituted cyclohexanones: stereoselective preparation of tetronic acids. *Canadian Journal of Chemistry* **80**, 671–679 (2002).

[73] Effenberger, F. & Eichhorn, J. Stereoselective synthesis of thienyl and furyl analogues of ephedrine. *Tetrahedron: Asymmetry* **8**, 469–476 (1997).

[74] Effenberger, F. & Jäger, J. Synthesis of the adrenergic bronchodilators (*R*)-terbutaline and (*R*)-salbutamol from (*R*)-cyanohydrins. *Journal of organic chemistry* **62**, 3867–3873 (1997).

[75] Effenberger, F. & Jäger, J. Stereoselective synthesis of (*S*)-3,4-methylenedioxyamphetamines from (*R*)-cyanohydrins. *Chemistry - A European Journal* **3**, 1370–1374 (1997).

[76] Johnson, D., Fischer, R. & Griengl, H. A novel stereoselective access to substituted l-2-deoxypentono-1,4-lactones and l-2-deoxypentoses. *Tetrahedron* **56**, 9289–9295 (2000).

[77] Effenberger, F. & Roos, J. Stereoselective synthesis of 3-amino-4,5-dihydroxyaldehydes – a novel preparation of n-acetyl-l-daunosamine. *Tetrahedron: Asymmetry* **11**, 1085–1095 (2000).

[78] Effenberger, F., Gutterer, B. & Syed, J. Stereoselective synthesis of (1r,2s)-2-amino-1,3-diols from (r)-cyanohydrins. *Tetrahedron: Asymmetry* **6**, 2933–2943 (1995).

[79] Warmerdam, E., van Rijn, R., Brussee, J., Kruse, C. & van der Gen, A. Synthesis of α-hydroxy-β-amino acids from chiral cyanohydrins. *Tetrahedron: Asymmetry* **7**, 1723–1732 (1996).

[80] Tromp, R. *et al.* Chemoenzymatic synthesis of fmoc-protected (2s,3s)-2-hydroxy-3-amino acids and their application in the synthesis of an α-hydroxylated β-hexapeptide. *Tetrahedron: Asymmetry* **12**, 1109–1112 (2001).

[81] van den Nieuwendijk, A., Ghisaidoobe, A., Overkleeft, H., Brussee, J. & van der Gen, A. Conversion of chiral unsaturated cyanohydrins into chiral carba-and heterocycles via ring-closing metathesis. *Tetrahedron* **60**, 10385–10396 (2004).

[82] Nazabadioko, S., Perez, R., Brieva, R. & Gotor, V. Chemoenzymatic synthesis of (*S*)-2-cyanopiperidine, a key intermediate in the route to (*S*)-pipecolic acid and 2-substituted piperidine alkaloids. *Tetrahedron: Asymmetry* **9**, 1597–1604 (1998).

[83] Brussee, J. & Marcus, J. Intramolecular cycloaddition reactions of ω-unsaturated chiral nitrones. *European Journal of Organic Chemistry* **1998**, 2513–2517 (1998).

[84] Solle, D., Geissler, D., Stärk, E., Scheper, T. & Hitzmann, B. Chemometric modelling based on 2d-fluorescence spectra without a calibration measurement. *Bioinformatics* **19**, 173–177 (2003).

[85] Carrea, G. & Riva, S. Properties and synthetic applications of enzymes in organic solvents. *Angewandte Chemie International Edition* **39**, 2226–2254 (2000).

[86] Klibanov, A. Improving enzymes by using them in organic solvents. *Nature* **409**, 241–246 (2001).

[87] Torres, S. & Castro, G. Non-aqueous biocatalysis in homogeneous solvent systems. *Food Technology And Biotechnology* **42**, 271–277 (2004).

[88] Bauer, M. *Enzyme kinetics of an (S)-hydroxynitrile lyase from Hevea brasiliensis in aqueous buffer and two-phase systems.* Ph.D. thesis, TU-Graz (1998).

[89] Poechlauer, P., Skranc, W. & Wubbolts, M. The large-scale biocatalytic synthesis of enantiopure cyanohydrins. In Blaser, H. & Schmidt, E. (eds.) *Asymmetric Catalysis on Industrial Scale: Challenges, Approaches and Solutions*, 151–164 (Wiley-VCH Verlag GmbH & Co. KGaA, 2004).

[90] Diels, O. & Alder, K. Synthesen in der hydroaromatischen reihe. *Justus Liebig's Annalen der Chemie* **460**, 98–122 (1928).

[91] nobelprize.org. The nobel prize in chemistry 1950: "for their discovery and development of the diene synthesis". webside (1950). Available online at http://nobelprize.org/nobel_prizes/chemistry/laureates/1950/index.html visited July 22th 2008.

[92] Becker, H. *Organikum* (Wiley-VCH Weinheim, 1999).

[93] Fringuelli, F. & Taticchi, A. *Dienes in the Diels-Alder reaction* (Wiley, 1990).

[94] Nicolaou, K. & Bulger, P. *Asymmetric synthesis - The essentials*, chap. Asymmetric reactions in total synthesis, 225–240 (Wiley-VCH GmbH&Co.KGaA, Weinheim, 2007).

[95] Mikami, K., Motoyama, Y. & Terada, M. Asymmetric catalysis of diels-alder cycloadditions by an ms-free binapthol-titanium complex: Dramatic effect of ms, linear vs positive nonlinear relationshop, and synthetic applications. *Journal of American Chemical Society* **116**, 2812–2820 (1994).

[96] Liu, P. & Jacobsen, E. Total synthesis of (+)-ambruticin. *Journal of American Chemical Society* **123**, 10772–10773 (2001).

[97] Knapen, J. *et al.* Homogeneous catalysts based on silane dendrimers functionalized with arylnickel(II) complexes. *Nature* **372**, 659–663 (1994).

[98] Bayer, E. & Mutter, M. Liquid phase synthesis of peptides. *Nature* **237**, 512–513 (1972).

[99] Ribourdouill, Y., Engel, G. & Gade, L. The immobilization of chiral catalyst on and inside dendrimers. *C.R. Chimie* **6**, 1087–1096 (2003).

[100] Kwiatkowski, P., Asztemboraskab, M. & Jurczaka, J. The enantioslective diels-alder reaction of 1-methoxybuta-1,3-diene with n-butyl glyoxylaate catalyzed by the (salen)cr(iii)cl and co(ii) complexes. *Tetrahedron: Asymmetry* **15**, 3189–3194 (2004).

[101] Uchida, T. *et al.* New asymmetric catalysis by (salen)cobalt(iii) complexes(salen=[bis(salicylidene)ethylenediaminato]={{2,2'-[ethane-1,2-diyl]bis[(nitrilo-κn)methylidyne]bis[phenolato-kappa o]}(2-)}) of cis-β-structure: Enantioselective *Baeyer-Villiger* oxidation of prochiral cyclobutanones. *Helvetica Chimica Acta* **85**, 3078–3089 (2002).

[102] Hajji, C., Roller, S., Beigi, M., Liese, A. & Haag, R. Polyglycerol-supported chromium-salen as a high-loading dendritic catalyst for stereoselective diels-alder reactions. *Advanced Synthesis & Catalysis* **348**, 1760–1771 (2006).

[103] Combes, A. Sur l'action des diamines sur les diacétones. *Comptes rendus de l'Académie Française* **108**, 1252 (1889).

[104] Beleizao, C. & Garcia, H. Chiral salen complexes: An overview to recoverable and reusable homogeneous and heterogeneous catalysts. *Chemical Reviews* **106**, 3987–4043 (2006).

[105] Pfeiffer, P., Breith, E., Löbbe, E. & Tsumaki, T. Tricyclische orthokondensierte nebenvalenzringe. *Justus Liebig's Annalen der Chemie* **503**, 84–130 (1933).

[106] Beigi, M. *Polyglycerol Supported Salen: Preparation, Catalysis and Sustainability in a Chemical Membrane Reactor*. Ph.D. thesis, Westfälische Wilhelms-Universität Münster (2007).

[107] Crosman, A. *et al. Asymmetric synthesis with chemical and biological Methods*, chap. Immobilization of Transition Metal Complexes and Their Application to Enantioselective Catalysis, 277–297 (Wiley-VCH GmbH&Co.KGaA, Weinheim, 2007).

[108] Beigi, M., Roller, S., Haag, R. & Liese, A. Polyglycerol-supported co- and mn-salen complexes as efficient and recyclable homogeneous catalysts for the hydrolytic kinetic resolution of terminal epoxides and asymmetric olefin epoxidation. *European Journal of Organic Chemistry* **2008**, 2135–2141 (2008).

[109] Hajji, C. & Haag, R. unpublished work (2007).

[110] Chaudhari, R., Seayad, A. & Jayasree, S. Kinetic modeling of homogeneous catalytic processes. *Catalysis Today* **66**, 371–380 (2001).

[111] Natta, G., Ercoli, R., Castellano, S. & Barbieri, F. The influence of hydrogen and carbon monoxide partial pressures on the rate of the hydroformulation reaction. *Journal of the American Chemical Society* **76**, 4049 (1954).

[112] Gholap, R., Kunt, O. & Bourne, J. Hydroformylation of propylene using unmodified cobalt carbonyl catalyst: selectivity studies. *Industrial & Engineering Chemistry Research* **31**, 2446 (1992).

[113] Kamiya, Y. & Kotake, M. Catalysis of manganese salts in the autoxidation of cyclohexanone. *Bulletin of the Chemical Society of Japan* **46**, 2780 (1973).

[114] Ubale, R. *Studies in homogeneous catalysis: Carbonylation of alcohols and esters*. Ph.D. thesis, University of Pune (1981).

[115] Chorkendorff, I. & Niemantsverdriet, J. *Concepts of modern catalysis and kinetics* (WILEY-VCH, Weinheim, 2007).

[116] Haag, R. Communication with institute of chemistry and biochemistry - organic chemistry, freie universität berlin, dendritic polymer research group, prof. dr. rainer haag.

[117] Segel, I. *Enzyme Kinetics: Behavior and Analysis of Rapid Equilibrium and SteadyState Enzyme Systems: Behavior and Analysis of Rapid Equilibrium and Steady-State Enzyme Systems* (John Wiley & Sons, 1993).

[118] Beigi, M., Haag, R. & Liese, A. Continuous application of polyglycerol-supported salen in a membrane reactor: Asymmetric epoxidation of 6-cyano-2,2-dimethylchromene. *Advanced Synthesis & Catalysis* **350**, 919–925 (2008).

[119] Laue, S., Greiner, L., Wöltinger, J. & Liese, A. Continuous application of chemzymes in a membrane reactor: Asymmetric transfer hydrogenation of acetophenone. *Advanced Synthesis & Catalysis* **343**, 711–720 (2001).

[120] Schurig, V. & Bayer, E. Soluble metal complexes of polymers for catalysis. *Angewandte Chemie International Edition in English* **14**, 493–494 (1975).

[121] Brinkmann, N., Giebel, D., Lohmer, G., Reetz, M. & Krag, U. Allylic substitution with dendritic palladium catalysts in a continuously operating membrane reactor. *Journal of Catalysis* **183**, 163–168 (1999).

[122] de Groot, D. & Reek, J. Palladium complexes of phosphane-functionalised carbosilane dendrimers as catalysts in a continuous-flow membrane reactor. *European Journal of Organic Chemistry* **2002**, 1085–1095 (2002).

[123] Dwars, T., Haberland, J., Grassert, I., Oehme, G. & Kragl, U. Asymmetric hydrogenation in a membrane reactor: recycling of the chiral catalyst by using a retainable micellar system. *Journal of Molecular Catalysis A: Chemical* **168**, 81–86 (2001).

[124] De Smet, K., Aerts, S., Ceulemans, E., Vankelecom, I. & Jacobs, P. Nanofiltration-coupled catalysis to combine the advantages of homogeneous and heterogeneous catalysis. *Chemical Communications* 597 – 598, (2001).

[125] van Heerbeek, R., Kamer, P., van Leeuwen, P. & Reek, J. Dendrimers as support for recoverable catalysts and reagents. *Chemical Reviews* **102**, 3717–3756 (2002).

[126] van Koten, G. & Jastrzebski, J. Periphery-functionalized organometallic dendrimers for homogeneous catalysis. *Journal of Molecular Catalysis A: Chemical* **146**, 317–323 (1999).

[127] Vankelecom, I. Polymeric membranes in catalytic reactors. *Chemical Reviews* **102**, 3779–3810 (2002).

[128] Wöltinger, J., Drauz, K. & Bommarius, A. The membrane reactor in the fine chemicals industry. *Applied Catalysis A: General* **221**, 171–185 (2001).

[129] Membrane Extraction Technology, London, UK. *Grace Davison Solvent Nanofiltration Membranes: Starmem™* (2005).

[130] Eggeling, E. & Hovestad, N. Selective hydrovinylation of styrene in a membrane reactor: Use of carbosilane dendrimers with hemilabile p,o ligands. *Angewandte Chemie International Edition* **38**, 1655–1658 (1999).

[131] Eggeling, E., Hovestad, N., Jastrzebski, J., Vogt, D. & van Koten, G. Phosphino carboxylic acid ester functionalized carbosilane dendrimers: Nanoscale ligands for the pd-catalyzed hydrovinylation reaction in a membrane reactor. *Journal of Organic Chemistry* **65**, 8857 – 8865 (2000).

[132] de Groot, D. *et al.* Palladium complexes of phosphine functionalised carbosilane dendrimers as catalysts in a continuous flow membrane reactor. *Chemical Communications* 1623 – 1624 (1999).

[133] Winckler, F. Organische bildungstheile von pflanzen, als alkaloide, fette, zucker, gummi, farbstoffe u. s. w. und deren produkte. *Annalen der Pharmacie* **4**, 242–247 (1832).

[134] Winckler, F. über die Mandelsäure und einige Salze derselben. *Annalen der Pharmacie* **18**, 310–319 (1836).

[135] Winckler, F. Zusammensetzung und Constitution der Mandelsäure. *Annalen der Pharmacie* **18**, 319–327 (1836).

[136] Lapworth, A. Reactions involving the addition of hydrogen cyanide to carbon compounds. *J. Chem. Soc* **83**, 995–1005 (1903).

[137] Kulkarni, B., Sharma, A., Gamre, S. & Chattopadhyay, S. Synthesis of the marine compound (2r,5z,9z)-2-methoxyhexacosa-5,9-dienoic acid via a lipase-catalyzed resolution and a novel o-alkylation protocol. *Synthesis* 595–599 (2004).

[138] Watanabe, A., Matsumoto, K., Shimada, Y. & Katsuki, T. Oxovanadium(v)-catalyzed enantioselective meerwein-ponndorf-verley cyanation of aldehydes using acetone cyanohydrin. *Tetrahedron Letters* **45**, 6229–6233 (2004).

[139] Nanda, S., Kato, Y. & Asano, Y. Pmhnl catalyzed synthesis of (*R*)-cyanohydrins derived from aliphatic aldehydes. *Tetrahedron: Asymmetry* **17**, 735–741 (2006).

[140] Watanabe, S., Cordova, A., Tanaka, F. & Barbas, C. One-pot asymmetric synthesis of β-cyanohydroxymethyl α-amino acid derivatives: Formation of three contiguous stereogenic centers. *Organic Letters* **4**, 4519–4522 (2002).

[141] Belokon, Y. *et al.* Chiral ti(iv) complexes of hexadentate schiff bases as precatalysts for the asymmetric addition of tmscn to aldehydes and the ring opening of cyclohexene oxide. *Tetrahedron: Asymmetry* **17**, 2328–2333 (2006).

[142] Mei, L. *et al.* Research on the cyanosilylation of prochiral aldehydes catalyzed by alkyldimethoxyl silylene-bridged lanthanide complexes. *Synthetic Communications* **36**, 2483 – 2490 (2006).

[143] Lundgren, S., Wingstrand, E., Penhoat, M. & Moberg, C. Dual lewis acid-lewis base activation in enantioselective cyanation of aldehydes using acetyl cyanide and cyanoformate as cyanide sources. *Journal of the American Chemical Society* **127**, 11592–11593 (2005).

[144] Poirier, D., Berthiaume, D. & Boivin, R. Unexpected formation of o-methoxycarbonyl cyanohydrin showing potential as a protective group of ketones. *Synlett* 1423–1425 (1999).

[145] Purkarthofer, T. *et al.* One-pot chemoenzymatic synthesis of protected cyanohydrins. *Tetrahedron* **60**, 735–739 (2004).

[146] Dadashipour, M. *et al. S*-selective hydroxynitrile lyase from a plant baliospermum montanum: Molecular characterization of recombinant enzyme. *Journal of Biotechnology* **153**, 100–110 (2011).

[147] Hasslacher, M. *et al.* Molecular cloning of the full-length cdna of (s)-hydroxynitrile lyase from hevea brasiliensis. functional expression in escherichia coli and saccharomyces cerevisiae and identification of an active site residue. *Journal of Biological Chemistry* **271**, 5884–91 (1996).

[148] Fukuta, Y. *et al.* Characterization of a new (*R*)-hydroxynitrile lyase from the japanese apricot prunus mume and cdna cloning and secretory expression of one of the isozymes in pichia pastoris. *Bioscience Biotechnology and Biochemistry* **75**, 214–220 (2011).

[149] Trummler, K. *et al.* Expression of the zn2+-containing hydroxynitrile lyase from flax (linum usitatissimum) in pichia pastoris- utilization of the recombinant enzyme for enzymatic analysis and site-directed mutagenesis. *Plant Science* **139**, 19–27 (1998).

[150] Forster, J. S., Roos, J., Effenberger, F., Wajant, H. & Sprauer, A. The first recombinant hydroxynitrile lyase and its application in the synthesis of (S)-cyanohydrins. *Angewandte Chemie - International Edition* **35**, 437–439 (1996). Diesen Articel habe ich noch nicht.

[151] Griengl, H. *et al.* Enzymatic cleavage and formation of cyanohydrins: a reaction of biological and synthetic relevance. *Chemical Communications (Cambridge)* **20**, 1933–1940 (1997).

[152] Griengl, H. *et al.* Enzyme catalysed formation of (*S*)-cyanohydrins derived from aldehydes and ketones in a biphasic solvent system. *Tetrahedron* **54**, 14477–14486 (1998).

[153] Effenberger, F., Ziegler, T. & Förster, S. Enzymkatalysierte Cyanhydrin-Synthese in organischen lösungsmitteln. *Angewandte Chemie* **99**, 491–492 (1987).

[154] Wehtje, E., Adlercreutz, P. & Mattiasson, B. Activity and operational stability of immobilized mandelonitrile lyase in methanol/water mixtures. *Applied Microbiology and Biotechnology* **29**, 419–425 (1988).

[155] Wehtje, E., Adlercreutz, P. & Mattiasson, B. Formation of C–C bonds by mandelonitrile lyase in organic solvents. *Biotechnology and Bioengineering* **36**, 39–46 (1990).

[156] Bauer, M., Griengl, H. & Steiner, W. Parameters influencing stability and activity of a (*S*)-hydroxynitrile lyase from *hevea brasiliensis* in two-phase systems. *Enzyme and Microbial Technology* **24**, 514–522 (1999).

[157] Sheldon, R. Cross-linked enzyme aggregates as industrial biocatalysts. *Organic Process Reserach & Development* **15**, 213–223 (2011).

[158] Faber, K. *Biotransformations in Organic Chemistry. A Textbook, 4th Edition* (Springer, Berlin, 2004), fifth edn.

[159] Straathof, A. & Adlercreutz, P. *Applied Biocatalysis* (CRC, 2000).

[160] Halling, P. Thermodynamic predictions for biocatalysis in nonconventional media: Theory, tests, and recommendations for experimental design and analysis. *Enzyme and Microbial Technology* **16**, 178–206 (1994).

[161] Lilly, M. Two-liquid-phase biocatalytic reactions. *Journal of Chemical Technology and Biotechnology* **32**, 162–169 (1982).

[162] Brink, L., Tramper, J., Luyben, K. & van't Riet, K. Biocatalysis in organic media. *Enzyme and Microbial Technology* **10**, 736–743 (1988).

[163] Dordick, J. Enzymatic catalysis in monophasic organic solvents. *Enzyme and Microbial Technology* **11**, 194–211 (1989).

[164] Khmelnitsky, Y., Levashov, A., Klyachko, N. & Karel, M. Engineering biocatalytic systems in organic media with low water content. *Enzyme and Microbial Technology* **10**, 710–724 (1988).

[165] Klibanov, A. Asymmetric transformations catalyzed by enzymes in organic solvents. *Accounts of Chemical Research* **23**, 114–120 (1990).

[166] Tramper, J., Vermue, M. & von Beeftink, H. *Biocatalysis in Non-Conventional Media: Proceedings of an International Symposium Noordwijkerhout, 26-29 April 1992 (Progress in Biotechnology)* (Elsevier Publishing Company, 1992).

[167] Verume, M. & Tramper, J. Biocatalysis in non-conventional media: Medium engineering aspects (technical report). *Pure and Applied Chemistry* **67**, 345–373 (1995).

[168] Vulfson, E., Halling, P. & Holland, H. (eds.) *Enzymes in Nonaqueous Solvents: Methods and Protocols (Methods in Biotechnology)* (Humana Press Inc.,U.S., 2001).

[169] Cooke, R. & Kuntz, I. The properties of water in biological systems. *Annual Review of Biophysics and Bioengineering* (1974).

[170] Bell, G. *et al.* Methods for measurement and control of water in non-aqueous biocatalysis. In Vulfson, E. N., Halling, P. J. & Holland, H. L. (eds.) *Enzymes in Nonaqueous Solvents: Methods and Protocols*, chap. 11, 105–126 (Humana Press Inc.,U.S., 2001).

[171] Paravidino, M., Sorgedrager, M., Orru, R. & Hanefeld, U. Activity and enantioselectivity of the hydroxynitrile lyase mehnl in dry organic solvents. *Chemistry - A European Journal* **16**, 7596–7604 (2010).

[172] Halling, P. Salt hydrates for water activity control with biocatalysts in organic media. *Biotechnology Techniques* **6**, 271–276 (1992).

[173] Luethi, P. & Luisi, P. Enzymic synthesis of hydrocarbon-soluble peptides with reverse micelles. *Journal of the American Chemical Society* **106**, 7285–7286 (1984).

[174] Laane, C., Boeren, S. & Vos, K. On optimizing organic solvents in multi-liquid-phase biocatalysis. *Trends in Biotechnology* **3**, 251–252 (1985).

[175] Kise, S. & Hayashida, M. Two-phase system membrane reactor with cofactor recycling. *Journal of Biotechnology* **14**, 221–228 (1990).

[176] Bauer, M., Griengl, H. & Steiner, W. Kinetic studies on the enzyme (*S*)-hydroxynitrile lyase from hevea brasiliensis using initial rate methods and progress curve analysis. *Biotechnology and Bioengineering* **62**, 20–29 (1999).

[177] Bauer, M., Geyer, R., Griengl, H. & Steiner, W. The use of lewis cell to investigate the enzyme kinetics of an (*S*)-hydroxynitrile lyase in two-phase systems. *Food Technology and Biotechnology* **40**, 9–19 (2002).

[178] Filho, M., Stillger, T., Müller, M., Liese, A. & Wandrey, C. Is log p a convenient criterion to guide the choice of solvents for biphasic enzymatic reactions? *Angewandte Chemie International Edition* **42**, 2993–2996 (2003).

[179] Reich, B. J. E. *Cyanide-catalyzed carbon-carbon bond formation: The synthesis of novel compounds, materials, and ligands utilized in homogeneous catalysis*. Ph.D. thesis, Texas A&M University, Texas (2005).

[180] Briggs, G. & Haldane, J. A note on the kinetics of enzyme action. *Biochemical Journal* **19**, 338–339 (1925).

[181] Straathof, A. & Heijnen, J. New constraints between kinetic parameters explain the (un)identifiability of enzymatic rate constants. *Biotechnology and Bioengineering* **52**, 433–437 (1996).

[182] Duggleby, R. Analysis of biochemical data by nonlinear regression: is it a waste of time? *Trends in Biochemical Sciences* **16**, 51–52 (1991).

[183] Duggleby, R. & Morrison, J. The analysis of progress curves for enzyme-catalysed reactions by non-linear regression. *Biochimica et Biophysica Acta (BBA) - Enzymology* **481**, 297–312 (1977).

[184] Duggleby, R. & Morrison, J. Progress curve analysis in enzyme kinetics. model discrimination and parameter estimation. *Biochimica et Biophysica Acta (BBA) - Enzymology* **526**, 398–409 (1978).

[185] Duggleby, R. & Morrison, J. The use of steady-state rate equations to analyse progress curve data. *Biochimica et Biophysica Acta (BBA) - Enzymology* **568**, 357–362 (1979).

[186] Duggleby, R. Experimental designs for estimating the kinetic parameters for enzyme-catalysed reactions. *Journal of Theoretical Biology* **81**, 671–684 (1979).

[187] Duggleby, R. Progress curves of reactions catalyzed by unstable enzymes. a theoretical approach. *Journal of Theoretical Biology* **123**, 67–80 (1986).

[188] Duggleby, R. Fitting the double michaelis-menten equation to kinetic data. *Journal of Theoretical Biology* **130**, 123–124 (1988).

[189] Duggleby, R. & Wood, C. Analysis of progress curves for enzyme-catalysed reactions. automatic construction of computer programs for fitting integrated rate equations. *Biochemical Journal* **258** (1989).

[190] Duggleby, R. & Clarke, R. Experimental designs for estimating the parameters of the michaelis-menten equation from progress curves of enzyme-catalyzed reactions. *Biochimica et Biophysica Acta (BBA) - Protein Structure and Molecular Enzymology* **1080**, 231–236 (1991).

[191] García-Sevilla, F. *et al.* Use of a windows program for simulation of the progress curves of reactants and intermediates involved in enzyme-catalyzed reactions. *Biosystems* **54**, 151–164 (2000).

[192] Markus, M., Plesser, T. & Kohlemeier, M. Analysis of progress curves in enzyme kinetics: Bias and convergent set in the differential and in the integral method. *Journal of Biochemical and Biophysical Methods* **4**, 81–90 (1981).

[193] Romein, B. & Rakels, J. Kinetic analysis of enzymatic chiral resolution by progress curve evaluation. *Biotechnology and Bioengineering* **43**, 411–422 (1994).

[194] Brereton, R. *Chemometrics. Data Analysis for the Laboratory and Chemical Plant* (Wiley & Sons, 2003).

[195] Otto, M. *Chemometrics. Statistics and Computer Application in Analytical Chemistry* (Wiley-Vch, 2007).

[196] Andersson, C. & Bro, R. The n-way toolbox for matlab. *Chemometrics and Intelligent Laboratory Systems* **52**, 1–4 (2000).

[197] Bro, R. Multiway calibration. multilinear pls. *Journal Of Chemometrics* **10**, 47–61 (1996).

[198] Gauß, J. C. F. *a Motus Corporum Coelestium in sectionibus conicis solem ambientium* (Gauß, Johann Carl Friedrich, 1809).

[199] MathWorks, T. Optimization toolbox user's guide version 3.1.1 (r2007a). Tech. Rep., The MathWorks,Inc., Natick, MA, USA (2007).

[200] The MathWorks, Inc., 3 Apple Hill Drive, Natick, MA 01760-2098. *Genetic Algorithm and Direct Search Toolbox 2: User's Guide* (2008).

[201] Rao, C., Sathish, T., Mahalaxmi, M., Laxmi, R., G.and Rao & Prakasham, R. Modelling and optimization of fermentation factors for enhancement of alkaline protease production by isolated bacillus circulans using feed-forward neural network and genetic algorithm. *Journal Of Applied Microbiology* **104**, 889–898 (2008).

[202] Findrilk, Z., Poijanac, M. & Vasic-Racki, D. Modelling and optimization of the (*R*)-(+)-3,4-dihydroxyphenyllactic acid production catalyzed with d-lactate dehydrogenase from lactobacillus leishmannii using genetic algorithm. *Chemical And Biochemical Engineering Quarterly* **19**, 351–358 (2005).

[203] Hoh, C., Dudziak, G. & Liese, A. Optimization of the enzymatic synthesis of o-glycan core 2 structure by use of a genetic algorithm. *Bioorganic & Medicinal Chemistry Letters* **12**, 1031–1034 (2002).

[204] Ghasemi, J., Ebrahimi, D., Hejazi, L., Leardi, R. & Niazi, A. Simultaneous kinetic-spectrophotometric determination of sulfide and sulfite and genetic algorithim variable selection using partial least squares calibration. *Journal Of Analytical Chemistry* **61**, 92–98 (2006).

[205] Fang, B., Chen, H., Xie, X., Wan, N. & Hu, Z. Using genetic algorithms coupling neural networks in a study of xylitol production: medium optimisation. *Process Biochemistry* **38**, 979–985 (2003).

[206] Roeva, O. *et al.* Multiple model approach to modelling of escherichia coli fed-batch cultivation extracellular production of bacterial phytase. *Electronic Journal Of Biotechnology* **10**, 592–603 (2007).

[207] Gheorghe, M. Model-based heuristic optimized operating policies for d-glucose oxidation in a batch reactor with pulsate addition of enzyme. *Computers & Chemical Engineering* **31**, 1231–1241 (2007).

[208] Weuster-Botz, D., Pramatarova, V., Spassov, G. & Wandrey, C. Use of a genetic algorithm in the development of a synthetic growth medium for *Arthrobacter simplex* with high hydrocortisone δ^1-dehydrogenase activity. *Journal of Chemical Technology & Biotechnology* **64**, 386–392 (1995).

[209] Bauer, M., Geyer, R., Boy, M., Griengl, H. & Steiner, W. Stability of the enzyme (*S*)-hydroxynitrile lyase from *hevea brasiliensis*. *Journal of Molecular Catalysis B: Enzymatic* **5**, 343–347 (1998).

[210] Lindner, P. & Hitzmann, B. Experimental design for optimal parameter estimation of an enzyme kinetic process based on the analysis of the fisher information matrix. *Journal of Theoretical Biology* **238**, 111–123 (2006).

[211] Zavrel, M. *et al.* Mechanistic kinetic model for symmetric carboligations using benzaldehyde lyase. *Biotechnology and Bioengineering* **101**, 27–38 (2008).

[212] de Brito Alves, R. M., do Nascimento, C. A. O. & Biscaia, E. C., Jr. (eds.). *Online Experimental Design for Model Validation* (Proceedings of 10th International Symposium on Process Systems Engineering - PSE2009., 2009).

[213] Resindion S.R.L., Via Roma 22, 20082 Binasco (Italy). *Sepabeads: Enzyme carriers* (2005).

[214] Hilterhaus, L. *et al.* Practical application of different enzymes immobilized on sepabeads. *Bioprocess and Biosystems Engineering* **31**, 163–171 (2008).

[215] Pollegioni, L. *et al.* Cephalosporin c acylase mutants: European patent 1553175a (2005).

[216] Arroyo, M., de la Mata, I., Acebal, C. & Castillon, M. Biotechnological applications of penicillin acylases: state-of-the-art. *Applied Microbiology and Biotechnology* **60**, 507–524 (2003).

[217] Hildebrand, F. & Lütz, S. Immobilisation of alcohol dehydrogenase from lactobacillus brevis and its application in a plug-flow reactor. *Tetrahedron: Asymmetry* **17**, 3219–3225 (2006).

[218] Palomo, J. *et al.* Resolution of (+/-)-5-substituted-6-(5-chloropyridin-2-yl)-7-oxo-5,6-dihydropyrrolo[3, 4b]pyrazine derivatives-precursors of (*S*)-(+)-zopiclone, catalyzed by immobilized candida antarctica b lipase in aqueous media. *Tetrahedron: Asymmetry* **14**, 429–438 (2003).

[219] Crangle, R. *Minerals yearbook: Volume I.– Metals and Minerals*, chap. Diatomite (U.S. Geological Survey, 2008).

[220] Bertram, M. *et al.* Characterization of lipases and esterases from metagenomes for lipid modification. *Journal of the American Oil Chemists' Society* **85**, 47–53 (2008).

[221] Gaffar, S., R.and Kermasha & Bisakowski, B. Biocatalysis of immobilized chlorophyllase in a ternary micellar system. *Journal of Biotechnology* **75**, 45–55 (1999).

[222] Persson, M. & Bornscheuer, U. Increased stability of an esterase from bacillus stearothermophilus in ionic liquids as compared to organic solvents. *Journal of Molecular Catalysis B: Enzymatic* **22**, 21–27 (2003).

[223] Alloue, W. *et al.* Comparison of yarrowia lipolytica lipase immobilization yield of entrapment, adsorption, and covalent bond techniques. *Applied Biochemistry and Biotechnology* **150**, 51–63 (2008).

[224] Arcos, J. & Otero, C. Enzyme, medium, and reaction engineering to design a low-cost, selective production method for mono- and dioleoylglycerols. *Journal of the American Oil Chemists' Society* **73**, 673–682 (1996).

[225] Anthonsen, T. *et al.* Phospholipids hydrolysis in organic solvents catalysed by immobilised phospholipase c. *Journal Of Molecular Catalysis B: Enzymatic* **6**, 125–132 (1999).

[226] Bagi, K. & Simon, L. Comparison of esterification and transesterification of fructose by porcine pancreas lipase immobilized on different supports. *Biotechnology Techniques* **13**, 309–312 (1999).

[227] Banfi, L., Guanti, G., Mugnoli, A. & Riva, R. Lipase catalyzed asymmetrization of quinolyl substituted 1,3-propanediols. *Tetrahedron: Asymmetry* **9**, 2481–2492 (1998).

[228] Basri, M., Yunus, W., Yoong, W., Ampon, K. & Razak, C. Immobilization of lipase from candida rugosa on synthetic polymer beads for use in the synthesis of fatty esters. *Journal of Chemical Technology & Biotechnology* **66**, 169–173 (1996).

[229] Bisht, K., Henderson, L., Gross, R., Kaplan, D. & Swift, G. Enzyme-catalyzed ring-opening polymerization of pentadecalactone. *Macromolecules* **30**, 2705–2711 (1997).

[230] Carbone, K., Casarci, M. & Varrone, M. Crosslinked poly(vinyl alcohol) supports for the immobilization of a lipolytic enzyme. *Journal of Applied Polymer Science* **74**, 1881–1889 (1999).

[231] Chang, S., Chang, S., Yen, Y. & Shieh, C. Optimum immobilization of candida rugosa lipase on celite by rsm. *Applied Clay Science* **37**, 67–73 (2007).

[232] de Castro, H., de Oliveira, P., Soares, C. & Zanin, G. Immobilization of porcine pancreatic lipase on celite for application in the synthesis of butyl butyrate in a nonaqueous system. *Journal of the American Oil Chemists' Society* **76**, 147–152 (1999).

[233] Fadiloglu, S. & Soylemez, Z. Olive oil hydrolysis by celite-immobilized candida rugosa lipase. *Journal of Agricultural and Food Chemistry* **46**, 3411–3414 (1998).

[234] Ferrer, M. *et al.* Effect of the immobilization method of lipase from thermomyces lanuginosus on sucrose acylation. *Biocatalysis and Biotransformation* **20**, 63–71 (2002).

[235] Fishman, A. & Cogan, U. Bio-imprinting of lipases with fatty acids. *Journal of Molecular Catalysis B: Enzymatic* **22**, 193–202 (2003).

[236] Furukawa, S. & Kawakami, K. Characterization of candida rugosa lipase entrapped into organically modified silicates in esterification of menthol with butyric acid. *Journal of Fermentation and Bioengineering* **85**, 240–242 (1998).

[237] Ghazali, H., Hamidah, S. & Che Man, Y. Enzymatic transesterification of palm olein with nonspecific and 1,3-specific lipases. *Journal of the American Oil Chemists' Society* **72**, 633–639 (1995).

[238] Gorokhova, I., Ivanov, A. & Zubov, V. Coprecipitation of pseudomonas fluorescens lipase with hydrophobic compounds as an approach to its immobilization for catalysis in nonaqueous media. *Russian Journal of Bioorganic Chemistry* **28**, 38–43 (2002).

[239] Guanti, G., Narisano, E. & Riva, R. Enzyme catalysed asymmetrization of pyridyl substituted 1,3-propanediols and of the corresponding diacetates. *Tetrahedron: Asymmetry* **8**, 2175–2187 (1997).

[240] Haas, M., Cichowicz, D., Jun, W. & Scott, K. The enzymatic hydrolysis of triglyceride-phospholipid mixtures in an organic solvent. *Journal of the American Oil Chemists' Society* **72**, 519–525 (1995).

[241] Hari Krishna, S., Persson, M. & Bornscheuer, U. Enantioselective transesterification of a tertiary alcohol by lipase a from candida antarctica. *Tetrahedron: Asymmetry* **13**, 2693–2696 (2002).

[242] Ivanov, A. & Schneider, M. Methods for the immobilization of lipases and their use for ester synthesis. *Journal of Molecular Catalysis B: Enzymatic* **3**, 303–309 (1997).

[243] Jeong, S., Hwang, B., Kim, J. & Kim, B. Lipase-catalyzed reaction in the packed-bed reactor with continuous extraction column to overcome a product inhibition. *Journal of Molecular Catalysis B: Enzymatic* **10**, 597–604 (2000).

[244] Kaewthong, W., Sirisansaneeyakul, S., Prasertsan, P. & H-Kittikun, A. Continuous production of monoacylglycerols by glycerolysis of palm olein with immobilized lipase. *Process Biochemistry* **40**, 1525–1530 (2005).

[245] Kaga, H., Siegmund, B., Neufellner, E., Faber, K. & Paltauf, F. Stabilization of candida lipase against acetaldehyde by adsorption onto celite. *Biotechnology Techniques* **8**, 369–374 (1994).

[246] Kawakami, K. & Yoshida, S. Thermal stabilization of lipase by sol-gel entrapment in organically modified silicates formed on kieselguhr. *Journal of Fermentation and Bioengineering* **82**, 239–245 (1996).

[247] Kermasha, S. & Bisakowski, B. The effect of immobilization on the hydrolytic/interesterification activity of lipase from rhizopus niveus. *Journal of the American Oil Chemists' Society* **75**, 1791–1799 (1998).

[248] Khare, S. & Nakajima, M. Immobilization of rhizopus japonicus lipase on celite and its application for enrichment of docosahexaenoic acid in soybean oil. *Food Chemistry* **68**, 153–157 (2000).

[249] Lee, C. & Parkin, K. Effect of water activity and immobilization on fatty acid selectivity for esterification reactions mediated by lipases. *Biotechnology and Bioengineering* **75**, 219–227 (2001).

[250] Liljeblad, A. & Kanerva, L. Enzymatic methods for the preparation of enantiopure malic and aspartic acid derivatives in organic solvents. *Tetrahedron: Asymmetry* **10**, 4405–4415 (1999).

[251] Marlot, C., Langrand, G., Triantaphylides, C. & Baratti, J. Ester synthesis in organic solvent catalyzed by lipases immobilized on hydrophilic supports. *Biotechnology Letters* **7**, 647–650 (1985).

[252] Matsumura, S., Mabuchi, K. & Toshima, K. Novel ring-opening polymerization of lactide by lipase. *Macromolecular Symposia* **130**, 285–304 (1998).

[253] Melo, L., Pastore, G. & Macedo, G. Optimized synthesis of citronellyl flavour esters using free and immobilized lipase from rhizopus sp. *Process Biochemistry* **40**, 3181–3185 (2005).

[254] Millqvist, A., Adlercreutz, P. & Mattiasson, B. Lipase-catalyzed alcoholysis of triglycerides for the preparation of 2-monoglycerides. *Enzyme and Microbial Technology* **16**, 1042–1047 (1994).

[255] Ming, L., Ghazali, H. & Let, C. Effect of enzymatic transesterification on the fluidity of palm stearin-palm kernel olein mixtures. *Food Chemistry* **63**, 155–159 (1998).

[256] Mojovic, L., Siler-Marinkovic, S., Kukic, G., Bugarski, B. & Vunjak-Novakovic, G. Rhizopus arrhizus lipase-catalyzed interesterification of palm oil midfraction in a gas-lift reactor. *Enzyme and Microbial Technology* **16**, 159–162 (1994).

[257] Persson, M., Costes, D., Wehtje, E. & Adlercreutz, P. Effects of solvent, water activity and temperature on lipase and hydroxynitrile lyase enantioselectivity. *Enzyme and Microbial Technology* **30**, 916–923 (2002).

[258] Pinsirodom, P. & Parkin, K. Selectivity of celite-immobilized patatin (lipid acyl hydrolase) from potato (solanum tuberosum l.) tubers in esterification reactions as influenced by water activity and glycerol analogues as alcohol acceptors. *Journal of Agricultural and Food Chemistry* **48**, 155–160 (2000).

[259] Pinsirodom, P. & Parkin, K. Selectivity of potato tuber lipid acyl hydrolase toward long-chain unsaturated fa in esterification reactions with glycerol analogs in organic media. *Journal of the American Oil Chemists Society* **80**, 335–340 (2003).

[260] Plou, F. *et al.* Acylation of sucrose with vinyl esters using immobilized hydrolases: demonstration that chemical catalysis may interfere with enzymatic catalysis. *Biotechnology Letters* **21**, 635–639 (1999).

[261] Pu, W., Li-rong, Y. & Jian-ping, W. Immobilization of lipase by salts and the transesterification activity in hexane. *Biotechnology Letters* **23**, 1429–1433 (2001).

[262] Rosu, R., Uozaki, Y., Iwasaki, Y. & Yamane, T. Repeated use of immobilized lipase for monoacylglycerol production by solid-phase glycerolysis of olive oil. *Journal of the American Oil Chemists' Society* **74**, 445–450 (1997).

[263] Sagiroglu, A. & Telefoncu, A. Immobilization of lipases on different carriers and their use in synthesis of pentyl isovalerates. *Preparative Biochemistry and Biotechnology* **34**, 169–178 (2004).

[264] Serri, N., Kamaruddin, A. & Long, W. Studies of reaction parameters on synthesis of citronellyl laurate ester via immobilized candida rugosa lipase in organic media. *Bioprocess and Biosystems Engineering* **29**, 253–260 (2006).

[265] Shah, S. & Gupta, M. Lipase catalyzed preparation of biodiesel from jatropha oil in a solvent free system. *Process Biochemistry* **42**, 409–414 (2007).

[266] Shih, I., Chiu, L., Lai, C., Liaw, W. & Tai, D. Enzymes catalyzed esterification of n-protected amino acids with secondary alcohols. *Biotechnology Letters* **19**, 857–859 (1997).

[267] Stevenson, D., Stanley, R. & Furneaux, R. Near-quantitative production of fatty acid alkyl esters by lipase-catalyzed alcoholysis of fats and oils with adsorption of glycerol by silica gel. *Enzyme and Microbial Technology* **16**, 478–484 (1994).

[268] Temesvari, J., Banky, E. & Biacs, P. Use of immobilized lipase in transesterification of triglicerides. *Acta Alimentaria* **23**, 215–220 (1994).

[269] Triantafyllou, A., Wang, D., Wehtje, E. & Adlercreutz, P. Polyacrylamides as immobilization supports for use of hydrolytic enzymes in organic media. *Biocatalysis and Biotransformation* **15**, 185–203 (1997).

[270] Tweddell, R., Kermasha, S., Combes, D. & Marty, A. Immobilization of lipase from rhizopus niveus: A way to enhance its synthetic activity in organic solvent. *Biocatalysis and Biotransformation* **16**, 411–426 (1999).

[271] Uyama, H., Takeya, K., Hoshi, N. & Kobayashi, S. Lipase-catalyzed ring-opening polymerization of 12-dodecanolide. *Macromolecules* **28**, 7046–7050 (1995).

[272] Valivety, R., Halling, P., Peilow, A. & Macrae, A. Relationship between water activity and catalytic activity of lipases in organic media effects of supports, loading and enzyme preparation. *European Journal of Biochemistry* **222**, 461–466 (1994).

[273] Wehtje, E., Adlercreutz, P. & Mattiasson, B. Improved activity retention of enzymes deposited on solid supports. *Biotechnology and Bioengineering* **41**, 171–178 (1993).

[274] Wisdom, R., Dunnill, P. & Lilly, M. Enzymic interesterification of fats: The effect of non-lipase material on immobilized enzyme activity. *Enzyme and Microbial Technology* **7**, 567–572 (1985).

[275] Xie, Y., Liu, H. & Chen, J. Kinetics of lipase catalyzed enantioselective esterification of racemic ibuprofen in isooctane. *Chinese Hournal of Chemical Engineering* **8**, 6–14 (2000).

[276] Xu, J., Zhou, R. & Bornscheuer, U. Comparison of differently modified pseudomonas cepacia lipases in enantioselective preparation of a chiral alcohol for agrochemical use. *Biocatalysis and Biotransformation* **23**, 415–422 (2005).

[277] Zhou, R. & Xu, J. Enantioselective synthesis of (*S*)-α-cyano-3-phenoxybenzyl alcohol by lipase-catalyzed alcoholysis of racemic ester in organic medium. *Biochemical Engineering Journal* **23**, 11–15 (2005).

[278] Ertan, F., Yagar, H. & Balkan, B. Some properties of free and immobilized alpha-amylase from penicillium griseofulvum by solid state fermentation. *Preparative Biochemistry & Biotechnology* **36**, 81–91 (2006).

[279] Gargouri, M., Smaali, I., Maugard, T., Legoy, M. & Marzouki, N. Fungus β-glycosidases: immobilization and use in alkyl-β-glycoside synthesis. *Journal of Molecular Catalysis B: Enzymatic* **29**, 89–94 (2004).

[280] Gaur, R., Pant, H., Jain, R. & Khare, S. Galacto-oligosaccharide synthesis by immobilized aspergillus oryzae β-galactosidase. *Food Chemistry* **97**, 426–430 (2006).

[281] Hansson, T., Andersson, M., Wehtje, E. & Adlercreutz, P. Influence of water activity on the competition between β-glycosidase-catalysed transglycosylation and hydrolysis in aqueous hexanol. *Enzyme and Microbial Technology* **29** (2001).

[282] Hansson, T. & Adlercreutz, P. Enzymatic synthesis of hexyl glycosides from lactose at low water activity and high temperature using hyperthermostable β-glycosidases. *Biocatalysis and Biotransformation* **20**, 167–178 (2002).

[283] Mansour, E. & Dawoud, F. Immobilization of invertase on celite and on polyacrylamide by an absorption procedure. *Journal of the Science of Food and Agriculture* **83**, 446–450 (2003).

[284] Sekeroglu, G., Fadiloglu, S. & Gögüs, F. Immobilization and characterization of naringinase for the hydrolysis of naringin. *European Food Research and Technology* **224**, 55–60 (2006).

[285] Adlercreutz, P. Activation of enzymes in organic media at low water activity by polyols and saccharides. *Biochimica et Biophysica Acta (BBA) - Protein Structure and Molecular Enzymology* **1163**, 144–148 (1993).

[286] Barros, R., Wehtje, E. & Adlercreutz, P. Modeling the performance of immobilized α-chymotrypsin catalyzed peptide synthesis in acetonitrile medium. *Journal of Molecular Catalysis B: Enzymatic* **11**, 841–850 (2001).

[287] Bemquerer, M. P., Adlercreutz, P. & Tominaga, M. Pepsin-catalyszed peptide-synthesis in organic media - studies with free and immobilized enzyme. *International Journal of Peptide and Protein Reserach* **44**, 448–456 (1994).

[288] Bjorup, P., Adlercreutz, P. & Clapés, P. Useful methods in enzymatic synthesis of peptides: A comparative study focussing on kinetically controlled synthesis of ac-phe-ala-nh2 catalyzed by alpha-chymotrypsin. *Biocatalysis and Biotransformation* **17**, 319–345 (1999).

[289] Bovara, R., Carrea, G., Gioacchini, A., Riva, S. & Secundo, F. Activity, stability, and conformation of methoxypoly(ethylene glycol)-subtilisin at different concentrations of water in dioxane. *Biotechnology and Bioengineering* **54**, 50–57 (1997).

[290] Calvet, S., Torres, J. & Clapes, P. Enzymatic peptide synthesis in organic media. synthesis of cck-8 dipeptide fragments. *Biocatalysis and Biotransformation* **13**, 201–216 (1996).

[291] Capellas, M. *et al.* Enzymatic synthesis of a cck-8 tripeptide fragment in organic media. *Biotechnology and Bioengineering* **50**, 700–708 (1996).

[292] Clapés, P., Valencia, G. & Adlercreutz, P. Influence of solvent and water activity on kinetically controlled peptide synthesis. *Enzyme and Microbial Technology* **14**, 575–580 (1992).

[293] Fité, M. *et al.* Reactivity of easily removable protecting groups for glycine in peptide synthesis using papain as catalyst. *Enzyme and Microbial Technology* **23**, 199–203 (1998).

[294] Gill, I. & Valivety, R. Pilot-scale enzymatic synthesis of bioactive oligopeptides in eutectic-based media. *Organic Process Research & Development* **6**, 684–691 (2002).

[295] Huang, X., Catignani, G. & Swaisgood, H. Comparison of the properties of trypsin immobilized on 2 celite(tm) derivatives. *Journal of Biotechnology* **53**, 21–27 (1997).

[296] Jönsson, A., Wehtje, E., Adlercreutz, P. & Mattiasson, B. Temperature effects on protease catalyzed acyl transfer reactions in organic media. *Journal of Molecular Catalysis B: Enzymatic* **2**, 43–51 (1996).

[297] Levitsky, V., Lozano, P. & Iborra, J. Designing enzymatic kyotorphin synthesis in organic media with low water content. *Enzyme and Microbial Technology* **26**, 608–613 (2000).

[298] Lozano, P., de Diego, T., Belleville, M., Rios, G. & Iborra, J. A dynamic membrane reactor with immobilized α-chymotrypsin for continuous kyotorphin synthesis in organic media. *Biotechnology Letters* **22**, 771–775 (2000).

[299] Miyazawa, T., Masaki, S., Tanaka, K. & Yamada, T. Peptide syntheses mediated by bacillus subtilis protease. *Letters in Peptide Science* **10**, 83–87 (2003).

[300] Pérez-Victoria, I. & Morales, J. Regioselectivity in acylation of oligosaccharides catalyzed by the metalloprotease thermolysin. *Tetrahedron* **62**, 2361–2369 (2006).

[301] Richards, A., Gill, I. & Vulfson, E. Continuous enzymatic production of oligopeptides: Synthesis of an enkephalin pentapeptide in a multistage bioreactor. *Enzyme and Microbial Technology* **15**, 928–935 (1993).

[302] Triantafyllou, A., Wehtje, E., Adlercreutz, P. & Mattiasson, B. How do additives affect enzyme activity and stability in nonaqueous media? *Biotechnology and Bioengineering* **54**, 67–76 (1997).

[303] Ulijn, R., Erbeldinger, M. & Halling, P. Comparison of methods for thermolysin-catalyzed peptide synthesis including a novel more active catalyst. *Biotechnology and Bioengineering* **69**, 633–638 (2000).

[304] Zhang, X. *et al.* Protease-catalyzed small peptide synthesis in organic media. *Enzyme and Microbial Technology* **19**, 538–544 (1996).

[305] Barros, R., Wehtje, E. & Adlercreutz, P. Mass transfer studies on immobilized alpha-chymotrypsin biocatalysts prepared by deposition for use in organic medium. *Biotechnology and Bioengineering* **59**, 364–373 (1998).

[306] Basso, A., Martin, L., Ebert, C., Gardossi, L. & Linda, P. Selectivity of penicillin g acylase towards phenylacetic acid derivatives in amide bond synthesis in toluene. *Journal of Molecular Catalysis B: Enzymatic* **16**, 73–80 (2001).

[307] Basso, A. *et al.* Activity of covalently immobilised pga in water miscible solvents at controlled aw. *Journal of Molecular Catalysis B: Enzymatic* **11**, 851–855 (2001).

[308] Basso, A. *et al.* Kinetically controlled synthesis of ampicillin and cephalexin in highly condensed systems in the absence of a liquid aqueous phase. *Journal of Molecular Catalysis B: Enzymatic* **39**, 105–111 (2006).

[309] de Martin, L., Ebert, C., Garau, G., Gardossi, L. & Linda, P. Penicillin g amidase in low-water media: immobilisation and control of water activity by means of celite rods. *Journal of Molecular Catalysis B: enzymatic* **6**, 437–445 (1999).

[310] Adlercreutz, P. On the importance of the support material for enzymatic synthesis in organic media. *European Journal of Biochemistry* **199**, 609–614 (1991).

[311] Adlercreutz, P. Effects of the support material and the thermodynamic water activity on enzymatic synthesis in organic media. *Annals of the New York Academy of Sciences* **672**, 314–317 (1992).

[312] Andersson, M., Samra, B., Holmberg, K. & Adlercreutz, P. Use of celite-immobilised chloroperoxidase in predominantly organic media. *Biocatalysis and Biotransformation* **17**, 293–303 (1999).

[313] Chaplin, J., Budde, C. & Khmelnitsky, Y. Catalysis by amine oxidases in non-aqueous media. *Journal of Molecular Catalysis B: Enzymatic* **13**, 69–75 (2001).

[314] Day, S. & Legge, R. Immobilization of tyrosinase for use in nonaqueous media: Enzyme deactivation phenomena. *Biotechnology Techniques* **9**, 471–476 (1995).

[315] Johansson, A., Mosbach, K. & Mansson, M. Horse liver alcohol dehydrogenase can accept nadp as coenzyme in high concentrations of acetonitrile. *European Journal of Biochemistry* **227**, 551–555 (1995).

[316] Katan, T. & Galun, E. A rapid and efficient method for the purification of tyrosinase from neurospora. *Analytical Biochemistry* **67**, 485–492 (1975).

[317] Khan, A. & Husain, Q. Decolorization and removal of textile and non-textile dyes from polluted wastewater and dyeing effluent by using potato (solanum tuberosum) soluble and immobilized polyphenol oxidase. *Bioresource Technology* **98**, 1012–1019 (2007).

[318] Leontievsky, A. *et al.* Transformation of 2,4,6-trichlorophenol by free and immobilized fungal laccase. *Applied Microbiology and Biotechnology* **57**, 85–91 (2001).

[319] Shim, J. *et al.* Degradation of azo dye by an electroenzymatic method using horseradish peroxidase immobilized on porous support. *Korean Journal of Chemical Engineering* **24**, 72–78 (2007).

[320] Shuttleworth, K. & Bollag, J. Soluble and immobilized laccase as catalysts for the transformation of substituted phenols. *Enzyme and Microbial Technology* **8**, 171–177 (1986).

[321] Virto, C., Svensson, I., Adlercreutz, P. & Mattiasson, B. Catalytic activity of non-covalent complexes of horse liver alcohol dehydrogenase, nad and polymers, dissolved or suspended in organic solvents. *Biotechnology Letters* **17**, 877–882 (1995).

[322] Yang, Z. & Robb, D. Comparison of tyrosinase activity and stability in aqueous and nearly nonaqueous environments. *Enzyme and Microbial Technology* **15**, 1030–1036 (1993).

[323] Costes, D., Wehtje, E. & Adlercreutz, P. Hydroxynitrile lyase-catalyzed synthesis of cyanohydrins in organic solvents. parameters influencing activity and enantiospecificity. *Enzyme and Microbial Technology* **25**, 384–391 (1999).

[324] Costes, D., Wehtje, E. & Adlercreutz, P. Cross-linked crystals of hydroxynitrile lyase as catalyst for the synthesis of optically active cyanohydrins. *Journal of Molecular Catalysis B: Enzymatic* **11**, 607–612 (2001).

[325] Effenberger, F., Eichhorn, J. & Roos, J. Enzyme catalyzed addition of hydrocyanic acid to substituted pivalaldehydes - a novel synthesis of (r)-pantolactone. *Tetrahedron: Asymmetry* **6**, 271–282 (1995).

[326] Poraver. Dennert poraver gmbh (2011). Available online at http://www.poraver.de/downloads/PDF/101117_IB_PORAVER_TDS_EN.pdf visited July 12th 2011.

[327] Goldberg, K. *et al.* Novel immobilization routes for the covalent binding of an alcohol dehydrogenase from rhodococcus ruber dsm 44541. *Tetrahedron: asymmetry* **19**, 1171–1173 (2008).

[328] Krüger, A., Liang, Y., Jarre, G. & Stegk, J. Surface functionalisation of detonation diamond suitable for biological applications. *Journal of Materials Chemistry* **16**, 2322–2328 (2006).

[329] Krüger, A. Hard and soft: Biofunctionalized diamond. *Angewandte Chemie, International Edition* **45**, 6426–6427 (2006).

[330] Krüger, A. New carbon materials: Biological applications of functionalized nanodiamond materials. *Chemistry - A European Journal* **14**, 1382–1390 (2008).

[331] Ozawa, M. *et al.* Preparation and behavior of brownish, clear nanodiamond colloids. *Advanced Materials* **19**, 1201–1206 (2007).

[332] Yuryev, R., Briechle, S., Gruber-Khadjawi, M., Griengl, H. & Liese, A. Asymmetric retro-henry reaction catalyzed by hydroxynitrile lyase from hevea brasiliensis. *ChemCatChem* **2**, 981–986 (2010).

[333] Straathof, A. & Jongejan, J. The enantiomeric ratio: origin, determination and prediction. *Enzyme and Microbial Technology* **21**, 559 – 571 (1997).

[334] Barros, R., Wehtje, E. & Adlercreutz, P. Enhancement of immobilized protease catalyzed dipeptide synthesis by the presence of insoluble protonated nucleophile. *Enzyme and Microbial Technology* **24**, 480–488 (1999).

[335] Hanefeld, U., Gardossi, L. & Magner, E. Understanding enzyme immobilisation. *Chemical Society Reviews* **38**, 453–468 (2009).

[336] Avi, M. *et al.* α- and β-oxygenated aldehydes derived from diels-alder reactions as substrates for hydroxynitrile lyases. *Journal of Molecular Catalysis B: Enzymatic* **61**, 268 – 273 (2009).

[337] U., N. *Untersuchungen zur enzymatischen C-C Verknüpfung am Beispiel der chiralen Cyanhydrinbildung*. Ph.D. thesis, Forschungszentrum Jülich,, Germany (1996).

[338] of Medicine, U. N. L. Chemidplus advanced database. Website (2008). Available online at http://chem.sis.nlm.nih.gov/chemidplus/ visited July 12th 2008.

[339] on Chemical Safety, I. P. Chemical safety information from intergovernmental organizations. Website (2008). Available online at http://www.inchem.org/; visited July 12th 2008.

[340] Shriver-Lake, L., Gammeter, B., Bang, S. & Pazirandeh, M. Covalent binding of genetically engineered microorganisms to porous glass beads. *Analytica Chimica Acta* **470**, 71–78 (2002).

Typeset May 28, 2013

Lebenslauf: Sebastian Briechle

	Schulausbildung
1983 – 1996	Grundschule und Gymnasium in Bergheim
	Zivildienst
1996 – 1997	Erftverband, Bergheim, im Bereich der Gewässerpflege
	Hochschulausbildung
10/1997 – 05/2004	Studium des Maschinenbaus an der RWTH Aachen Vertiefungsrichtung: **Bioverfahrenstechnik**
	Auslandsaufenthalte
08/2001 – 07/2002	Auslandsstudium an der Königlichen Technischen Hochschule in Stockholm, Schweden
09 – 12/2002	Studienarbeit an der Universität Lund, Schweden
09/2003 – 01/2004	Diplomarbeit bei Novozymes Biopharma AB in Lund, Schweden
	Promotion
06/2004 – 06/2005	Wissenschaftlicher Mitarbeiter am Institut für Biochemie, WWU Münster. Beginn der Promotion. Doktorvater Prof. Dr. rer. nat. Andreas Liese
07/2005 – 06/2008	Wissenschaftlicher Mitarbeiter am Institut für Technische Biokatalyse, TU Hamburg–Harburg. Weiterführung der Promotion. Doktorvater Prof. Dr. rer. nat. Andreas Liese
	Berufstätigkeit
11/2008 – heute	Entwicklungsingenieur im Bereich der industriellen Biotechnologie bei BASF SE in Ludwigshafen

Frankenthal, den 19. Februar 2013